

CHARACTERISING THE NEUROPHYSIOLOGY OF POST-TRAUMATIC
OSTEOARTHRITIS IN RATS AND THE INVOLVEMENT OF PROTEASE
ACTIVATED RECEPTOR-4

By

Melissa S. O'Brien

Submitted in partial fulfilment of the requirements
for the degree of Doctor of Philosophy

at

Dalhousie University
Halifax, Nova Scotia
February 2021

© Copyright by Melissa O'Brien, 2021

Table of Contents

| | |
|---|-------------|
| List of Tables | viii |
| List of Figures | ix |
| Abstract | xi |
| List of Abbreviations and Symbols Used: | xii |
| Acknowledgments: | xv |
| Chapter 1: Introduction | 1 |
| 1.1 Overview | 1 |
| 1.2 Anatomy of the Human Knee Joint | 2 |
| 1.2.1 Knee Joint Innervation | 5 |
| 1.2.2 Vascular Supply of the Human Knee Joint | 8 |
| 1.3 Arthritis | 9 |
| 1.3.1 Osteoarthritis | 10 |
| 1.3.1.1 Aetiology of Osteoarthritis..... | 11 |
| 1.3.1.2 Pathophysiology of Osteoarthritis | 13 |
| 1.3.1.3 Current treatments in Osteoarthritis..... | 16 |
| 1.3.2 Rheumatoid Arthritis | 18 |
| 1.3.2.1 Aetiology of Rheumatoid Arthritis | 20 |
| 1.3.2.2 Pathophysiology of Rheumatoid Arthritis..... | 21 |
| 1.3.2.3 Current Treatments in Rheumatoid Arthritis..... | 22 |
| 1.3.3 Preclinical Models of Osteoarthritis | 23 |
| 1.3.3.1 The Medial Meniscal Transection (MMT) Model of Post-Traumatic Osteoarthritis..... | 23 |
| 1.3.3.2 The Monoiodoacetate (MIA) Model of Osteoarthritis..... | 24 |
| 1.4 Pain in Arthritis | 25 |
| 1.4.1 The Pain Pathway | 26 |
| 1.4.2 Pain mechanisms and mediators in OA | 33 |
| 1.5 Assessment of Nociceptive Behaviour in Preclinical Models of Pain | 39 |
| 1.5.1 von Frey Hair Algesiometry | 40 |
| 1.5.2 Dynamic Weight Bearing | 40 |
| 1.6 Electrophysiology as a Measure of Nociceptive Tone in Preclinical Models of Pain | 41 |
| 1.6.1 Teased Nerve Recordings | 41 |
| 1.7 Assessment of Inflammation in Preclinical Models of Pain | 42 |
| 1.7.1 Intravital Microscopy (IVM) | 43 |
| 1.7.2 LAser Speckle Contrast Analysis (LASCA) | 44 |
| 1.8 Serine Proteases | 45 |

| | |
|---|-----------|
| 1.8.1 <i>The Role of Serine Proteases in Arthritis</i> | 46 |
| 1.8.2 <i>Protease Activated Receptors (PARs)</i> | 50 |
| 1.8.3 <i>The Role of PARs in Pain and Inflammation</i> | 55 |
| 1.8.4 <i>The Role of PARs in Arthritis</i> | 58 |
| 1.8.5 <i>The Role of PAR4 in Inflammation and Pain</i> | 59 |
| 1.9 Aims, Objectives & Hypotheses | 61 |
| Chapter 2: Methods | 62 |
| 2.1 Animals | 62 |
| 2.2 Animal Models | 62 |
| 2.2.1 <i>Medial Meniscal Transection Surgery and Sham Surgery</i> | 62 |
| 2.2.2 <i>Monoiodoacetate Model Induction</i> | 63 |
| 2.3 Single Unit Electrophysiology | 64 |
| 2.3.1 <i>Surgical Preparation</i> | 64 |
| 2.3.2 <i>Single Unit Recordings</i> | 65 |
| 2.4 Histology | 67 |
| 2.4.1 <i>Fluoro-gold Labelling of Joint Afferents</i> | 67 |
| 2.4.2 <i>Immunohistochemistry of DRG tissue</i> | 68 |
| 2.5 Saphenous Nerve Electron Microscopy | 69 |
| 2.6 Joint Histopathology | 71 |
| 2.7 Pain Behaviour | 73 |
| 2.7.1 <i>von Frey Hair Algesiometry</i> | 73 |
| 2.7.2 <i>Dynamic Incapacitance</i> | 74 |
| 2.8 Inflammatory Measurements | 74 |
| 2.8.1 <i>Surgical Preparation</i> | 74 |
| 2.8.2 <i>Laser Speckle Contrast Analysis (LASCA)</i> | 75 |
| 2.8.3 <i>Intra-vital Microscopy (IVM)</i> | 76 |
| 2.9 Measurement of Protein Analytes in Rat Serum | 77 |
| 2.9.1 <i>Luminex</i> | 78 |
| 2.9.2 <i>Enzyme Linked Immunosorbent Assay</i> | 78 |
| 2.10 Mass Spectrometry | 78 |
| 2.10 Materials | 80 |
| 2.11 Statistical Analysis | 80 |

| | |
|---|------------|
| Chapter 3: Nociceptive Characterisation of the MMT Model of PTOA..... | 92 |
| 3.1 Background and Hypotheses | 92 |
| 3.2 Characterisation of Pain Phenotype in the MMT model of PTOA | 93 |
| 3.2.1 Methods | 93 |
| 3.2.2 Results | 94 |
| 3.2.2.1 Effect of Medial Meniscal Transection on Joint Diameter..... | 94 |
| 3.2.2.2 Medial Meniscal Transection Induced Nociceptive Behaviour that was Sex-Specific | 94 |
| 3.3 Characterisation of Joint Damage in the MMT Model..... | 96 |
| 3.3.1 Methods | 96 |
| 3.3.2 Results | 96 |
| 3.3.2.1 Medial Meniscal Transection induced Joint Pathology..... | 96 |
| 3.4 Measurement of Joint Nociceptors in the MMT Model | 97 |
| 3.4.1 Methods | 97 |
| 3.4.2.1 Medial Meniscal Transection Induced Sex-specific Changes in Joint Afferent Sensitization...98 | |
| 3.5 Assessment of Saphenous Nerve Morphology in the MMT Model | 99 |
| 3.5.1 Methods | 99 |
| 3.5.2 Results | 99 |
| 3.5.2.1 Medial Meniscal Transection Resulted in Neuropathy, But Not Demyelination, of the Saphenous Nerve in Male Animals | 99 |
| 3.6 Assessment of Joint Neurones at the Level of the Dorsal Root Ganglia | 100 |
| 3.6.1 Methods | 100 |
| 3.6.1 Results | 100 |
| 3.6.1.1 Medial Meniscal Transection Did Not Induce Neuronal Apoptosis but Activated Satellite Glial Cells..... | 100 |
| 3.7 Effect of Amitriptyline on PTOA Pain | 101 |
| 3.7.1 Methods | 101 |
| 3.7.1.1 Pain Behaviour | 101 |
| 3.7.1.2 Single Unit Electrophysiology..... | 102 |
| 3.7.2 Results | 102 |
| 3.7.2.1 Systemic Amitriptyline Attenuated Pain Behaviour in Male PTOA Animals | 102 |
| 3.7.2.2 Local Administration of Amitriptyline Attenuated Joint Afferent Firing in both Sexes | 103 |
| 3.8 The Role of β-Endorphin and Noradrenaline in the MMT Model..... | 103 |
| 3.8.1 Methods | 103 |
| 3.8.1.1 Measurement of Serum β -Endorphin and Noradrenaline..... | 103 |
| 3.8.1.2 Correlations Between Serum β -Endorphin or Noradrenaline, and Firing Rates..... | 104 |
| 3.8.1.3 Systemic Naloxone Treatment in Female MMT Animals | 104 |
| 3.8.2 Results | 105 |
| 3.8.2.1 Serum β -Endorphin and Noradrenaline Concentration in MMT Animals..... | 105 |

| | |
|--|------------|
| 3.8.2.2 Correlation of Serum β -Endorphin or Noradrenaline Concentrations and Afferent Firing Rates | 105 |
| 3.8.2.3 Endogenous Opioids Mediate Antinociception in Female MMT Animals | 106 |
| 3.9 Chapter Summary..... | 106 |
| 3.9.1 Medial Meniscus Transection Induces Histological Damage in Both Sexes but Sexually Disparate Pain Responses | 106 |
| 3.9.2 Assessment of Neuropathic-like Pain in the Medial Meniscus Transection Model ... | 107 |
| 3.9.3 Endogenous Opioids Mediate Antinociception in Female MMT Animals..... | 108 |
| Chapter 4: The role of PAR4 in Early and Late-Stage Experimental OA | 134 |
| 4.1 Background and Hypothesis | 134 |
| 4.2 Characterising Early and Late Stages in the MIA and MMT Models of Experimental OA..... | 134 |
| 4.2.1. Methods | 135 |
| 4.2.1.1 Induction of MIA and MMT Models..... | 135 |
| 4.2.1.2 Characterising Saphenous Nerve Integrity in Early and Late Stages in the MIA and MMT models of Experimental OA | 137 |
| 4.2.2 Results | 137 |
| 4.2.2.1 Peripheral nerve damage and demyelination is present in the late phase of the MIA model | 137 |
| 4.2.2.2 Peripheral nerve damage but not demyelination is present in the late phase of the MMT model..... | 138 |
| 4.3 Characterising Systemic Inflammation in Early and Late Stages in the MIA and MMT models of Experimental OA..... | 138 |
| 4.3.1 Methods | 138 |
| 4.3.1.1 Measurement of Systemic Inflammatory Mediators..... | 138 |
| 4.3.2 Results | 139 |
| 4.4 Single-Unit Recordings of Joint Afferent Fibres in MIA and MMT Models of OA and the Effect of PAR4 Blockade on Evoked Firing..... | 140 |
| 4.4.1 Methods | 140 |
| 4.4.2 Results | 140 |
| 4.4.2.1 Characterisation of Joint Afferent Electrophysiological Activity in the Early and Late Phases of Experimental OA | 140 |
| 4.4.2.2 PAR4 Blockade Attenuates Joint Afferent Firing in Early Experimental OA..... | 141 |
| 4.4.2.3 PAR4 Blockade Fails to Affect Joint Afferent Firing in Late Experimental OA..... | 142 |
| 4.5 Effect of PAR4 Blockade on Pain Behaviour in the Early and Late Phases of Experimental OA | 142 |
| 4.5.1 Methods | 143 |
| 4.5.2 Results | 143 |
| 4.5.2.1 PAR4 Blockade Improves Referred Pain in Early Phases of Experimental OA | 143 |

| | |
|--|------------|
| 4.6 Measuring Joint Inflammation in Experimental OA and the Effects of Systemic PAR4 Blockade | 145 |
| 4.6.1 Methods | 145 |
| 4.6.1.1 IVM..... | 145 |
| 4.6.1.2 LASCA | 146 |
| 4.6.2 Results | 146 |
| 4.6.2.1 Comparison of Joint Inflammation in Early and Late OA | 146 |
| 4.6.2.2 Effect of PAR4 Blockade on Joint Inflammation in Early Timepoints | 147 |
| 4.7 Evaluation of PAR4 expression in DRG Joint Neurons..... | 148 |
| 4.7.1 Methods | 148 |
| 4.7.2 Results | 148 |
| 4.7.2.1 PAR4 Expression is Higher in Joint DRG Neurons at Early OA Timepoints..... | 148 |
| 4.8 Chapter Summary..... | 149 |
| 4.8.1 The MIA and MMT models of OA Exhibit Enhanced Inflammation at Early Timepoints and Nerve Damage at Later Timepoints | 149 |
| 4.8.3 PAR4 Expression in DRG Joint Neurons is Greater During Early Timepoints in the MIA and MMT Models | 151 |
| Chapter 5: Human Arthritic Synovial Fluid Contributes to Joint Afferent Sensitisation, in Part by Activation of PAR4 | 176 |
| 5.1 Background and Hypotheses: | 176 |
| 5.2 Effect of Human Synovial Fluid on Rodent Joint Nociceptors and the Contribution of PAR4 | 177 |
| 5.2.1. Methods | 177 |
| 5.2.2. Results | 178 |
| 5.2.2.1 Neuronal Characteristics of Afferent Fibres..... | 178 |
| 5.2.2.2 Human Arthritic Synovial Fluid Sensitised Rodent Nociceptors | 179 |
| 5.3 Proteomic Analysis of Arthritic Synovial Fluid | 180 |
| 5.3.1. Methods | 180 |
| 5.3.2. Results | 180 |
| 5.3.2.1 Proteomic Analysis Reveals High Levels of Proteases and Protease Inhibitors in Synovial Fluid | 180 |
| 5.4 Chapter Summary..... | 181 |
| 5.4.1 PAR4 cleaving proteins are present in OA and RA synovial fluid | 181 |
| 5.4.2 Human Arthritic Synovial Fluid Sensitises Rodent Nociceptors in part via PAR4 Activation | 182 |
| Chapter 6: Discussion | 196 |

| | |
|--|------------|
| 6.1 Medial Meniscus Transection Causes Sexually Disparate Nociceptive Responses in Rats | 197 |
| 6.2 Effects of PAR4 Antagonism in Early and Late Phases of MMT and MIA..... | 204 |
| 6.3 Arthritic Synovial Fluid is Pro-Nociceptive and Contains Serine Proteases | 211 |
| 6.3.1 Summary | 216 |
| 6.4 Limitations of Experimentation | 216 |
| 6.4.1 The Use of Animals to Study Arthritis and Pain..... | 216 |
| 6.4.2 Electrophysiology..... | 218 |
| 6.4.3 Pain Behaviour..... | 219 |
| 6.4.4 Measures of Inflammation | 220 |
| 6.4.4.1 Preparatory Surgery-Induced Inflammation | 220 |
| 6.4.4.2 Rhodamine 6-G Staining of Leukocytes | 221 |
| 6.4.4.3 LASCA | 221 |
| 6.4.4.4 Measurement of Serum Cytokines | 221 |
| 6.4.5 Pharmacological Tools..... | 222 |
| 6.4.5.1 PAR4 Antagonism..... | 222 |
| 6.4.5.2 Male vs Female Animals..... | 223 |
| 6.4.5.3 Testing a Single Dose of Pepducin P4pal10 | 223 |
| 6.4.5.4 The Use of Post-Surgical Buprenorphine | 223 |
| 6.4.6 Untargeted Mass Spectrometry..... | 224 |
| 6.4.7 Immunohistochemistry | 225 |
| 6.5 Future Directions | 225 |
| 6.5.1 Determine What Other Receptors are Inhibited by Pepducin P4pal10 | 225 |
| 6.5.2 Assess PAR4 Antagonism using another Agent | 226 |
| 6.5.3 Use Serine Protease Probes in Mass Spectrometry and Activity-Based Probes to Ascertain Protease Bioactivity in Synovial Fluid | 226 |
| 6.5.4 Assess the Effect of Complement Factor C4a on Afferent Firing and Pain..... | 226 |
| 6.5.5 Future Electrophysiology Experiments | 227 |
| 6.6 Conclusion | 227 |
| References..... | 230 |
| Appendix A: OARSI Scoring of Knee Joints | 253 |
| Appendix B: Drugs, Reagents, and Devices..... | 258 |
| Appendix C: Comparison of Day 14 MIA in Male and Female Animals | 263 |
| Appendix D: Synovial Fluid Proteomics Result | 269 |
| Appendix E: Copyright Permission | 274 |

List of Tables

| | |
|--|-----|
| TABLE 1. 1: AFFERENT AND EFFERENT INNERVATION OF THE HUMAN KNEE JOINT. | 8 |
| TABLE 1. 2: THE AMERICAN COLLEGE OF RHEUMATOLOGY GUIDELINES FOR KNEE OA DIAGNOSIS. ... | 11 |
| TABLE 1. 3: CLASSIFICATION CRITERIA FOR RHEUMATOID ARTHRITIS. | 20 |
| TABLE 1. 4: SERINE PROTEASES IN ARTHRITIC JOINTS. | 49 |
| TABLE 1. 5: PAR ACTIVATING PROTEASES, DISARMING PROTEASES, AND SYNTHETIC ACTIVATING PEPTIDES. | 55 |
| TABLE 3. 1: ELECTROPHYSIOLOGICAL CHARACTERISTICS OF JOINT AFFERENTS IN MMT ANIMALS. ... | 113 |
| TABLE 4. 1: MEASUREMENT OF SERUM CYTOKINES IN MIA AND MMT ANIMALS. | 157 |
| TABLE 4.2: ELECTROPHYSIOLOGICAL PROPERTIES OF MIA AND MMT JOINT AFFERENTS. | 158 |
| TABLE 4. 3: MEASUREMENT OF LEUKOCYTE TRAFFICKING AND JOINT PERFUSION IN MIA AND MMT ANIMALS. | 169 |
| TABLE 5. 1: ELECTROPHYSIOLOGICAL PROPERTIES OF NAÏVE JOINT AFFERENT FIBRES TREATED WITH HUMAN ARTHRITIC SYNOVIAL FLUID. | 184 |

List of Figures

| | |
|--|-----|
| FIGURE 1. 1 ANATOMY OF THE HUMAN KNEE JOINT. | 4 |
| FIGURE 1. 2 INNERVATION OF THE HUMAN KNEE JOINT. | 6 |
| FIGURE 1. 3 VASCULATURE OF THE HUMAN KNEE JOINT..... | 9 |
| FIGURE 1. 4 COMPARISON OF NORMAL AND OSTEOARTHRITIC KNEE..... | 16 |
| FIGURE 1. 5 COMPARISON OF NORMAL KNEE AND RHEUMATOID ARTHRITIS KNEE JOINT..... | 22 |
| FIGURE 1. 6 ACTION POTENTIAL GENERATION IN SENSORY NEURON..... | 28 |
| FIGURE 1. 7 THE PAIN PATHWAY. | 29 |
| FIGURE 1. 8 MECHANISM OF PERIPHERAL SENSITISATION. | 31 |
| FIGURE 1. 9 LEUKOCYTE TRAFFICKING..... | 44 |
| FIGURE 1. 10 STRUCTURE OF PROTEASE ACTIVATED RECEPTOR-4. | 51 |
| FIGURE 1. 11 ACTIVATION AND DISARMAMENT OF PROTEASE ACTIVATED RECEPTOR-1..... | 53 |
| FIGURE 2. 1 PROCEDURE FOR MMT AND SHAM SURGERIES..... | 81 |
| FIGURE 2. 2 SINGLE UNIT ELECTROPHYSIOLOGY SET-UP FOR JOINT AFFERENT RECORDING..... | 82 |
| FIGURE 2. 3 SINGLE UNIT CONDUCTION VELOCITY MEASUREMENT ON AN OSCILLOSCOPE..... | 83 |
| FIGURE 2. 4 SAPHENOUS NERVE ORIENTATION ON COPPER GRID FOR ELECTRON MICROSCOPY ANALYSIS..... | 84 |
| FIGURE 2. 5 G-RATIO ANALYSIS OF SAPHENOUS NERVE AXONS..... | 85 |
| FIGURE 2. 6 SET-UP FOR VON FREY HAIR ALGESIOMETRY ASSESSMENT..... | 86 |
| FIGURE 2. 7 DYNAMIC INCAPACITANCE ASSESSMENT OF HINDLIMB WEIGHTBEARING..... | 87 |
| FIGURE 2. 8 SET-UP OF LASER SPECKLE CONTRAST ANALYSIS (LASCA) ASSESSMENT OF JOINT BLOOD FLOW..... | 88 |
| FIGURE 2. 9 DEPICTION OF INTRAVITAL MICROSCOPY (IVM) MEASUREMENT. | 89 |
| FIGURE 2. 10 SYNOVIAL FLUID SAMPLING..... | 90 |
| FIGURE 2. 11 LC-MS/MS SAMPLE PREPARATION..... | 91 |
| FIGURE 3. 1 MMT INDUCED JOINT INFLAMMATION AND PAIN..... | 110 |
| FIGURE 3. 2 MMT SURGERY CAUSES JOINT DAMAGE IN BOTH MALE AND FEMALE RATS. | 111 |
| FIGURE 3. 3 THE MMT MODEL INDUCED SENSITIZATION OF JOINT AFFERENTS IN MALE ANIMALS. | 116 |
| FIGURE 3. 4 MMT INDUCED SAPHENOUS NERVE DAMAGE. | 119 |
| FIGURE 3. 5 IMMUNOHISTOCHEMICAL ANALYSIS OF DORSAL ROOT GANGLIA IN THE MMT MODEL. | 122 |
| FIGURE 3. 6 EFFECT OF SYSTEMICALLY ADMINISTERED AMITRIPTYLINE ON MMT-INDUCED PAIN. | 124 |
| FIGURE 3. 7 EFFECT OF CLOSE-INTRAARTERIAL ADMINISTRATION OF AMITRIPTYLINE ON JOINT AFFERENT FIRING..... | 127 |
| FIGURE 3. 8 MEASUREMENT OF SERUM BETA-ENDORPHIN AND NORADRENALINE IN PTOA ANIMALS. | 132 |
| FIGURE 3. 9 EFFECT OF NALOXONE IN FEMALE MMT ANIMALS..... | 133 |

| | |
|---|------------|
| FIGURE 4. 1 EXPERIMENTAL TIMELINE FOR MIA AND MMT ANIMALS. | 136 |
| FIGURE 4. 2 MIA AND MMT-INDUCED NERVE DAMAGE. | 156 |
| FIGURE 4. 3 EFFECT OF PAR4 BLOCKADE ON JOINT AFFERENT FIRING IN EARLY AND LATE STAGES OF THE MIA AND MMT MODELS..... | 162 |
| FIGURE 4. 4 EFFECT OF PAR4 BLOCKADE ON PAIN BEHAVIOUR IN EARLY AND LATE STAGES OF THE MIA AND MMT MODELS. | 167 |
| FIGURE 4. 5 EFFECT OF PAR4 BLOCKADE ON JOINT INFLAMMATION IN MIA AND MMT MODELS..... | 173 |
| FIGURE 4. 6 PAR4 EXPRESSION IN DRG JOINT NEURONES IN MIA AND MMT MODELS..... | 175 |
| FIGURE 5. 1 THE EFFECT OF PAR4 BLOCKADE ON OA SYNOVIAL FLUID-INDUCED JOINT NOCICEPTOR SENSITISATION..... | 187 |
| FIGURE 5. 2 THE EFFECT OF PAR4 BLOCKADE ON RA SYNOVIAL FLUID-INDUCED JOINT AFFERENT SENSITISATION. | 190 |
| FIGURE 5. 3 BIOINFORMATIC ANALYSIS OF OA AND RA PROTEOMIC CONTENT. | 194 |
| FIGURE 5. 4 ABUNDANCE OF SERINE PROTEASES AND SERPINS OF INTEREST..... | 195 |

Abstract

Osteoarthritis (OA) affects 1 in 10 Canadians and is more prevalent in women than men. Remarkably, 60% of OA patients cite inadequate pain relief with current treatments. This may in part be due to multiple OA phenotypes and obscure mechanisms of OA pain. To investigate these phenomena, the neurophysiology of post-traumatic OA (PTOA) was assessed in both sexes and the contribution of pain subtypes was explored. The role of algogenic proteases was examined as a potential mechanism of OA pain.

In the medial meniscal transection (MMT) model of PTOA, similar levels of joint damage were observed in male and female animals; however, marked sex-differences in joint neurobiology were detected. At endstage disease, only male MMT animals exhibited secondary allodynia, weight bearing deficits, and joint nociceptor sensitisation. Saphenous nerve damage was observed in male but not female MMT animals and the neuropathic analgesic amitriptyline reduced pain in males suggesting that peripheral neuropathy may be contributing to PTOA pain in male animals. The lack of nociception in female MMT animals may have been afforded by the endogenous opioid beta-endorphin whose levels were elevated in female animals.

Serine proteases are elevated in the joints of OA patients and contribute to catabolic destruction of joint tissue as well as joint pain and inflammation. Through activation of protease activated receptor 4 (PAR4), some serine proteases cause pain in inflamed joints but in a neuropathic state the actions of PAR4 are unknown. In this thesis, PAR4 antagonism with pepducin P4pal10 attenuated pain behaviour and joint afferent firing in the early inflammatory phases of the MMT and monoiodoacetate (MIA) models of OA. During endstage OA, however, PAR4 antagonism was not effective, suggesting that the role of PAR4 in neuropathic pain may be minimal.

In other experiments, human arthritic synovial fluid was found to sensitise rodent joint nociceptors, increasing both evoked and spontaneous firing. Proteomic analysis of the synovial fluid revealed a diverse protein composition including PAR4-cleaving serine proteases. Pretreatment with pepducin P4pal10 prevented the sensitising effects of arthritic synovial fluid suggesting that PAR4 cleaving proteases are, in part, responsible for the pain of arthritis.

In conclusion, MMT is a viable model of PTOA to study pain in male but not female rats. The reason for this discrepancy is due to joint neuropathy in males and a hyperactive endogenous opioid system in females. Furthermore, antagonist studies demonstrate that blockade of PAR4 represents a viable target for the treatment of OA pain.

List of Abbreviations and Symbols Used:

| | |
|--------------|--|
| ACL | Anterior cruciate ligament |
| ACPA | anti-citrullinated protein antibody |
| ACR | American College of Rheumatology |
| AMPA | α -amino-3-hydroxy-5-methyl-4-isoxazolepropionic acid |
| ANOVA | Analysis of variance |
| ARRIVE | Animal Research: Reporting of In Vivo Experiments |
| ASIC | Acid sensing ion channel |
| BDNF | Brain derived neurotrophic factor |
| CGRP | Calcitonin gene related peptide |
| COX | Cyclooxygenase |
| CRP | C-reactive protein |
| CTx | C-terminal telopeptides |
| DAMPs | Damage-associated molecular patterns |
| DMARDs | Disease-modifying-anti-rheumatic drugs |
| DRG | Dorsal root ganglia |
| ELISA | Enzyme Linked Immunosorbent Assay |
| EM | Electron microscopy |
| ESR | Erythrocyte sedimentation rate |
| EULAR | European League Against Rheumatism |
| FG | Fluoro-Gold |
| GAPDH | Glyceraldehyde-3-phosphate dehydrogenase |
| GFAP | Glial fibrillary acidic protein |
| NGS | Normal goat serum |
| GRKs | G protein receptor kinases |
| i.artic. | Intra-articular |
| ICAM | Intercellular adhesion molecule |
| IL-1 β | Interleukin-1 β |
| IL-10 | Interleukin-10 |

| | |
|------------------|---|
| IL-15 | Interleukin-15 |
| IL-17A | Interleukin-17A |
| IVM | Intravital microscopy |
| JAM | Junctional adhesion molecules |
| KOOS | Knee Injury and Osteoarthritis Outcome Score |
| LASCA | LAser Speckle Contrast Analysis |
| LC-MS | Liquid chromatography – Mass Spectrometry |
| LCL | Lateral collateral ligament |
| MCL | Medial collateral ligament |
| MHC | Major histocompatibility complex |
| MIA | Monoiodoacetate |
| MMPs | Matrix metalloproteases |
| MMT | Medial meniscal transection |
| MRI | Magnetic resonance imaging |
| NGF | Nerve growth factor |
| NMDA | N-methyl-D-aspartate |
| NSAIDs | Non-steroidal anti-inflammatory drugs |
| NTx | N-terminal telopeptides |
| OA | Osteoarthritis |
| OARSI | Osteoarthritis research society international |
| PAG | Periaqueductal grey |
| PAR | Protease activated receptor |
| PBS | Phosphate buffered saline |
| PCL | Posterior cruciate ligament |
| PECAM | Platelet endothelial cell adhesion molecule |
| PGE ₂ | Prostaglandin E2 |
| PKA | Protein kinase A |
| PKC | Protein kinase C |
| PTOA | Post-traumatic osteoarthritis |
| RA | Rheumatoid Arthritis |

| | |
|---------------|---|
| Rac1 | Ras-related C3 botulinum toxin substrate 1 |
| RF | Rheumatoid factor |
| RhoA | Ras homolog gene family, member A |
| RVM | Rostral ventromedial medulla |
| SEM | Standard error of the mean |
| SERPIN | Serine Protease INhibitor |
| SF | Synovial Fluid |
| SNL | Sciatic nerve ligation |
| STZ | Streptozotocin |
| TACAN | Transmembrane protein 120A |
| TNF- α | Tumor necrosis factor- α |
| tPA | Tissue plasminogen activator |
| trkA | Tropomyosin receptor kinase A |
| TRP | Transient receptor potential |
| TRPM8 | Transient receptor potential Melastatin-8 |
| TRPV1 | Transient receptor potential Vanilloid- 1 |
| uPA | Urokinase Plasminogen Activator |
| VCAM | Vascular cell adhesion molecule |
| VSGCs | Voltage-gated sodium channels |
| WOMAC | Western Ontario and McMaster Universities Arthritis Index |

Acknowledgments:

First and foremost, I would like to thank my supervisor Dr. Jason McDougall for his guidance and continued support over the past four years.

I would like to thank the members of the McDougall lab both past and present with whom I have had the pleasure of working. The assistance and advice of Allison Reid and Holly Philpott is especially appreciated.

I am also grateful to my advisory committee members, Drs. Robertson, Kelly, and Sawynok for their valued expertise.

I would also very much like to thank all of members of the Department of Pharmacology, including the administrative staff: Luisa Vaughn, Sandi Leaf, and Lori Lawson, and graduate student coordinators: Drs. Pasumarthi, Pelis, and Langille for creating a welcoming scientific environment.

Finally, I have to thank my family and friends for all of their support during my graduate studies.

Chapter 1: Introduction

1.1 Overview

Arthritis encompasses over 100 distinct conditions that affect the joints of the body and causes debilitating pain. The most prevalent form of arthritis is osteoarthritis (OA) which affects 9.6% of men and 18.0% of women worldwide and is ranked within the top 10 most disabling diseases in developed countries by the World Health Organization [1]. The most recent Global Burden of Diseases report (2016) estimates 302 million people globally live with OA representing a significant burden.

Despite the clinical need, there are no pharmacological therapies available to prevent, slow, or modify disease progression [2]. The only drug-based therapeutic approach available to people living with OA are analgesic medications; however, many have serious side-effects with long-term use. The advent of new therapies to treat OA effectively are sorely needed but require a better understanding of fundamental pain mechanisms.

The prevalence of OA is higher in women and women report greater pain and disability from the disease [3]. Despite this, the majority of preclinical studies have been carried out solely in male animals with little consideration being given to females. The first aim of this thesis was to compare the neurophysiological characteristics of OA pain in male versus female joints.

Serine proteases are a class of enzymes that are found within the arthritic joint and contribute to the catabolic destruction of joint tissue and to OA pain [4]. Promising preclinical and clinical data support blocking the activity of serine proteases as a way to

provide pain relief. A second aim of this thesis was to explore the role of protease signalling in OA pain.

1.2 Anatomy of the Human Knee Joint

The knee is the second largest joint in the human body and the most common lower-limb joint to be affected by OA. Functionally, the knees are essential to maintaining balance and locomotion [5]. In concert with the hip and ankle joints, movement of the knee allows for locomotory movements such as walking, climbing stairs, and bending. Under constant compression, the knee joint requires a tightly controlled musculoskeletal, nervous, and vascular systems to maintain joint health.

The knee is a synovial joint that is capable of extension and flexion and minimal rotation. It consists of three bones; the femur, tibia and patella, and five ligaments; the anterior cruciate ligament (ACL), the posterior cruciate ligament (PCL), the medial collateral ligament (MCL), the lateral collateral ligament (LCL), and the patellar ligament. The MCL and LCL provide stability to the hinge-like motion of the knee by preventing mediolateral translation of the joint, while the cruciate ligaments prevent anterior or posterior movement of the tibia relative to the femur [5]. The articular surfaces of the femur and tibia are covered in hyaline cartilage that acts to reduce mechanical forces applied to the bone and ensure near-frictionless movement. Additionally, two crescent-shaped fibrocartilaginous structures called menisci (medial and lateral) attached to the tibial plateau provide another joint stabilising mechanism to reduce and distribute forces over the surface of the tibia [6].

The entire joint is encased in an articular capsule with an outer fibrous layer and a thin inner membrane called the synovial membrane (or synovium). While the outer layer

provides protection, the synovium actively provides nourishment and clearance of unwanted mediators or cells from the joint space. Despite being just 1-3 cells thick, the cells of the synovial membrane (synoviocytes) produce and secrete synovial fluid that bathe the joint cavity as well as actively phagocytose cell debris and waste from the joint space [7]. Synovial fluid is composed of hyaluronic acid, lubricin, and plasma filtrate and acts as a lubricant and source of nutrients for avascular hyaline cartilage. In addition to providing nutrients, it also acts as a vehicle for the diffusion of biochemical molecules (eg: oxygen, growth factors, etc.). A healthy adult joint contains just four mL of synovial fluid and is subjected to sub-atmospheric pressures (-15 mmHg [8]). Increases in both synovial fluid volumes and intra-articular pressures are observed in arthritic conditions, though more dramatic changes are detected in RA rather than OA [9, 10]. Excess synovial fluid is commonly aspirated from diseased joint which can be used for diagnostic testing.

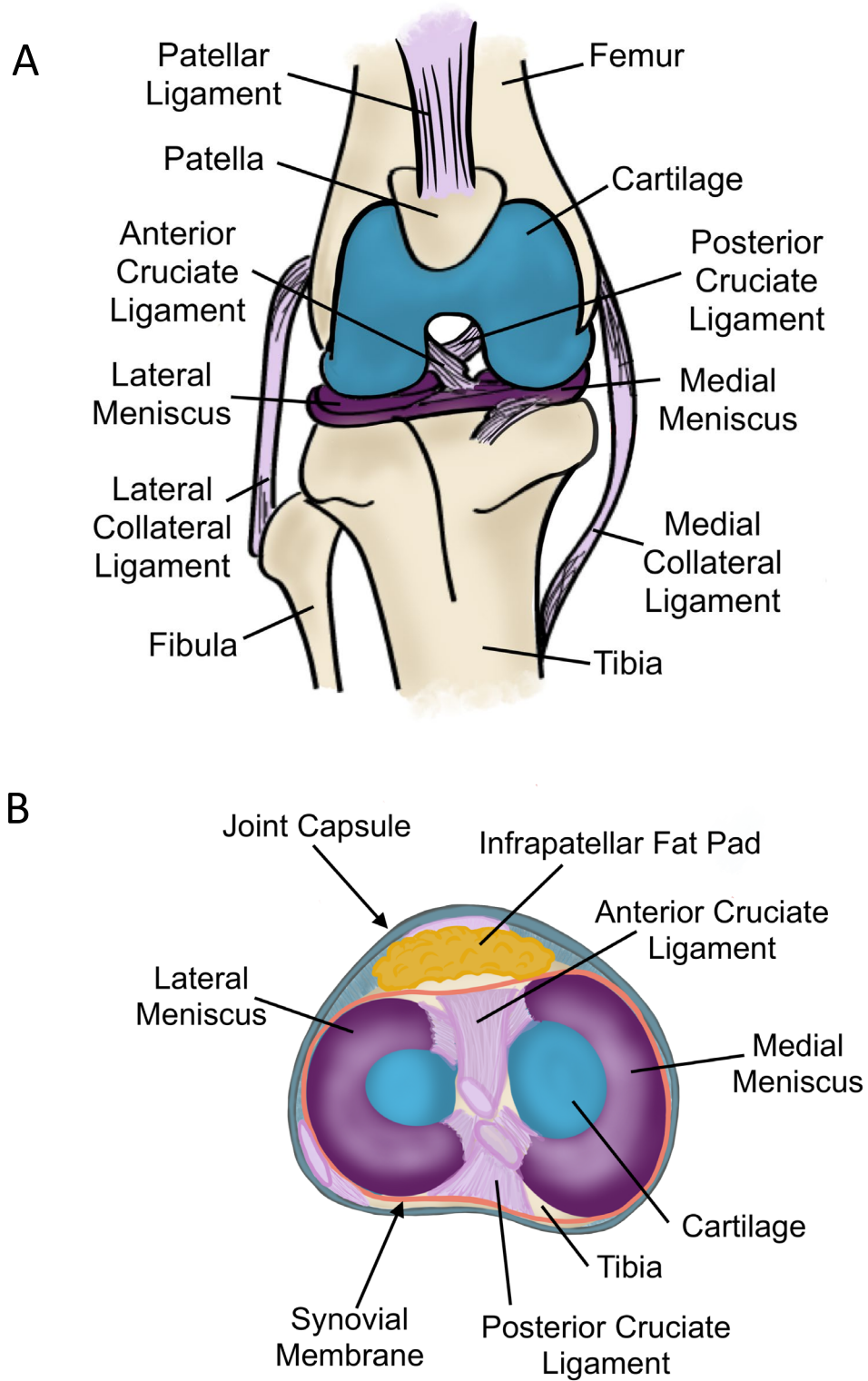


Figure 1. 1 Anatomy of the human knee joint.

Coronal view (A) and transverse view (B) of a human knee joint.

1.2.1 *Knee Joint Innervation*

The joint is a densely innervated organ, with nerves that sense position, regulate blood flow, and alert the brain to potentially harmful forces or movements. The major sources of sensory innervation come from branches of the sciatic and femoral nerves which include the saphenous, common peroneal, and tibial nerves [5]. Within these nerves are four types of sensory afferents (Table 1.1) that convey information about joint position, movement, and potential noxious information. $A\alpha$ fibres, the fastest and largest afferents, are found in ligaments and quickly send proprioceptive information to the CNS. Another type of proprioceptor, $A\beta$ fibres, are also found in the joint but are more widely distributed across multiple tissues including ligaments, tendons, the joint capsule, as well as axillary muscles. They also sense proprioceptive changes but are more receptive to changes in pressure and touch [11].

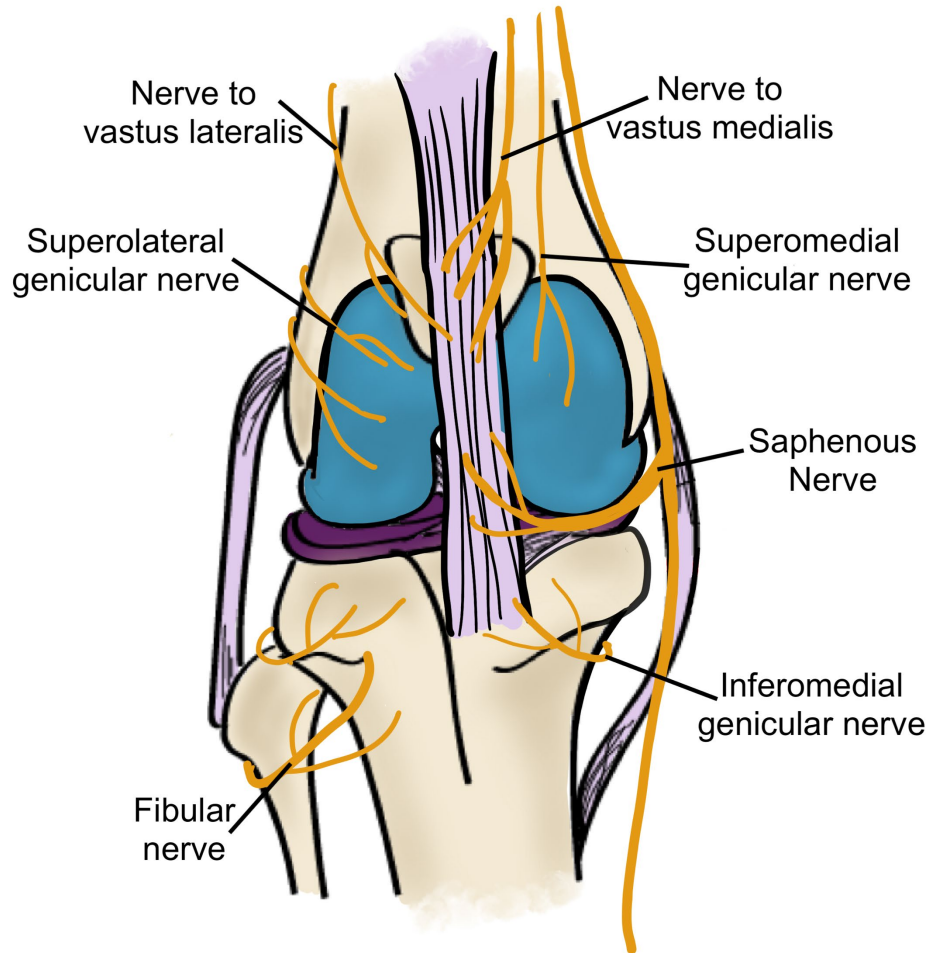




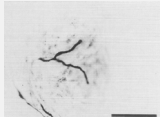
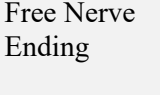
Figure 1. 2 Innervation of the human knee joint.

A simplified depiction of the innervation of the human knee joint. The joint capsule and synovium, which are highly innervated, were omitted for clarity.

Anatomical studies carried out in animals and humans have similarly discerned that nociceptors are the most abundant nerve type found within the joint; making up approximately 80% of all fibres [12, 13]. Two types of nociceptive fibres, A δ and C fibres, innervate all joint tissue with the exception of cartilage and the inner two-thirds of the menisci. A δ fibres are thinly myelinated, and many of these fibres exhibit high threshold to activation when recorded in animals, meaning that high forces were needed to elicit action potential generation [14]. Activation of these fibres are responsible for the

fast sharp pain following a sprain or injury. C-fibres also exhibit high thresholds but in contrast are unmyelinated and the slowest conducting of all afferents. While also transmitting nociceptive-information, a number of these C fibres are called ‘silent nociceptors’ because they don’t initially respond to stimulation. In experimental conditions, these fibres only respond to mechanical stimuli once an inflammatory insult has been introduced [15]. Activation of C fibres elicits the *delayed* dull pain that follows a noxious stimulus.

In addition to afferents, the joint is innervated by sympathetic efferents that terminate near joint blood vessels [16]. Of particular importance to maintaining joint health, blood flow within the organ is not autoregulated, and thus vasoregulation lies entirely upon nervous control [17]. However, in addition to sympathetic control, free endings of nociceptive A δ and C-fibres also release vasoactive peptides such as substance P, calcitonin gene-related peptide (CGRP), and endomorphin-1[18-22].

| Fibre Subtype | Ending Type | Myelinated | Diameter | Conduction Velocity | Function | Location |
|-------------------------|--|------------|-------------------|---------------------|-------------------------------|--|
| Sympathetic | | No | 0.4 - 2.4 μ m | 1 m/s | Vasoregulation Nociception | Near Blood Vessels |
| Class I (A α) | Golgi  | Yes | 10 – 18 μ m | 60 – 100 m/s | Proprioception | Ligaments |
| Class II (A β) | Ruffini:  | Yes | 5 – 13 μ m | 20 – 70 m/s | Proprioception | Ligaments Joint Capsule Muscles |
| | Pacinian:  | | | | | |
| Class III (A δ) | Free Nerve Ending  | Thinly | 1 – 5 μ m | 2.5 – 20 m/s | Nociception | Joint Capsule Synovium |



| | | | | | | |
|-----------------|---|----|------------------|-----------|-------------------------------|--|
| Class IV (C) |  | No | <1 μm | < 2.5 m/s | Nociception Vasoregulation | Subchondral Bone Meniscus Ligaments Infrapatellar Fat-Pad |
| |  | | | | | Joint Capsule Synovium Subchondral Bone Meniscus Ligaments Infrapatellar Fat-Pad |

Table 1. 1: Afferent and efferent innervation of the human knee joint.

Summary of the type of afferent and efferent nerve fibres identified in the human knee joint classified by: the type of fibre ending, myelination, diameter, conduction velocity, role in the joint, and location of innervation. Adapted from [23].

1.2.2 Vascular Supply of the Human Knee Joint

To sustain healthy joint tissue and repair potential trauma, a regulated vascular supply is critical. Bone, ligaments, synovium and the outer third of the menisci are vascularised to varying degrees. Joint tissue that lacks blood supply are cartilage and the inner two-thirds of the menisci; these tissues rely on either contact with synovial fluid or vascular rich synovial membrane for nutrients [5].

Blood supply to the knee originates from branches of the femoral artery that form a rich network around the joint. On the medial side of the femur, the femoral artery bifurcates into the descending genicular artery which passes anteriorly and the popliteal artery which follows posteriorly. The descending genicular artery further branches into the saphenous artery which feeds the anteromedial portion of the knee, and five additional genicular branches which collectively supply the femoral condyles, synovium, menisci, and articular ligaments [5].

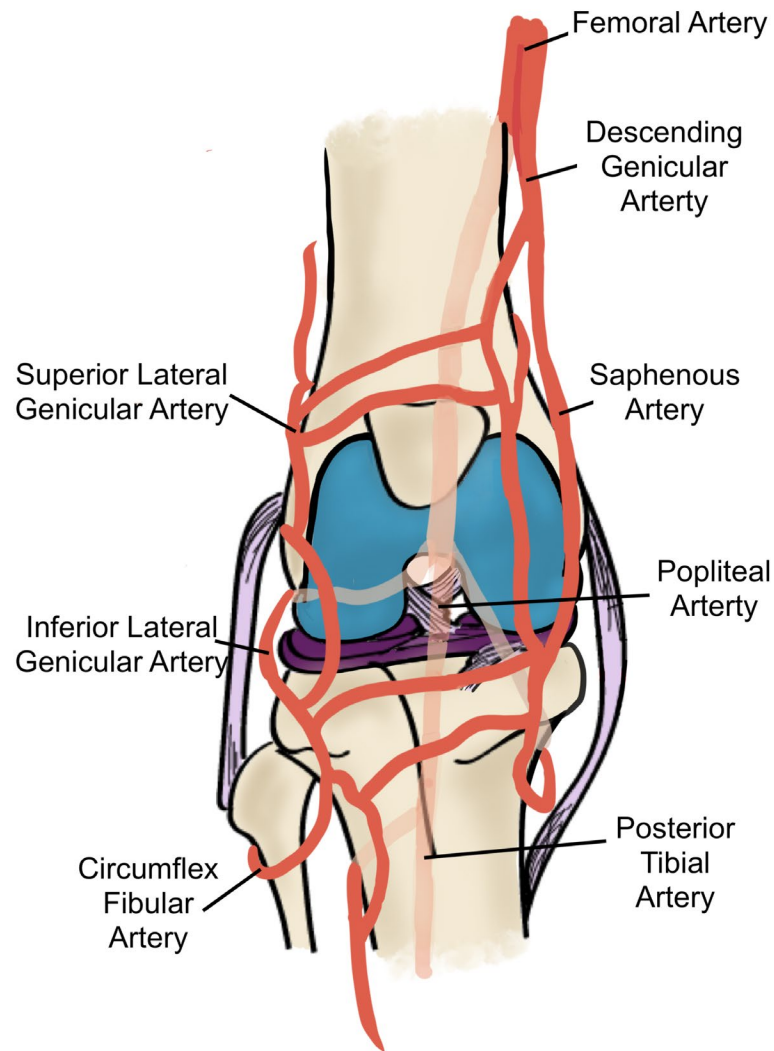


Figure 1. 3 Vasculature of the human knee joint.

A simplified depiction of the vascularisation of the human knee joint. The joint capsule and synovium, which are highly vascularised, were omitted for clarity.

1.3 Arthritis

Arthritis is an umbrella term that covers over 100 different conditions and affects 1 in 5 Canadians [24]. Depending on the type of arthritis it may affect only one joint, multiple joints, the tissues that surround the joint, or it may be a systemic condition. One

defining feature of all joint conditions, however, is pain. The two most common forms of arthritis are OA and rheumatoid arthritis (RA).

1.3.1 Osteoarthritis

Osteoarthritis had long been defined as simply a degenerative disorder, resulting from ‘wear and tear’ on joints and as a natural part of aging; however, OA is now defined as a disease of moveable joints that is initiated by micro- or macro- injuries that activate a maladaptive repair response within the joint [25]. All joint tissues are affected, resulting in cartilage degeneration, bone remodeling, synovial inflammation, meniscal damage, osteophyte formation, and neural reorganisation. These joint changes lead to pain, stiffness, loss of normal joint function, and increase the likelihood of developing a comorbidity [26].

The joints most commonly affected by OA are the weight bearing knee and hip joints as well as the joints of the hand. Upon presentation to the clinic, knee OA is diagnosed upon physical examination, patient history, and if necessary, radiographic and laboratory testing [27]. Several different organisations have developed diagnostic criteria for OA including the American College of Rheumatology (ACR) and the European League Against Rheumatism (EULAR) [27, 28]. According to the ACR guidelines, in addition to knee pain, the patient must present with at least 3 of the following: age > 50 years, morning stiffness < 30 minutes, crepitus, bony tenderness, bony enlargement, and/or no palpable warmth. Fewer criteria are needed if radiographs are taken; however, both the ACR and EULAR stress the possibility that plain radiographs may not detect early OA [28]. Laboratory testing is used when the need to exclude RA is necessary. This includes serum measurements of rheumatoid factor (RF) and erythrocyte sedimentation

rates (ESR) and synovial fluid aspiration for assessment of physical appearance and white blood cell count.

| American College of Rheumatology Diagnostic Criteria for Osteoarthritis | | |
|---|--|---|
| Clinical | Clinical & Radiographic | Clinical & Laboratory |
| Knee pain + at least 3 others: <ul style="list-style-type: none"> - Age >50 years - Stiffness < 30 mins - Crepitus - Bony Tenderness - Bony Enlargement - No Palpable Warmth | Knee pain + at least 1 other: <ul style="list-style-type: none"> - Age >50 years - Stiffness < 30 mins - Crepitus - Osteophytes | Knee pain + at least 5 others: <ul style="list-style-type: none"> - Age >50 years - Stiffness < 30 mins - Crepitus - Bony Tenderness - Bony Enlargement - No Palpable Warmth - ESR < 40 mm/hour - RF < 1:40 - SF OA |

Table 1. 2: The American College of Rheumatology Guidelines for knee OA diagnosis.

The ACR guidelines, developed in 1986, for clinical, clinical and radiographic, and clinical and laboratory determination of OA. ESR = erythrocyte sedimentation rate, RF = rheumatoid factor, SF OA = synovial fluid signs in OA (clear, viscous, or white blood cell count < 2000/mm³). [27]

1.3.1.1 Aetiology of Osteoarthritis

Risk factors that contribute to the development of OA include age, sex, obesity, joint trauma, and genetics [29]. The effects of age are multifactorial. For example, the loss of chondrocytes and changes in the make-up of the extracellular matrix (ECM) weaken the cartilage, loss of proprioceptors impair joint biomechanics, and an increase in senescent cells increase joint inflammation [30-32]. These age-related changes to joint structures prime the organ to increase the susceptibility and the progression of OA. Traumatic joint injury also substantially increases the risk of developing OA with 12% of all knee OA cases estimated to be post-traumatic osteoarthritis (PTOA) [33]. Both ACL and meniscal injuries carry a high risk of PTOA development due to altered joint biomechanics and joint instability [34]. In patients with isolated ACL injuries, 13% go on to develop PTOA while those with a combined ACL and meniscal injury, 48% develop PTOA within 10 years [35]. While joint reconstruction aims to repair the damaged tissue and joint function, PTOA is still high in patients that undergo surgical intervention [36]. Obesity (BMI > 30 kg/m²) is strongly associated with OA of the knee and hip; however, the fact that hands can develop OA suggests that the disease is not only a consequence of heightened weight-bearing [37]. Levels of the adipokine leptin are elevated in obesity and are also elevated in OA joints. In synovial fluid, leptin has been found to have catabolic effects on cartilage and subchondral bone [38], corroborating a metabolic association with OA. Genetics can play a role in OA development where individuals born with joint malalignment have abnormal joint biomechanics which could lead to premature tissue degradation. Genetic mutations have also been identified, particularly in genes that encode for type II collagen and interleukins which have both been linked to an increased susceptibility to OA [39-43]. Women also have an increased risk of developing OA. Due

to an increased incidence around menopause, several studies explored the role that sex-hormones may be playing in OA; however, the results were largely conflicting [44-46]. There are several anatomical differences between men and women that may predispose women to joint damage. These include: decreased cartilage thickness, femur width, quadriceps angle, and differences in tibial chondylar size [47].

1.3.1.2 Pathophysiology of Osteoarthritis

Osteoarthritis begins with a rapid reorganisation of joint architecture that sets in motion a gradual, progressive decline in joint structure. Due to the heterogeneous nature of OA, the initiating event can differ greatly depending on the individual. For example, in a professional athlete, years of repetitive micro and macro- injuries may culminate in not only altering the biomechanics of the joint but also permanently weakening the cartilage. In contrast, in an aged joint, a gradual loss of cartilage and proprioceptors, hardening of subchondral bone, and a state of protracted inflammation has the potential to prime the joint for injury. Regardless of the initiating factor, however, the osteoarthritic joint fails to balance anabolic and catabolic mediators successfully, ultimately leading to joint destruction.

The pathophysiology of OA during early and late stages of the diseases are distinct. One of the earliest detected features of OA is an increase in bone remodeling, which results in a thinned subchondral plate [48]. Elevated levels of bone resorption markers, such as the C-terminal and N-terminal telopeptides CTx and NTx, are found in the joints of individuals with early as well as progressive OA [49, 50]. Since cartilage and bone are

both structurally linked, changes to the composition of either tissue can affect the mechanical properties of the other. Hence, a seven-fold increase in cartilage loss is found in areas where there is also bone attrition [51]. Under changing tensile loading in OA joints, the water content of articular cartilage increases leading to a reduction in the tensile properties of the tissue. The resulting swollen cartilage is less able to deform under load rendering the joint more susceptible to damage [52]. Other metabolic changes have been detected in cartilage with alterations in proteoglycan synthesis noted during OA even before major fibrillation is observed [53]. Concurrently in this early phase, an amplification of catabolic activity occurs, where elevated levels of metalloproteases (MMPs) degrade cartilage (eg, MMP-9 and MMP-3) [54] and cleaved cartilage fragments can trigger local inflammatory responses in the nearby synovium [55].

Inflammation of the synovium, called synovitis, plays a key role in the pathogenesis of early OA and subsequent disease progression. Magnetic resonance imaging (MRI) studies have demonstrated synovitis during the early stages of OA [56-58]. When a small cohort of early OA patients were followed for 4-years, MRI consistently detected synovial thickening in 73% of patients, reasoning that joint inflammation persisted throughout early stages of the disease [56]. Larger longitudinal imaging studies have found that the presence of synovitis in early OA correlates with patient reported pain, and also is predictive of disease progression [58-60]. Histopathology of synovial tissue from early OA patients reveals hyperplasia, increased mononuclear cell infiltration and angiogenesis [61]. Overexpression of metallo- and serine proteases and proinflammatory cytokines such as interleukin-1 β (IL-1 β), interleukin-15 (IL-15), and tumor necrosis factor- α (TNF- α) in early OA synovial tissue have also been reported [61-65]. These

inflammatory mediators have been found to potentiate cartilage destruction and are also capable of sensitizing nociceptors to generate pain [66-69].

Once initiated, the osteoarthritic joint continues to degrade. As cartilage and bone architecture change, abnormal mechanical stresses lead to further production of cytokines, including IL-6, and proteases (MMP-1 and MMP-3) by chondrocytes and the process of OA becomes self-perpetuating [70]. End-stage OA is characterised by complete cartilage degeneration, severe meniscal damage, development of subchondral bone sclerosis and lesions, intermittent synovitis, and nerve damage in a subset of patients. While synovitis has been examined at end-stage disease, the literature is conflicting. Imaging and histological studies have both reported widespread inflammation as well as minute synovitis compared to early disease stages [61]. This may represent heterogeneity within the OA population or may suggest synovitis flares rather than chronic synovitis are more common at end-stage disease. Abnormal nerve morphology has been detected in severe OA joints of humans and in animals following joint injury [71, 72]. In patients, increased sensory innervation in the meniscus was observed in late-onset disease compared with early [71], and in rabbits, following an ACL injury, small-diameter fibres rich in pain-producing neuropeptides also increased in density and became contorted [72]. These data support the finding that approximately 23% of OA patients experience neuropathic-like pain caused by sensory nerve damage [73].

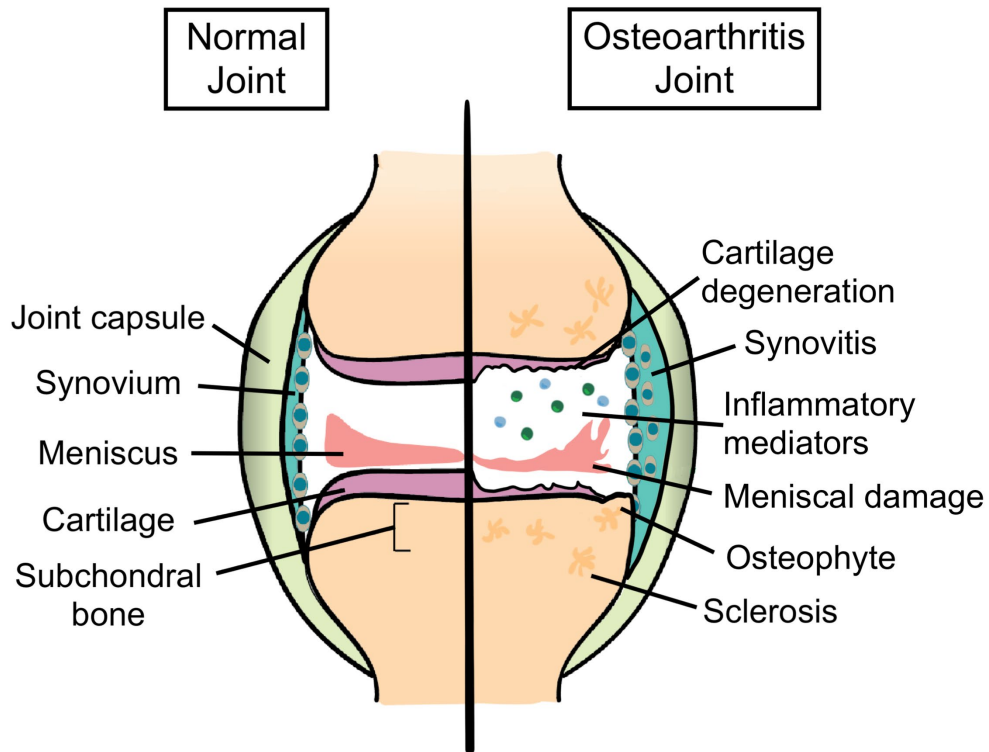


Figure 1. 4 Comparison of normal and osteoarthritic knee.

Depiction of a normal and osteoarthritic knee joint. While the normal joint has smooth cartilage, an intact meniscus, clear synovial fluid, a thin synovium, and undamaged subchondral bone, the OA joint shows many signs of destruction. The arthritic joint has degenerated cartilage and meniscus, synovitis, inflammatory mediators within the joint space, and the bone is badly damaged with osteophytes and subchondral sclerosis.

1.3.1.3 Current treatments in Osteoarthritis

No disease-modifying agents are available for osteoarthritis and thus analgesics and non-pharmacological interventions to manage pain are the only outlet for patients [2]. It is recognised that people that live with osteoarthritis do so for decades and often are treated with many different pharmacological agents during this time. It is also noted that many of these treatments have deleterious side-effects with long-term use which makes treating OA pain increasing difficult [74]. In 2010, the Osteoarthritis Research Society

International (OARSI) developed guidelines for the non-surgical management of knee OA with a group of experts from thirteen countries [2]. In addition to the quality of evidence, and estimated effect sizes for a given treatment, they paid particular attention to potential patient co-morbidities, and side effect profiles. For the treatment of knee OA without co-morbidity, non-pharmacological interventions included: water-based exercise, weight management, and moderate land-based exercise. Pharmacological treatments that were recommended by the OARSI guidelines and are considered first-line are oral and topical non-steroidal anti-inflammatory drugs (NSAIDs) and acetaminophen which provide relief of mild to moderate pain. NSAIDs provide analgesia by blocking cyclooxygenase (COX) and preventing the production of prostaglandin and thromboxane synthesis. Agents that block both COX-1 and COX-2 isoforms, such as ibuprofen, are associated with stomach ulcers, liver damage, and cardiovascular events with long term use. Selective COX-2 agents such as celecoxib, provide a similar amount of pain relief but less GI side effects. Topical NSAIDs reduce the risk of serious adverse events and are better tolerated by patients because the systemic levels of drugs are reduced. Other topical options include capsaicin which acts on TRPV1 to deplete nociceptors of algogenic neuropeptides; however, this effect is short lived and may cause skin irritation [75].

For moderate to severe pain, a limited number of therapeutics are effective. Intraarticular injection of corticosteroids are a potent anti-inflammatory that are recommended for moderate to severe pain but their effect is short lived and administration comes with potential harm [76]. Long term use has recently been found to

correlate with cartilage degeneration and thus its therapeutic use is precarious [77, 78]. For end-stage OA patients with neuropathic-pain like symptoms, a serotonin-norepinephrine reuptake inhibitor such as duloxetine may be prescribed [2, 74]. Severe pain that is refractory to first line-treatment may be treated with an opioid such as tramadol. Both classes of drugs are potent analgesics but are contraindicated in geriatric patients, limiting their potential usefulness in this population [2].

An emerging new therapy for OA pain is monoclonal antibodies directed against nerve growth factor (anti-NGF). Tanezumab and fasinumab have demonstrated clinical efficacy against OA pain compared to placebo but excitement for the new therapeutics has been tempered by a particularly negative side-effect of progressive joint degeneration [79-82]. After initial successful phase III trials, it was discovered that patients that received tanezumab were also regularly taking NSAIDs and the combination was associated with atrophy [83]. New clinical trials that excluded the concomitant use of NSAIDs while administering low doses of tanezumab or fasinumab, have improved the safety profile of the drugs [81, 82].

1.3.2 Rheumatoid Arthritis

Rheumatoid arthritis is a chronic inflammatory autoimmune disorder that primarily affects joints but also causes systemic manifestations in the skin, eyes, and heart [84]. Global estimates suggest that RA affects approximately 1% of the population (WHO), where it is associated with severe disability and premature mortality [1]. The hallmarks of RA are joint synovitis and degeneration, extra-articular nodules, and systemic inflammation that can be measured using serology. RA affects both large (knee, hip,

shoulder, elbow) and small (metacarpophalangeal, second through fifth metatarsophalangeal, wrist) joints in a symmetrical pattern [84].

Clinically, RA is associated with the presence of autoantibodies such as rheumatoid factor (RF) and anti-citrullinated protein antibody (ACPA) years prior to the onset of disease symptoms but unfortunately these often go undetected [84, 85]. Patients also often have elevated systemic inflammatory markers such as C-reactive protein. ACR and EULAR devised new guidelines in 2010 for the classification of RA (Table 1.3). Upon presentation, the patient must have one or more swollen joints that cannot be explained by another cause (eg: OA, gout). They are assessed for the presence of autoantibodies and acute inflammatory markers using serology and evaluated based on the duration of their symptoms to compile a score. A minimum score of 6 is required for a probable RA classification [85]. Early treatment with disease modifying agents are critical to control the progression of the disease [86].

| American College of Rheumatology / European League Against Rheumatism - Classification criteria for rheumatoid arthritis | |
|---|-------|
| Criterion | Score |
| Joint involvement | |
| 1 large joint | 0 |
| 2-10 large joints | 1 |
| 1-3 small joints (with or without involvement of large joints) | 2 |
| 4-10 small joints (with or without involvement of large joints) | 3 |
| 10 joints (at least 1 small joint) | 5 |
| Serology (at least 1 test result is needed for classification) | |
| Negative RF <i>and</i> negative ACPA | 0 |
| Low-positive RF <i>or</i> low-positive ACPA | 2 |
| High-positive RF <i>or</i> high-positive ACPA | 3 |
| Acute-phase reactants (at least 1 test result is needed for classification) | |
| Normal CRP <i>and</i> normal ESR | 0 |
| Abnormal CRP <i>or</i> abnormal ESR | 1 |
| Duration of symptoms | |
| <6 weeks | 0 |
| ≥6 weeks | 1 |

Table 1. 3: Classification criteria for rheumatoid arthritis.

The ACR and EULAR 2010 classification criteria for probable RA. RF = rheumatoid factor, ACPA = anti-citrullinated protein antibody, ESR = erythrocyte sedimentation rate, CRP = C-reactive protein. (Adapted from [85])

1.3.2.1 Aetiology of Rheumatoid Arthritis

The cause of RA is unknown but genetic factors and environmental triggers are thought to play a large role in disease susceptibility. Genetic studies have demonstrated through familial and genome-wide approaches, that over 100 loci are associated with RA [87, 88]. Many of these are genes encoding major histocompatibility complex (MHC) molecules and post-translational modification enzymes – having downstream effects on immune activation. Environmental triggers associated with RA include smoking, and other forms of bronchial stress such as inhaling silica dust [89].

Additionally, a sex-difference also exists in RA where women are three times more likely to develop the disease than men [90].

1.3.2.2 Pathophysiology of Rheumatoid Arthritis

The pre-rheumatoid phase is characterised by an increase in the generation of autoantibodies against post-translationally modified proteins, including those with citrulline residues [84]. Antibodies develop against multiple proteins found in the joint, including fibronectin, fibrinogen, and collagen. It is unknown what the initial precipitating factor for joint inflammation is; whether it is an immune response to these proteins, or potentially an aberrant immune response to joint micro-trauma. Regardless of the initiating factor, the outcome is an infiltration of adaptive and innate immune cells that mediate synovial hyperaemia, pannus formation, and bone destruction and pain.

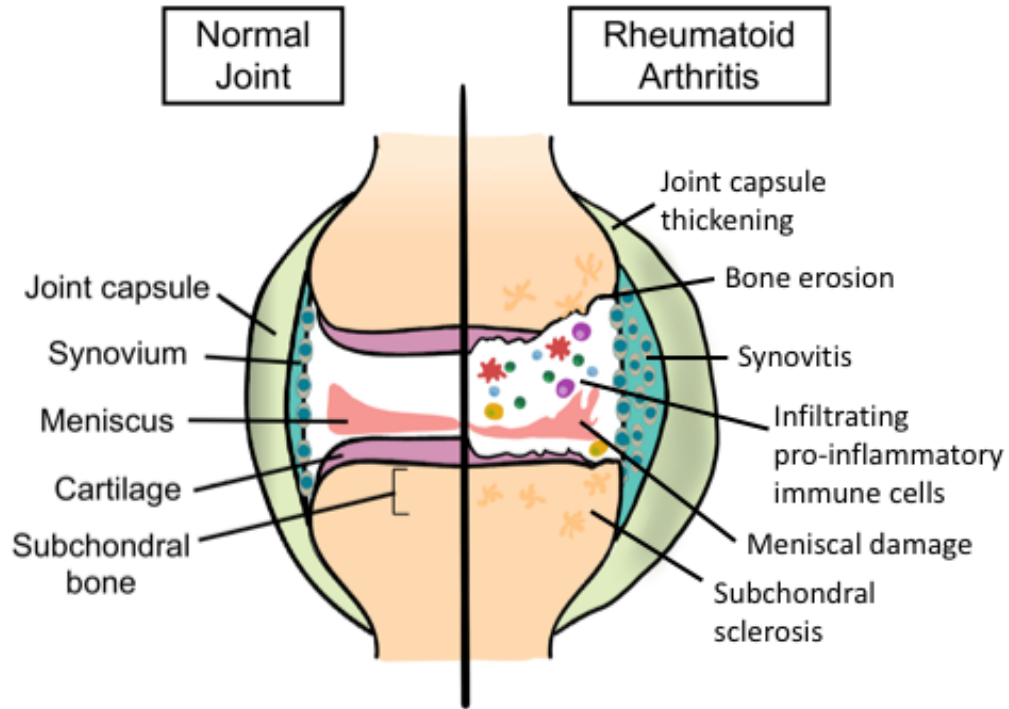


Figure 1. 5 Comparison of normal knee and rheumatoid arthritis knee joint.

Depiction of a normal and RA knee joint where the arthritic joint has joint capsule thickening as well as pronounced synovitis with synovial cell proliferation. The RA joint is also infiltrated by immune cells and pro-inflammatory mediators that contribute to the destruction of cartilage, meniscus, and vast bone remodeling. Ultimately, erosion and sclerosis of subchondral bone is widespread in the joint.

1.3.2.3 Current Treatments in Rheumatoid Arthritis

Unlike OA, RA treatments include therapeutics that can modify the progression of the disease (but not cure it). The two main classes of drugs used for RA patients are disease-modifying-anti-rheumatic drugs (DMARDs) and biologics [86]. DMARDs, such as methotrexate, have been the mainstay of RA treatment since the 1950s. They are considered a frontline therapy for RA patients [86]. As inflammatory mediators became more strongly implicated in disease pathogenesis, biological agents targeted towards these molecules emerged as new drugs. Today, several monoclonal antibodies against

TNF- α or its receptor (adalimumab, certolizumab pegol, etanercept, golimumab, or infliximab), the IL-6 receptor (tocilizumab), B-cells (rituximab), T-cells (abatacept), and janus kinases (JAK) (tofacitinib, baricitinib, and upadacitinib) are available. These biologic therapies can be combined with methotrexate as disease severity increases to moderate or severe or if the patient doesn't respond to methotrexate therapy alone. Additionally, intraarticular corticosteroid injections are also used to control inflammatory flares but do not have the disease-modifying capabilities that other agents do.

1.3.3 Preclinical Models of Osteoarthritis

In vivo preclinical models of OA have been employed to recapitulate aspects of the disease. Use of these models has contributed to greater understanding of disease pathophysiology and successfully identified new therapeutic targets which have subsequently been tested in clinical trials.

Preclinical models of OA are often categorised as 'spontaneous', 'surgical', or 'chemical' models [91]. Animals that naturally develop joint degeneration consistent with OA include mice, rabbits, guinea pigs, dogs, sheep, and horses. The study of the joints in these animals as they age provide a spontaneous model that mimics the human condition. Both surgical and chemical models offer rapid onset of joint damage and mimic OA-related pain and were utilised in this thesis.

1.3.3.1 The Medial Meniscal Transection (MMT) Model of Post-Traumatic Osteoarthritis

The MMT model of PTOA is a surgical model that involves destabilising the joint by transecting both the MCL as well as the medial meniscus. The result is a progressive mild to moderate OA – causing mild proteoglycan loss as early as 1 week following surgery, and full thickness cartilage degeneration and mild sclerosis on the medial tibial plateau by 3-4 weeks [92-94]. Most studies have found the presence of joint inflammation is mild in this model, with low synovitis scores denoting minor mononuclear cell infiltration and negligible synovial hyperplasia [94, 95]. One study stands out in contrast, however, Mapp *et al*, assessed synovial inflammation in the MMT model by measuring the thickness of the synovium and further quantified vascular density weekly following surgery. The data suggest a significant increase in synovial lining thickness and cellularity 7 days following induction that's maintained until day 28 [93]. The disparity in these results may have to do with the method of induction in the model as the authors cauterized and removed the connective tissue and muscle surrounding the joint which would induce more trauma and instability. Relatively few studies have assessed pain behaviour in this model but those that have used male animals exclusively [94, 96]. Animals exhibit mild weight bearing deficits and heightened mechanical sensitivity by 3-days post-surgery [94, 96]. Attenuation of pain behaviour with the neuropathic analgesic gabapentin, but not a COX-2 specific inhibitor, rofecoxib, suggest a centrally-mediated mechanism to pain in this model [94]. Further mechanistic work is needed to elucidate the pain mechanism in this model as have been carried out other models of OA.

1.3.3.2 The Monoiodoacetate (MIA) Model of Osteoarthritis

The moniodocetate (MIA) model is a commonly used chemical model that results in rapid joint damage and measurable pain behaviour [97]. The chemical MIA is injected into the knee joint where it inhibits glyceraldehyde-3-phosphate dehydrogenase (GAPDH), a key enzyme in the glycolysis pathway [98]. In the presence of MIA, chondrocytes are no longer able to produce adequate energy, and they die [99]. The model is biphasic in nature. Within the first few days of the model there is an initial inflammatory flare with increased levels of joint cytokines, including IL-6 and TNF- α , and local immune cell infiltration, including macrophages, neutrophils, and mast cells [97, 100]. This coincides with measurable pain responses [101]. By days 5-7, the inflammation subsides, and pain responses diminish. At day 14, moderate to severe cartilage degeneration is present as well as subchondral bone loss and peripheral nerve damage [101]. At this timepoint animal pain behaviour increases again. Criticism of the model includes that aspects of the joint damage are not consistent with human OA; however, this model does recapitulate inflammatory flares and neuropathic elements of the disease that contribute to OA pain.

1.4 Pain in Arthritis

Pain is the foremost concern of people living with arthritis and the number one reason for visiting their primary physician. One community-based study estimated patient dissatisfaction with analgesics at an alarming 60% [102]. This dissatisfaction exists, in part, because of poorly managed pain and undesirable side effects of prescribed drugs. An incomplete understanding of pain mechanisms in OA and the use of analgesics that are not targeted toward the disease may contribute to the lack of efficacy reported by patients. Heterogeneity within the patient population poses an additional hurdle for treating OA pain as different pain phenotypes require individualised treatment.

1.4.1 *The Pain Pathway*

Pain is defined as “an unpleasant sensory and emotional experience associated with, or resembling that associated with, actual or potential tissue damage” [103]. It is influenced to varying degrees by an individual’s biology, but also physiological and sociological factors.

The joint is heavily innervated by myelinated A δ and unmyelinated C-nociceptive fibres that are silent until activated by a noxious stimulus [14, 15]. Most nociceptors are polymodal and respond to more than one type of noxious stimulus which is either mechanical (eg: pin-prick, abnormal joint rotation), chemical (eg: H⁺, NGF), or thermal (temperatures < 15°C and > 42°C) [104]. Free nerve endings on these pseudounipolar cells are equipped with mechano-, chemo-, and thermo-receptors – capable of transducing potentially harmful stimuli into electrical impulses. Thermal and chemical receptors are well known to researchers, with members of the transient receptor potential (TRP) family of receptors detecting noxious temperature, and multiple receptor types implicated in the detection of chemical danger (eg: acid sensing ion channel (ASICs), tropomyosin receptor kinase A (TrkA)). Nociceptive mechanoreceptors remained elusive until recent years; while candidate genes had been identified in bacteria no eukaryote homologs had been identified until recently. However, two mechanosensitive ion channels have now been identified in nociceptors; Peizo2 and transmembrane protein 120A (TACAN), sparking excitement for new understanding of this pathway [105-108]. Following a noxious stimulus, activation of a specialised receptor causes local depolarization of the axon membrane leading to the generation of a

receptor potential [109]. This depolarization spreads to the spike trigger zone, an area enriched with voltage-gated sodium channels, and if large enough to pass the threshold, an action potential is generated. The electrical signal is transmitted from the site of actual or potential damage along axons through the dorsal root ganglion and centrally into the dorsal horn of the spinal cord. A δ fibres synapse onto projection neurones or interneurones in lamina I and V of the dorsal horn while C fibres primarily terminate in lamina II [110]. Projection neurones cross the spinal cord and propagate pain signals via either the spinothalamic tract to the thalamus or along the spinoreticular tract to the brainstem [110]. Multiple areas of the brain are involved in the sensory-discrimination and affective-cognitive encoding of pain signals, they include the somatosensory and anterior cingulate cortices and the amygdala.

Importantly, pain input is prioritized along with other homeostatic and physiological demands [111] and can be modulated by descending inhibitory and facilitatory pathways. Originating in somatosensory and limbic cortices, these descending pathways project through the periaqueductal grey (PAG) and the rostral ventromedial medulla (RVM) before reaching dorsal horn interneurons. Whether or not peripheral nociceptive signals are amplified or diminished is dependent upon the descending pain-control system which is largely controlled by serotonergic, noradrenergic, and GABAergic neurones [110].

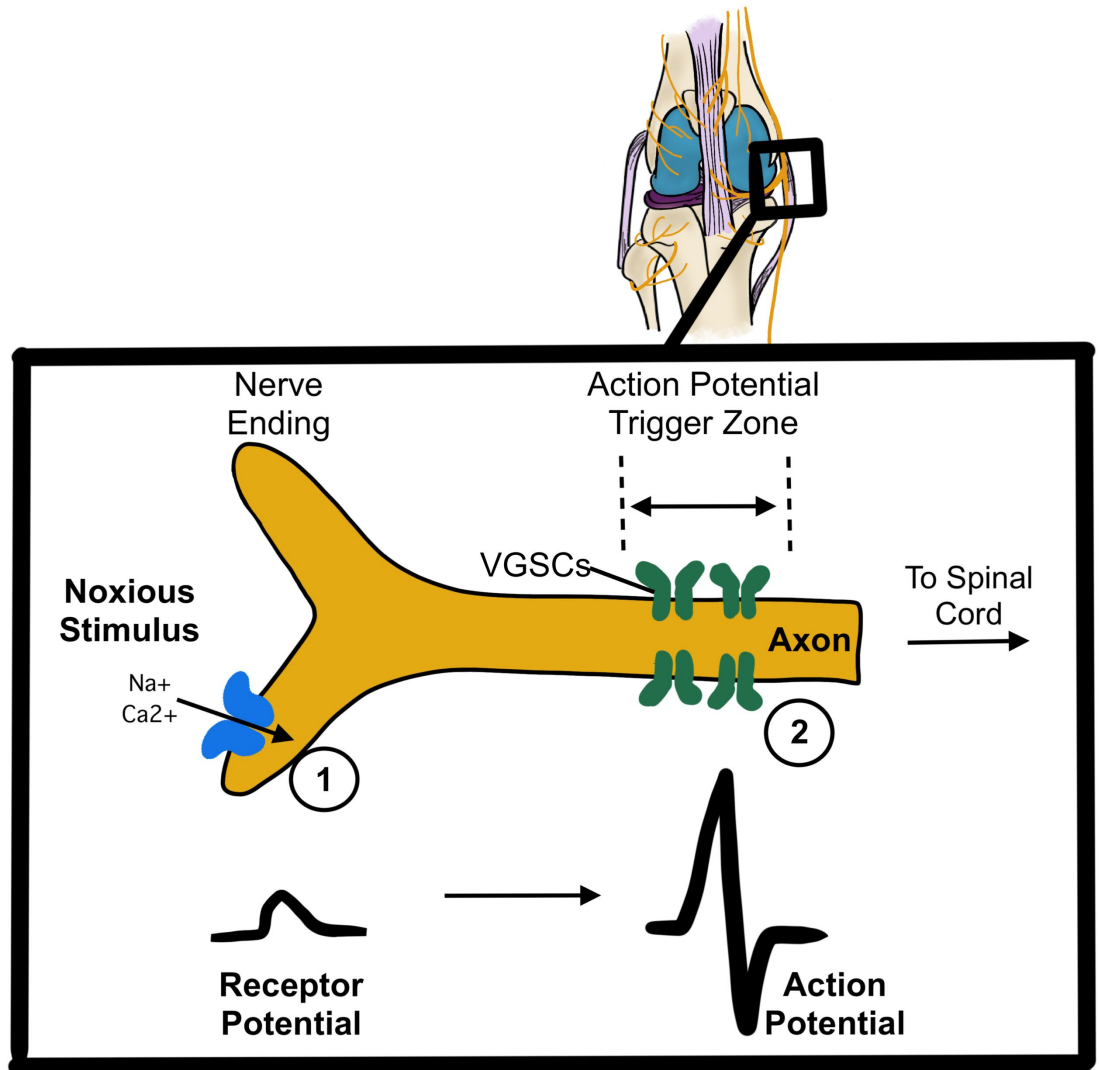


Figure 1. 6 Action potential generation in sensory neuron.

Simplified depiction of an action potential generated in a nociceptor. (1) receptor responds to noxious stimulus by allowing the entry of sodium and calcium ions, and the generation of a receptor potential. The receptor potential moves along the nerve ending until it reaches the action potential trigger zone (2) that is densely occupied by voltage-gated sodium channels (VSGCs). If the potential is amplified enough to reach the threshold to fire, an action potential will move along the axon towards the spinal cord.

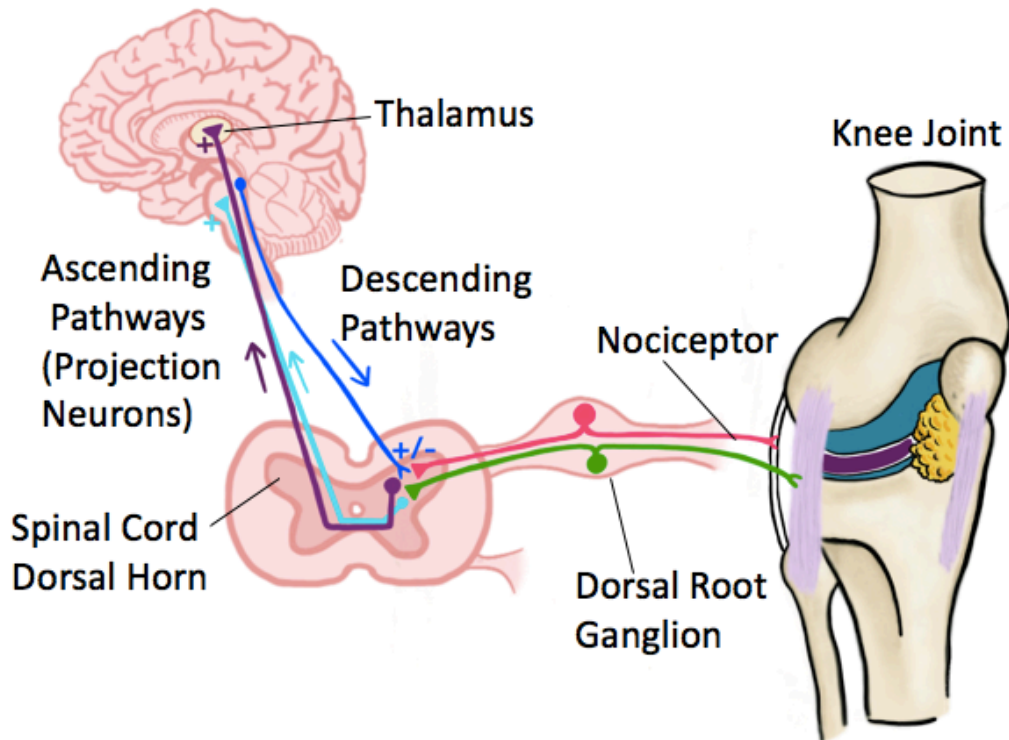


Figure 1. 7 The pain pathway.

Simplified pain pathway highlighting a nociceptor innervating the knee joint. The cell body of joint afferent resides in the dorsal root ganglia and it desiccates in the dorsal horn of the spinal cord. Here the primary afferent synapse with either projection neurons or inter neurons that project nociceptive information to the brainstem or thalamus via the spinothalamic tract or spinoreticular tract. Other sensory, affective, and cognitive brain centers are involved in sensory discrimination and emotional responses to nociceptive input but were omitted for clarity. Spinal dorsal horn neurones also receive descending inhibitory and facilitatory input.

In addition to sensing noxious stimuli in an acute setting, nociceptors are also highly plastic and have been implicated in driving pathological pain conditions [112]. Allodynia, defined as pain sensation in response to a stimulus that normally does not evoke a painful response, and hyperalgesia, which is increased pain from a normally painful stimuli are two common pain states. Two neuronal mechanisms represent the underpinnings of these phenomena: peripheral sensitisation and central sensitisation.

Using electrophysiology to measure the activity of nociceptors, it has been shown that following tissue injury or inflammation, a decrease in the activation threshold and increase in the responsiveness of nociceptors occurs following a stimulus at the site of injury [113]. This means that following injury: (1) less stimuli are needed to transmit nociceptive signals and (2) nociceptors transmit an exaggerated signal in response to the same stimulus, when compared to a non-injured setting. This neuronal sensitisation also causes nociceptors to now respond to stimuli that are non-noxious explaining the phenomenon of allodynia. The molecular mechanisms behind these changes in nociceptor signaling (peripheral sensitisation) includes changes in receptor expression at both the nerve endings and along axons, infiltration of immune cells and the release of inflammatory mediators, and the activation of intracellular signalling cascades that modulate the responsiveness of individual receptors (Figure 1.8) [112].

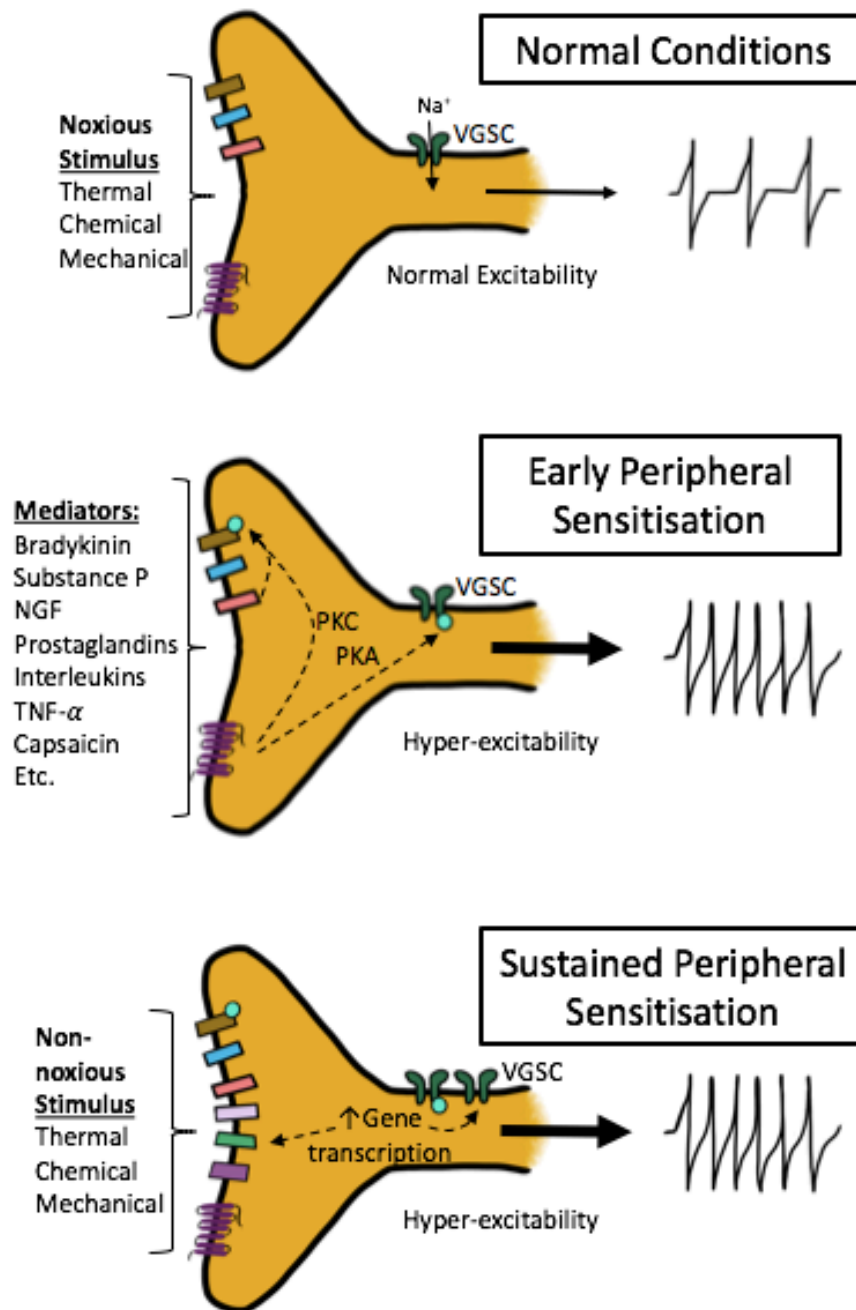


Figure 1. 8 Mechanism of Peripheral Sensitisation.

Simplified depiction of a nociceptor under normal conditions and during peripheral sensitisation. Under normal conditions, a noxious stimulus is required to elicit the generation of an action potential via specialised receptors on the nerve ending and voltage-gated sodium channels (VGSCs). Peripheral sensitisation is induced following injury or inflammation by a variety of algogenic mediators, some examples are provided which include bradykinin, substance P, nerve growth factor (NGF), prostaglandins, interleukins, TNF- α , and capsaicin. Once these molecules activate their respective

receptors, they initiate intracellular signalling cascades that result in phosphorylation (blue circles) of other receptors via intracellular kinases (PKA, PKC). Some also cause transcriptional changes such that the receptor expression in the neuron is modified. These changes contribute to hyperexcitability of the nociceptors such that non-noxious stimuli can evoke activation of the cells.

Central sensitisation is a form of use-dependent plasticity that follows aberrant peripheral afferent input. Following inflammation, injury, or neuronal damage, enhanced peripheral input from nociceptors results in homo- and heterosynaptic facilitation of dorsal horn neurones in the spinal cord [112, 114]. In the case of homosynaptic plasticity, a consistent barrage of nociceptive input results in a progressive increase in the output from the affected dorsal horn neuron (termed: wind-up). The physiological response would be feeling increased pain from repetitive stimuli even though the same stimuli are being consistently applied. Importantly, this synaptic plasticity is only observed while peripheral input is maintained. In heterosynaptic circuitry, two nociceptive afferents with divergent receptive fields can synapse on the same dorsal horn neurone or conversely a nociceptive and non-nociceptive A- β fibre that transmits signals for touch can share a synapse on the same neurone. Heterosynaptic facilitation occurs when nociceptive input increases causing a prolonged post-synaptic potentiation, which long outlasts the peripheral input. In this scenario, the threshold for both nociceptive and potentially non-nociceptive inputs are reduced because the responsiveness of the post-synaptic dorsal horn neurone has improved. Given the above scenarios, the neighbouring nociceptor with a different receptive field can become activated because of the shared synapse (secondary hyperalgesia). Alternatively, an A β fibre that's transmitting non-nociceptive information can act as a nociceptor giving rise to allodynia. The increase in synaptic strength is

mediated in-part by changes in receptor activity and density namely by N-methyl-D-aspartate (NMDA) and α -amino-3-hydroxy-5-methyl-4-isoxazolepropionic acid (AMPA) glutamate receptors. However, enhanced glial cell activation and loss of inhibitory functions have also been implicated in the mechanisms of central sensitisation [114].

1.4.2 Pain mechanisms and mediators in OA

Much of what is known about pain in OA has come from a culmination of human studies as well as pre-clinical animal experiments. During the early stages of OA, patients report joint pain with movement or loading of the joint but are afforded some relief at rest [115]. This type of pain is likely caused by mechanical stimulation of nociceptors (*nociceptive pain*) as the joint adapts to altered loading and joint degeneration. It can be described as dull, aching, or throbbing. A subset of patients may also notice mild swelling and associated pain – which is also described as – dull, aching, or throbbing. This type of pain is *inflammatory pain*.

As the disease progresses, people living with OA report persistent pain that radiates away from the joint and that is present even when resting [115]. The quality of pain also changes. Specialized pain questionnaires, such as the Western Ontario and McMaster Universities Arthritis Index (WOMAC), modified painDETECT questionnaire, and Knee Injury and Osteoarthritis Outcome Score (KOOS) capture these changes in OA patients [26]. Pain that is described as sharp, stabbing, radiating, or as ‘pins and needles’ is synonymous with *neuropathic pain*. Estimates suggest that as many as 25% of OA patients experience neuropathic-like pain caused by damage to the nerves themselves [73]. This type of pain is often not present until endstage disease.

While the patient reported pain is fundamental to understand symptomatology, much of what we know about each type of pain as it pertains to OA has been discerned from animal studies. The type of pain reported early in OA, pain with movement or exercise but not at rest, is likely nociceptive in nature occurring with loading of the joint. This pain serves a protective purpose to prevent overuse of the damaged joint. Many studies have sought to examine the relationship between joint damage and pain, but conflicting reports of radiological evidence of OA and pain exist [116-119]. In awake humans with non-diseased joints, noxious stimulation of ligaments and joint capsule with mechanical, chemical, and thermal stimuli elicits pain [120-122]. In contrast, stimulation of aneural cartilage fails to evoke pain. In diseased joints, however, changes in joint innervation may change which structures are susceptible to pain upon stimulation. While longitudinal studies present a clear narrative of increasing pain with an individual's disease progression, the ability to pinpoint joint structures that contribute to OA pain has been more challenging [123]. This may be due to the heterogeneity associated with the disease and the fact that many factors contribute to the development of OA. Using an animal model, the contribution of structural damage to joint sensitisation was examined in aged Dunkin Hartley guinea pigs [124]. While joint afferent sensitisation was observed in aged animals, no correlation between nociceptor activity and joint damage was observed mirroring what is observed clinically.

The use of MRI has afforded a more thorough analysis of joint pathology and identified inflammatory flares as a feature of pain in OA patients. The level of synovitis and bone marrow oedema are higher in joints of patients with pain compared to those that are asymptomatic [60, 125]. Changes in these inflammatory markers have been shown to

correlate with patient reported pain where improvement in synovitis is associated with lower pain scores and worsening of both are associated with more persistent, severe pain [125]. Histological analysis of synovial tissue from patients undergoing joint arthroplasty also reveal higher levels of synovitis with synovial hypertrophy and leukocyte infiltration in patients with higher pain scores [126]. Importantly, patients with synovitis also reported pain with activities including walking and bending of the knee. In these patients, synovial fluid levels of IL-6 also correlate with KOOS-measured pain scores [126]. Proinflammatory cytokines, including IL-6, have been implicated in the pathogenesis of several models of OA, and their sensitising effects on joint nociceptors has been thoroughly examined. In the MIA model, joint levels of IL-6 and TNF- α are elevated soon after induction where it is associated with synovial hypertrophy and mechanical allodynia [100]. Local administration of these cytokines to the knee joint causes robust sensitisation of A δ (TNF- α) and C (TNF- α and IL-6) fibres [127, 128]. Electrophysiology experiments also revealed that acute joint inflammation and pro-inflammatory mediators such as bradykinin, prostaglandin E2, IL-6, and TNF- α also activate silent nociceptors such that previously quiescent afferents now respond to normal mechanical stimulation of the joint [127-130]. Several of these molecules have been found to modulate joint afferents not only by direct activation via their cognate receptors but also by inducing phosphorylation of other neural elements including VGSCs and TRPV1 to enhance neuronal activity [131, 132]. This represents one mechanism whereby allodynia can occur in OA patients.

Central sensitisation at spinal and supraspinal sites has also been documented following joint inflammation. Both acute (e.g. kaolin-carrageen, bradykinin, TNF- α) and

chronic (adjuvant-induced arthritis) joint inflammation increases the activity of dorsal horn neurones with joint input [133-135]. Following inflammation, the spinal cord neurones exhibit decreased mechanical thresholds at the joint and also areas around the joint such that the receptive field has expanded into non-inflamed adjacent areas. The neurones also exhibit enhanced firing in response to non-noxious and noxious mechanical stimulation of the joint. These changes in dorsal horn neurone responsiveness underlie primary hyperalgesia (pain at the joint) and secondary hyperalgesia (pain at an adjacent site) commonly observed in patients and observed in animal models of OA. In established OA, patients report pain at rest and widespread pain beyond the region of the affected joint. Quantitative pain testing in these patients reveals that they exhibit widespread hyperalgesia and temporal summation indicating that central sensitisation is ongoing [136]. Using a pressure algometer, a patient's pressure pain threshold can be determined at the site of OA and at distal sites. Consistent evidence of decreased pain thresholds at remote sites are found among OA patients compared with healthy controls [137, 138]. Temporal summation is a proxy of central sensitisation whereby the same stimuli are applied repeatedly, and the pain response recorded. If their pain responses increase without an increasing stimulus then this can be taken as evidence of sensitisation. In OA, temporal summation is present but does not correlate with disease severity [139, 140]. The molecular basis of these changes is only partly understood. In MIA animals, elevated levels of glutamate, bradykinin, substance P, and CGRP are found in the spinal cord and are important mediators of neuronal sensitization [141, 142]. NMDA and NK receptors, in part, potentiate second order spinal cord neurones, as pre-treatment with antagonists against both of these mediators attenuate the sensitising effects of joint inflammation

[143-145]. Descending circuitry also contributes to the neurophysiology of these spinal cord neurones as spinalised animals exhibit further enhanced responses to joint inflammation compared to animals with intact spinal circuitry [146].

1.4.2.1 Neuroplastic Changes in OA

Neuroplastic changes have been discovered in both the peripheral and central pain pathway in OA patients and animal models. In the synovium of patients undergoing joint arthroplasty, normal innervation is observed in non-inflamed tissue; however, decreased peptidergic innervation is observed in hypertrophic tissue [147]. In contrast, in diseased meniscus and subchondral bone increased innervation and vascularisation has been detected [71, 148]. Aneural cartilage can also become painful as aberrant innervation crosses the subchondral bone tidemark into calcified cartilage in OA joints [148]. In the MIA model, the nerve damage marker ATF3 has been detected in DRG neurones and the saphenous nerve also undergoes demyelination [101, 149]. NGF is also elevated in human OA where it acts as a trophic factor in addition to directly sensitising nociceptors via its receptor TrkA. As such, limiting the activity of NGF with a monoclonal antibody has recently emerged as a promising analgesic option for OA pain [79, 80]. Building on these clinical findings, Aso *et al.*, have examined whether inhibiting TrkA in animals can prevent aberrant peptidergic joint innervation observed at endstage OA [150]. A chronic oral dosing of the TrkA antagonist AR786 prior to the induction of post-traumatic OA prevented the development of pain behaviour and algogenic CGRP. While further studies are needed, these results suggest that targeting NGF or TrkA may prevent the neuropathic pain observed in some OA patients.

Plastic changes have also been noted in the brain of OA patients. Those with chronic OA pain exhibit atrophy in the anterior cingulate cortex, amygdala, thalamus, and brainstem [151, 152]. In a subset of patients that underwent joint arthroplasty, there was a complete recovery from pain and an improvement in grey matter volume. While grey matter loss is commonly reported in chronic pain patients, this finding suggests that the absence of peripheral drive can improve the neural integrity of the CNS [153].

1.4.2.2 Other Mediators in OA Pain

Serine proteases are elevated in the joints of OA patients and contribute to pain and inflammation via protease activated receptors (PARs) [4]. Activation of PAR2 and PAR4 sensitises joint nociceptors while inhibition of joint proteases attenuates pain in MIA animals [154-157]. Recent evidence also suggests that PARs mediate inflammatory and arthritic joint pain at the level of the spinal cord since intrathecal blockade of PAR2 abolishes joint pain [158].

The endocannabinoid system (ECS) has been shown to modulate OA pain at the level of the joint as well as in the spinal cord. In rodents and humans with OA, cannabinoid receptors 1 and 2 (CB1-2) are found in synovial tissue [159, 160]. The endocannabinoids anandamide (AEA) and 2-arachidonoylglycerol (2-AG) are also found in arthritic synovial fluid but not healthy joints [159, 161]. In MIA animals, treatment with the phytocannabinoid cannabidiol (CBD) attenuates pain, inflammation, and early, chronic treatment prevents neuropathy at endstage disease [149]. In the same model, CB2 receptors are upregulated in the spinal cord and local administration of the CB2 agonist

JWH133 attenuates central sensitisation and prevents astrocyte activation [162]. This suggests that the ECS may be regulating OA pain via a descending inhibitory pathway.

Another molecule studied in people living with OA and corroborated in animals is the lipid mediator lysophosphatidic acid (LPA). In humans, LPA has been found to be elevated in OA joints and correlates with disease severity [163]. In animals, administration of LPA causes a dose-dependent mechanical allodynia, joint afferent sensitisation, and saphenous nerve demyelination. Interestingly, in this model, nerve damage is more severe in female animals compared to males, but further investigation is needed to elucidate the reasons for this [163, 164].

1.5 Assessment of Nociceptive Behaviour in Preclinical Models of Pain

Measuring nociceptive behaviour in laboratory animals can be divided into evoked and spontaneous tests [165]. The majority of assays fall within the evoked testing category and involve either mechanical, chemical, or thermal stimulus. Only mechanical stimuli, however, bears any resemblance to a clinically relevant external stimulus that affects an arthritis patient [91]. Examples of evoked nociceptive tests are von Frey hair algometry, pressure application measurement, and vocalisations. Spontaneous nociceptive behaviour can be obtained from observations rather than direct application of stimuli and is thought to be more clinically relevant than an evoked response. Examples of spontaneous behaviour include dynamic weight bearing, facial grimacing, and activity-based assessments. In both types of assessment, special care is needed to ensure the testing environment is quiet, scent-free, and that the animals have been previously habituated to the room and experimenter. These precautions will minimize stress-induced analgesia as well as startle responses which can confound results [166, 167].

1.5.1 *von Frey Hair Algesiometry*

Von Frey hair algesiometry is an evoked nociceptive test used to measure tactile sensitivity and mechanical allodynia that has been applied to models of arthritis [165]. Originally invented by Maximilian von Frey in 1896, the process consists of a set of hairs of various thickness with corresponding bending force. To assess tactile sensitivity, the lowest force von Frey hair is applied perpendicular to the skin just until the hair bends. A positive response to the hair would be considered when the animal pulls the stimulated area away or licking the stimulus area, while a lack of response would be a negative response. If the animal doesn't respond, thicker hairs are applied in series of increasing forces until a response is elicited. In naïve animals, the animals usually do not respond to any of the hairs that are applied; however, in arthritic models, the animal withdraws their paws to hairs that previously didn't elicit a response. This change in mechanosensitivity in arthritic animals is indicative that the animals are experiencing allodynia. Since most arthritis models are induced in the knee and von Frey hairs are applied to the glabrous skin of the ipsilateral hindpaw, the assay is actually testing for referred pain (secondary allodynia) because the primary site of injury is not being tested.

1.5.2 *Dynamic Weight Bearing*

Gait changes in human OA are a possible sign of pain [168, 169]. In animals, dynamic weight bearing can be used as a measurement of the weight distribution between the hind-limbs. The animals are placed in a Perspex chamber with a pressure-sensitive floor. The weight applied and the surface area for each paw is calculated and any deficits in injured limbs can be determined. While weight bearing deficits have been observed in

animal models of OA, including MIA and MMT, the true degree of gait changes may be disguised in the experimental setting. It is important to be cognisant of the fact that rodents like other prey animals may try to disguise any injuries and this may occur more often in spontaneous assays than evoked pain behaviour procedures [149, 170, 171]. Additionally, since the MMT model is inducing joint instability, the weight bearing deficits may be due to structural changes or joint instability and not linked to pain observed clinically.

1.6 Electrophysiology as a Measure of Nociceptive Tone in Preclinical Models of Pain

Electrophysiology was first used to measure the activity of joint afferent fibres in the cat by Ernest Gardner in 1947 [172]. Noting the importance of ‘crippling joint disorders’, his study provided insight into the type of sensory neurones present and their stimulus modalities. The use of electrophysiology is still regarded as the gold-standard to assess nociception and can be utilised in both *in vivo* or *in vitro* assays. In pain research, objective measurement of both peripheral drive using a teased nerve preparation to measure single unit activity, or central input by recording field potentials in the dorsal horn of spinal cord or in specific regions of the brain such as the thalamus are regularly carried out *in vivo* [146, 173]. *In vitro* intracellular recordings in sliced spinal cord or brain sections and dissociated neurons provide insight into the molecular activity of nociceptive circuitry.

1.6.1 Teased Nerve Recordings

Single unit recordings from the medial articular branch of the saphenous nerve gained popularity following studies by Schaible and Schmidt. The recordings, first in cats and

then in rats, characterised the type of nociceptive and non-nociceptive joint afferents present and how they responded to mechanical and chemical stimuli [14, 15]. The A δ and C afferent fibres identified, could be categorised into those with low or high mechanical thresholds, or a third class called “silent nociceptors” that were mechanically insensitive until activated by an inflammatory mediator. They built on this work to find that the nociceptors were sensitised following acute joint inflammation, as such, ongoing spontaneous firing was enhanced, the threshold to activate the fibres was reduced, and the evoked firing rate was increased [174-176]. Using clinically-relevant analgesics such as aspirin or indomethacin, this afferent sensitization was abolished highlighting that a powerful tool now existed to not only measure the activity of afferents following injury but also to test analgesics in a variety of disease states [177]. Since these early studies were carried out, other seminal work has contributed to our understanding of joint neurophysiology. Clinically, the disparity between patient reported pain and joint degeneration has been an enigma. However, by examining the neurophysiology of joint afferents from aged Dunkin Hartley guinea pigs, it has been demonstrated that the level of joint damage does not correlate with joint afferent sensitisation [124].

1.7 Assessment of Inflammation in Preclinical Models of Pain

Assessment of inflammation in preclinical models of pain and arthritis can range from minimally-invasive *in vivo* assays that measure leukocyte trafficking and blood flow, to non-invasive measurement of joint oedema. Quantification of inflammatory mediators in serum or synovial fluid provide an *ex-vivo* snapshot of the inflammatory milieu in arthritic and control animals.

1.7.1 Intravital Microscopy (IVM)

Inflammatory responses are mediated in part by immune cell migration from the general circulation to the site of injury or infection. This movement occurs as a result of a concerted effort by damaged tissue, endothelial cells, and leukocytes to mediate migration [178]. Under these conditions, leukocytes follow a series of recognisable steps on the path to extravasation which can be monitored in real time using intra-vital microscopy (IVM) [179].

Following tissue injury, damage-associated molecular patterns (DAMPs) stimulate resident immune cells including mast cells and macrophages to release cytokines and other proinflammatory mediators [178]. Nearby endothelial cells are activated, and selectins (P-selectin and E-selectin) are induced on the surface of the cells to first capture circulating leukocytes and then invoke the distinctive “rolling” phase of leukocyte trafficking where the immune cells are tethered by the selectins and move slowly along the endothelial wall [180]. As integrins become activated in the slow rolling leukocytes, they firmly adhere to the intimal surface of the venule wall under the influence of intercellular adhesion molecules 1 and 2 (ICAM1 and ICAM2) and vascular cell adhesion molecule 1 (VCAM1). Several endothelial cell adhesion molecules and receptors are involved in the subsequent diapedesis process including ICAM-1, platelet endothelial cell adhesion molecule-1 (PECAM-1), and junctional adhesion molecules (JAMs) [181-183]. Via these adhesion molecules and receptors, the leukocytes transmigrate out of the vasculature, through the endothelial barrier, and enter the tissue to exert their pro-inflammatory effects (Figure 1.9).

IVM can be utilised in arthritis models to visual fluorescently labelled leukocytes within the knee joint microvasculature and measure two key steps of the extravasation process: rolling and adherence [179, 184]. These two steps precede extravasation and provide a measure of local inflammation. Additionally, the anti-inflammatory potential of test agents can be assessed by their effects on leukocyte trafficking.

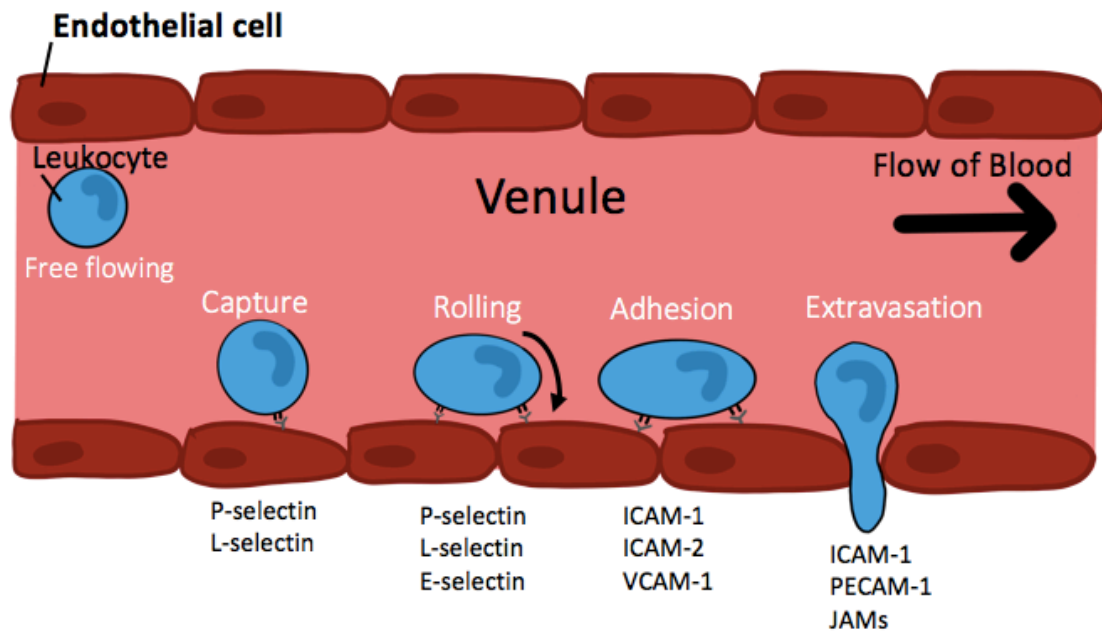


Figure 1. 9 Leukocyte Trafficking.

Following injury or during local inflammation, selectins (P and E) are induced on the surface of endothelial cells and initiate the capture of free-flowing leukocytes. Subsequent characteristic leukocyte rolling is mediated by P-, L- and E-selectins. During leukocyte adhesion, activated integrins bind to ICAM-1, ICAM-2, and VCAM-3 minimising further leukocyte movement. Extravasation usually occurs at endothelial barriers via endothelial receptors ICAM-1, PECAM-1 and junctional adhesion molecules (JAMs).

1.7.2 *LAser Speckle Contrast Analysis (LASCA)*

Hyperaemia is another component of inflammation that is observed in OA. Increased blood flow is an infrequent feature of OA and is observed during intermittent inflammatory flares [185]. Measuring the amount of joint blood flow between arthritic and non-arthritic joints introduces another tool to assess inflammation and test treatments with vasoregulatory potential. LAser Speckle Contrast Analysis (LASCA) is a tool that allows for the measurement of vascular conductance.

1.8 Serine Proteases

Proteases (or proteinases) are proteolytic enzymes that are capable of hydrolyzing peptide bonds in proteins to form smaller peptide fragments [186, 187]. Protease activity is implicated in a wide range of physiological processes, including the breakdown of dietary proteins, intracellular and extracellular protein metabolism, blood clotting, and complement activation. They are also involved in pathological conditions such as Alzheimer's disease, cardiovascular disease, and arthritis [4, 188-190]. Proteases were initially classified as endoproteases that targeted internal bonds or exoproteases that targeted cleavage sites in the NH₂- or COOH- termini of proteins. However, new functional and structural assays that allowed for the identification of the catalytic mechanism of proteases resulted in a new classification system. Six classes of proteases have now been identified based on their mode of catalysis. Serine, cysteine, threonine, aspartic, and metallo-proteases have all been identified in mammals, and glutamic proteases are present in bacteria [186]. Serine, cysteine, threonine proteases catalyse their substrates using an electron dense nucleophile residue in a two-step reaction that first produces a covalent intermediate before finally hydrolysing the amino-acid bond [187, 191]. In contrast, aspartic, metallo-, and glutamic proteases carry out their proteolytic

activity in a single step by polarising water which then hydrolyses the substrate [187]. In humans, genomic studies have ascertained that proteases make up 2% of the genome and it is becoming increasingly apparent that they are not passive catabolic molecules [192]. Rather, proteases are sophisticated protein-processing agents that also act as neurotransmitters, and their activity is tightly regulated by endogenous inhibitors [187, 193].

Serine proteases constitute about a third of all known proteases in humans and are considered the “workhorses” of the human body [187]. Their name is derived from the nucleophilic serine residue at the cleavage active site which is common among all member of the family, while the surrounding amino acids differ creating novel binding pockets that confer substrate specificity. The classic catalytic triad in serine proteases, His-Asp-Ser/Asp-His-Ser/Ser-Asp-His/Asp-Ser-His, is found in chymotrypsin, trypsin, thrombin, cathepsin G, and neutrophil elastase among others [187, 194]. While other amino acid sequences do exist, they are less common. Chymotrypsin was the first serine protease to be identified in the pancreas following which its enzymatic activity was extensively studied, and its crystal structure was successfully modelled [195]. From these early studies, much was gleaned about zymogen activation and substrate recognition, but a wider appreciation for protease activity outside of the digestive system was also growing.

1.8.1 The Role of Serine Proteases in Arthritis

With the destructive nature of arthritis long being a focus of research, proteases were considered important factors to explore. As such, many studies have demonstrated an elevated level of serine proteases in joint tissue of RA and OA patients (Table 1.4) [4,

196-198]. For the most part, levels of proteolytic enzymes are higher in RA when compared OA, owing to the greater catabolic and inflammatory nature of RA. The use of *ex-vivo* studies and pre-clinical models brought the study of proteases in arthritis beyond their purely degradative role by introducing the concept that proteases also act as signalling molecules contributing to disease pathogenesis and pain [154, 157, 158, 199-202].

Thrombin is a serine protease that is elevated in OA and RA joints and mediates not only cartilage degeneration but also inflammation and disease progression [196, 203, 204]. While levels are higher in arthritic joints compared to healthy controls, activity levels are eight-fold higher in RA than OA. In the context of arthritis, thrombin is part of the coagulation cascade and cleaves fibrinogen to form fibrin, the presence of which has been correlated with the severity of the disease. In a model of RA, fibrin has been found to stimulate synoviocytes [205] and promote synovitis and pannus formation. Fibrin also promotes joint inflammation by inducing leukocyte migration, stimulating TNF- α and IL-1 β expression in macrophages, and chemokines release by endothelial cells, synoviocytes, and neutrophils [206-210]. In mice that were deficient in fibrinogen, collagen-induced RA was milder, affecting less joints and with decreased severity. The levels of pro-inflammatory mediators TNF- α , IL-1 β , and IL-6, were also reduced in the mutant mice suggesting that altering the production of fibrin can profoundly alter the progression of the disease [211]. In fact, similar results have been found from inhibiting thrombin itself, where it resulted in decreased fibrin levels, reduced synovitis, and disease severity in models of collagen- and antigen- induced arthritis [204, 212].

Another serine protease, tissue plasminogen activator (tPA) is higher in OA joints compared to RA [198, 213, 214]. The role of tPA in disease pathogenesis has not been extensively studied. tPA is responsible for the production of plasmin from plasminogen, which in turn degrades fibrin and acts on multiple protease-activated receptors. Cultured synoviocytes from RA and OA patients produce tPA as well as its inhibitor, plasminogen inhibitor, but higher amounts of the former are produced from RA cells [214]. Like other proteases, an imbalance between proteolytic activity and inhibition of tPA has been found to have deleterious effects on joint health. While both tPA and plasmin also have catabolic effects on cartilage and subchondral bone *ex-vivo* and in animal models, knockdown of tPA exacerbates arthritis [215 , 216, 217]. Collagen-induced arthritis was more severe in tPA knockout mice where the joints had elevated fibrin deposition and synovial cytokine levels [217]. These data suggest that some level of tPA activity is necessary to counteract the destructive effects of fibrin.

The data presented here represent some of the ways in which serine proteases contribute to the pathogenesis of arthritis. Another way that proteases can contribute to arthritis and its symptoms is through protease-activated receptor signalling.

| Serine Protease | Level in RA Joint | Level in OA Joint |
|--|-------------------|-------------------|
| Thrombin | ↑↑ | ↑ |
| Tryptase | ↑ | ↑ |
| Proteinase-3 | ↑ | |
| Matriptase-1 | | ↑ |
| Cathepsin G | ↑ | |
| Urokinase Plasminogen Activator (uPA) | ↑ | |
| Tissue Plasminogen Activator (tPA) | | ↑ |
| Complement 4a | ↑ | ↑↑ |
| Elastase | ↑ | |
| Dipeptidyl peptidase | ↑ | |
| Granzyme A | ↑ | |
| HtrA serine peptidase | ↑ | ↑↑ |
| Fibroblast activation protein | ↑ | ↑↑ |
| Fibroleukin | ↑↑ | ↑ |
| Activated protein C | ↑↑ | ↑ |

Table 1. 4: Serine Proteases in Arthritic Joints.

Serine proteases that have been identified in the joints of RA and OA patients. An arrow indicates elevated in arthritis compared with other joint condition or control. (Adapted from [4]).

1.8.2 *Protease Activated Receptors (PARs)*

Protease activated receptors (PARs) are the cognate receptors of serine proteases of which four have been currently identified (PAR1-4). While PAR1 was cloned in 1991, PAR4 was discovered in 1998 using a database to search against thrombin and trypsin cleaving domains [218-220]. PARs are found in platelets, endothelial cells, myocytes, neurones, glial cells, and several types of immune cells [221]. Unlike classic ligand-binding receptors, PARs contain their own ligand within the N-terminal domain that is unmasked following peptide cleavage by a protease. The resulting tethered ligand binds to a specific ligand binding site on the second extracellular loop, activating the receptor and engaging G-proteins or β -arrestin [193]. Canonical and non-canonical pathways have been identified for PAR1, 2, and 4, while PAR3 appears to act mainly as a co-factor dimerizing with other PARs. Canonical cleavage of PARs 1 and 2 leads to coupling with the G proteins $G\alpha_q$, $G\alpha_i$, and $G\alpha_{12/13}$, and canonical cleavage of PAR4 results in $G\alpha_q$, and $G\alpha_{12/13}$ coupling (Figure 1.10) [222-227]. Synthetic agonists that mimic the amino acid sequence of the tethered ligand have also been developed as a tool to study the pharmacology of the receptors and are called ‘synthetic activating peptides’ [193]. While significant efforts have gone into elucidating the pharmacology of PAR1 and 2, limited information is available for PAR3 and PAR4, which is in part due to limited pharmacological agents.

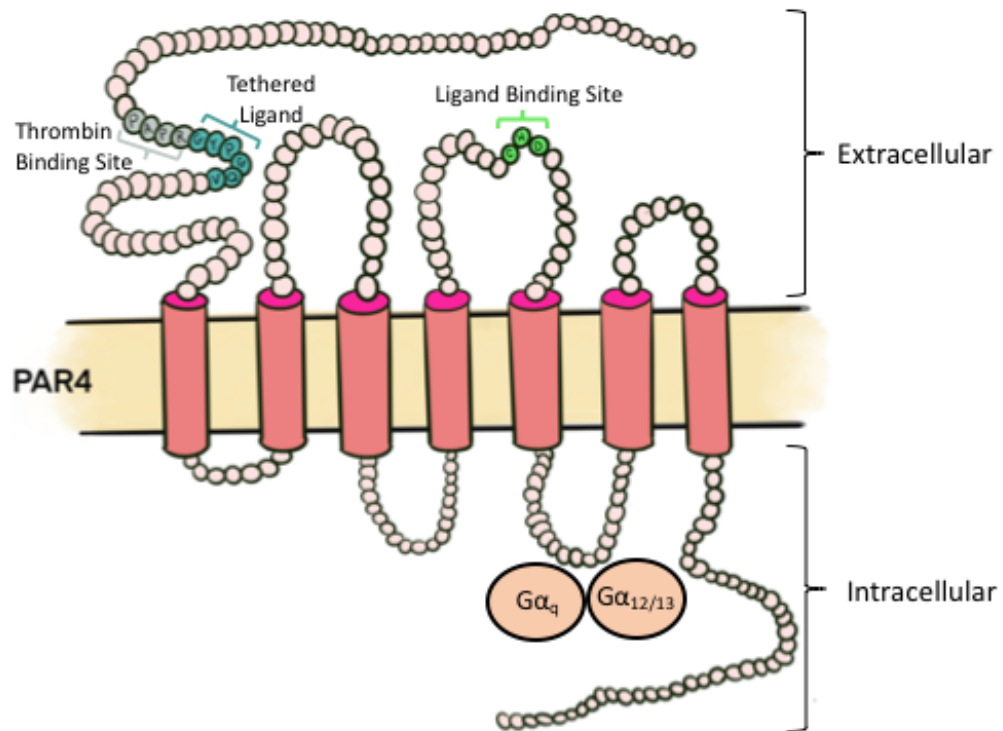


Figure 1. 10 Structure of Protease Activated Receptor-4.

A depiction of PAR4, highlighting the thrombin binding domain, the resulting tethered ligand following thrombin cleavage, and the ligand binding site on the second extracellular loop. PAR4 couples to α_q and $\alpha_{12/13}$ G-proteins following receptor activation. The best characterised downstream signalling following PAR4 activation is Ca^{2+} mobilisation (α_q) and Rho activation ($\alpha_{12/13}$).

Similar to biased signalling observed in other GPCRs, different serine proteases can cleave at distinct amino acid sequences on the N-terminus effectively revealing novel ligands which engage different G-proteins associated with the PARs. For example, in endothelial cells, thrombin-induced cleavage of PAR1 induces RhoA GTPase signalling, whereas activated protein C-induced cleavage of PAR1 increased Rac1 within the cells suggesting different intracellular signalling mechanisms following distinct protease cleavage [228]. With PAR4, only the canonical cleavage site (often simply referred to as

the thrombin site) has been identified. Importantly, proteolytic cleavage by the same protease has also been found to engage different signalling pathways for PARs expressed in different tissue. For example, activation of PAR4 in DRG neurons traced from the colon results in a decrease in intracellular calcium [229]. At the level of the joint, activation of PAR4 is excitatory, suggesting a different signalling pathway [155]. A final mechanism by which proteases can modulate PAR signalling is by disarming the receptors. Proteases can hydrolyse bonds downstream of the classical receptor-activating site rendering N-terminus unresponsive to further cleavage and any receptor binding [193] (Figure 1.11). Activating proteases, synthetic activating peptides, and disarming proteases for each PAR are compiled in Table 1.5.

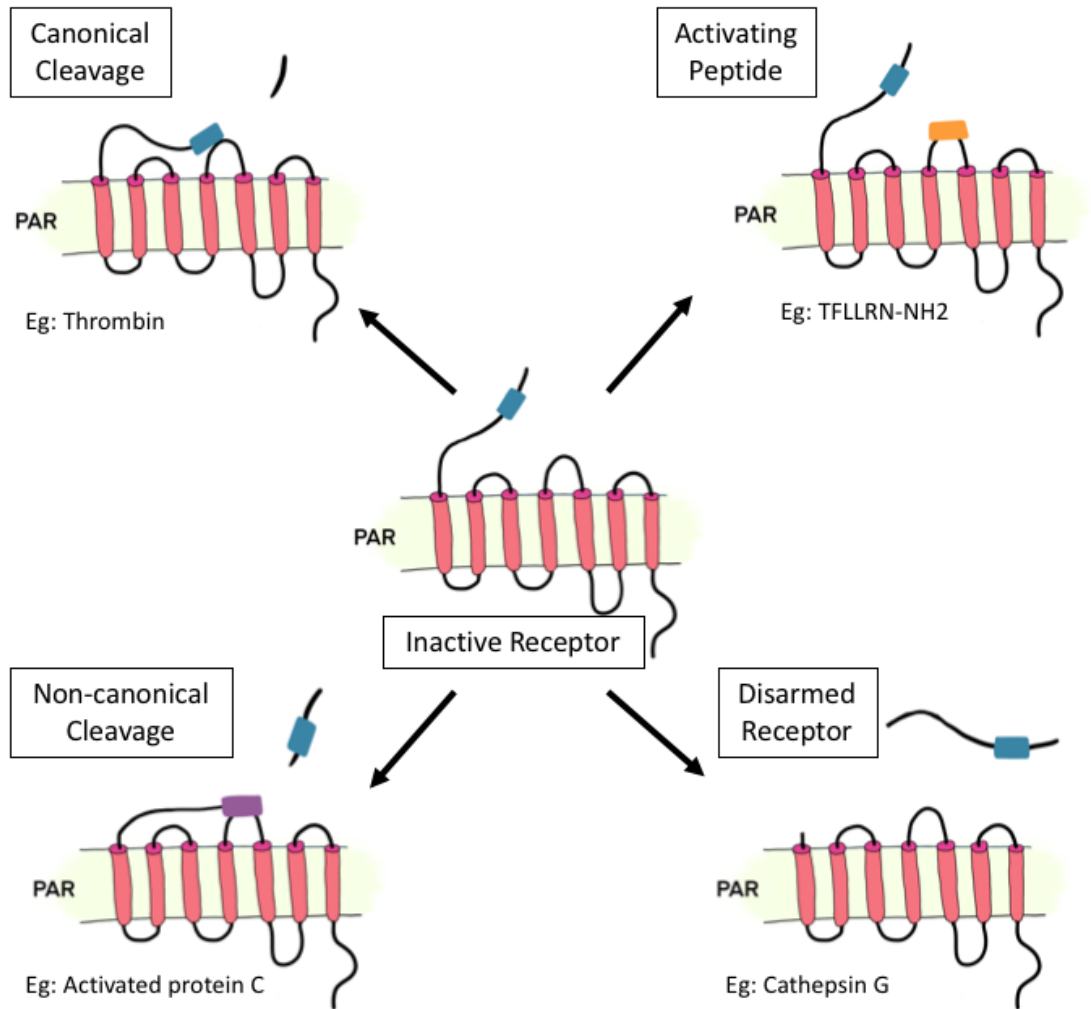


Figure 1. 11 Activation and disarmament of protease activated receptor-1.

Depiction of PAR1 and the various methods of cleavage and activation. PAR1 was chosen (rather than PAR4) because the pharmacology has been more thoroughly interrogated for this receptor. While canonical cleavage, disarming, and activation via a synthetic activating peptide has been confirmed in PAR4, non-canonical cleavage has yet to be identified.

PAR signalling is terminated by proteolytic desensitisation and receptor internalisation, but mechanisms differ greatly based on the receptor as well as the activating proteases. The general mechanism for receptor desensitisation in PARs is similar to other GPCRs, where activation of the receptor leads to receptor

phosphorylation by protein kinases such as G protein receptor kinases (GRKs) or second messenger kinases PKA or PKC. Canonical cleavage of PAR1 leads to GRK3 or 5 phosphorylation and depending on the protease activator β -arrestin recruitment can vary. With PAR1, for example, thrombin cleavage leads to β -arrestin-1 recruitment, while activated protein C cleavage causes β -arrestin-2 recruitment. In contrast, proteolytic cleavage by other enzymes fails to elicit any β -arrestin signalling (eg: elastase). Cleavage of PARs at canonical sites results in rapid receptor internalisation in either β -arrestin-dependent (PAR2) or -independent (PAR1) mechanisms [230, 231]. Although comparatively less is known about PAR4, signal termination and receptor trafficking appear to occur at a much slower pace and by different mechanisms than other protease receptors. PAR4 has been shown to have a shorter C-terminus and have fewer phosphorylation sites than PAR1 and PAR2, which dramatically lengthens the duration of signalling following PAR4 activation compared to its counterparts [232]. PAR4 internalisation also occurs independently of β -arrestin via clathrin-mediated endocytosis [233].

| | Activating proteases | Disarming proteases | Synthetic Activating Peptides |
|------|--|--|--------------------------------------|
| PAR1 | Thrombin Granzyme A Plasmin Activating protein C Trypsin Factor Xa Kallikrein- 4, 5, 6, 14 | Kallikrein-1 ADAM17 or MMP Protease 3 Trypsin Cathepsin G Elastase Plasmin | SFLLRN-NH2 TFLLRN-NH2 |

| | Activating proteases | Disarming proteases | Synthetic Activating Peptides |
|------|--|---|-------------------------------|
| | MMP-1 Cathepsin G Proatherocytin Pen C 13 Chymase | | |
| PAR2 | Trypsin Mast cell tryptase Factor Xa: Factor VIIa Acrosin Matriptase Serine 11D Trypsin Granzyme A Kallikrein-2, 4, 5, 6, 14 | Plasmin Protease 3 Calpain Cathepsin G Elastase | SLIGRL-NH2 FLIGRL-NH2 |
| PAR3 | Thrombin | Cathepsin G | N/A |
| PAR4 | Thrombin Trypsin Cathepsin G Trypsin IV Mannin-binding SP-1 Plasmin Factor Xa Kallikrein-1, 14 C4a | Kallikrein-14 | AYPGKF-NH2 GYPGKF-NH2 |

Table 1. 5: PAR activating proteases, disarming proteases, and synthetic activating peptides.

Summary of proteases known to cleave PARs and cause activation or disarming of the receptors as well as non-cleaving synthetic activating peptides. Some examples provided indicate a protease as activating and disarming the same receptor (Eg: kallikrein-14 with PAR4), these are examples where the receptor is expressed in different cells or tissue highlighting the importance of biased signalling in PAR pharmacology. (Adapted from [234]).

1.8.3 The Role of PARs in Pain and Inflammation

There is growing evidence to suggest that each member of the PAR family is implicated in the pain as either a positive or negative regulator of the nociceptive system. To date the majority of studies have explored the role of PAR1 and 2 in nociception and inflammation; however, evidence for a role for PAR 3 and PAR4 is emerging.

PAR1 is expressed peripherally on nociceptive neurones, myelin, and endothelial cells, and extensively in the CNS in neurons, microglia, and astrocytes. Data suggest PAR1 activation is associated with inflammatory and neuropathic pain [235-240]. Interestingly, PAR1 activation causes either pro- or anti- nociceptive responses in animals depending on the experimental conditions. Administration of thrombin alone into the hindpaw of mice, for example, increases the withdrawal and thermal thresholds of animals suggesting anti-nociceptive effects of receptor activation. Following acute inflammation with carrageenan in the paw, thrombin treatment reduced mechanical allodynia and thermal hyperalgesia [241]. Martin *et al.* (2009) explored the mechanism of PAR1-induced analgesia and determined that receptor activation by natural ligands or synthetic activating peptides were mediated by the endogenous opioid system. Proenkephalin mRNA increased in local immune cells following PAR1 agonist treatment and the antinociceptive effects were blocked by naloxone [242]. In contrast to the analgesic effects observed in inflammatory conditions, PAR1 activation in a neuropathic model resulted in hyperalgesia [237, 238]. In sciatic nerve ligation (SNL) and streptozotocin (STZ)-induced diabetic neuropathy models aberrant PAR1 expression has been demonstrated both peripherally at expanded nodes of Ranvier or spinally in the dorsal horn [237, 238]. Blocking thrombin activity in the SNL model suppressed mechanical allodynia while chronic inhibition of thrombin in the STZ model recovered node of Ranvier remodelling and PAR1 expression changes. A recent study has provided further evidence that PAR1 signalling directly affects myelination in the CNS through a brain derived neurotrophic factor (BDNF)- mechanism [243]. Following stroke in mice, blockade of PAR1 promotes repair of brain lesions which is prevented with BDNF

inhibitors; whether a similar phenomenon is mediating PAR1 in peripheral neuropathic pain warrants further research.

PAR2 is similarly expressed in the nociceptive pathway having been found in 60% of DRG neurons a large percentage of which co-express with peptidergic neurones. As such, activation of PAR2 with endogenous activators (eg. trypsin or neutrophil elastase) or synthetic activating peptides leads to the release of pro-inflammatory substance P and CGRP. PAR2 expression also colocalizes in DRG neurons with members of the transient receptor potential vanilloid (TRPV) family TRPV1 and 4 which encode noxious heat and mechanical stimuli, respectively [244]. Following PAR2 activation, animals exhibit thermal and mechanical hyperalgesia; however, coadministration of a TRP-channel antagonist prevents thermal hypersensitivity and reduces tactile hyperalgesia, suggesting the functional activity of the receptors were linked. Further studies found that activation of PAR2 potentiates the activity of TRP channels by phosphorylating the channels via PKA or PKC [244, 245]. PAR2 has also been widely studied in cancer pain, neuropathic pain, visceral pain, and arthritic pain, and blockade of the receptor or inhibition of its endogenous protease activators have been found to be analgesic [246-248].

PAR3 is expressed in DRG neurons along with CGRP and substance P suggesting that it may be implicated in nociceptive signalling [249]. There are currently no peer-reviewed articles that explore the role of PAR3 in either inflammatory or neuropathic pain as the development of a PAR3 activating peptide remains elusive.

1.8.4 The Role of PARs in Arthritis

In addition to serine proteases being implicated in arthritis pathogenesis, their receptors have also been found in arthritic joints and studied in animal models. PAR1 has been found in human synovium and fibroblasts from both RA and OA patients but little preclinical exploration has been carried out in the area of pain [196, 250]. Using human synovial fibroblasts, it has been discovered that thrombin acts on PAR1 to cause IL-6 release, the levels of which correlate with patient reported pain and disease progression [251]. In the collagen- and antigen-induced models of RA, enhanced gene expression of PAR1 is observed in the joint [252]. When arthritis is induced in PAR1 knockout mice the severity of disease is reduced with milder synovitis, cartilage degeneration, and lower IL-6 levels detected [203].

PAR2 expression has been widely detected in arthritic joints including in the synovium, mast cells, chondrocytes, and osteoblasts [253-257]. The Ferrell laboratory extensively examined PAR2 expression in the joints of mice with RA or post-traumatic OA and then assessed what effect knocking out PAR2 would have on the model progression. Using a combination of chronic and acute inflammatory joint models (Freund's complete adjuvant and kaolin and carrageen, respectively) in wildtype and PAR2^{-/-} mice, Ferrell *et al.*, demonstrated that PAR2 was necessary for the development of joint pathology. In wildtype but not PAR2^{-/-} mice, the inflammatory insult caused synovial hyperplasia, cellular infiltration and cartilage erosion [200]. Using the same animals in a post-traumatic model of OA, wildtype animals developed cartilage erosion with enhanced PAR2 expression in chondrocytes and increased subchondral bone formation. Mice lacking PAR2 develop very mild joint pathology. However, treatment of

wildtype animals with established PTOA with a PAR2 monoclonal antibody, SAM-11, was able to reduce the progression of OA [199]. Finally, gene rescue experiments were conducted using a human-PAR2 expressing adenovirus. When SAM-11 was administered to PAR2^{-/-} mice in the early stages of PTOA, their disease progression worsened, validating the importance of the receptors in OA pathogenesis [201].

Further studies have examined the role of PAR2 in OA-associated pain and neuropathy and found that PAR2 is implicated in both. Using mice, it was found that the MIA model caused an increase in the proteolytic activity of neutrophil elastase, a PAR2 cleaving serine protease, during the early inflammatory stage of the model[156]. Since robust inflammation can contribute to neuropathy, and PAR2 signalling has been implicated in both inflammatory as well as neuropathic pain, the authors blocked the activity of neutrophil elastase and PAR2 during the inflammatory phase of MIA to determine if it affected neuropathy observed later in the timecourse. By using either an endogenous (SERPINA1) or synthetic (sivelestat) inhibitor of neutrophil elastase early in the model, endstage nerve damage and associated hyperalgesia were attenuated. Similar results were observed using a PAR2 antagonist (GB83) or PAR^{-/-} mice, suggesting it was the activation of PAR2 that mediated subsequent damage and pain [156].

1.8.5 The Role of PAR4 in Inflammation and Pain

Similar to other PARs, PAR4 is expressed in the vascular system and peripheral nociceptive pathway. The initial *in-vivo* experiments were focused on the potential role of PAR4 in modulating the vascular system. However, while developing synthetic activating peptides and novel antagonists to study the pharmacology of PAR4, some interesting

observations were made. After identifying the best candidate activating peptide from binding assays, AYPGKF-NH₂, was injected into the paw of rats, where it produced long lasting oedema. Animals were then pretreated with capsaicin to deplete neuropeptides prior to PAR4 activation, but this treatment had no effect on oedema. This was the first evidence that PAR4 signalling did not depend on neurogenic mechanisms which had been observed with PAR1 and PAR2 [258]. Another study that pre-treated animals with the bradykinin-2 receptor antagonist, icatibant, attenuated the effects of AYPGKF-NH₂ [259]. Suggesting that PAR4 was instead acting in concert with the B2 receptor.

The first study to examine PAR4 in the nociceptive pathway was in 2007, where PAR4 expression and activation were investigated in the rat [241]. Expression of PAR4 in DRG neurons was just over 60%, with 90% of those co-expressing CGRP and 80% expressing substance P. Intraplantar injection of AYPGKF-NH₂ caused increased thermal and mechanical thresholds in naïve animals suggesting an anti-nociceptive effect. Administration of AYPGKF-NH₂ also attenuated the algogenic effects of carrageen. In contrast to this study, administration of the PAR4 activating peptide into the knee joint of mice and rats causes mechanical allodynia and oedema. In mice and rats, PAR4 expression was confirmed in articular cartilage, subchondral bone, menisci, synovium, and mast cells. Following AYPGKF-NH₂ administration, there were gradual increases in joint blood flow and mechanical allodynia which was blocked with pretreatment with either the PAR4 blocker pepducin P4pal10 or B2 receptor antagonist HOE-140. In kaolin/carrageen mice, pretreatment with pepducin P4pal10 also attenuated the synovitis and increase in joint perfusion associated with the model [260]. To understand the neurophysiology of PAR4 activation on joint nociceptors better, single-unit

electrophysiology was carried out on rats that were treated with AYPGKF-NH₂ [155]. PAR4 activation using the synthetic peptide significantly increased firing of joint afferent fibres. This effect was abolished by pretreatment with peptidase P4pal10 and HOE-140 demonstrating bradykinin B₂ receptor dependence. To discern whether TRPV1 activation was also mediating the sensitisation observed, the effect of the TRPV1 antagonist SB366791 was tested but it had no effect on AYPGKF-NH₂ induced firing. Again, the nociceptive effects of PAR4 appear to be divergent from PAR2 in that TRPV1 does not seem to be implicated.

Despite the abundance of PAR4 in joint tissue, the number of articles examining the role of PAR4 in arthritis is very limited. Further research is warranted given the promising results from the studies discussed and the completely unexplored avenue of PAR4 in neuropathic pain.

1.9 Aims, Objectives & Hypotheses

The objectives of this thesis were:

- 1) Characterise pain in the MMT model of post-traumatic osteoarthritis in male and female rats, and
- 2) Assess the involvement of PAR4 in mediating pain and inflammation in early and late stages of experimental OA, and
- 3) Determine the effect of human arthritic synovial fluid on joint nociceptors and whether PAR4 mediated the effects of synovial fluid

Our central hypothesis was:

In the MMT model of PTOA, female animals would experience an enhanced pain phenotype compared to males and that PAR4 would mediate this pain.

Chapter 2: Methods

2.1 Animals

All experimental protocols were approved by Dalhousie University Committee on the Use of Laboratory Animals, which follows standards mandated by the Canadian Council for Animal Care and acts in accordance with the ARRIVE (Animal Research: Reporting of In Vivo Experiments) guidelines. Animal ethics protocols: 16-122, 18-133, and 19-119.

Male and female Wistar rats (Charles River, Quebec, Canada) arrived at the Carelton Animal Care Facility at Dalhousie University in Halifax, Canada where they acclimated for a minimum of one week in the facility prior to introduction of an animal into a study. The rats were housed in pairs of the same sex in ventilated cages at 22°C ± 2°C on 12:12 hour light:dark cycles (light-on from 7:00-19:00). Cages were lined with woodchip bedding and Enviro-dri nesting material and animals were provided with environmental enrichment. Standard lab chow and water were provided *ad libitum*.

2.2 Animal Models

2.2.1 Medial Meniscal Transection Surgery and Sham Surgery

Male and female Wistar rats were anaesthetised using isoflurane (2.5-4%; 100% O₂ at 0.8L/min) to maintain the cessation of both flexor withdrawal and eye blink reflexes. Ocular lubricant was applied throughout the surgery to prevent corneal irritation. The right hindlimb was shaved, cleaned three times with chlorohexidine, and swabbed with 70% ethanol and betadine in triplicate to disinfect the surgical field.

With the right leg held in an extended position, the joint space was visualised, and a scalpel was used to make a 7mm incision in the skin on the medial aspect of the knee (Figure 2.1). Reflection of the skin and gentle blunt dissection of tissue beneath revealed the medial collateral ligament (MCL). The MCL was subsequently cut in the mid-substance to expose the medial meniscus which is located between the tibial plateau and femoral head. With light palpation of the tibia, the medial meniscus was transected mid-substance; the newly severed anterior and posterior sections were checked to ensure they were both freely mobile and that the transection was complete. Care was taken not to damage the articular cartilage of the tibial plateau with the scalpel.

Sham surgery consisted of blunt dissection to visualise the MCL, but neither the MCL nor the medial meniscus were transected.

All skin incisions were closed with 5-0 non-absorbable poly-propylene sutures (Ethicon, New Jersey, United States) and animals were treated with sustained release buprenorphine (1.2 mg/kg; Chiron Compounding, Ontario, Canada) that lasted 48-72 hours. Animals were allowed a minimum of seven days to recover before any testing commenced.

2.2.2 Monoiodoacetate Model Induction

Male Wistar rats were deeply anaesthetised with isoflurane (2.5-4%; 100% O₂ at 0.8L/min) until cessation of paw-withdrawal and eye-blink reflexes. Ipsilateral knee joints were shaved and cleaned three times with chlorohexidine. Alternating swabs of 70% ethanol and betadine acted as an anti-septic. Sodium monoiodoacetate (MIA: 3 mg in 50 µL of saline) was injected into the knee joint capsule (intra-articular; i.artic.)

through the patellar ligament. The knee was then manually extended and flexed for 30 seconds to disperse the solution throughout the joint capsule. Animals were allowed a minimum of three days to recover before any testing commenced.

2.3 Single Unit Electrophysiology

2.3.1 Surgical Preparation

Single unit joint afferent fibres were measured using electrophysiology. Male and female Wistar rats were deeply anaesthetised with urethane (25% in saline, 2 g/kg i.p.) until a surgical plane of anaesthesia was reached as measured by ablation of sensory reflexes. Core body temperature was measured via a rectally-inserted thermometer and maintained at 37°C by a thermostatically-controlled heating blanket (CWE Inc, Pennsylvania, United States). In a supine position, an incision was made in the neck and the trachea was exposed and cannulated to allow for artificial ventilation with a Harvard rodent respiratory pump (100% O₂ stroke volume: 2.5 ml; respiratory frequency: 52 breaths/min) (Harvard Apparatus, MA, USA). A heparinised saline-filled cannula was inserted into the carotid artery to allow for continuous measurement of mean arterial blood pressure using a pressure transducer and monitor (World Precision Instruments, Florida, United States). Finally, the jugular vein was similarly cannulated to allow for administration of the muscle relaxant gallamine triethiodide (50 mg/kg) which acted to minimize neural activity of hindlimb musculature that would interfere with the joint recordings.

A specialized clamp was attached to the femur and used to both immobilise the hip joint and also anchor the lower limb to a stereotaxic frame. The ipsilateral paw was

placed in a specialized boot connected in series with a force transducer and torque meter (Data Track 244-1-R, Intertechnology, Ontario, Canada). The boot acted to immobilise the ankle joint. With both the hip joint and ankle joint fixed, rotation of the boot applied torque directly to the knee joint which was recorded on a torque meter.

A 5 cm longitudinal incision was made in the skin of the medial aspect of the hindlimb extending from the inguinal region to below the knee joint. The skin was reflected and sewn onto a metal O-ring suspended above the limb thereby creating a pool around the knee. This pool was subsequently filled with warmed mineral oil (37°C) to prevent tissue desiccation. The medial articular branch of the saphenous nerve was isolated, cut in the inguinal region to prevent spinal reflexes and cut distal to the knee to prevent sensory input from the lower limb. The isolated saphenous nerve was placed on a Perspex stage lowered into the pool and the epineurium was peeled back revealing the exposed nerve stump. Using fine-tipped Dumonts forceps, fine neurofilaments were teased apart and serially placed on a platinum recording electrode. The knee joint was gently probed with a rounded glass rod in order to identify afferents that innervated the knee joint rather than surrounding muscle or skin. Once a joint afferent had been identified, single unit extracellular recordings were then undertaken.

2.3.2 Single Unit Recordings

Once a joint afferent was identified, the mechanosensitivity of the fibre was assessed by determining the mechanical threshold, and responsiveness to non-noxious and noxious mechanical stimuli during ‘baseline activity’. First the mechanical threshold was determined by slowly rotating the knee until an action potential was generated. The

minimum torque required to elicit neuronal activity was designated the mechanical threshold. Non-noxious and noxious outward rotations were then applied to the knee and the number of action potentials produced during the rotations were counted (Figure 2.2). Non-noxious rotation was within the normal working range of the knee and would not be considered painful in an alert animal. Noxious rotation refers to torque occurring outside the normal working range of the knee, but not severe enough to cause soft tissue injury. These rotations lasted 5 seconds in duration, except in the case of synovial fluid experiments in which torque was maintained for 10 seconds. The same experimental design was consistently followed in that the baseline activity of the joint afferent was assessed via three sets of rotations separated by five-minute intervals. Following this baseline assessment, a test drug was administered either via a close-local intra-arterial injection into the saphenous artery or by intra-peritoneal injection. Rotations were then continued to determine if neuronal activity (movement-evoked action potentials) changed compared to baseline. The duration of time-courses changed in each experiment depending on the drug and route of administration used and specific details for each experiment are found in chapters 3-5.

Following completion of a recording, the electrical threshold and conduction velocity of the fibre were assessed. A pair of bipolar silver stimulating electrodes were applied to the receptive field of the fibre and current was applied (0.6Hz, 2ms pulse width, 1-6V) with increasing pulse voltage (0.25 V steps) until an action potential was elicited. The minimum electrical current needed to produce an action potential was denoted the electrical threshold of the fibre. The distance between stimulating and recording

electrodes was measured using a piece of suture and a ruler. The difference in time between when the stimulus was applied and an impulse was observed was determined using an oscilloscope (Figure 2.3). The conduction velocity was reported in metres per second (m/s) and calculated by the following equation:

$$\text{Conduction velocity} = \frac{\text{distance between stimulating and recording electrodes}}{\text{time}_{\text{stimulus applied}} - \text{time}_{\text{impulse recorded}}}$$

Joint afferents were categorized into nociceptive subtype based on their calculated conduction velocity; A δ (>2 m/s) or C (<2 m/s). In cases where electrical stimulation was not achieved, the subtype was categorized as ‘not determined’.

Single unit recordings were digitized using a data-acquisition system (CED Power1401; Cambridge Electronic Design, Cambridge, UK), recorded using Spike 2 software (Cambridge Electronic Design), and analysed offline.

2.4 Histology

The retrograde fluorescent tracer, Fluoro-gold (Fluorochrome, Denver, CO, United States) was utilized to label knee joint afferents. When injected into the knee joint, the dye is taken up by knee joint nerve terminals and retrogradely transported towards the DRG at a rate of approximately 2 cm/day. Five days after Fluoro-gold injection, DRGs were harvested and the cell bodies of neurones that project from the knee joint were visualised under wide band UV light (365 nm).

2.4.1 Fluoro-gold Labelling of Joint Afferents

Male and female Wistar rats were anaesthetised using isoflurane (2.5-4%; 100% O₂ at 0.8L/min) until cessation of sensory reflexes. The ipsilateral knee joint was shaved, cleaned with chlorohexidine, and swabbed with 70% ethanol. Using a Hamilton syringe, 10 µL of Fluoro-gold (2% solution in 0.9% saline) was injected i.artic. through the patellar ligament five days before the model (histological) endpoint. The knee was subsequently flexed and extended to disperse the dye through the joint capsule.

Five days following Fluoro-gold injection, the animals were again deeply anaesthetised with isoflurane (4-5%; 100% O₂ at 0.8L/min). Once sensory reflexes were ablated, the chest cavity was exposed, and the animals were transcardially perfused with 120 mL of 0.9% saline followed by 120 mL of 4% paraformaldehyde. Ipsilateral L3-L4 DRGs were harvested and placed in paraformaldehyde overnight at 4°C. DRGs were then cryoprotected by serial incubations in 20% and 40% sucrose for 5 days each. Tissues were embedded in optimal cutting temperature (OCT) compound (Sakura Finetek, Torrance, CA, USA) within plastic molds and stored at -20°C until specimen sectioning.

2.4.2 Immunohistochemistry of DRG tissue

DRGs were sectioned at 12 µm using a HM525 cryostat (ThermoFisher Scientific, Waltham, MA, USA). Five non-consecutive sections were mounted on Superfrost Plus slides (Fischer Scientific, Nepean, Ottawa, Canada) and stored at 4°C until fluorescently stained.

The expression of epitopes of interest by Fluoro-gold-labelled neurones were assessed using commercially available antibodies. DRG sections were first treated with 10% normal goat serum (NGS) in phosphate buffered saline (PBS) to block non-specific

binding sites on the tissue. Following washing with PBS, the tissue was incubated with primary antibodies against cleaved caspase-3, glial fibrillary acidic protein (GFAP), or PAR4, all diluted in a 1% NGS solution and stored overnight at 4°C. Following four washes with PBS, the DRG tissues were incubated with secondary antibodies for one hour in the dark, washed and mounted with Fluoromount-G mounting medium (Invitrogen, Carlsbad, CA, USA). Details regarding species and concentrations of primary and secondary antibodies are found in chapters 3 and 4. Positive and negative control experiments were carried out for immunohistochemistry experiments. As a negative control, primary antibodies were omitted from the assay protocol. Spinal cord tissue was stained for epitopes of interest as positive immunoreactivity has been shown in this tissue.

Slides were viewed with a Zeiss Axio Imager 2 (Zeiss, Oberkochen, Germany) at 10x magnification. Photomicrographs were taken using an AxioCam HRm camera (Zeiss, Oberkochen, Germany) and analysed offline using Image J software. The total number of Fluoro-gold-positive neurones were counted and the percentage that expressed cleaved caspase-3 or PAR4 were calculated. Additionally, the number of double labelled Fluoro-gold and caspase-3 positive neurones that were associated with GFAP-positive satellite glial cells was recorded.

2.5 Saphenous Nerve Electron Microscopy

Transverse sections of the saphenous nerve were visualized using electron microscopy (EM) to assess axon morphology, myelin integrity and myelin thickness,

These parameters would determine whether neuropathy was present in MMT, sham-operated, and MIA animals.

Briefly, animals were deeply anaesthetised using isoflurane (2.5-4%; 100% O₂ at 0.8L/min) until cessation of sensory reflexes. A longitudinal incision was made in the skin of the ipsilateral hindlimb and a ~ 5mm section of the saphenous nerve proximal to the knee joint was gently dissected free from the surrounding tissue and harvested. The nerve segment was fixed in a solution of 2.5% glutaraldehyde in 0.1M sodium cacodylate buffer (pH 7.3) for seven days at 4°C. Further preparation for EM was carried out by Mary Ann Trevors in the Electron Microscopy Lab through the Faculty of Medicine Cores Facilities at Dalhousie University.

Additional fixation was achieved with incubation of the nerves in 1% osmium tetroxide for 2 hours. An *en bloc* stain with uranyl acetate (0.25%) was carried out overnight at 4°C to provide additional stability to tissue membranes and improve protoplasmic contrast [261]. The samples were then dehydrated in a graded series of acetone (50%, 70%, 95%, and 100%). Epon araldite resin was used to embed the saphenous nerves. The samples were subjected to increasing concentrations of acetone/resin solutions. The first mixture was a 3:1 ratio of dried 100% acetone to resin for 3 hours, which was followed by a 1:3 ratio of dried 100% acetone to resin overnight. Finally, the nerves were embedded in 100% Epon araldite resin for 3 hours and cured in an oven at 60°C for 48 hours. Saphenous nerves were sectioned at 100nm thickness using LKB Huxley ultramicrotome fitted with a diamond knife. Transverse slices of nerves were placed onto a copper wire grid consisting of 300 individual squares per inch (each square measuring 83µm x 58µm) that would later be loaded into the electron microscope.

The sections were stained with the electron dense heavy metals, uranyl acetate (2% aqueous solution for 10 minutes) and lead citrate (3% aqueous solution for 4 min) and stored at room temperature until viewing.

To visualise the saphenous nerve axons, the copper wire grids were inserted into a JEOL JEM 1230 transmission electron microscope (JEOL Corp. Ltd., Tokyo, Japan). Using the 3X3 copper grid as a backdrop, the cross-section of the saphenous nerve could be easily partitioned into nine quadrants. To ensure equitable sampling from each nerve section, three photomicrographs were captured (from quadrants one, five, and nine) at 2500x magnification using a Hamamatsu ORCA-HR digital camera (Hamamatsu Photonics, Hamamatsu City, Japan) (Figure 2.4). The photomicrographs were analysed offline in a blinded fashion using ImageJ processing software. Myelin integrity was assessed whereby axons that had disrupted or extruding myelin were considered damaged and non-damaged axons were fibres that were surrounded by compact and uniform myelin. The G-ratio was calculated as a measure of myelin thickness using the equation $G = \sqrt{\frac{a}{A}}$ where a is the internal axonal area, and A is the total axonal area of the fibre (Figure 2.5). The larger the G-ratio, the thinner the myelin around the axon. Fibres were classified as small diameter (internal axonal diameter < 3µm) or large diameter (internal axonal diameter > 3µm) for G-ratio calculations. Previous studies in rat have used 3 µm as the as the cutoff for small diameter axons (presumably Aδ fibres) [262].

2.6 Joint Histopathology

Following terminal experiments ipsilateral knee joints were excised from male and female Wistar rats from MMT and sham-surgery animals. Fixation of joint tissue was

achieved by a seven-day incubation in 4% paraformaldehyde at room temperature. For longer term storage, joints were transferred to 70% ethanol.

Decalcification, sectioning, staining, and scoring of joint tissue was carried out by Bolder Biopath (Boulder, CO, United States). Tissues were decalcified in 5% formic acid for 4-5 days and subsequently cut in two coronally prior to paraffin embedding. Three sections from each half were cut at approximately 160 μ m steps and stained with toluidine blue. The joint half with the most damage was used for scoring using a modified OARSI scoring system (Appendix A). Measures of joint OA included cartilage degeneration, presence of osteophytes, subchondral bone damage, and synovitis. All measurements were scored on a five-point scale where zero was no damage and five was the most severely damaged. Tibial and femoral cartilage degeneration scores were calculated by examining proteoglycan loss and collagen damage for the outer, middle and inner zones of the joint. The cartilage damage score was calculated for each zone and the sum of all zones was calculated. Osteophytes were scored according to size, ranging from < 200 μ m which was scored zero and > 600 μ m which scored the highest ranking of five. Only the largest osteophyte was scored. A 'total joint score' was also calculated and consisted of the sum of the cartilage degeneration and the osteophyte score. Subchondral bone damage included the loss of subchondral bone, fragmentation of calcified cartilage, and an increase in the number of basophilia. The synovium was examined for infiltration of mononuclear cells and hyperplasia as indicators of synovitis. Additionally, to account for sex-differences in the thickness of cartilage between male and female animals, the depth of cartilage lesions was measured and normalised by dividing by the thickness of undamaged cartilage.

2.7 Pain Behaviour

von Frey hair algesiometry and dynamic incapacitance experiments were carried out concurrently on the same groups of either male or female Wistar rats. Animals of the opposite sex were not tested on the same day.

2.7.1 von Frey Hair Algesiometry

von Frey hair algesiometry testing was carried out to measure secondary mechanical allodynia in male and female Wistar rats. Animals were placed in a clear Perspex chamber (31.5 cm long x 9.5cm wide x 24cm tall) with metal mesh flooring (Figure 2.6) (Concept Plastics, Dartmouth, Nova Scotia, Canada). Animals acclimated to the testing chamber for 10-15 minutes until exploratory behaviour had ceased. Mechanosensitivity of the ipsilateral hindpaw was assessed using a graded series of six von Frey hairs (North Coast Medical, Gilroy, California, USA), which increase in bending force (2, 4, 6, 8, 10, and 15g) when applied to the paw. A modified version of the Dixon's up-down method [263] was used to assess mechanosensitivity. Starting with the lightest filament (2g), the hair was applied to the plantar surface of the hindpaw, avoiding the toe pads, until the hair bent. The filament was held for up to 3 seconds or until a positive response was elicited. If the animal responded with paw withdrawal and licking or shaking of the paw, this was deemed a 'positive response' and the next lower force hair was applied. If the animal did not respond to the hair, the next higher force hair was applied to the paw in the same fashion up to a 15g cutoff. The withdrawal threshold was calculated using the following formula:

$$\text{Withdrawal threshold} = 10^{[X_f + k\delta]} / 10,000$$

Where X_f = value (in log units) of the final von Frey hair used, k = tabular value for the pattern of the last 6 positive/negative responses, and δ = mean difference (in log units) between stimuli. The unit for withdrawal threshold is gram (g).

2.7.2 Dynamic Incapacitance

Following each von Frey hair testing, animals underwent hindlimb incapacitance assessment which is a measure of spontaneous, non-evoked pain (Figure 2.7). Animals were placed in a Perspex chamber (24cm long x 24cm wide x 32cm tall) (model BIO-DWB-AUTO-R, Bioseb, Boulogne, France) with a pressure sensitive floor. An overhead camera (DFK22AUC03 ImagingSource, Charlotte, NC, USA) was used to track animal movement. Animals were allowed to freely move throughout the chamber for three minutes while dynamic weight bearing measurements and contemporaneous video were recorded. Videos were analyzed offline to calculate the percentage weight borne on the ipsilateral hindlimb relative to the weight borne on the contralateral hindlimb.

2.8 Inflammatory Measurements

2.8.1 Surgical Preparation

Laser speckle contrast analysis (LASCA) and intra-vital microscopy (IVM) experiments were carried out consecutively in the same animals to assess inflammation. The surgical preparation carried out on an animal preceded both inflammatory measurements described below. Male Wistar rats were deeply anaesthetised using urethane (25% solution; 2g/kg i.p.) until cessation of sensory reflexes was confirmed. In a

supine position, a longitudinal incision was made in the neck to expose the trachea, which was cannulated with PE-200 tubing to permit unrestricted breathing. Core body temperature was measured via a rectally-inserted thermometer and maintained at 37°C by a thermostatically-controlled heating blanket (CWE Inc, Pennsylvania, United States). To allow for continual measurement of mean arterial pressure (MAP), the right carotid artery was cannulated, and blood pressure was recorded at each experimental timepoint. To prevent clotting within the cannula which would impede MAP measurement, the vascular conduits were flushed with 0.1% heparinised saline. The right jugular vein was cannulated with PE-50 tubing to allow for the administration of the nucleic stain Rhodamine 6G (0.05% in saline) which permitted the visualization of leukocytes *in vivo* under 590 nm fluorescent light. Finally, the ipsilateral knee was exposed by surgically removing the overlying skin and superficial fascia. Physiological buffer (135mM NaCl, 20mM NaHCO₃, 5mM KCl, 1mM MgSO₄*7H₂O, pH =7.4; 37 ± 1°C) was continuously perfused over the exposed joint to prevent tissue desiccation throughout the experiment.

2.8.2 Laser Speckle Contrast Analysis (LASCA)

The blood tissue perfusion of the exposed knee joint was measured in real time using a PeriCam PSI System (Perimed Inc., Ardmore, PA, USA) (Figure 2.8). Briefly, the exposed knee was placed at a working distance of 10 cm beneath the scanner head of the PeriCam PSI System. A 785 nm laser was directed over the exposed microcirculation of the joint, the backscatter of which created a speckle pattern. One-minute recordings of the exposed knee joint were taken with a frame capture rate of 25 images per second. Using dedicated software (PIMSoft, Version 1.5.4.8078), images were averaged to generate a

compressed 1 perfusion image per second. This pattern was stored offline and analyzed for blood flow. While a static object would generate a constant speckle pattern over time, a moving object (*i.e.* circulating erythrocytes) would cause a speckle pattern which fluctuated over the course of a recording.

At the end of the experiment rats were euthanized with euthansol (100 μ l, intracardiac) and a final recording called the ‘dead scan’ of the knee was taken. The purpose of the ‘dead scan’ was to account for any Brownian motion in the microvasculature. This “biological zero” value was subtracted from all measurements prior to analysis. Images were analysed offline where a defined region of interest approximating the knee joint was highlighted and the mean blood perfusion therein was calculated. To account for differences in MAP, which would influence tissue perfusion, vascular conductance was calculated at each timepoint by the following equation:

$$C = Q/P$$

Where C is vascular conductance, Q is mean perfusion, and P is MAP. The arbitrary unit of perfusion units (PU) was used for vascular conductance values.

2.8.3 Intra-vital Microscopy (IVM)

Intravital microscopy (IVM) was used to assess leukocyte trafficking within the microcirculation of the knee joint, as described previously [264]. Straight, unbranched post-capillary venules were identified using a Leica DM2500 microscope under 200X magnification. The i.v. administered rhodamine 6G accumulated in mitochondria and acted as a fluorescent marker for microvascular leukocytes [265]. Incident 590nm light caused excitation of the rhodamine 6G-labelled leukocytes causing them to fluoresce

which allowed for easy visualization as the cells moved through the synovial microcirculation. Three one-minute fluorescent videos were captured for each time point using a Leica DFC 3000 camera (Leica Microsystems Inc., Ontario, Canada). Videos were analysed offline for leukocyte trafficking.

Leukocytes were stratified by their leukocyte-endothelial interactions and quantified to assess articular inflammation. Two types of leukocyte activity were counted: (i) rolling leukocytes and (ii) adherent leukocytes. Rolling leukocytes were defined as positively-stained blood cells travelling slower than the surrounding blood flow. They were counted by drawing an arbitrary line perpendicular to the venule and counting the number of leukocytes moving across that line during one minute. Adherent leukocytes were defined as positively-stained cells that remained stationary for a minimum of 30 seconds. These leukocytes were quantified by counting the number of cells that remained stationary within a 100 μ m length of the venule.

2.9 Measurement of Protein Analytes in Rat Serum

Several cytokines, β -endorphin, and noradrenaline were measured in the serum of Wistar rats from different experimental models, sexes, and timepoints. A Luminex assay and an Enzyme Linked Immunosorbent Assay (ELISA) were used to quantify serum concentrations of the specific analytes. The experimental protocol for harvesting blood, extracting and subsequently storing serum was the same for both assays. Following terminal experiments, intra-cardiac blood samples were taken and stored for a minimum of 20 minutes at room-temperature prior to centrifugation (2000xg) and serum isolation. The serum samples were stored at -20°C until testing.

2.9.1 *Luminex*

Luminex assays were utilized to measure serum cytokines from different experimental models and timepoints in male and female Wistar rats. Serum samples were thawed over ice, aliquoted (25 μ L), and the concentrations of five cytokines (IL-17A, IL-1 β , IL-10, IL-6, and TNF- α) were measured using a Luminex microbead-based suspension array (Invitrogen, Carlsbad, CA, USA). Samples were deposited onto a 96 well plate and assessed using the manufacturer's processing protocol. The plate was read using a Bio-Plex 200 system (Bio-Rad, Hercules, California, USA) and analyzed using Bio-Plex Manager 6.0 software (Bio-Rad, Hercules, California, USA). Samples were run in duplicate and mean values were calculated.

2.9.2 *Enzyme Linked Immunosorbent Assay*

ELISAs were used to measure serum noradrenaline (Biomatik, Cambridge, Canada) and β -endorphin (Novus Biologicals, Oakville, Canada) in male and female Wistar rats. Serum samples were thawed over ice, and the manufacturer processing instructions were followed. A FLUOstar Omega plate reader (BMG Labtech, Ortenberg, Germany) was used to measure the absorbance of enzyme-conjugated antibodies in the samples in each respective plate. Samples were run in duplicate and mean concentration values were calculated.

2.10 *Mass Spectrometry*

Two synovial fluid samples were used in these analyses. The osteoarthritic sample was from a 64-year old man. The rheumatoid arthritis sample was from a 58-year old

woman. Both samples were diluted 1:1 in serum-free macrophage medium upon joint aspiration (Figure 2.10).

Synovial Fluid protein content was measured using a Coomassie Bradford assay (Thermo Fisher Scientific, Waltham, MA, USA). Aliquots of OA and RA synovial fluid containing 100 µg of protein were dissolved in 500 mM ammonium bicarbonate and denatured using 8M urea. Cysteine residues were reduced using 10 mM dithiothreitol and alkylated using 60 mM iodoacetamide. Overnight digestion was carried out using the bacterial endoprotease Glu-C (Promega) at 37°C. Digested peptide solutions were desalted using hydrophilic-lipophilic-balanced reverse phased cartridges (Waters, Milford, MA), dried by SpeedVac and stored at -80°C.

Peptides were resuspended in 20µl Mobile Phase A prior to LC-MS/MS analysis. Briefly, peptides were fractionated using an Ultimate 3000 nanoRSLC chromatograph and underwent untargeted tandem mass spectrometry using the Q-Exactive Orbitrap mass spectrometer in the Dalhousie Biological Mass Spectrometry Cores Facility. Protein identification was performed using the Proteome Discoverer 2.1 software. Data are presented as relative abundance of protein.

Metascape [266] was used to classify the molecular mechanisms of the proteins found in the RA and OA synovial fluid. The proteins were screened against pathways in common ontology catalogs including: the Gene Ontology (GO) consortium, Reactome gene sets, BioGrid, and OmniPath. Enriched pathways (containing ≥ 3 proteins) were reported in a heatmap generated by Metascape. To elucidate potential protein associations, such as functional and physical interactions, a string network was generated by inputting the entire data set of synovial fluid proteins into the String Consortium

software (October 18, 2020). Functional and physical interactions between the proteins found in the synovial fluid were inspected by screening against relevant curated human datasets and against Pubmed publications that included our proteins of interest. A level of ‘high confidence’ was set as the minimum threshold to include an interaction.

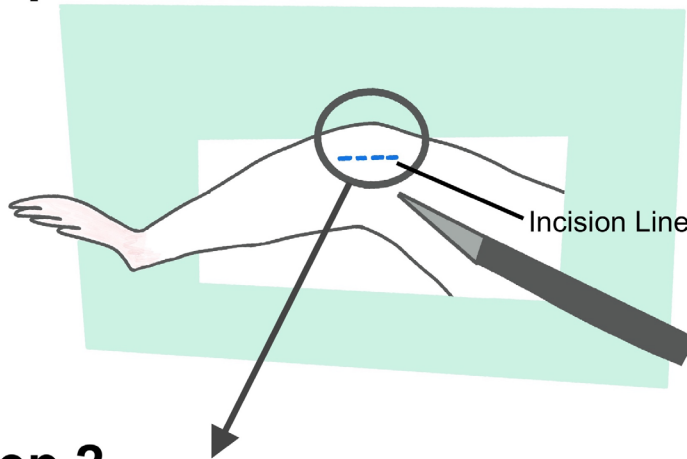
2.10 Materials

Found in Appendix B.

2.11 Statistical Analysis

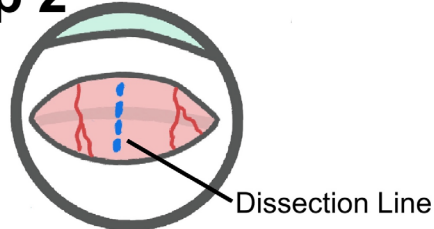
Data are presented as either median with interquartile ranges (IQR) or mean \pm standard error of the mean (SEM). Joint histopathology is presented as median with IQR as the data were ordinal. Data were tested for Gaussian distribution by examining the residuals in Quantile-Quantile (QQ) plots. Joint histopathology and spontaneous firing data were non-parametric and therefore analysed using the Kruskal- Wallis test. All other experimental data (behavioural pain, G-ratio, Luminex, ELISA, immunohistochemistry, electrophysiology, LASCA, and IVM) were normally distributed and were analysed using parametric statistics. Depending on the nature of the experiment, either an unpaired Student’s t-test, 1-way analysis of variance (ANOVA), or a 2-way repeated measures (rm) ANOVA was employed. Variables in parametric testing included sex, treatment, and time, the latter of which was treated as a repeated measure when the same animals were tested. ‘Treatment’ included experimental model, drug, or experimental timepoints when different cohorts of animals were used. A *p* value less than 0.05 was considered statistically significant.

Step 1



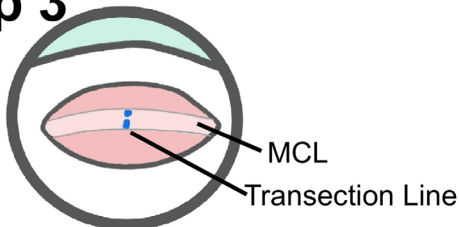
**Medial skin
incision over
the knee joint**

Step 2



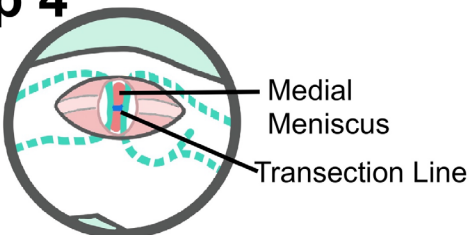
**Blunt dissection of
tissue overlying MCL**

Step 3



**Transection of MCL
exposing the medial
meniscus**

Step 4



**Midsubstance
transection of the
medial meniscus**

Figure 2. 1 Procedure for MMT and Sham Surgeries.

An illustration of an anaesthetised animal undergoing MMT or sham surgery. MMT surgery consisted of steps 1-4 while sham surgery followed steps 1 and 2. Following both surgeries the incision was closed with polypropylene sutures.

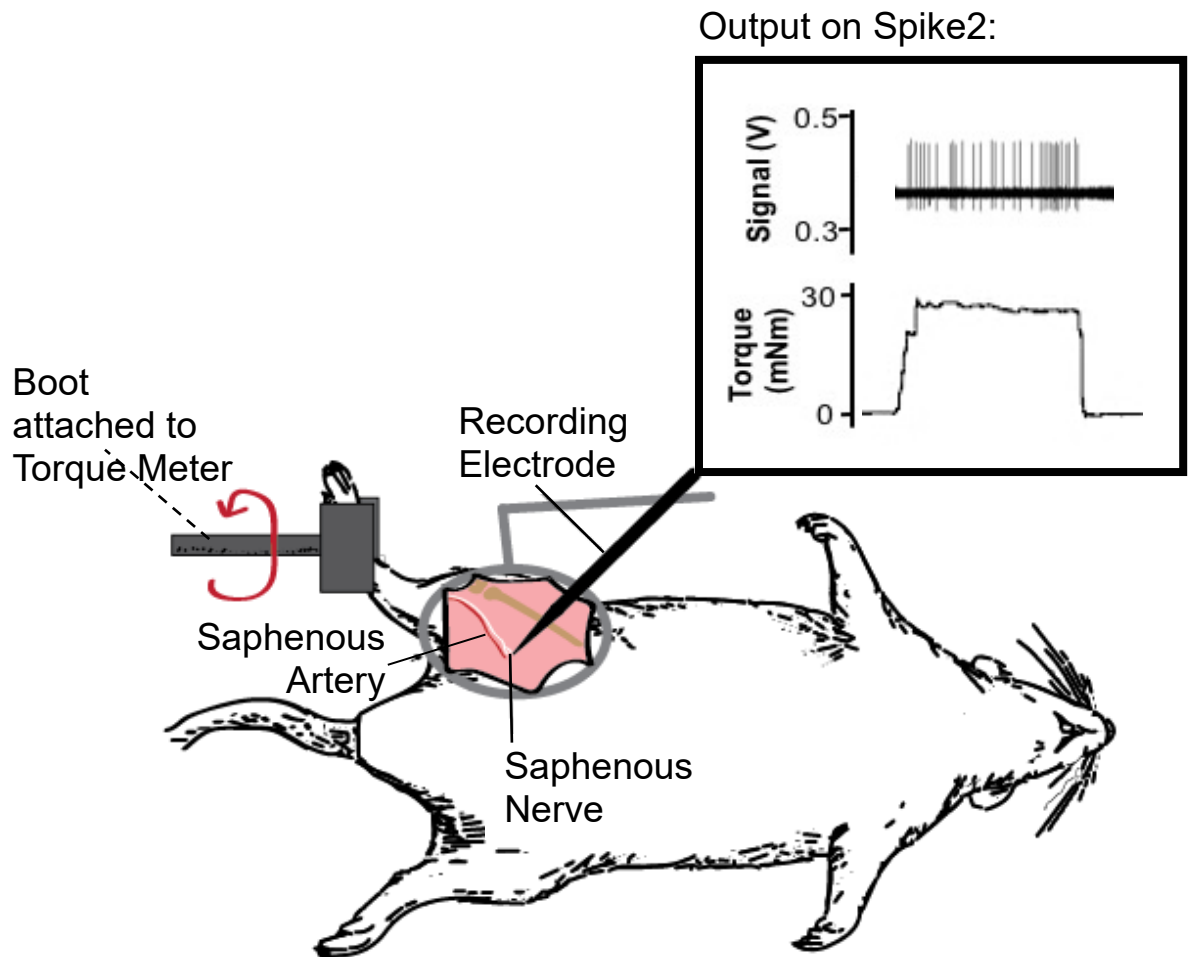


Figure 2. 2 Single Unit Electrophysiology Set-up for Joint Afferent Recording.

The skin over the ipsilateral knee of an anaesthetised animal was reflected and sewn into a metal O-ring creating pool which was filled with warm mineral oil. A teased neurofilament from the saphenous nerve was placed over the recording electrode and following rotation of the boot attached to the torque meter, action potentials were evoked. The evoked firing and corresponding readout from the torque meter as seen using Spike 2 software are depicted.

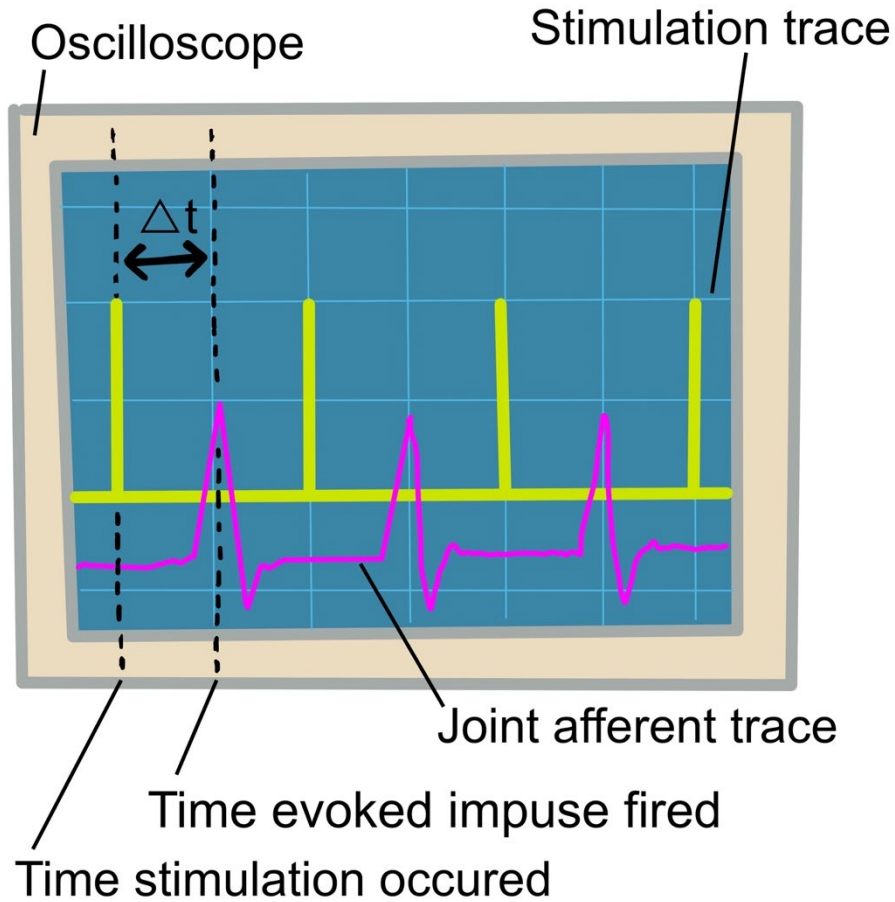


Figure 2. 3 Single Unit Conduction Velocity Measurement on an Oscilloscope.

An oscilloscope displaying electrical pulses applied to the receptive field of a single unit (*stimulation trace*, yellow) and the resulting impulse recorded from the afferent (*single unit trace*, pink). The time between the peak of the stimulation artefact and the resulting impulse are marked with a dotted line to illustrate how Δt is obtained for conduction velocity calculations.

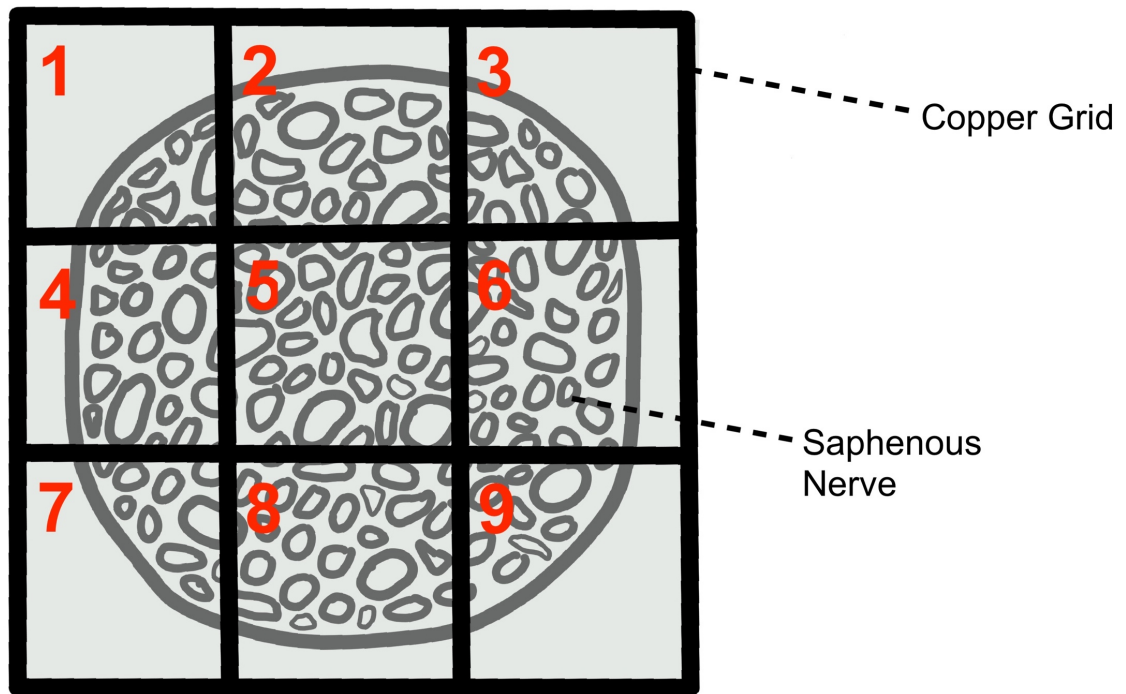


Figure 2. 4 Saphenous Nerve Orientation on Copper Grid for Electron Microscopy Analysis.

The illustration depicts a cross-section of the saphenous nerve on a copper grid as viewed under an electron microscope. The nerve was partitioned across nine quadrants of the grid and photomicrographs of quadrants 1, 5, and 9 were taken to sample the nerve fibre.

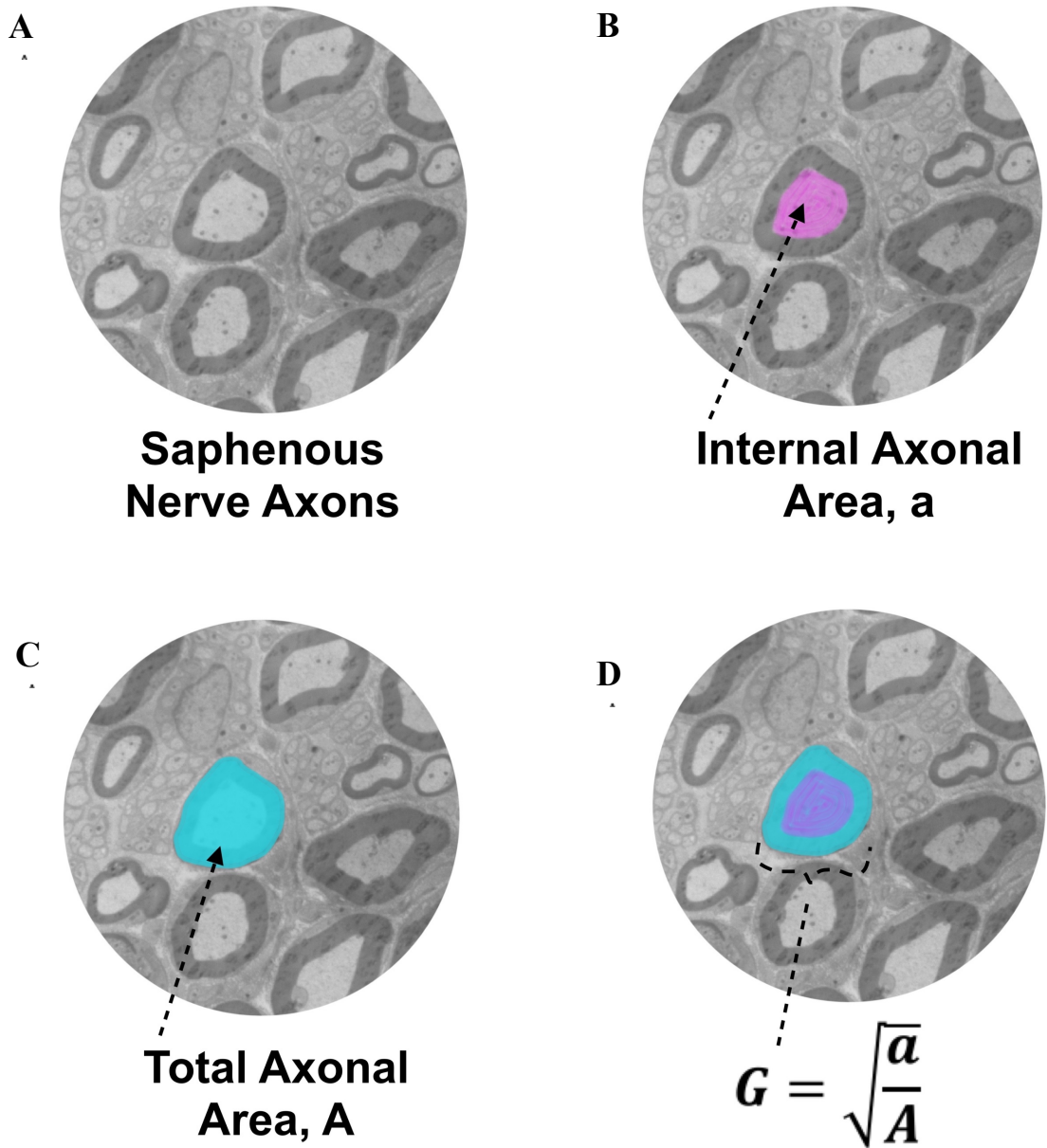


Figure 2. 5 G-ratio Analysis of Saphenous Nerve Axons.

The G-ratio of saphenous nerve axons (A) was determined by measuring the internal axonal area (shown in B), and the total axonal area (shown in C) and calculating the G-ratios (shown in D). G-ratios are unitless and a ratio approaching 1 indicates decreasing myelin thickness.

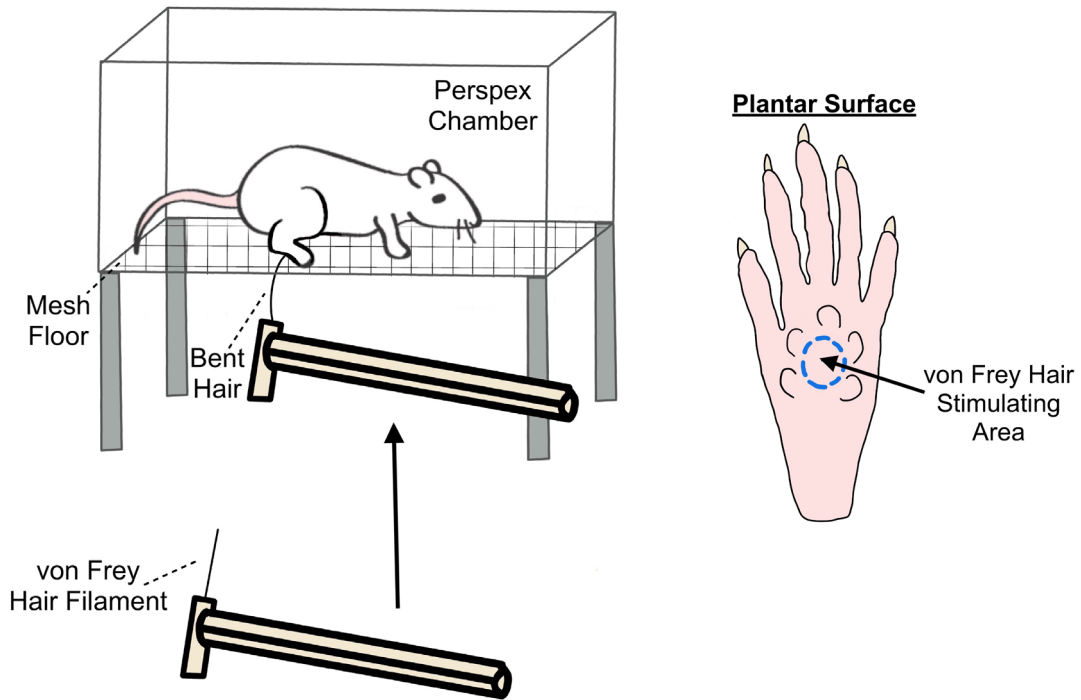


Figure 2. 6 Set-up for von Frey Hair Algesiometry Assessment.

A Wistar rat was placed in a clear Perspex chamber with a mesh floor. A von Frey hair filament was applied to the plantar surface of the ipsilateral hindpaw until the hair bent. On the right, the von Frey hair application area is shown. Care was taken to avoid the toe pads and to apply the force to the volar surface of the hindpaw. The filament was applied for 3 seconds

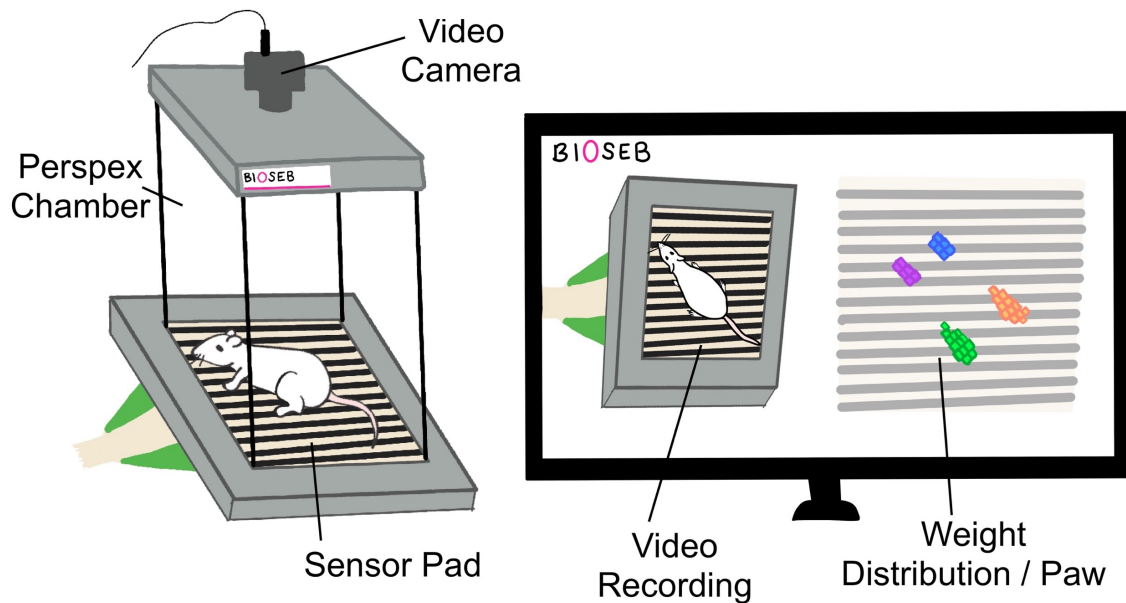


Figure 2. 7 Dynamic Incapitance Assessment of Hindlimb Weightbearing.

An animal was allowed to move freely around a Perspex chamber containing a pressure-sensitive pad. The video camera above recorded the animal over a 3-minute testing period during which dynamic weight bearing data were recorded. An example of the video recording and image output is portrayed at right. The weight distribution for each paw was determined throughout the testing period allowing for the calculation of the percentage weight borne on the ipsilateral hindlimb relative to the weight borne on the contralateral hindlimb.

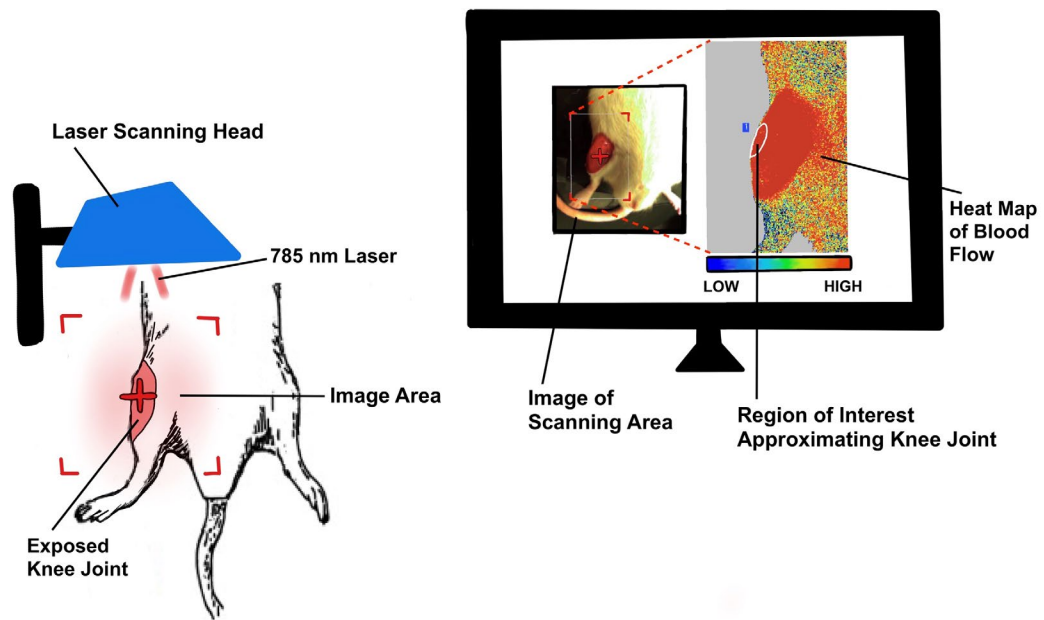


Figure 2. 8 Set-up of LAsER Speckle Contrast Analysis (LASCA) Assessment of Joint Blood Flow.

Joint blood flow was measured in an anaesthetised animal using LASCA. A 785 nm laser was directed towards the exposed knee joint, and the back-scattered photons created a speckle pattern. Proprietary software was used to create a perfusion map (right) which represents relative blood flow. A region of interest that approximated the area of the knee joint was used to calculate articular blood flow.

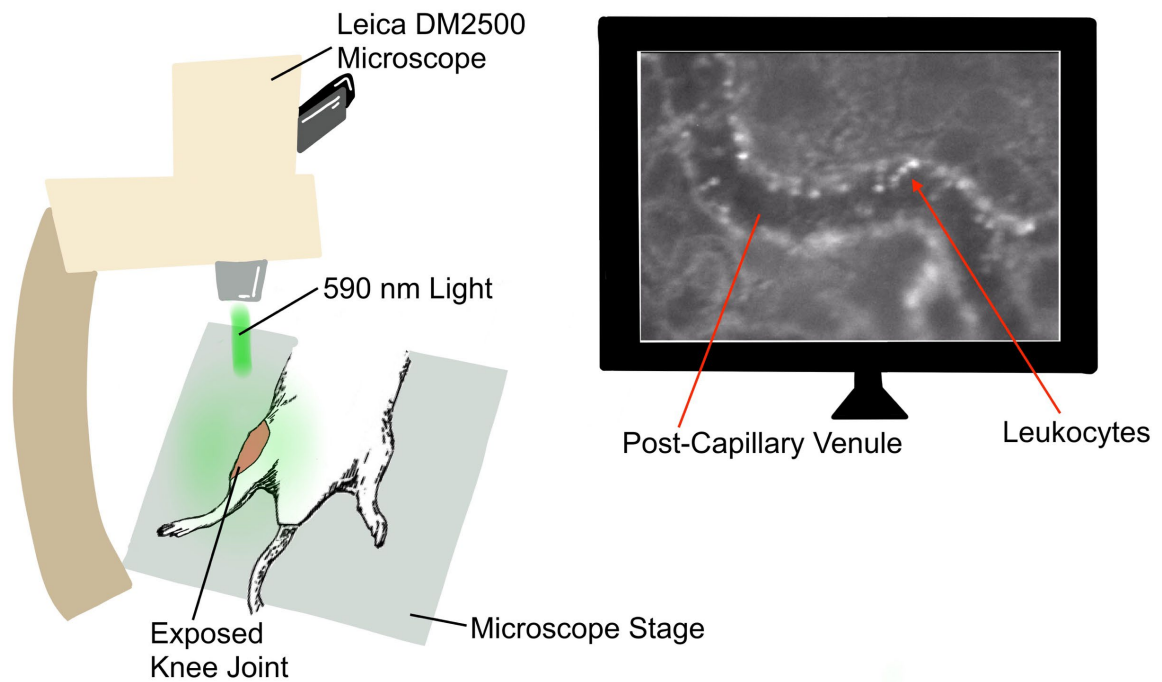


Figure 2. 9 Depiction of Intravital Microscopy (IVM) Measurement.

The illustration portrays an IVM experiment where leukocyte trafficking was recorded in an anaesthetised animal. A Leica DM2500 microscope with 590 nm incident light was used to visualize fluorescent leukocytes as they migrated through the synovial microcirculation. The computer screen depicts a still from a video of a post-capillary venule with positively stained leukocytes.

Synovial Fluid extraction and aliquoting:

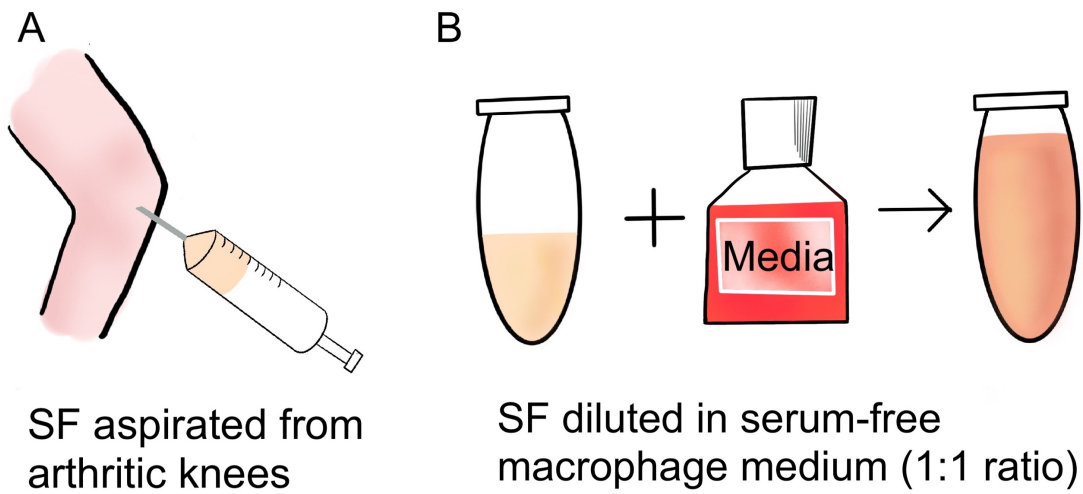


Figure 2. 10 Synovial Fluid Sampling.

Synovial fluid samples were aspirated from a male OA patient and female RA patient (A). Samples were diluted 1:1 in serum-free macrophage medium and stored at -80°C (B).

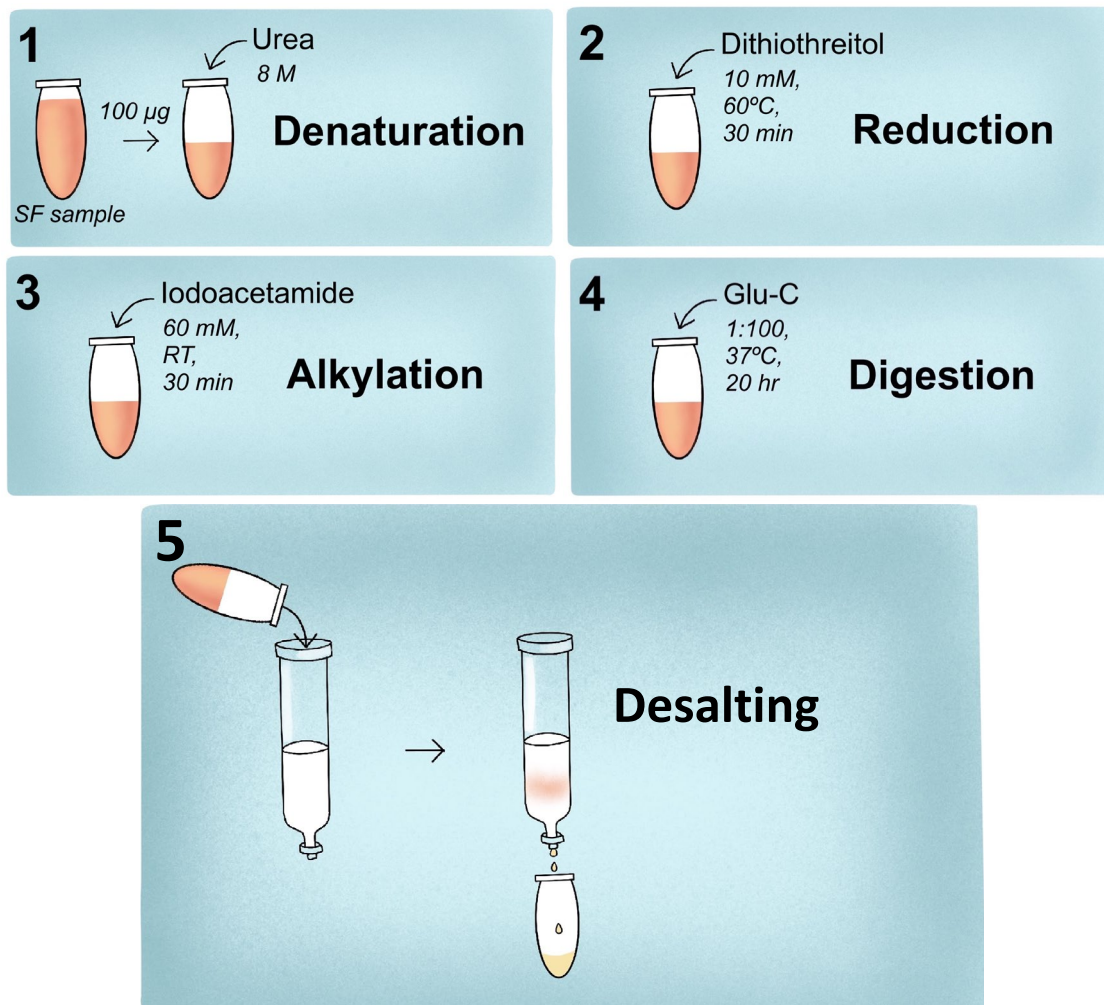


Figure 2. 11 LC-MS/MS Sample Preparation.

Synovial fluid samples were aliquoted and first denatured using urea (1). Serial reduction and alkylation were carried out with dithiothreitol (2) and iodoacetamide (3), respectively. Overnight digestion was carried out with the protease Glu-C (4) before sample desalting and clean-up (5).

Chapter 3: Nociceptive Characterisation of the MMT Model of PTOA

Disclosures: Data from this chapter have been published in O'Brien, MS & McDougall, JJ., 2020; Osteoarthritis & Cartilage.

3.1 Background and Hypotheses

Osteoarthritis (OA) does not affect males and females equally. Approximately 10% of men and 20% of women over the age of 60 years old suffer from OA while prevalence is increasing in younger adults [1]. In addition to the occurrence of OA being greater in women, their pain scores are also higher than men with the same level of joint damage [267].

Preclinical animal models serve as useful tools to study disease pathogenesis and provide target validation. Despite clear sex differences in the presentation of OA, female rodents have rarely been used in pre-clinical OA pain studies until recently. Thus, most pain mechanisms have been elucidated in males which have been shown to have a different pain neurobiology from females [171]. Therefore, a comparison of OA pain circuitry between the sexes requires further investigation.

Traumatic joint injury is a risk factor for the development of OA. For example, a meniscal tear or extrusion alters joint biomechanics that can lead to cartilage degeneration and an increased risk for the development of PTOA [33]. The prevailing clinical evidence suggests that the pain phenotypes associated with PTOA likely consist of nociceptive, inflammatory, and neuropathic components [268, 269]. Understanding the relative contribution of each type of pain is important since they require different classes of analgesics to treat effectively.

The MMT model of PTOA involves transection of the medial meniscus and the medial collateral ligament. Despite the widespread use of the MMT model, its underlying

neurophysiology has not been thoroughly examined. Furthermore, the effect of MMT surgery on female nociception has not been studied.

The aim of the present study was to characterise the peripheral nociceptive pathway in the MMT model. The possible presence of sex-differences and peripheral neuropathy were also examined.

Hypotheses Evaluated in this Study:

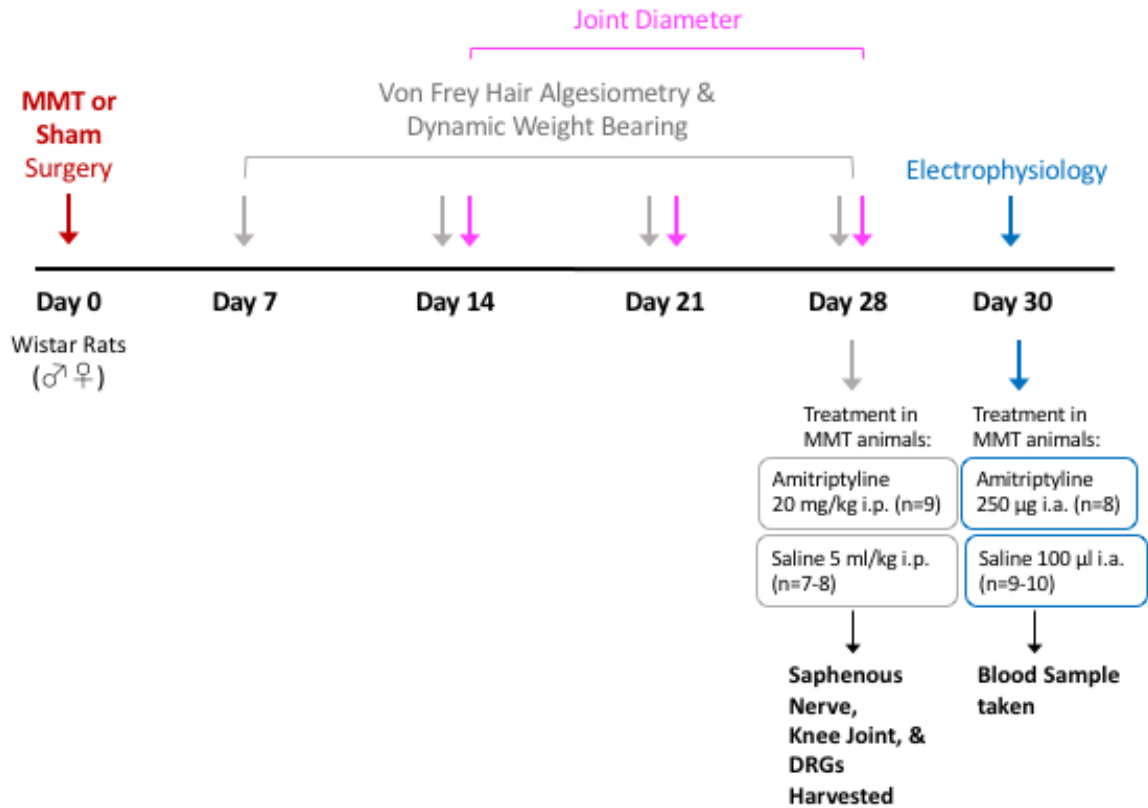
- I: Female animals develop more pronounced pain in response to MMT compared to males.**
- II: Post-traumatic osteoarthritis pain induced by MMT is mediated in part by neuropathy.**

3.2 Characterisation of Pain Phenotype in the MMT model of PTOA

3.2.1 Methods

Male and female Wistar rats (Male: 230-361 g – Female: 209-286 g) were deeply anaesthetised with isoflurane (2-4%, O₂ 0.8L/min) and underwent either MMT or a sham-surgery of the right knee joint. The MMT surgery (described in detail in section 2.2) involved a destabilization of the joint where both the MCL and medial meniscus were transected. The sham surgery only involved blunt dissection of the connective tissues overlying the joint with no transection of either the medial meniscus nor the MCL. Following surgery, pain behaviour was tested weekly for 4 weeks using von Frey hair algometry and dynamic incapacitance testing. Knee joint diameters were also

measured on days 14, 21, and 28 following MMT and sham surgeries.



3.2.2 Results

3.2.2.1 Effect of Medial Meniscal Transection on Joint Diameter

The joint diameter of MMT and sham surgery animals were not significantly different at days 14, 21, or 28 post-surgery in either sex (n=8-17 animals per group; 2-way RM ANOVA).

3.2.2.2 Medial Meniscal Transection Induced Nociceptive Behaviour that was Sex-Specific

MMT produced secondary mechanical allodynia in both male and female animals over the course of the 28-day model (Figure 3.3). In day 7 male animals, withdrawal

thresholds were reduced compared to baseline (baseline: $14.92 \pm 0.09\text{g}$; day 7: $11.14 \pm 0.72\text{g}$). The hindlimb mechanosensitivity continued to increase up to day 14 ($8.18 \pm 0.82\text{g}$) and persisted on days 21 and 28. In contrast, male animals (baseline: $14.94 \pm 0.06\text{g}$) that underwent the sham surgery demonstrated a mild reduction in withdrawal threshold on day 7 ($14.02 \pm 0.91\text{g}$) before recovering to baseline levels on days 14, 21, and 28.

In female MMT animals (baseline: $14.08 \pm 0.49\text{g}$), a similar pattern was observed where withdrawal thresholds decreased on days 7 and 14 ($12.59 \pm 0.74\text{g}$ and $11.79 \pm 1.0\text{g}$ respectively). However, unlike the males, mechanosensitivity recovered over the last 2 weeks of the model (day 21: $13.39 \pm 0.85\text{g}$ and day 28: $13.34 \pm 0.67\text{g}$). While an overall significant reduction was observed in withdrawal threshold compared to female sham animals ($p < 0.05$, $n = 8-16$, 2-way RM ANOVA) *post hoc* analysis revealed that there was no statistical significance at any of the individual days tested. Comparison of MMT male and female animals revealed that males presented with significantly lower hindpaw withdrawal thresholds compared to females from 2 weeks post-surgery until the end of the study.

Hindlimb weight bearing deficits were observed in male, but not female MMT animals (Figure 3.1C). Following MMT surgery, male animals placed significantly less weight on their injured ipsilateral hindlimb on days 7, 14, and 28 compared to sham-operated animals ($p < 0.001$, $n = 8-17$). In female animals, there was no statistical difference in weight-bearing between the hindlimbs in MMT or sham surgery animals ($p > 0.05$, $n = 16-17$). Comparison of MMT male and female animals revealed that male

weight bearing deficits were significantly greater compared to females only on day 14 post-surgery ($-4.9\% \pm 1.4\%$, $p < 0.05$, $n = 16-17$).

3.3 Characterisation of Joint Damage in the MMT Model

3.3.1 Methods

Knee joints were harvested on day 28 following MMT or sham surgery, preserved in 4% paraformaldehyde, and decalcified with formic acid. Tissue was sectioned in the frontal plane, stained with toluidine blue and assessed for damage using the OARSI scoring system as described in section 2.6.

3.3.2 Results

3.3.2.1 Medial Meniscal Transection induced Joint Pathology

Analysis of knee joints from both male and female animals 28 days following MMT surgery revealed histopathology consistent with PTOA (Figure 3.2). Loss of chondrocytes and proteoglycans on the outer and middle zones of the tibial plateau and femoral head of the joint resulted in marked to severe cartilage degeneration. Large osteophytes were also visible in MMT joints but were absent in sham surgery knees. Control animals also lacked cartilage damage, and presented with healthy, smooth cartilage with normal chondrocyte and rich proteoglycan staining. Total joint damage scores in both male (median: 23.5, IQR: 19.75-26.5) and female (18.0, IQR: 14.7-22.9) PTOA joints were significantly larger than their sham-surgery counterparts (male sham: 0.5, IQR: 0.0-0.05, female sham: 0.5, IQR: 0.2-0.5) ($p < 0.05$, $n = 5-7$, Kruskal Wallis test). Significant tibial bone damage was present in MMT animals of both sexes,

consisting of subchondral bone loss and epiphyseal trabecular bone sclerosis. This damage was absent in the joints of sham animals ($p > 0.05$, $n = 5-7$, Kruskal Wallis test).

3.4 Measurement of Joint Nociceptors in the MMT Model

3.4.1 Methods

Thirty days following MMT or sham surgery, male and female animals were deeply anaesthetised with urethane (25% solution, 2 g/kg i.p.) and underwent surgical preparation for single unit electrophysiology recording experiments, as outlined in section 2.3.1. Briefly, the saphenous nerve was cut in the inguinal region and the distal nerve stump was teased to isolate knee joint afferent fibres. The joint afferents were characterised by the following parameters: mechanical thresholds, evoked firing in response to rotation of the knee joint, spontaneous firing, electrical thresholds, and conduction velocities.

Mechanosensitivity was assessed by applying rotational force within the normal working range of the joint (normal rotation), and beyond its working range (hyper-rotation). The rotational stimuli were applied in pairs, with the normal and hyper-rotations each lasting for five seconds in duration. Three sets of rotations were initially applied to acquire a 'baseline activity' measurement. Each movement cycle was performed at 5-minute intervals. The mean evoked firing during the baseline was calculated for each type of rotational stimulus. At the end of the recording session, the receptive field of the afferent fibre was electrically stimulated with a pair of bipolar silver electrodes to determine the electrical threshold and conduction velocity of the fibre (See Section 2.3.2).

3.4.2 Results

3.4.2.1 Medial Meniscal Transection Induced Sex-specific Changes in Joint Afferent Sensitization

Mechanonociceptive A δ - and C-fibres were recorded from MMT and sham operated animals and electrophysiological characteristics are summarized in Table 3.1. Overall, sensitization of joint afferents was observed in male MMT animals when compared to sham-operated, but not in female PTOA animals. Mechanical thresholds were significantly reduced in male MMT fibres compared to their sham-surgery counterparts ($p < 0.05$, $n = 13-20$, 2-way RM ANOVA). In female animals, fibres from MMT and sham surgery animals did not differ in the minimum force required to evoke firing ($p > 0.05$, $n = 10-14$). Rotation of the knee within the normal working range of the joint caused on average 17 ± 4 and 12 ± 2 action potentials for male and female PTOA animals respectively. This firing frequency was not significantly different between the sexes ($p > 0.05$, $n = 9-18$ fibres per group, Figure 3.3). In response to hyper-rotation, male MMT fibres fired 50 ± 7 action potentials/movement which was significantly greater compared to 25 ± 4 action potentials/movement recorded in male sham animals ($p < 0.01$, $n = 13-20$). When compared to female PTOA afferents, male animal fibres fired significantly more action potentials in response to hyper rotation of the knee joint ($p < 0.05$, $n = 14-20$). The same stimuli evoked 33 ± 4 and 22 ± 3 action potentials from female MMT and sham-surgery animals respectively, revealing that female PTOA joint nociceptors were not sensitized compared to control animals ($p > 0.05$, $n = 10-14$). Spontaneous firing was observed in all experimental groups but was greatest in MMT-operated rats with around 35% of fibres showing non-evoked activity in both sexes.

Measurement of joint afferent conduction velocity revealed slower neurotransmission in nociceptors recorded from male ($p < 0.01$, $n = 8-10$, Table 3.1) but not in female ($p > 0.05$, $n = 7$) MMT animals compared to their sham-surgery controls.

3.5 Assessment of Saphenous Nerve Morphology in the MMT Model

3.5.1 Methods

Saphenous nerve samples were harvested proximal to the ipsilateral knee joint on day 28 following MMT or sham-surgery in male and female Wistar rats. Tissues were then processed for electron microscopy as described in section 2.5. Photomicrographs of saphenous nerve samples were scored for nerve integrity and g-ratios.

3.5.2 Results

3.5.2.1 Medial Meniscal Transection Resulted in Neuropathy, But Not Demyelination, of the Saphenous Nerve in Male Animals

Analysis of day 28 saphenous nerve photomicrographs revealed a higher proportion of axons were morphologically irregular in male animals following MMT surgery ($29 \pm 5\%$) compared with sham-surgery ($15 \pm 1\%$) ($p < 0.05$, $n = 1074-1140$ fibres from 7 animals per group, 2-way ANOVA, Figure 3.4). In female animals, there was no significant difference in the percentage of damaged fibres between MMT ($15 \pm 1\%$) and sham ($15 \pm 3\%$) surgery animals ($p > 0.05$, $n = 974-1107$ fibres from 6-7 animals per group). There was significantly more damage observed in the saphenous axons of male PTOA animals ($p < 0.05$, Figure 3.4).

Myelin thickness, as measured by g-ratio analysis of the saphenous nerve, was not altered in either small (Figure 3.4F) or large (Figure 3.4G) diameter axons in PTOA animals of either sex ($p > 0.05$, $n = 246-427$ fibres from 6-7 animals per group).

3.6 Assessment of Joint Neurones at the Level of the Dorsal Root Ganglia

3.6.1 Methods

DRGs (L3-L4) from Fluoro-Gold-injected animals were harvested 28 days following MMT or sham-surgery as described in section 2.4.1. Tissues were stained with commercially available primary antibodies against cleaved-caspase 3 (rabbit-anti-cleaved-caspase 3; 1:800) and glial fibrillary acidic protein (mouse-anti-GFAP; 1:750) overnight at 4°C. Following washes with PBS, the sections were incubated with Alexa fluor 488 goat-anti-rabbit (1:1000) and Alexa Fluor 555 goat-anti-mouse (1:750) secondary antibodies for one hour. Photomicrographs were taken on a Zeiss Axio Imager 2 microscope at 10x magnification and analyzed offline using image J software (see Section 2.4.2). The percentage of Fluoro-Gold positive joint neurones that expressed cleaved-caspase 3 and were surrounded by GFAP positive satellite glial cells was calculated.

3.6.1 Results

3.6.1.1 Medial Meniscal Transection Did Not Induce Neuronal Apoptosis but Activated Satellite Glial Cells

Immunohistochemical analysis of L3 and L4 joint neurones did not reveal significant differences in cleaved-caspase 3 expression between PTOA and sham-

operated animals of either sex (Figure 3.5). In male animals, 35 ± 3 % of Fluoro-Gold positive neurones from MMT animals expressed the apoptotic marker, compared to 48 ± 3 % in sham animals ($p > 0.05$, $n = 6-8$ DRGs per group, 2-way ANOVA). Female MMT and sham-operated animals also expressed similar levels with 32 ± 4 % and 34 ± 5 % of neurones showing positive staining in each group ($p > 0.05$, $n = 6$ DRGs per group).

Association of joint neurones with activated GFAP-positive SGCs was also assessed in MMT and sham-operated animals. Increased GFAP immunofluorescence was observed in the SGCs which apposed 23 ± 3 % and 30 ± 4 % of Fluoro-gold positive neurones of male and female MMT rats respectively ($p < 0.001$, $n = 6-8$ DRGs per group). In contrast, joint neurones from control surgery animals were surrounded by very few SGCs that were positive for GFAP (male sham: 7 ± 2 %, female sham: 4 ± 1 %). When GFAP expression was compared between male and female MMT animals, there was no significant difference observed between the groups ($p > 0.05$).

Joint afferents that expressed both cleaved-caspase 3 and were also associated with GFAP-positive SGCs were also upregulated in MMT animals of both sexes compared to sham-operated animals ($p < 0.05$, $n = 6-8$ DRGs per group). Similar levels of co-expression were observed in MMT males and females (16 ± 5 % and 17 ± 5 %, respectively) ($p > 0.05$).

3.7 Effect of Amitriptyline on PTOA Pain

3.7.1 Methods

3.7.1.1 Pain Behaviour

On day 28 post MMT surgery, male and female animals were treated with either amitriptyline (20 mg/kg i.p.) or saline (5 ml/kg i.p.). Behavioural pain measurements were conducted at 30, 60, 120, and 180 minutes following drug administration.

3.7.1.2 Single Unit Electrophysiology

On day 30 post-MMT surgery, male and female animals were deeply anaesthetised with urethane (25% solution, 2 g/kg i.p.) and underwent surgical preparation for single unit electrophysiological recording as detailed in section 2.3.1. The saphenous artery was cannulated for close intra-arterial drug delivery of amitriptyline or saline to the knee joint. Following baseline rotations, amitriptyline (250 µg i.a.) or saline (100 µl i.a.) was administered and joint mechanosensitivity was assessed for an additional 40 minutes. The percentage change in afferent activity before and after administration of amitriptyline or vehicle was calculated.

3.7.2 Results

3.7.2.1 Systemic Amitriptyline Attenuated Pain Behaviour in Male PTOA Animals

When treated with the neuropathic analgesic amitriptyline, sexually disparate results were observed in PTOA animals. In male animals, amitriptyline treatment caused a reversal of both secondary allodynia ($p < 0.05$, $n = 8-9$, 2-way rm ANOVA, Figure 3.6A) and hindlimb weight bearing deficits ($p < 0.05$, $n = 8-9$, Figure 3.6B) 28 days post-MMT surgery. Female animals, in contrast, showed no significant response to amitriptyline with either pain readout ($p > 0.05$, $n = 7-8$, Figure 3.6A and Figure 3.6B).

3.7.2.2 Local Administration of Amitriptyline Attenuated Joint Afferent Firing in both Sexes

To assess the effect of amitriptyline on joint afferent firing, the drug was administered locally to the joint where it attenuated firing in response to normal and hyper-rotation of the knee (Figure 3.7). Evoked firing in response to normal joint rotation was significantly decreased in both male and female animals ($p < 0.05$, $n = 8-10$ fibres per group, 2-way rm ANOVA, Figure 3.7C-D). Strikingly, treatment also largely abolished firing in response to hyper-rotation in both sexes ($p < 0.01$, $n = 8-10$ fibres per group). With both types of stimuli, the response to amitriptyline was immediate in males, while in females a more gradual decrease in firing was observed.

3.8 The Role of β -Endorphin and Noradrenaline in the MMT Model

In previous studies where sex-specific nociceptive responses have been detected, enhancement of the endogenous opioid system and adrenergic system have been observed in female animals [270, 271]. As such, a comparison of systemic β -endorphin and noradrenaline were compared between male and female MMT animals.

3.8.1 *Methods*

3.8.1.1 Measurement of Serum β -Endorphin and Noradrenaline

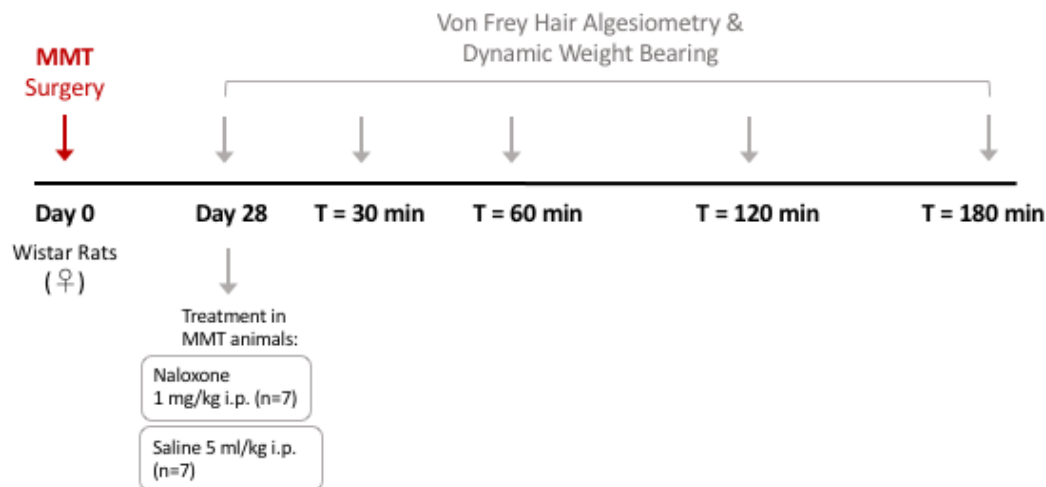
Following terminal experiments on day 30 post MMT or sham surgery, serum was isolated, and β -endorphin and noradrenaline concentrations were measured using commercially available ELISA kits as outlined in Sections 2.9 and 2.9.2.

3.8.1.2 Correlations Between Serum β -Endorphin or Noradrenaline, and Firing Rates

Following quantification of serum β -endorphin and noradrenaline, concentrations were plotted against baseline joint afferent firing rates for those animals which had been used for electrophysiological studies. Pearson's correlation coefficients were calculated using Prism software.

3.8.1.3 Systemic Naloxone Treatment in Female MMT Animals

As described previously in this chapter, MMT female animals do not present with observable pain behaviour or heightened joint afferent firing despite having joint histopathology consistent with PTOA. As a result of the elevated serum β -endorphin in female MMT animals, the aim of this experiment was to determine if systemic treatment with naloxone could reverse the effects of endogenous opioids in these animals. On day 28 following MMT surgery, female animals were administered either naloxone (1 mg/kg i.p.) or saline (5 ml/kg i.p.). von Frey hair algometry and dynamic weight bearing testing were then conducted at 30, 60, 120, and 180 minutes following treatment as depicted below.



3.8.2 Results

3.8.2.1 Serum β -Endorphin and Noradrenaline Concentration in MMT Animals

Quantification of serum β -endorphin revealed significantly elevated levels in female MMT animals (91.0 ± 10.4 pg/mL) compared to males (55.4 ± 7.8 pg/mL) ($p < 0.05$, $n = 10-12$, 2-way ANOVA, Figure 3.8A). When compared to sham-operated controls, however, there was no significant change in these neuromodulators in either sex ($p > 0.05$, $n = 5-12$, Figure 3.8A).

Serum noradrenaline levels were significantly elevated in female MMT animals (1377 ± 206 pg/mL) compared to sham (578 ± 197 pg/mL) ($p < 0.05$, $n = 7-12$, 2-way ANOVA, Figure 3.8D). Noradrenaline levels in male (1083 ± 185 pg/mL) and female (1377 ± 206 pg/mL) MMT serum did not differ from each other ($p > 0.05$, $n = 12-13$).

3.8.2.2 Correlation of Serum β -Endorphin or Noradrenaline Concentrations and Afferent Firing Rates

Correlations were made between serum β -endorphin or noradrenaline levels and baseline afferent firing rates in a subgroup of animals. When compared to joint nociceptor firing rates, serum β -endorphin was negatively correlated with afferent activity in female PTOA animals ($r = -0.92$, $p < 0.01$, $n = 8$, Pearson correlation coefficient, Figure 3.8B). Despite being elevated in female MMT serum, noradrenaline levels did not correlate with joint afferent firing rate ($r = -0.43$, $p > 0.05$, $n = 8$, Pearson correlation coefficient, Figure 3.8E). In male animals, no relationship was observed between evoked firing and the serum concentration of either β -endorphin ($r = -0.12$, $p > 0.05$, $n = 6$, Pearson correlation coefficient, Figure 3.8C) or noradrenaline ($r = -0.05$, $p > 0.05$, $n = 7$, Pearson correlation coefficient, Figure 3.8F).

3.8.2.3 Endogenous Opioids Mediate Antinociception in Female MMT Animals

Treatment with naloxone significantly reduced withdrawal thresholds in day 28 female MMT animals when compared to saline vehicle ($p < 0.05$, $n = 7$, 2-way ANOVA, Figure 3.9A). The treatment effectively reduced secondary allodynia for the duration of the experiment. Hindlimb weight bearing was not affected by naloxone treatment ($p > 0.05$, $n = 7$, Figure 3.9B).

3.9 Chapter Summary

3.9.1 Medial Meniscus Transection Induces Histological Damage in Both Sexes but Sexually Disparate Pain Responses

On day 28 post MMT surgery, joint damage consistent with PTOA was present in both male and female animals. Sham-control animals had normal joint morphology.

When behavioural pain testing was employed, secondary allodynia and weight bearing deficits were present in males yet absent in females. Single unit electrophysiological recordings revealed that there was sensitization of male joint afferent fibres. Despite the occurrence of PTOA joint damage, joint nociceptors did not display heightened activity in female MMT animals.

3.9.2 Assessment of Neuropathic-like Pain in the Medial Meniscus Transection

Model

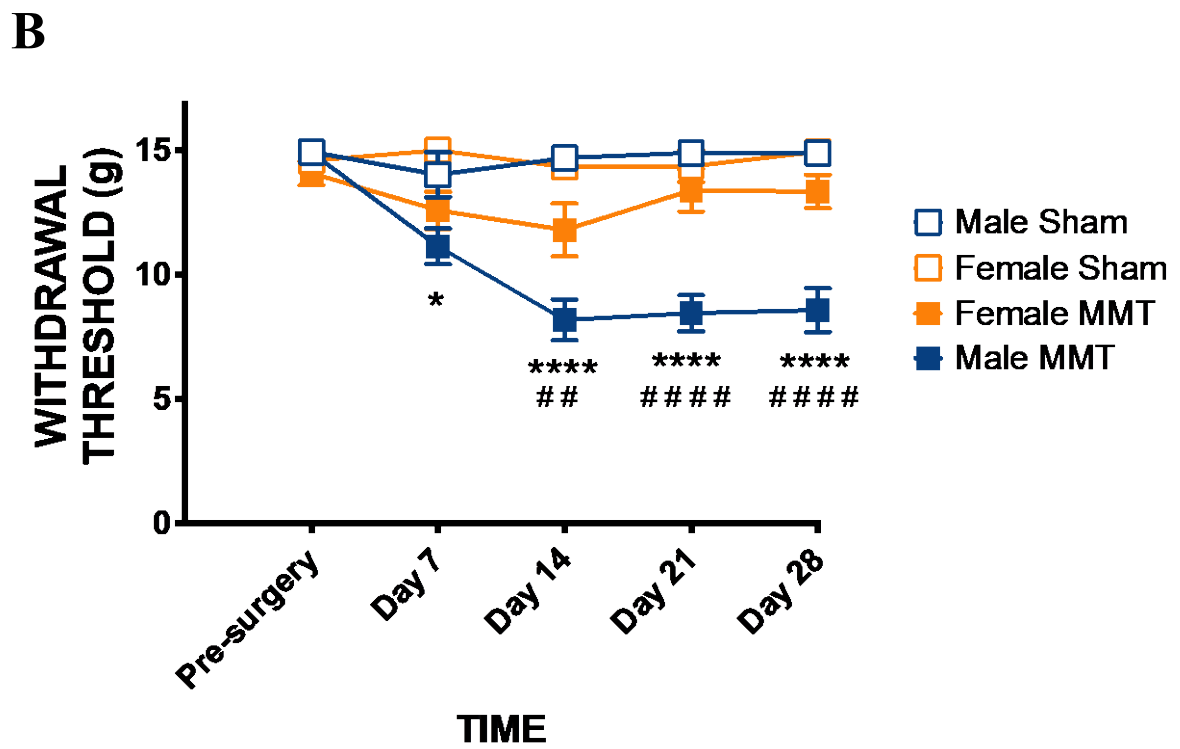
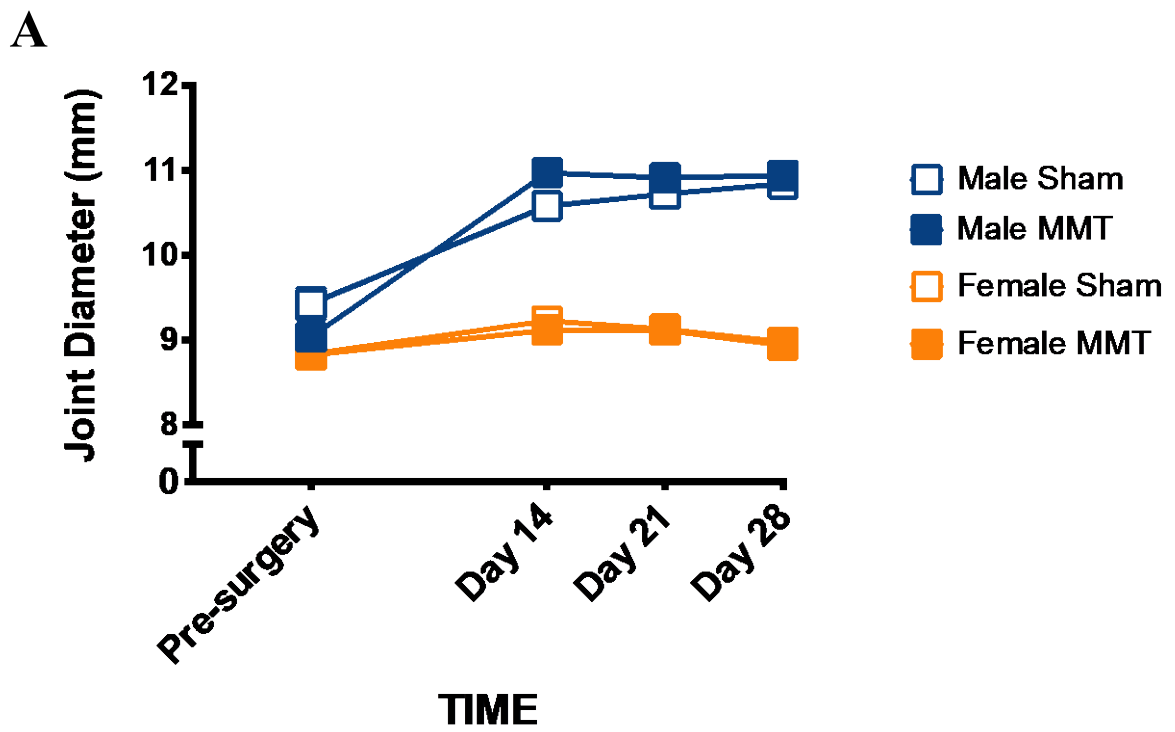
To examine the neurophysiology of the MMT model in greater detail, the morphology of the saphenous nerve was examined and joint neurones in the DRG were assessed for an association between cleaved-caspase-3 and GFAP-positive-SGCs. Demyelination was absent in both male and female MMT animals, but nerve damage was only present in males. At the level of the DRGs, elevated levels of GFAP expressing SGCs were associated with joint neurones in both sexes suggesting an activation of SGCs in the MMT model.

When treated with systemic administration of amitriptyline, pain was attenuated in male MMT animals only. Furthermore, local administration of amitriptyline to the knee attenuated joint afferent firing in both sexes.

Taken together, the data suggest that the heightened pain response observed in male PTOA animals may be a combination of nociceptive and neuropathic pain. The lack of joint inflammation and synovitis implies that inflammatory pain may not be a major contributor at day 28 in the MMT model.

3.9.3 Endogenous Opioids Mediate Antinociception in Female MMT Animals

In order to elucidate possible mediators of the antinociception observed in female MMT animals, serum β -endorphin and noradrenaline levels were measured in MMT animals. The levels of β -endorphin were significantly elevated in female MMT animals compared to males, and the concentration of the opioid was negatively correlated with joint afferent firing. Systemic naloxone administered to female animals produced secondary allodynia but not hindlimb weight bearing deficits suggesting endogenous opioids are partially mediating the lack of a pain phenotype in female PTOA rats. While noradrenaline was elevated in female MMT compared to sham controls, it did not differ from male MMT animals. There was also no correlation between serum noradrenaline concentration and joint afferent firing. Thus, sympathetic tone appears to contribute less than the endogenous opioid system to the antinociception observed in female PTOA animals.



C

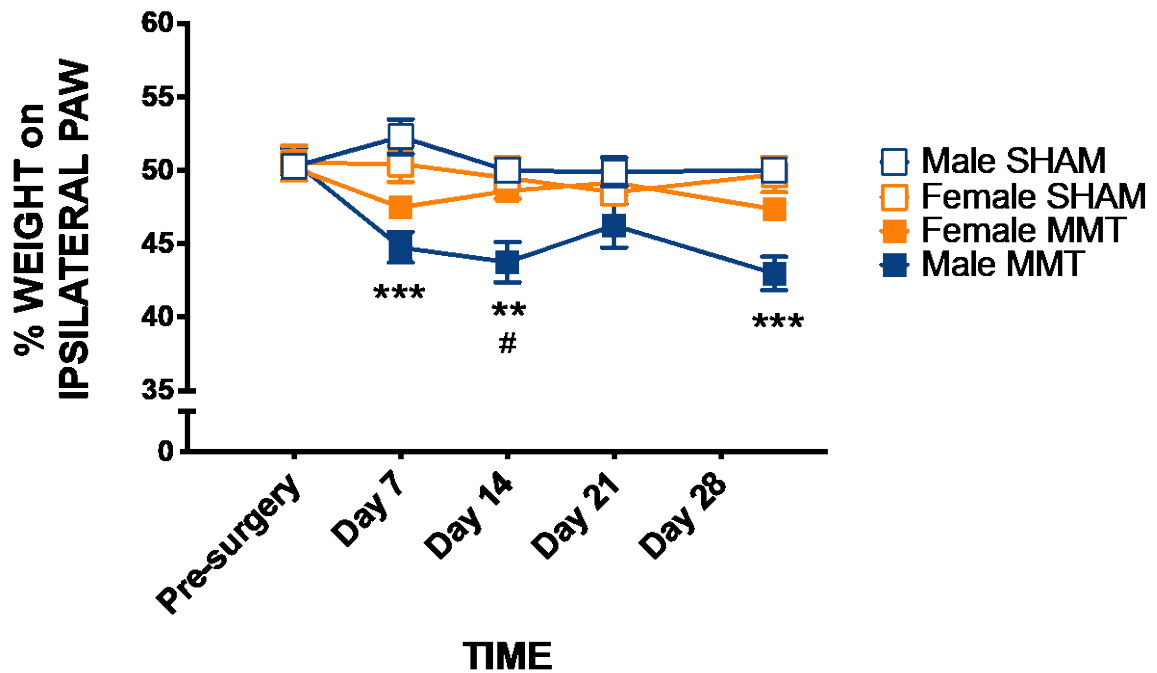
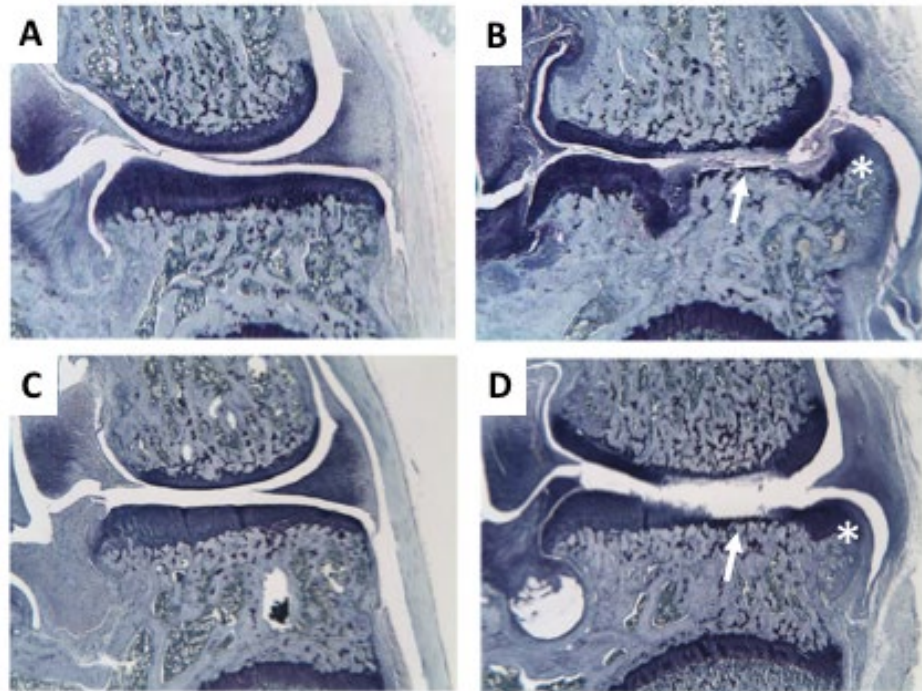


Figure 3. 1 MMT induced joint inflammation and pain.

(A) MMT surgery failed to elicit significant changes in knee joint diameter in either male or female animals compared to sham-surgery animals throughout the model development. (B) Decreased withdrawal thresholds were observed in male PTOA animals compared to sham controls for the duration of the model. In female PTOA animals, there was a small but significant decrease in withdrawal threshold compared to sham surgery animals ($P < 0.05$, 2-way rm ANOVA; $n = 8-17$). The reduction in withdrawal threshold was greater in male animals than females from days 14-28 following MMT surgery. (C) Hindlimb weight bearing deficits were observed in male PTOA animals compared to sham control animals on days 7, 14, and 28. Female animals did not display any weight bearing deficits over the 28-day timecourse. Data presented as mean values \pm SEM, an * denotes a male MMT vs male sham comparison, an # denotes a male MMT vs female MMT comparison, * $P < 0.05$, ** $P < 0.01$, *** $P < 0.001$, **** $P < 0.0001$, 2-way rm ANOVA with Bonferroni *post-hoc* test, $n = 8-17$ animals per group.



| Group | Total Joint Score | Cartilage Degeneration | Normalised Cartilage Damage | Osteophyte Score | Synovitis | Bone Damage Score | n |
|-------------|---------------------|------------------------|-----------------------------|------------------|----------------|-------------------|---|
| Male Sham | 0.5 (0.0-0.5) | 0.5 (0.3-0.5) | 0.01 (0.00-0.02) | 0.0 (0.0-0.0) | 0.5 (0.3-0.5) | 0.0 (0.0-0.0) | 5 |
| Male MMT | 23.5 (19.75-26.5)** | 18.5 (14.8-21.5)* | 0.69 (0.41-0.86)**** | 5.0 (5.0-5.0)** | 2.0 (0.8-2.0) | 5.0 (4.0-5.0)** | 5 |
| Female Sham | 0.5 (0.2-0.5) | 0.5 (0.1-0.6) | 0.00 (0.00-0.01) | 0.0 (0.0-0.0) | 0.0 (0.0-0.0) | 0.0 (0.0-0.0) | 7 |
| Female MMT | 18.0 (14.7-22.9)* | 16.0 (12.7-18.4) | 0.58 (0.24-0.68)**** | 2.5 (1.8-5.0)* | 0.5 (0.5-0.5)* | 2.0 (1.0-4.0)* | 6 |

Figure 3. 2 MMT surgery causes joint damage in both male and female rats.

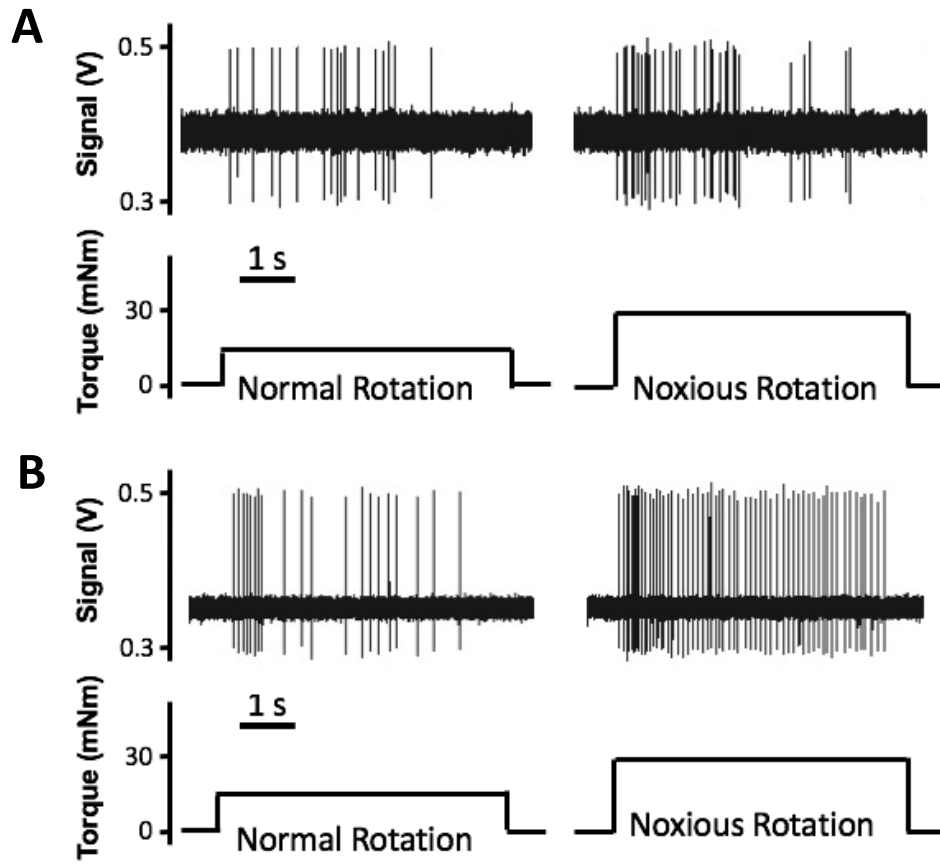
Representative frontal plane images of knee joints stained with toluidine blue 28 days following sham (A; male, C; female) or MMT (B; male, D; female) surgery, depicting cartilage degeneration (arrows) and formation of osteophytes (asterisks). Joint histopathology scores are summarised within the table *P<0.05, **P<0.01 and ****P<0.0001 denotes MMT vs sham (of the same sex) statistical significance using post hoc Dunn's Multiple Comparisons Test. Data are medians (interquartile range). Images are taken at 16X magnification.

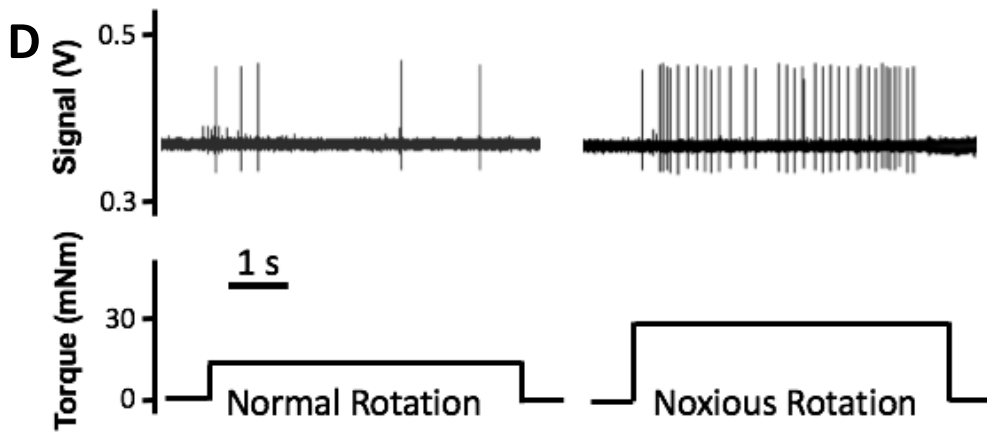
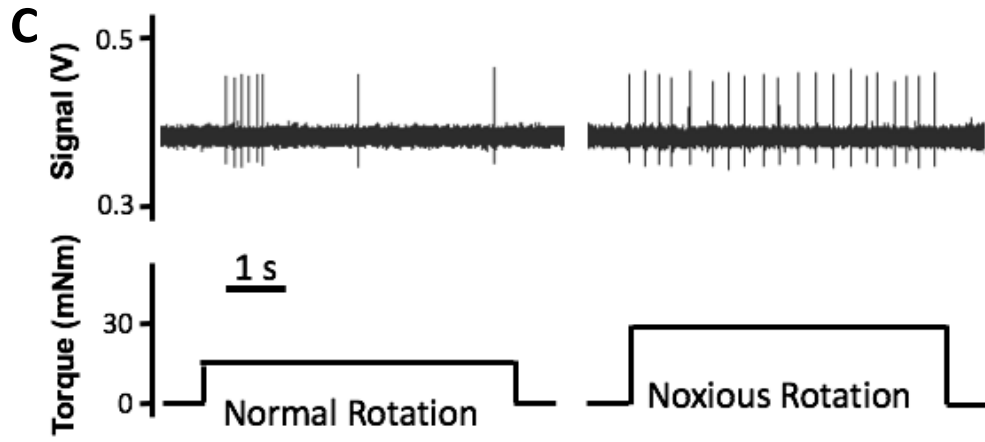
| Fibre type | Mechanical Threshold (mNm) | Hyper Rotation (mNm) | Normal Rotation (mNm) | Spontaneous Fibres (%) | Electrical Threshold (V) | Conduction Velocity (m/s) | n |
|--------------------|-----------------------------------|-----------------------------|------------------------------|-------------------------------|---------------------------------|----------------------------------|-----------|
| Male Sham | | | | | | | |
| All fibres | 14 ± 4 (3-30) | 24 ± 7 (18-35) | 15 ± 5 (8-20) | 21 | 3.8 ± 1 (2-4.25) | 2.5 ± 0.8 (1.07-5.26) | 13 |
| III | 17 ± 1 (15-20) | 24 ± 2 (18-28) | 18 ± 1 (16-20) | | 3.65 ± 0.7 (2-5) | 3.3 ± 0.6 (2.25-5.26) | 5 |
| IV | 14 ± 3 (8-20) | 26 ± 1 (25-27) | 16 ± 1 (15-16) | | 4.00 ± 0.1 (3.75-4.25) | 1.3 ± 0.1 (1.07-1.47) | 3 |
| ND | 12 ± 5 (3-30) | 25 ± 3 (20-35) | 13 ± 4 (8-16) | | N/A | N/A | 5 |
| Male MMT | | | | | | | |
| All fibres | 9 ± 2 (2-25)* | 23 ± 5 (15-35) | 13 ± 3 (6-20) | 35 | 4.3 ± 1 (2.75-6) | 1.4 ± 0.5 (0.74-2.73)# | 20 |
| III | 6 ± 1 (5-7) | 22 ± 2 (20-23) | 12 ± 0 (12) | | 4.75 ± 1.3 (3.5-6) | 2.4 ± 0.4 (2.04-2.73) | 2 |
| IV | 7 ± 2 (2-18) | 22 ± 2 (15-30) | 13 ± 2 (8-18) | | 4.14 ± 0.3 (2.75-5) | 1.2 ± 0.3 (0.74-1.67) | 8 |
| ND | 11 ± 3 (2-25) | 24 ± 2 (20-35) | 13 ± 2 (6-20) | | N/A | N/A | 10 |
| Female Sham | | | | | | | |
| All Fibres | 10 ± 3 (4-16) | 25 ± 8 (20-30) | 16 ± 5 (14-20) | 20 | 3.9 ± 1.5 (2.75-4.25) | 2.1 ± 0.8 (1.17-3.02) | 10 |
| III | 8 ± 1 (5-10) | 24 ± 2 (20-29) | 16 ± 2 (12-20) | | 3.88 ± 0.2 (3.5-4.25) | 2.4 ± 0.2 (2.14-3.02) | 4 |
| IV | 12 ± 1 (10-15) | 27 ± 2 (25-30) | 17 ± 2 (15-20) | | 3.83 ± 0.5 (2.75-4.25) | 1.6 ± 0.2 (1.17-1.78) | 3 |
| ND | 11 ± 4 (4-16) | 25 ± 2 (22-27) | 16 ± 1 (14-18) | | N/A | N/A | 3 |
| Female MMT | | | | | | | |
| All fibres | 8 ± 2 (4-15) | 19 ± 5 (15-22) | 12 ± 3 (8-18) | 36 | 4.1 ± 1.5 (2-6.5) | 1.9 ± 0.8 (1.45-2.76) | 14 |
| III | 8 ± 2 (4-10) | 19 ± 1 (18-20) | 11 ± 1 (10-12) | | 4.8 ± 1 (3-6.5) | 2.3 ± 0.2 (2.02-2.76) | 3 |
| IV | 8 ± 2 (4-13) | 20 ± 1 (17-22) | 12 ± 1 (10-14) | | 3.5 ± 0.6 (2-4.75) | 1.5 ± 0.1 (1.45-1.56) | 4 |

| | | | | | | | |
|----|--------------|-------------------|------------------|--|-----|-----|---|
| ND | 9 ± 2 (4-15) | 20 ± 1 (15-25) | 13 ± 2 (8-18) | | N/A | N/A | 7 |
|----|--------------|-------------------|------------------|--|-----|-----|---|

Table 3. 1: Electrophysiological characteristics of joint afferents in MMT animals.

Fibres recorded 30 days following MMT and sham-surgery animals are classified by mechanical threshold values, torque applied in normal and hyper rotation of the joint, the percentage of fibres that exhibited spontaneous firing, electrical thresholds, and are grouped into fibre type (III or IV) by calculation of conduction velocity. Data are means ± SEM (range).





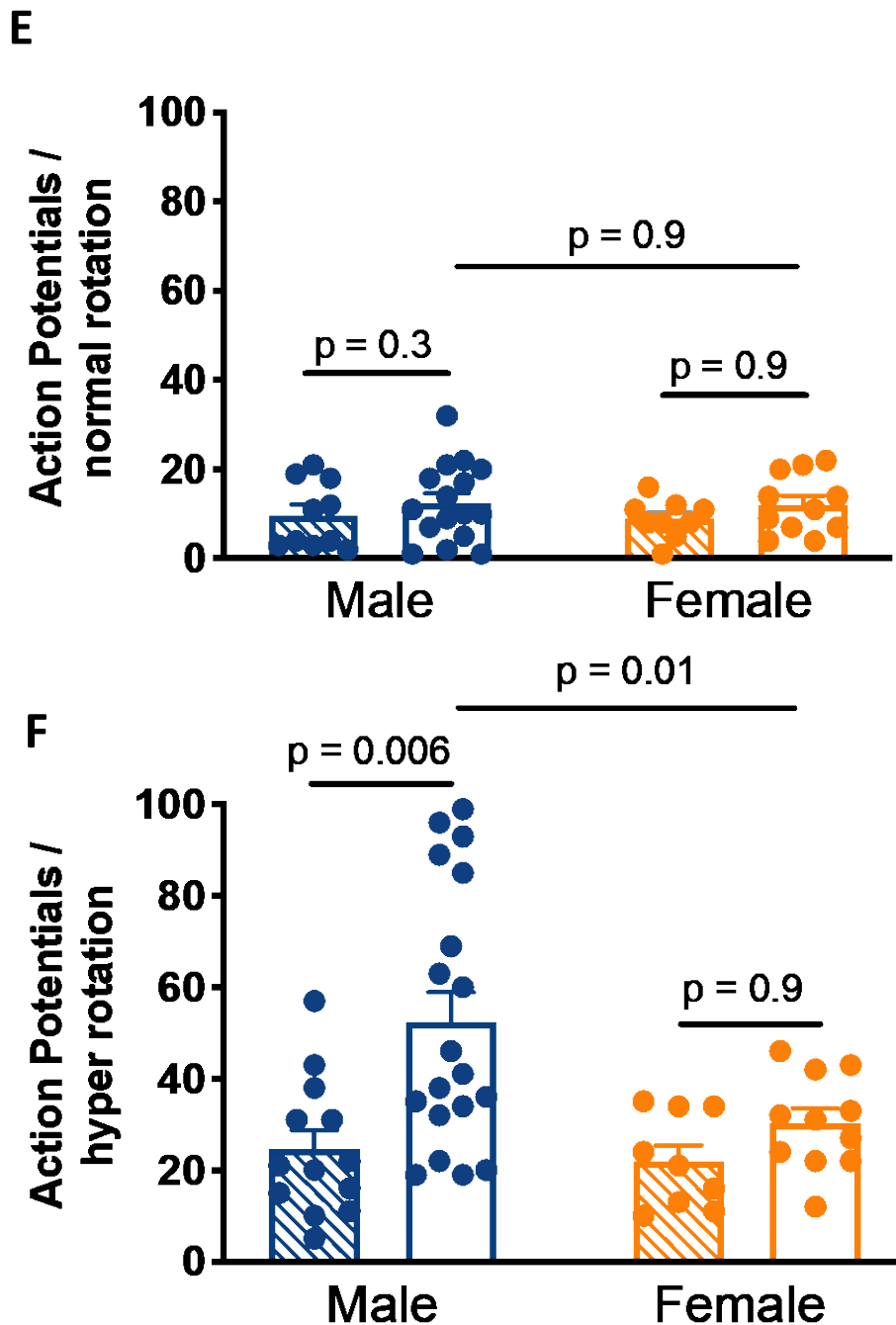
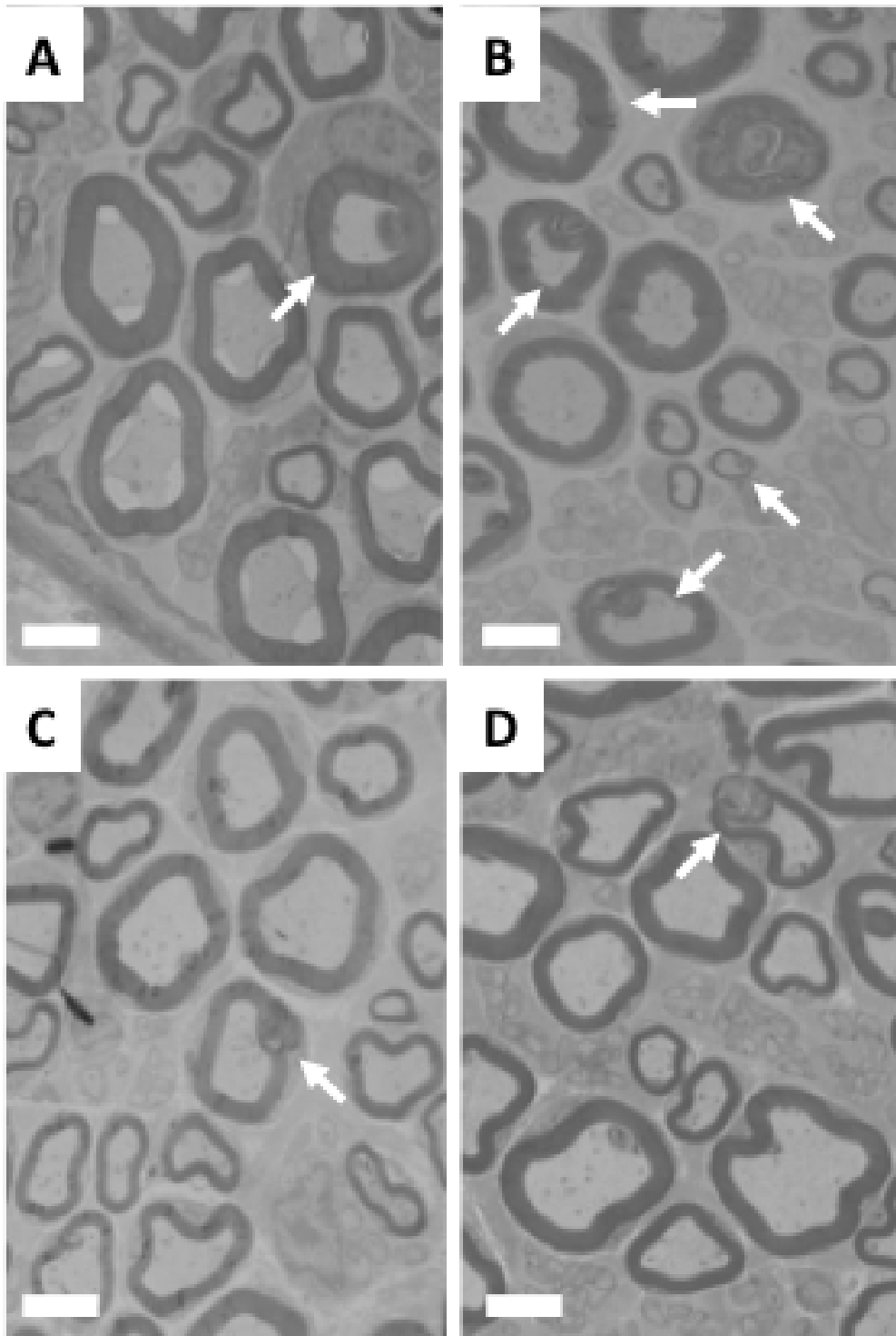
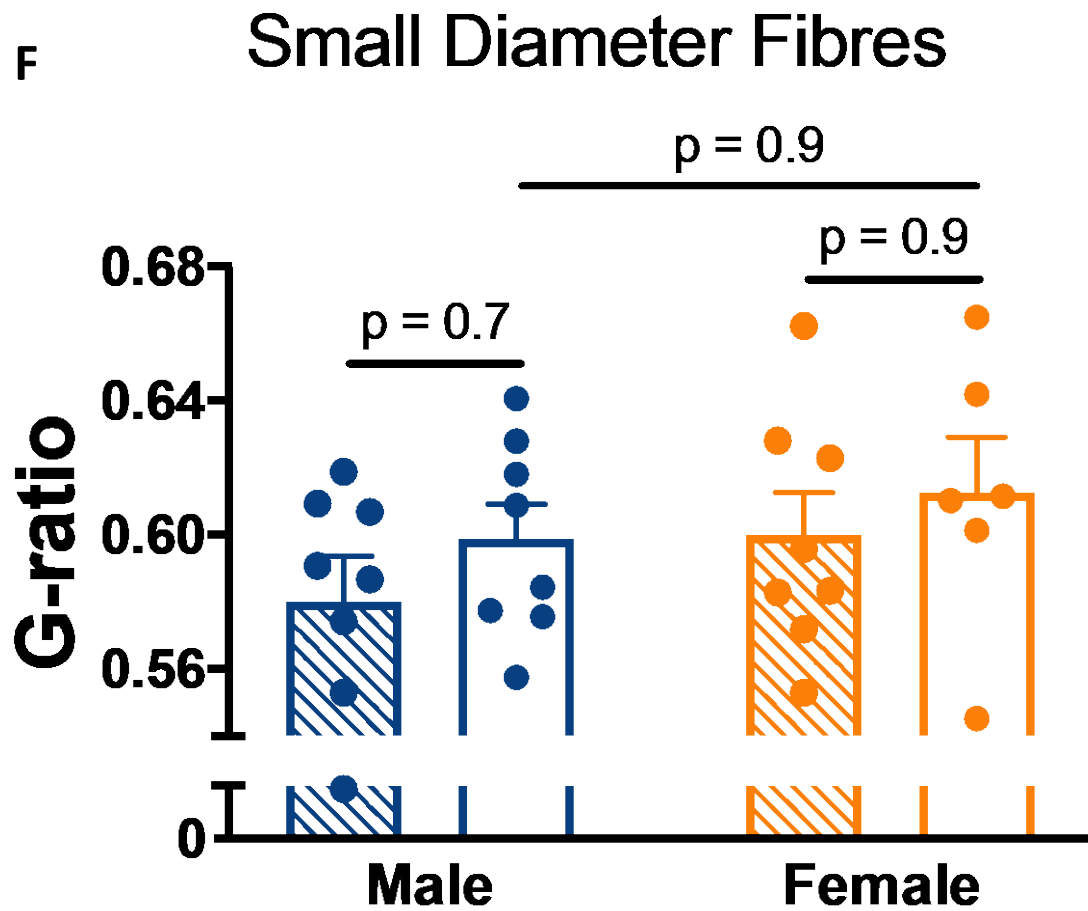
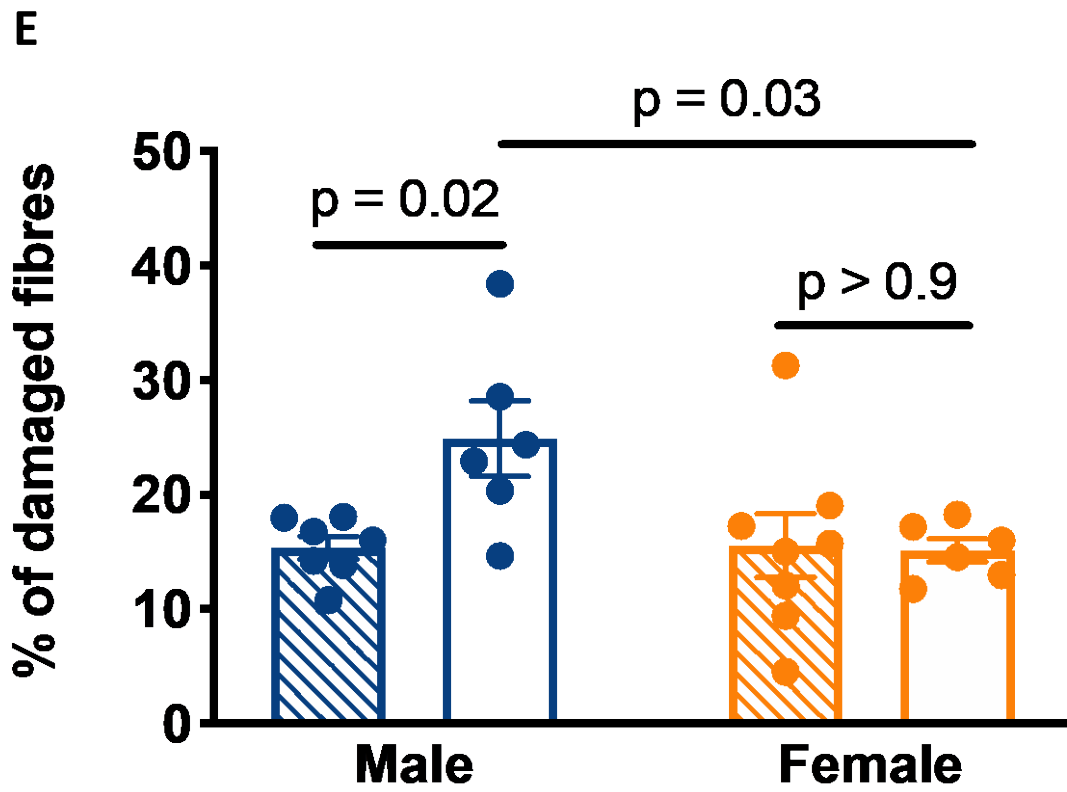


Figure 3. 3 The MMT model induced sensitization of joint afferents in male animals.

Representative traces of single unit recordings from male sham-(A) or MMT-(B) surgery animals or female sham-(C) or MMT-(D) surgery animals on day 30. Normal rotation of the joint failed to induce a significant difference in evoked firing between MMT and sham surgery animals of either sex (E). Following hyper-rotation of the knee joint, male MMT fibres fired significantly more action potentials compared to their sham-surgery counterparts and compared to female MMT animals (F). Data presented as mean values \pm SEM, 2-way ANOVA, $n = 10-20$ fibres per group.





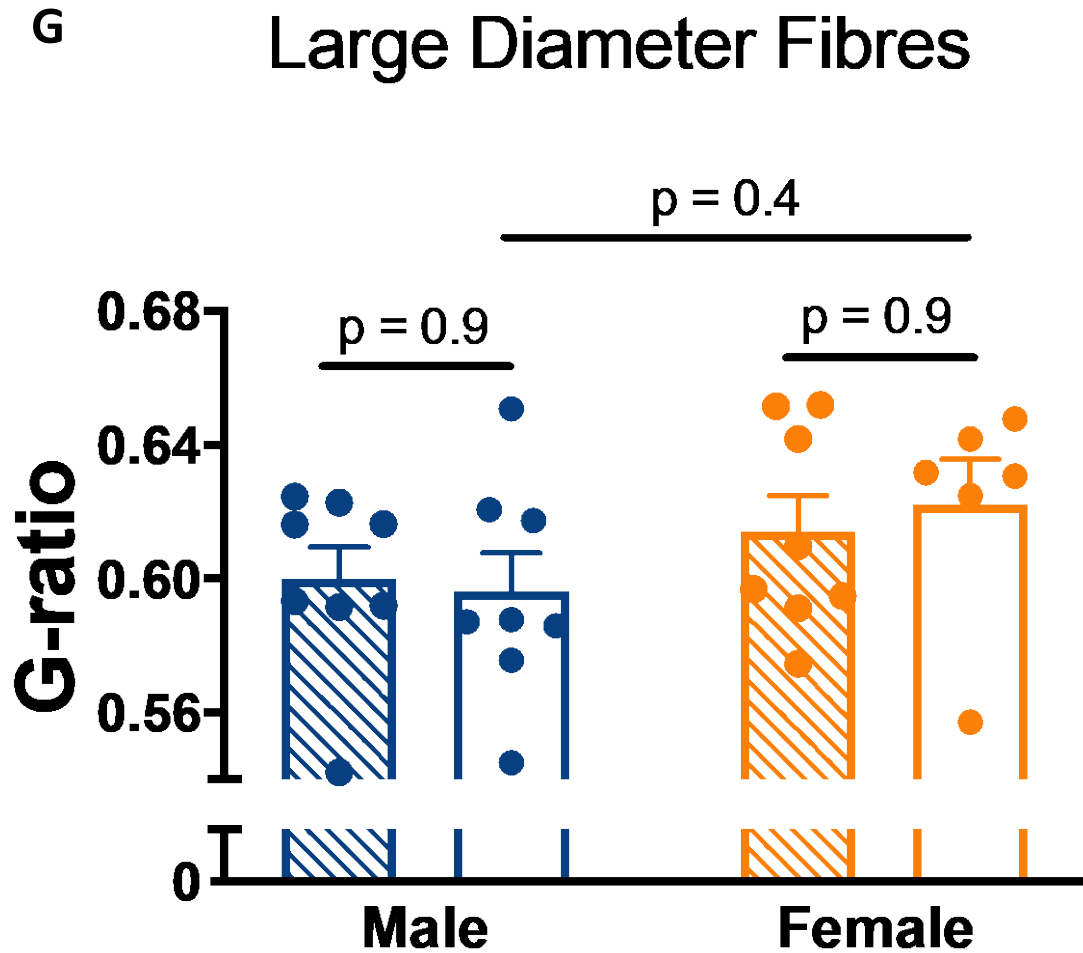
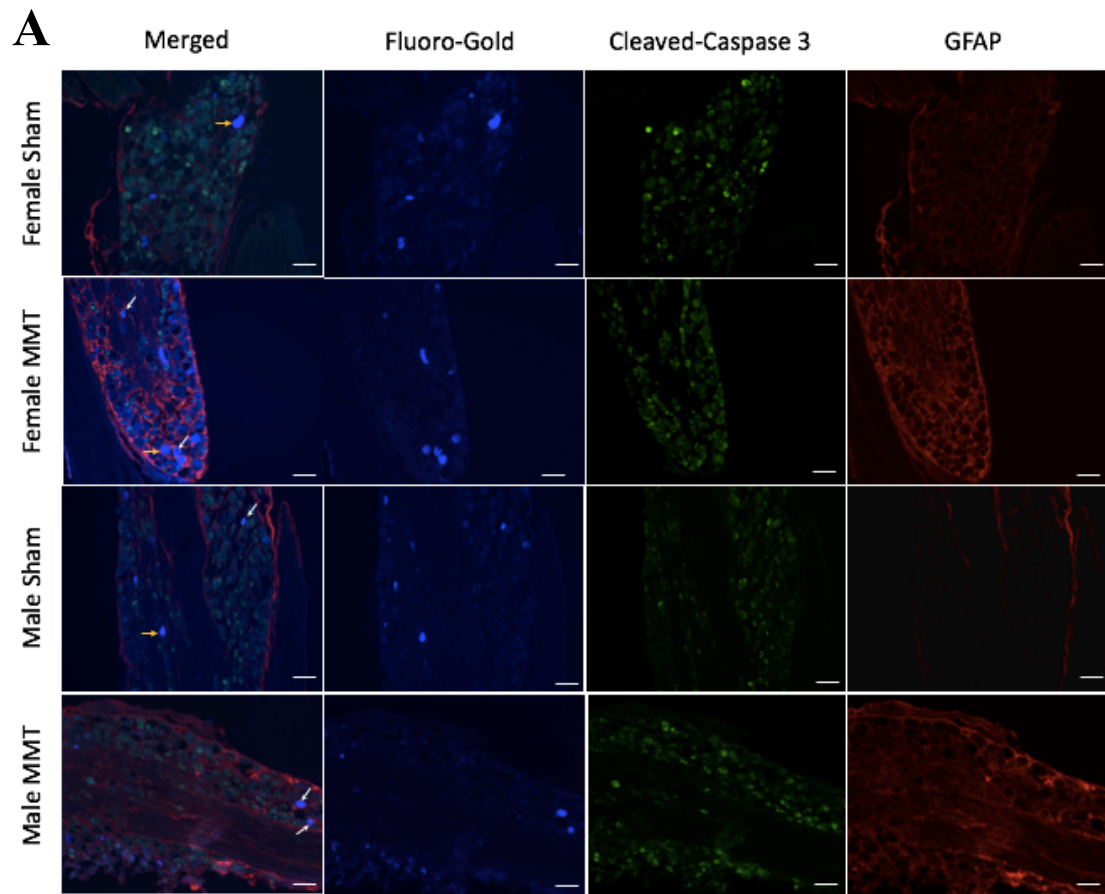
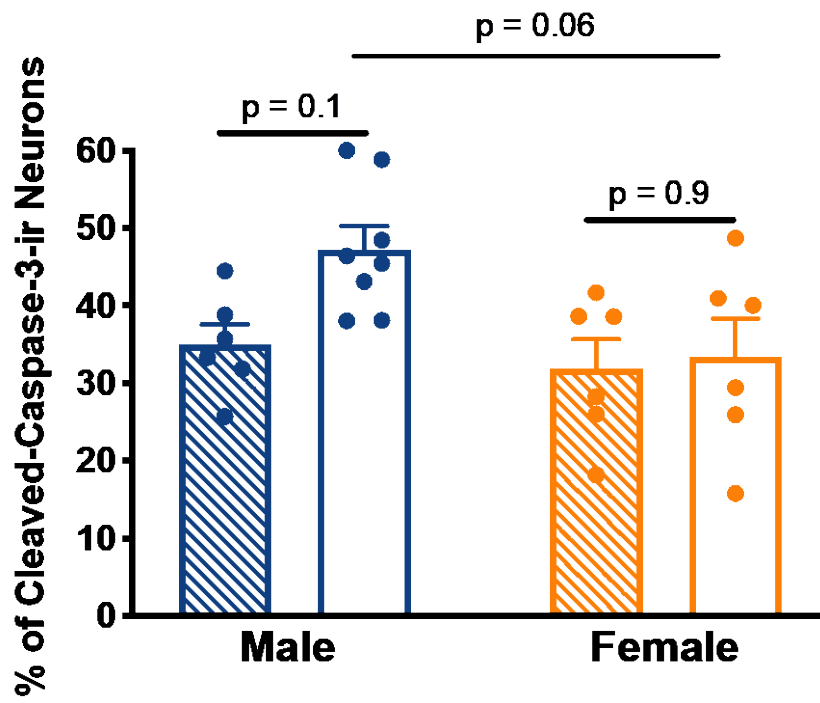


Figure 3. 4 MMT induced saphenous nerve damage.

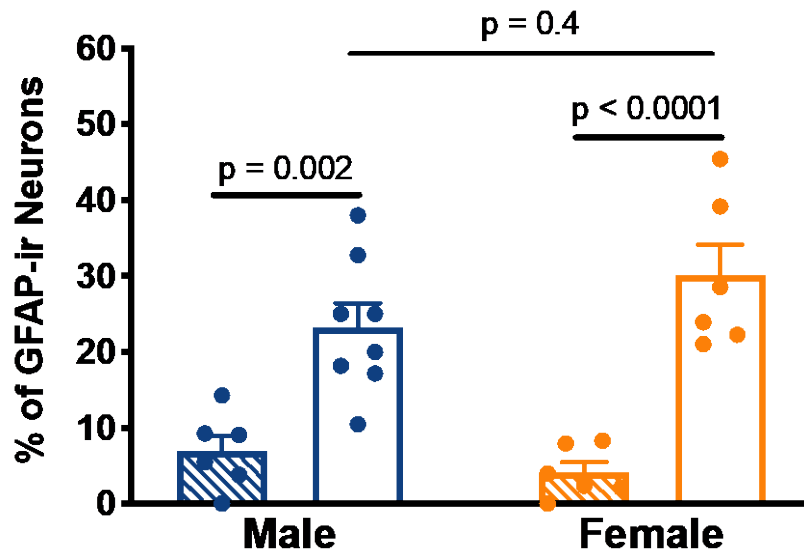
Representative electron micrographs of the saphenous nerve taken 28 days following MMT or sham surgery, **A**; male sham, **B**; male MMT, **C**; female sham, **D**; female MMT. The percentage of axons with irregular morphology was significantly higher in male MMT animals compared to their sham counterparts or female PTOA animals ($n= 974-1140$ axons from 7 animals per group) (**E**). G-ratio values were calculated for both large (**F**) and small (**G**) diameter axons; MMT surgery did not significantly affect the values calculated for either sex. Data presented as mean values \pm SEM. Arrows indicate damaged axons, scale bar = 6 μm . 2-way rm ANOVA, $n= 7$ animals per group.



B



C



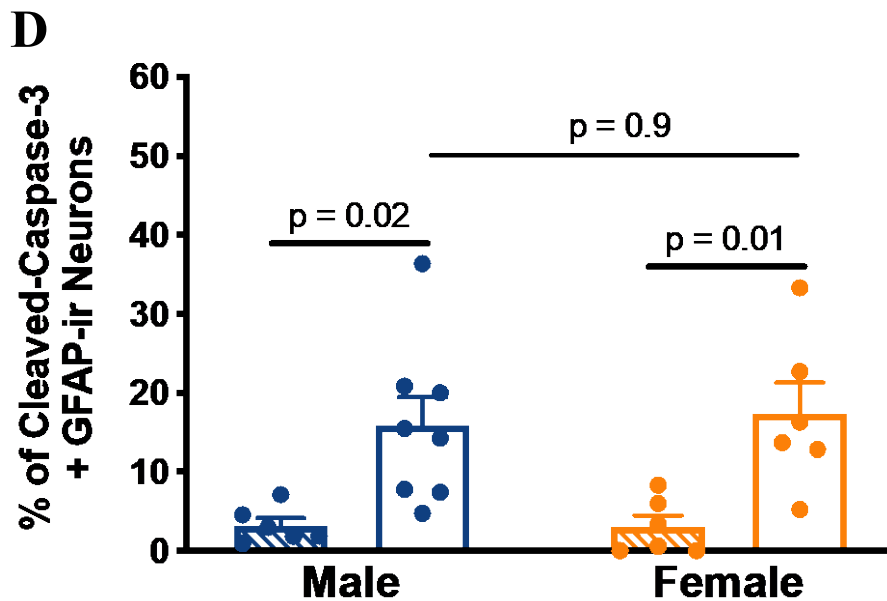
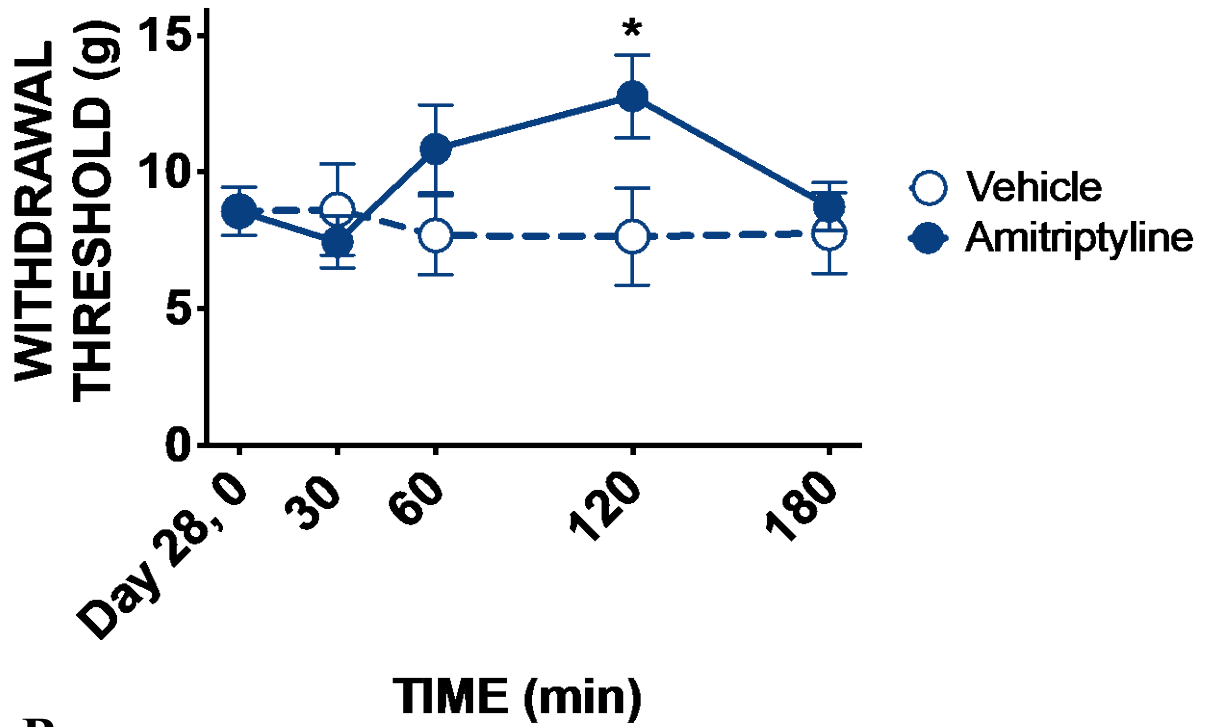


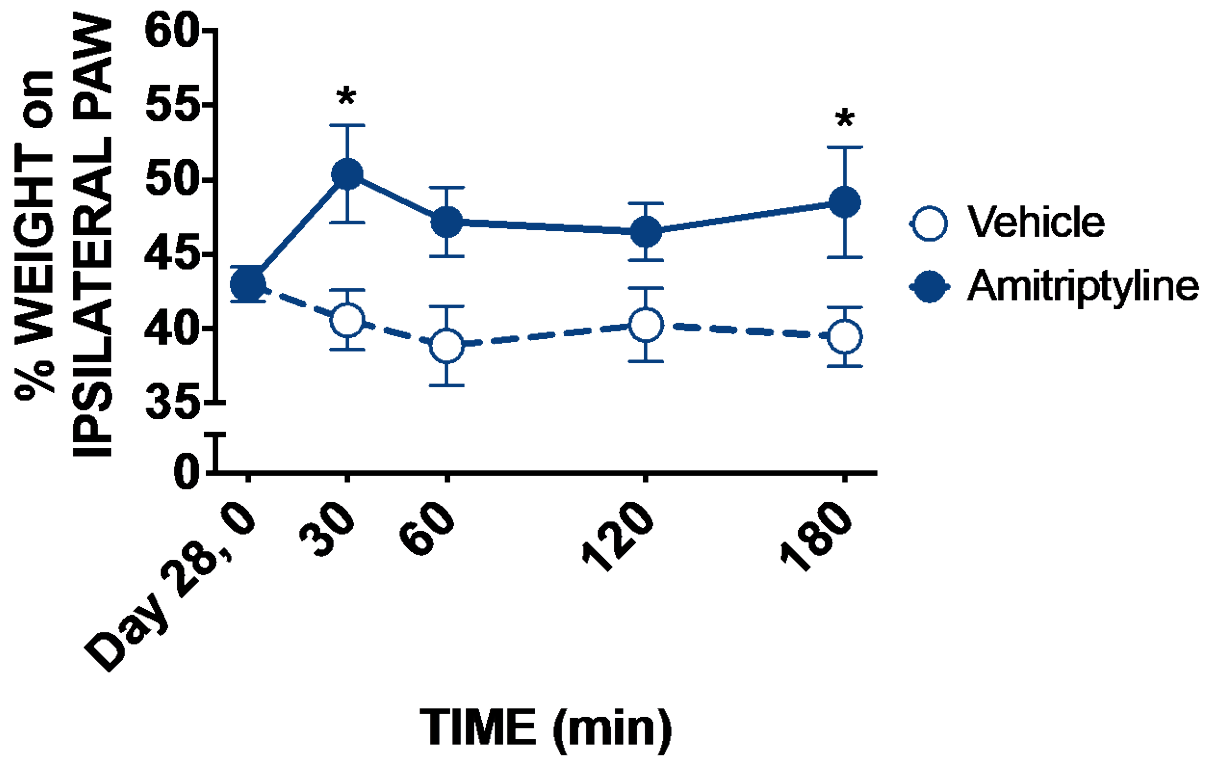
Figure 3. 5 Immunohistochemical analysis of dorsal root ganglia in the MMT model.

Cleaved caspase-3 expression was not statistically different in FG-positive neurones of MMT animals when compared to their sham counterparts in either sex (A). The number of FG-traced neurones that were associated with GFAP-positive SGCs were elevated in MMT animals of both sexes compared to sham-operated animals (B). The percentage of FG-neurones that expressed both cleaved caspase-3 and were associated with GFAP-positive SGCs was also higher in the DRGs of PTOA animals of both sexes (C). Data are presented as mean values \pm SEM, 2-way ANOVA, n=6-8 DRGs per group.

A



B



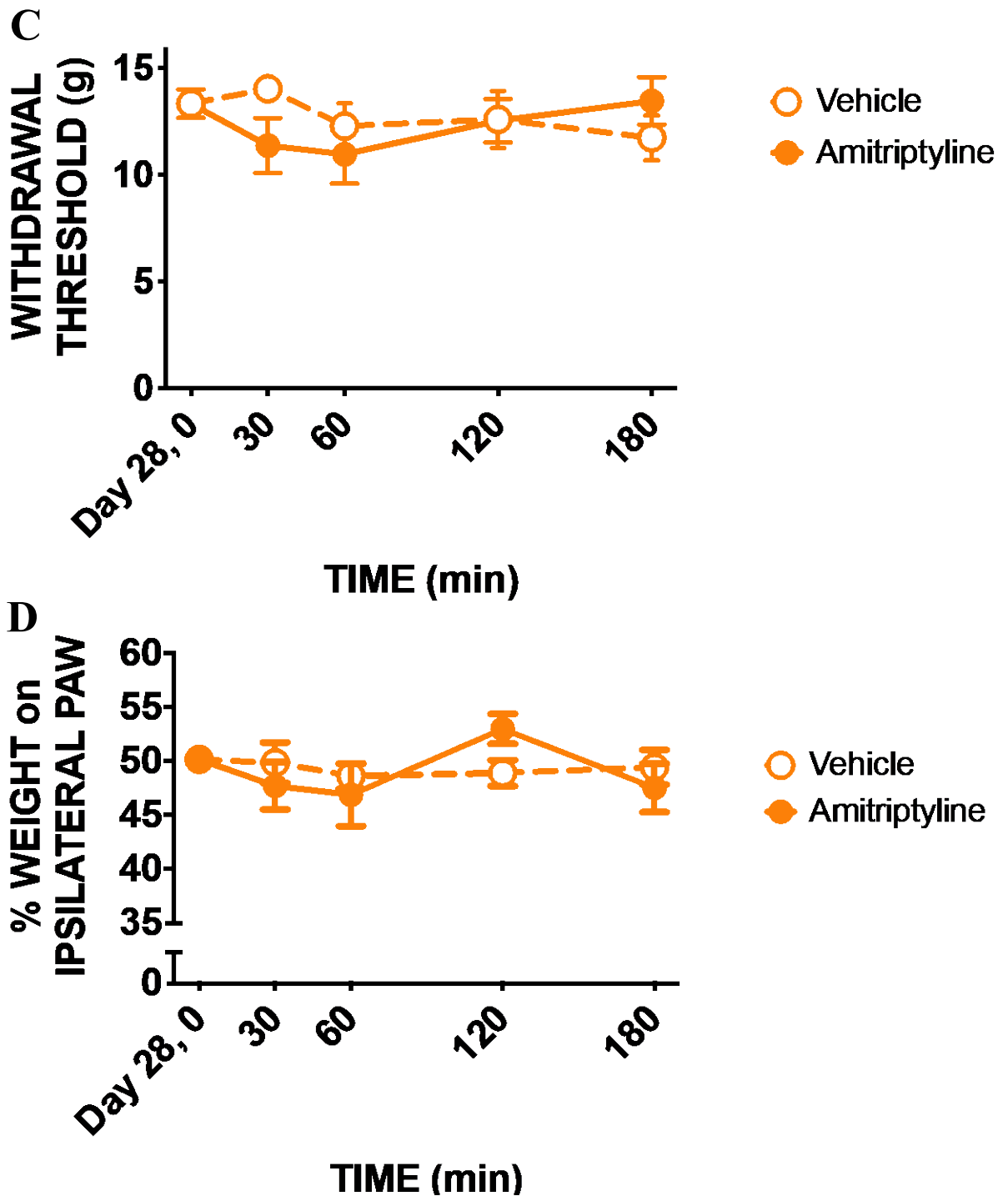
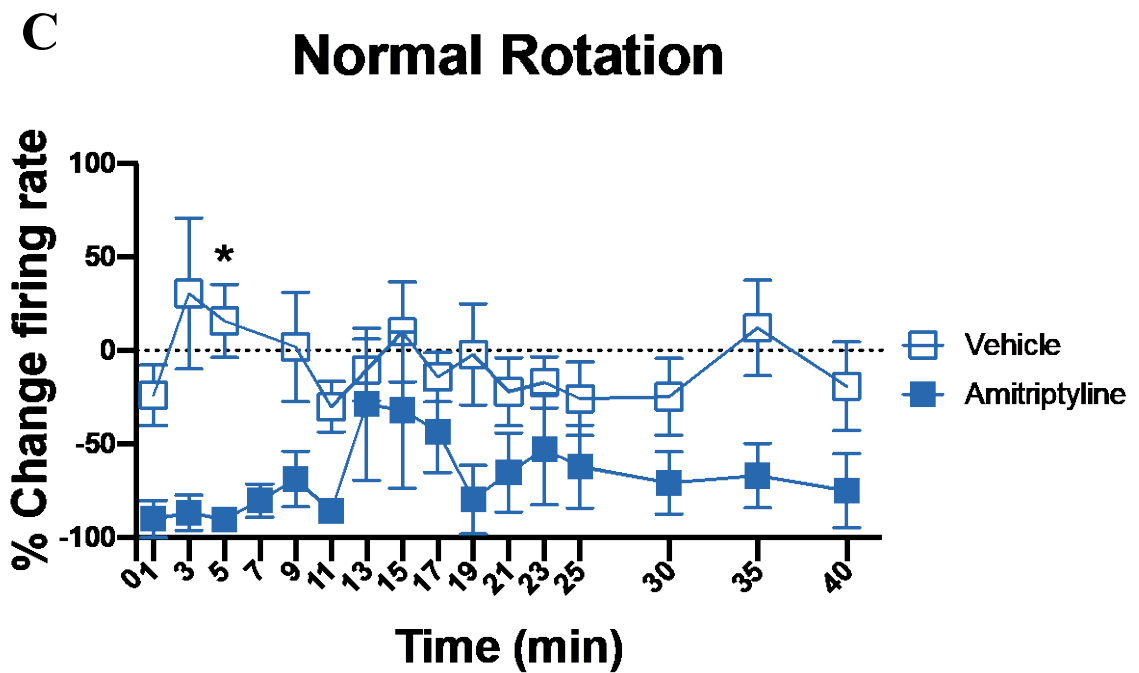
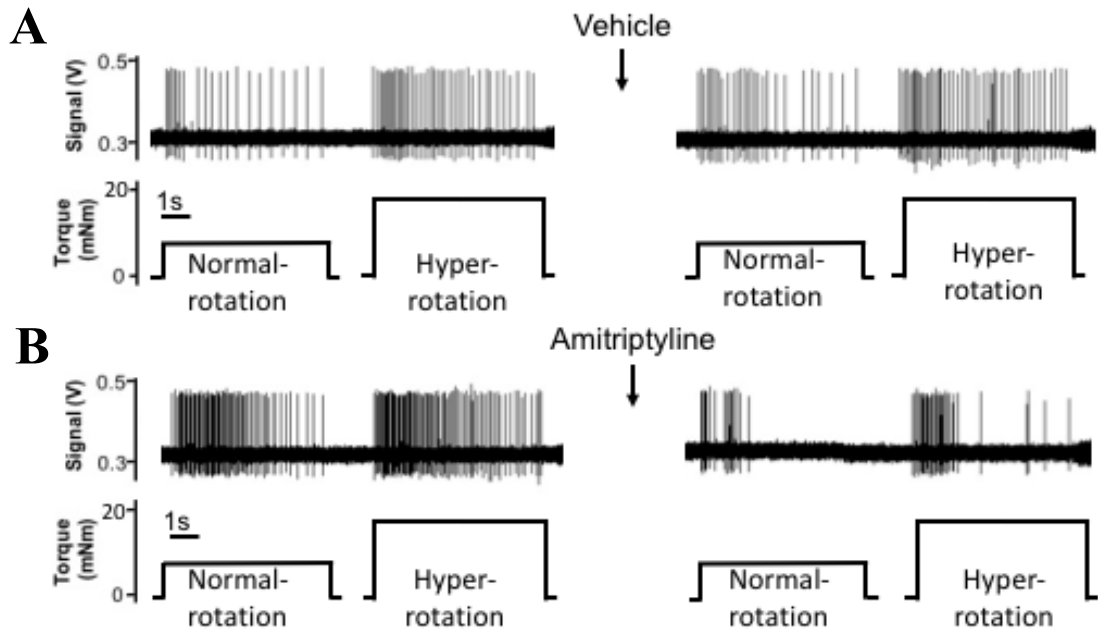
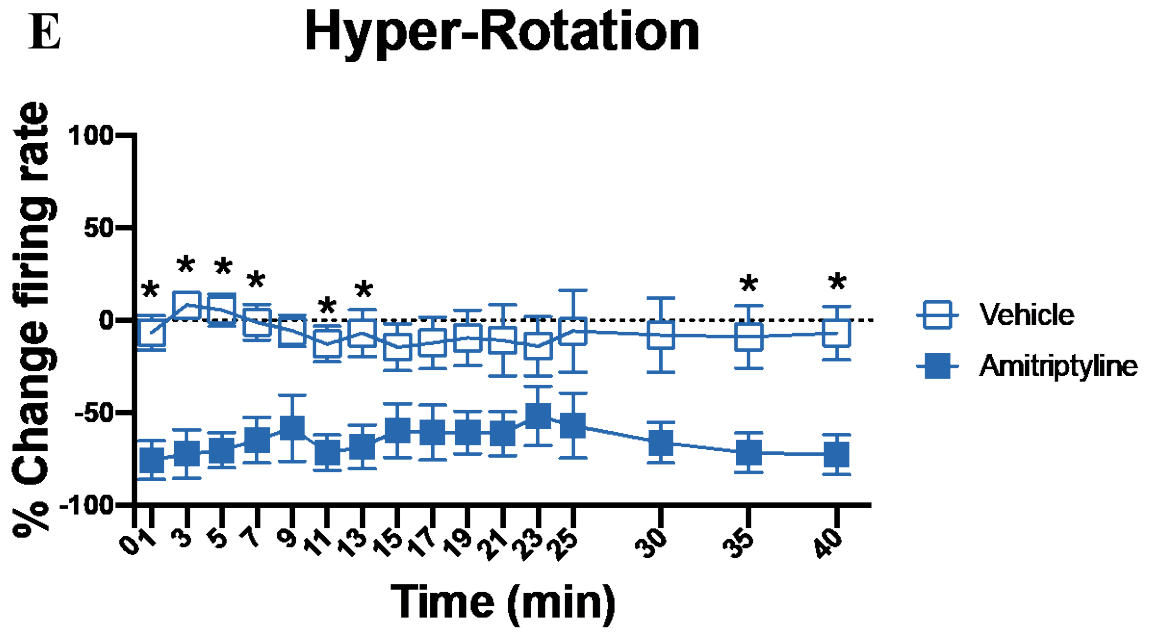
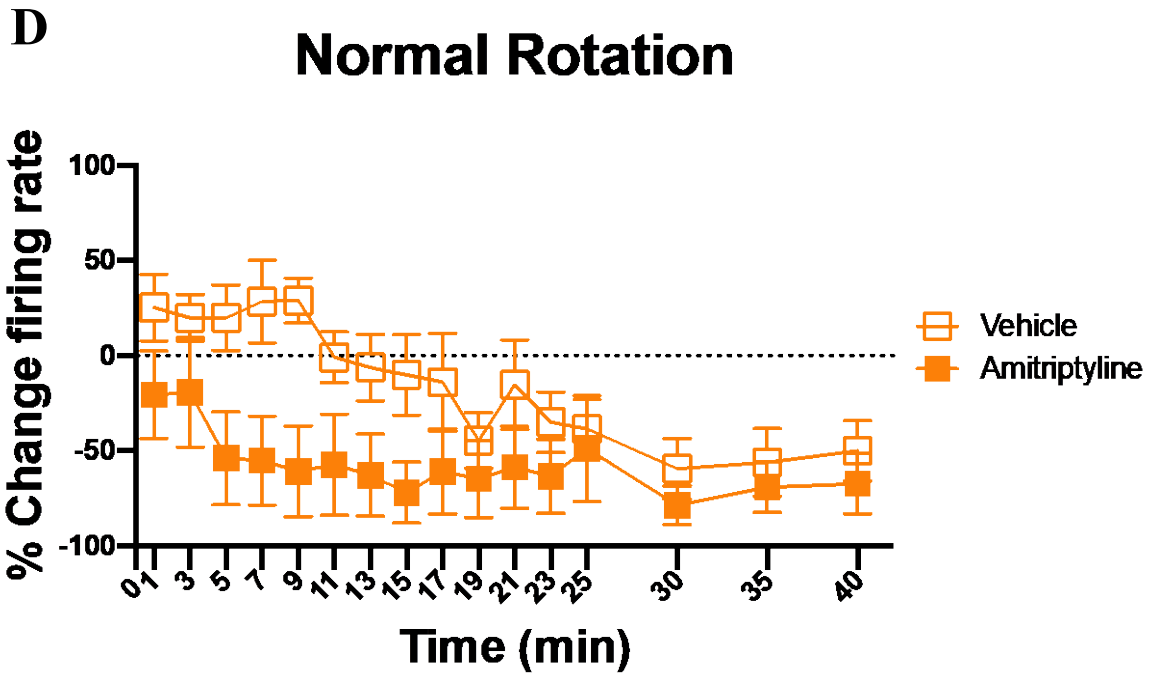


Figure 3. 6 Effect of systemically administered amitriptyline on MMT-induced pain.

When administered systemically on day 28 post MMT surgery, amitriptyline (20 mg/kg i.p.) significantly improved both hindpaw withdrawal threshold (A) and weight bearing deficits (B) in male animals, when compared to saline vehicle. In female PTOA animals, statistically significant differences were not observed in either outcome (C, D). Data are mean values \pm SEM, * $P < 0.05$, 2-way rm ANOVA with Bonferroni *post-hoc* test, $n = 7-9$ animals per group.





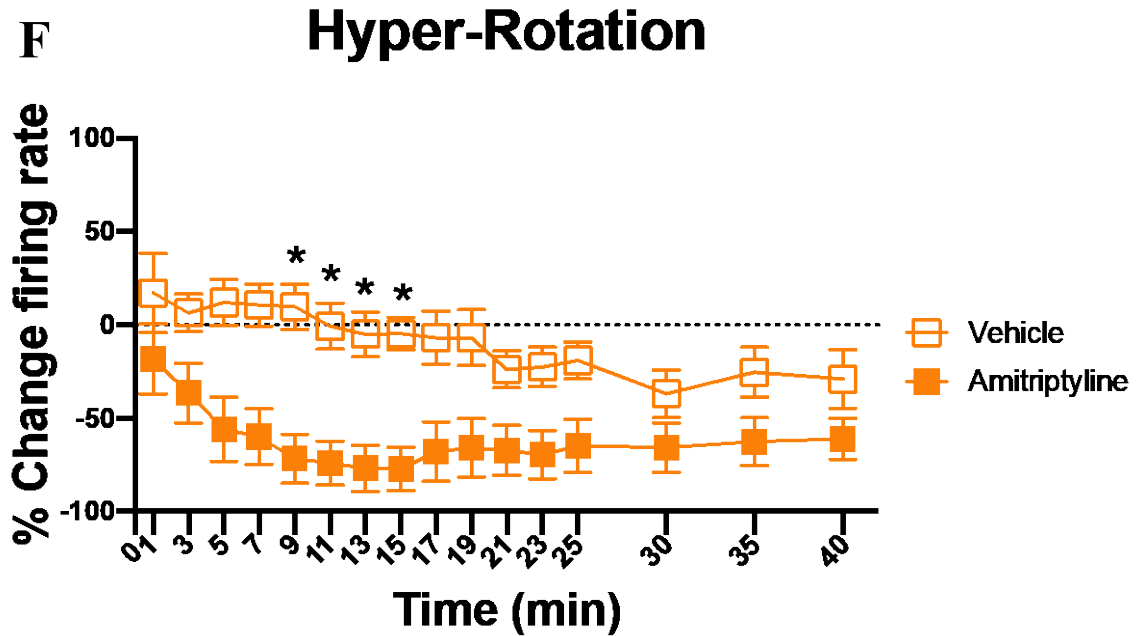


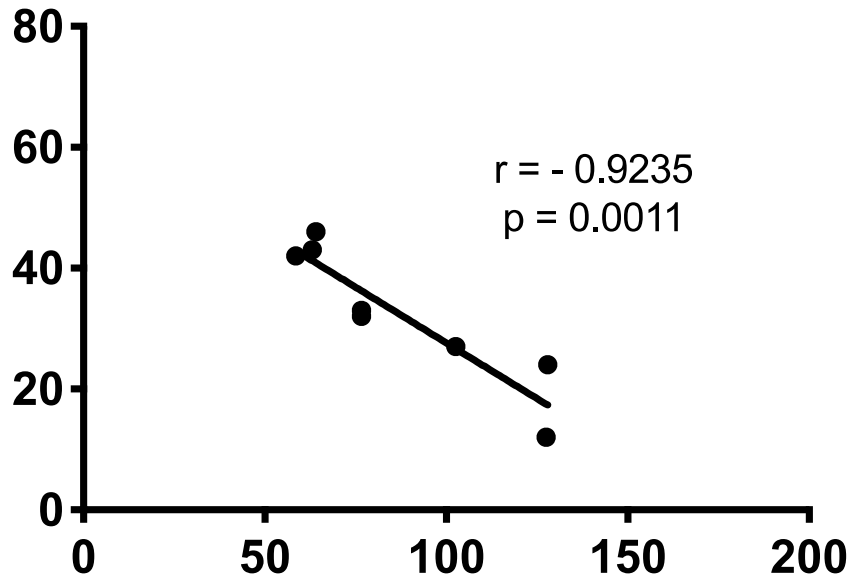
Figure 3. 7 Effect of close-intraarterial administration of amitriptyline on joint afferent firing.

Representative traces of the effect of (A) saline vehicle and (B) amitriptyline administration on joint afferent firing from a male MMT animal. Following close-intraarterial administration of amitriptyline (250 μg i.a.) into the saphenous artery, evoked firing was significantly reduced in response to both normal (C-D) and hyper (E-F) rotation of the joint in PTOA animals of both sexes. Data are mean values \pm SEM, 2-way ANOVA, $n=10-20$ fibres per group. * $P<0.05$, 2-way rm ANOVA with Bonferroni *post-hoc* test.

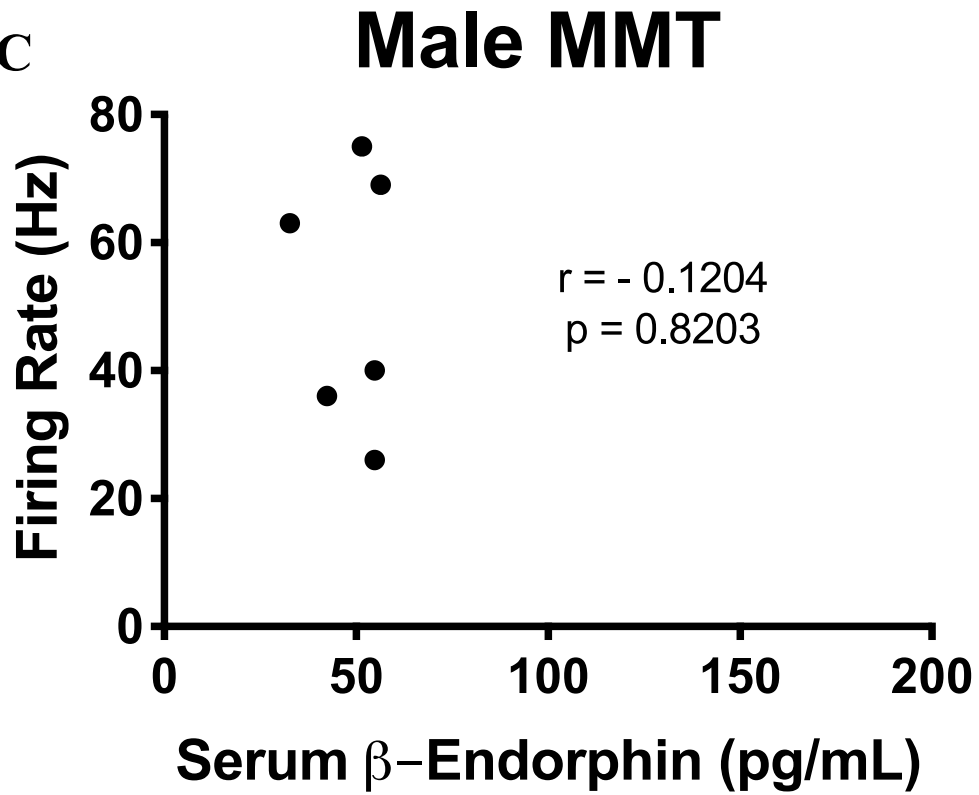
A

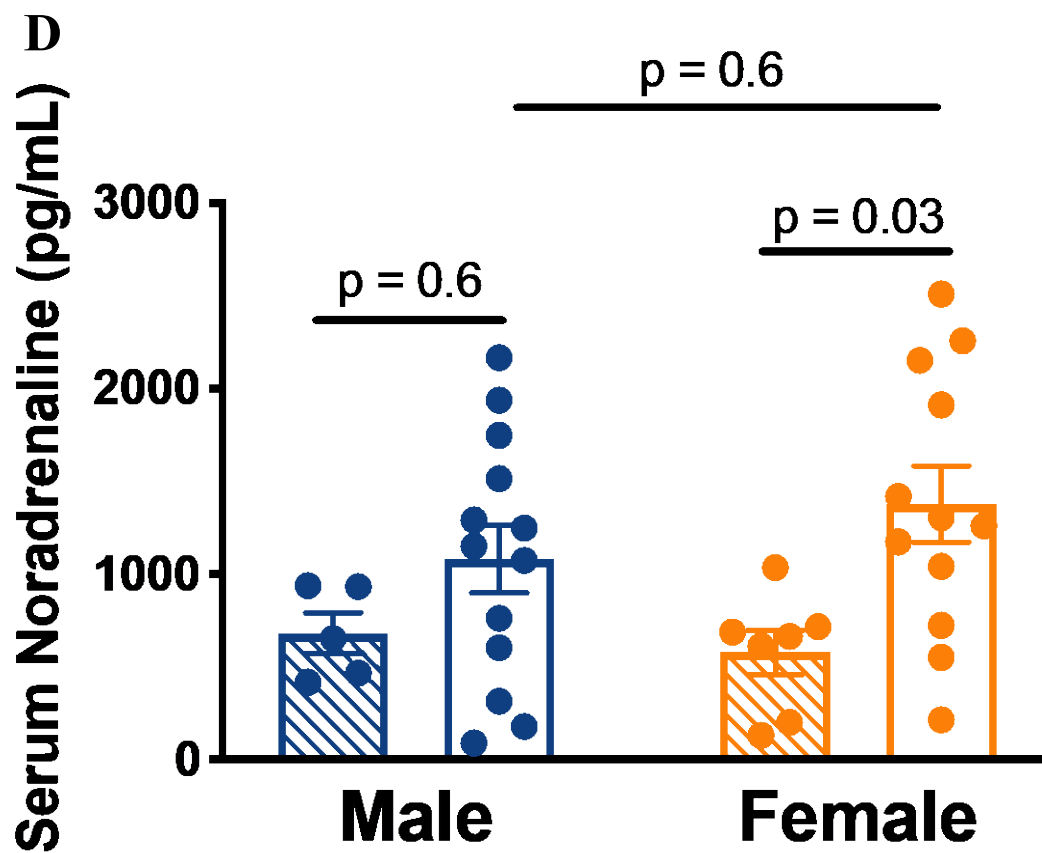


B



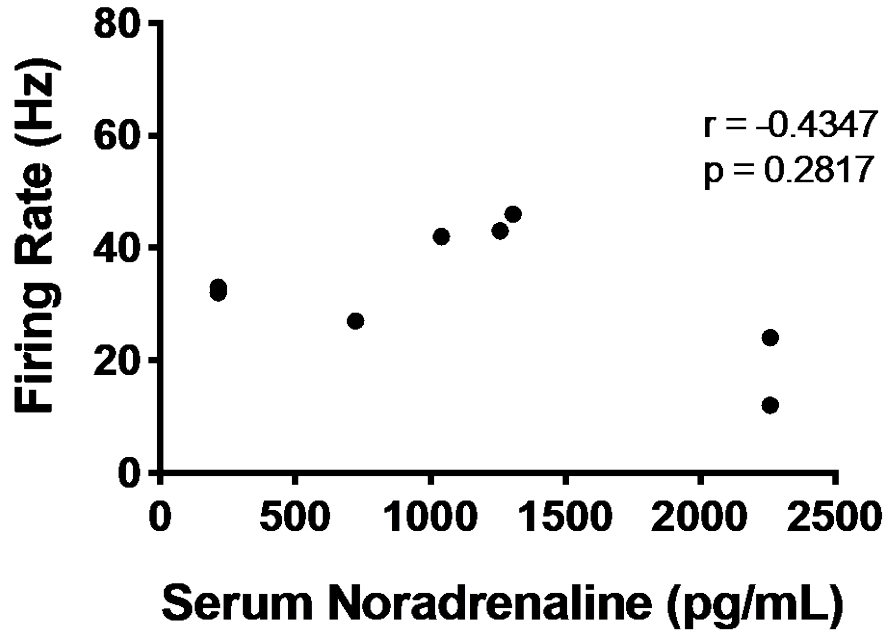
C





E

Female MMT



F

Male MMT

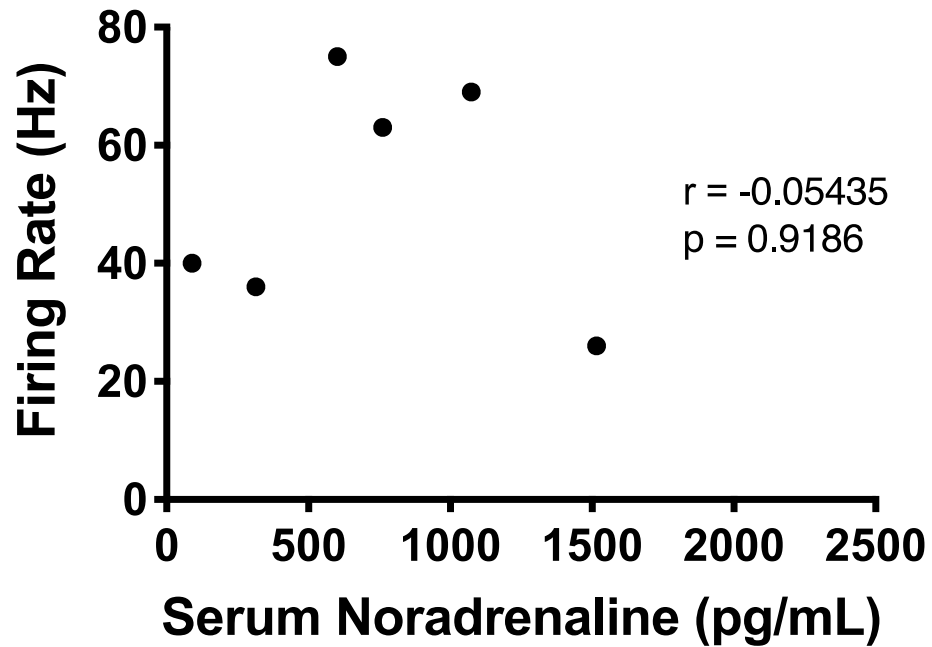


Figure 3. 8 Measurement of Serum Beta-Endorphin and Noradrenaline in PTOA animals.

Serum β -endorphin levels were significantly elevated in female MMT animals compared to males, but no differences were observed between surgical groups of either sex **(A)**. Serum β -endorphin levels were negatively correlated with baseline joint afferent firing rates in female PTOA animals **(B)**, but no relationship was found in male PTOA animals **(C)**. Serum noradrenaline was significantly elevated in female MMT animals compared to their sham counterparts but not males **(D)**. No relationships were observed between noradrenaline concentration and afferent firing rates in PTOA animals of either sex **(E, F)**. Data in A and D are presented as mean values \pm SEM, 2-way ANOVA, n = 5-13 animals per group. Correlations examined using Pearson's correlation coefficient.

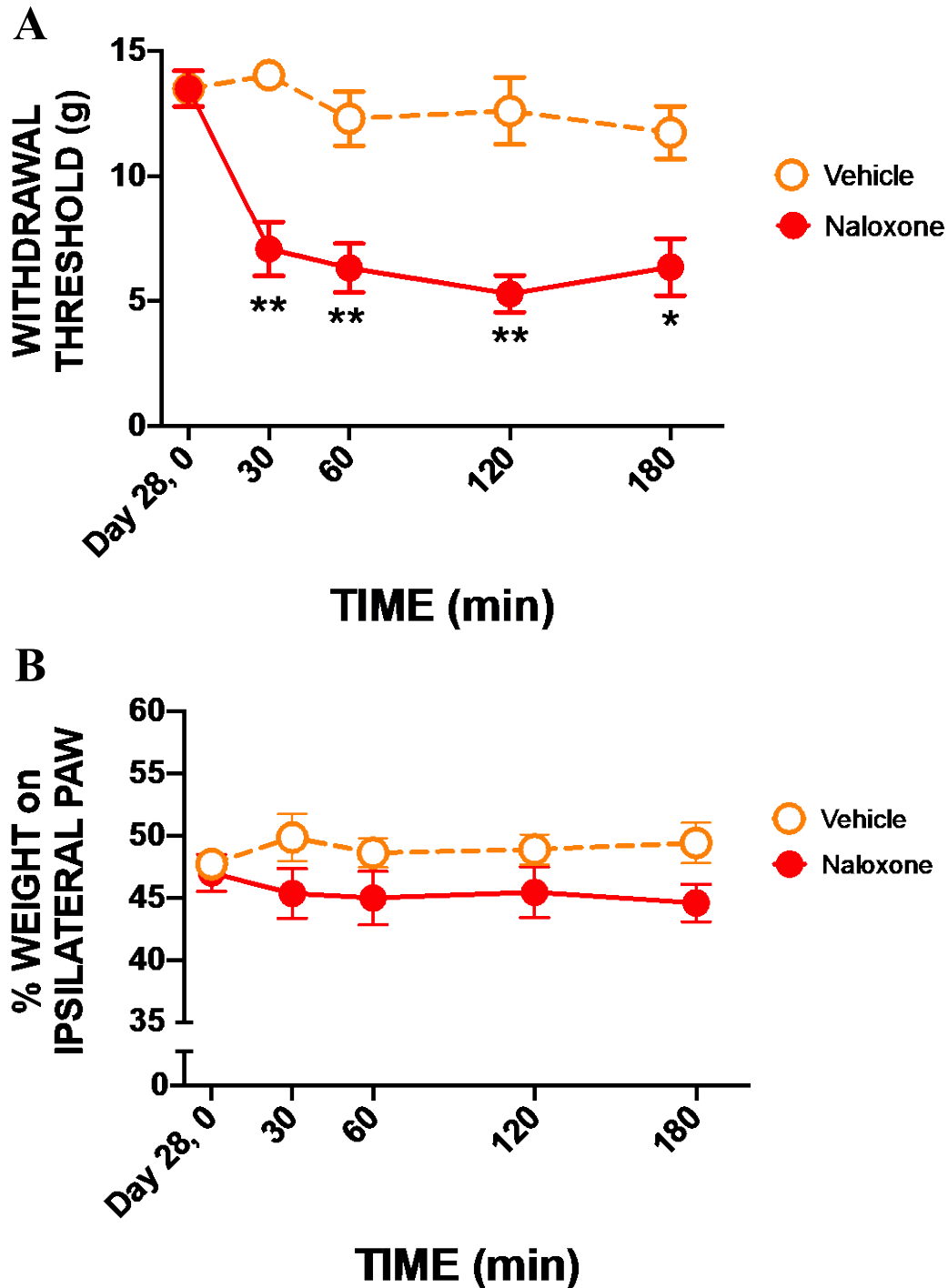


Figure 3. 9 Effect of naloxone in female MMT animals.

Systemic administration of naloxone (1 mg/kg i.p.) to day 28 female MMT rats produced a reduction in withdrawal threshold that was sustained over the 3-hour timecourse (A). Hindlimb weight bearing was not affected by naloxone treatment (B). Data are presented as mean values \pm SEM, * P <0.05, ** P <0.01, 2-way rm ANOVA with Bonferroni *post-hoc* test, $n = 7$ animals per group.

Chapter 4: The role of PAR4 in Early and Late-Stage Experimental OA

Disclosures: There are no disclosures to report for this chapter.

4.1 Background and Hypothesis

Serine proteases have been implicated in the catabolic destruction of joint tissue in OA and also found to mediate pain through their cognate receptors, PAR1-4 [156, 157, 200, 201, 260]. In pre-clinical models of inflammatory joint disease, PAR4 activation has been shown to modulate nociception and joint inflammation [155, 260, 272].

Additionally, local administration of PAR4-activating peptides into the joint sensitize joint nociceptors in a mechanism mediated partially by bradykinin-2 release from mast cells [155]. While PAR4 cleaving serine proteases are elevated in OA patients, the role of the receptor in the disease has not been widely studied.

Unlike PAR4, PAR2 has been studied extensively in the context of OA and blockade of the receptor has been found to be anti-nociceptive, anti-inflammatory, and neuroprotective in pre-clinical models [154, 156, 157]. It is unknown if PAR4 antagonism would exhibit the same beneficial properties in rodent OA models.

Hypotheses Tested in this Study:

- I: Blockade of PAR4 is antinociceptive in both inflammatory and neuropathic-driven pain in experimental OA models.**
- II: Blockade of PAR4 is anti-inflammatory in experimental OA models.**

4.2 Characterising Early and Late Stages in the MIA and MMT Models of Experimental OA

4.2.1. Methods

4.2.1.1 Induction of MIA and MMT Models

Two models were employed to induce experimental OA, the monoiodoacetate (MIA) model and the MMT model. Male and female MIA animals were compared on the basis of nociceptor activity and saphenous nerve thickness and did not differ from each other (Appendix C). Therefore, only male animals were used in these experiments.

Briefly, male Wistar rats (250-395g) were deeply anaesthetised with isoflurane (2-4%, O₂ 0.8L/min) until cessation of sensory reflexes. In the MIA model, 3 mg of MIA (50 µl saline) was administered into the right knee via intra-articular injection on day zero.

Naïve animals were used as controls in a sub-set of experiments.

A separate cohort of animals underwent the MMT surgery as previously described with sham-surgery animals acting as controls where appropriate.

Two timepoints were chosen to represent early phase and late phase OA in each model. The early phases are days 3 and 7 in the MIA and MMT models, respectively, while the late phases are days 14 and 28. Experimental timelines are depicted in figure 4.1.

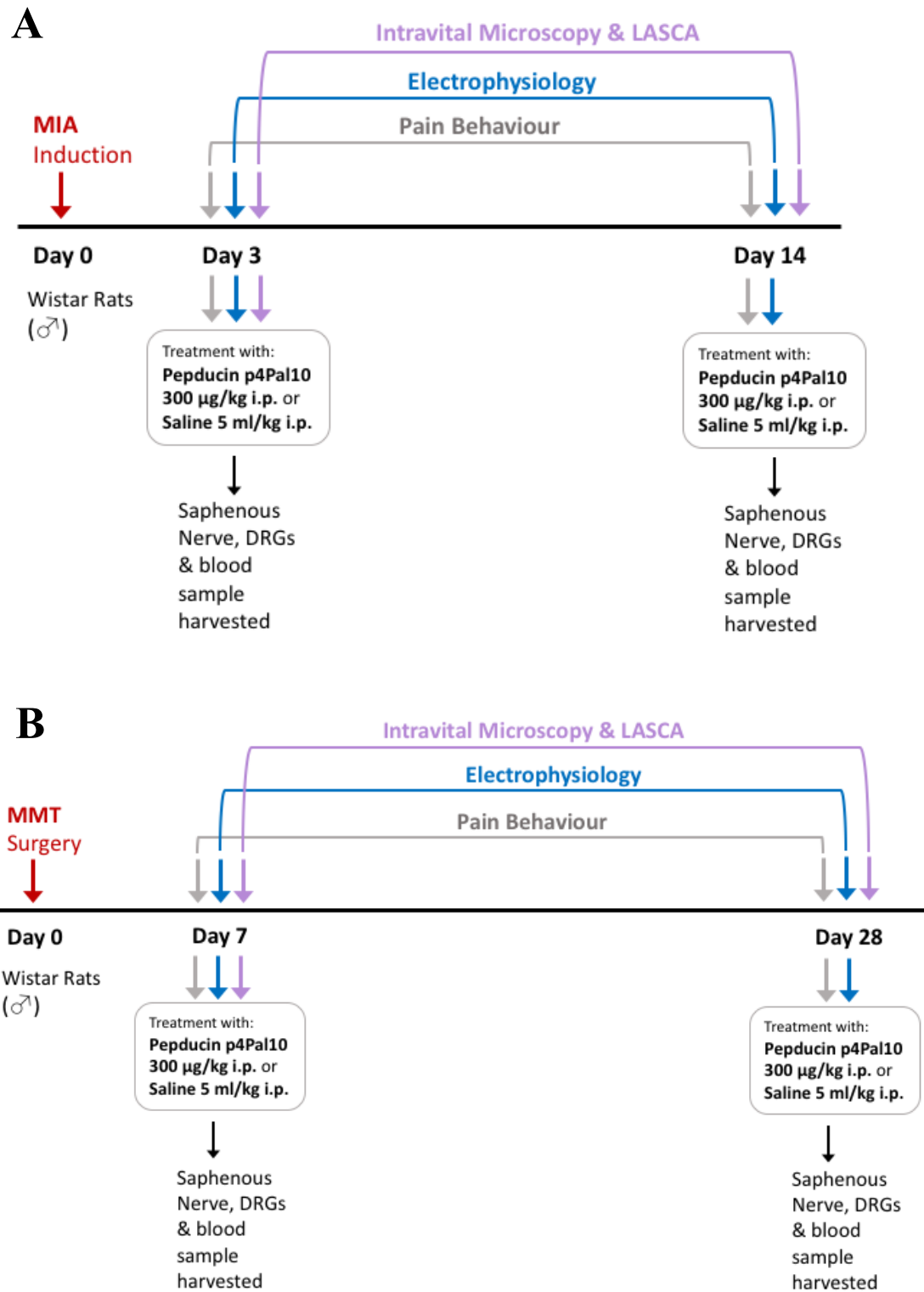


Figure 4. 1 Experimental Timeline for MIA and MMT Animals.

MIA animals (A) and MMT animals (B).

4.2.1.2 Characterising Saphenous Nerve Integrity in Early and Late Stages in the MIA and MMT models of Experimental OA

Saphenous nerve sections proximal to the ipsilateral knee were harvested from naïve, days 3 and 14 MIA and days 7 and 28 MMT animals and processed for electron microscopy as detailed in section 2.5. G-ratios were calculated to measure myelin thickness and the percentage of axons with irregular morphology was determined.

4.2.2 Results

4.2.2.1 Peripheral nerve damage and demyelination is present in the late phase of the MIA model

MIA caused an increase in g-ratio values 14 days following administration compared to both day 3 MIA and naïve animals as measured in both large diameter ($p < 0.05$, $n = 5-6$ animals per group, one-way ANOVA, Figure 4.2B) and small diameter axons ($p < 0.05$, $n = 5-6$ animals per group, Figure 4.2C), indicating nerve demyelination. G-ratio values were not significantly different between day 3 MIA and naïve animals ($p > 0.05$, $n = 5$ animals per group).

Examining nerve morphology also revealed a significantly higher proportion of axons in day 14 MIA animals were abnormal, 16.7 ± 1.1 %, compared with 10.3 ± 1.4 % and 9.3 ± 1.3 % in day 3 MIA and naïve nerve samples, respectively (Figure 4.2D). Abnormal morphology included disrupted or extruded myelin, whereas normal morphology was considered compact, uniform myelin.

4.2.2.2 Peripheral nerve damage but not demyelination is present in the late phase of the MMT model.

Comparison of g-ratio measurements from day 28 male MMT and sham-surgery saphenous nerves indicated a non-significant change in myelin thickness in the MMT model as presented in section 3.4.2. These data are presented again in Figure 4.2A to compare with the early timepoint in this model. G-ratios were calculated for saphenous nerves from day 7 MMT and sham-surgery animals and non-significant differences in myelin thickness were observed for both large diameter ($p>0.05$, $n=5-6$ animals per group, one-way ANOVA, Figure 4.2E) and small diameter axons ($p>0.05$, $n=5-6$ animals per group, Figure 4.2F). When day 7 and day 28 MMT axons were compared, no differences in g-ratios were detected ($p>0.05$, $n=6-8$ animals per group).

MMT surgery caused a significant increase in the percentage of damaged axons at day 28 compared to day 7 ($p<0.05$, $n=6$ animals per group, Figure 4.2G). However, comparison of nerve morphology at the early timepoint revealed a non-significant difference between day 7 MMT and sham-surgery axons ($p>0.05$, $n=5-6$ animals per group, Figure 4.2G), further supporting a lack of nerve damage early in this model.

4.3 Characterising Systemic Inflammation in Early and Late Stages in the MIA and MMT models of Experimental OA

4.3.1 Methods

4.3.1.1 Measurement of Systemic Inflammatory Mediators

Intra-cardiac blood samples were harvested from naïve animals, or three- and 14-days post MIA administration and seven- and 28-days post MMT or sham-surgery. Multiplex assays were performed as detailed in section 2.9 to measure IL-10, IL-17A, IL-6, IL-1 β , and TNF- α .

4.3.2 Results

Serum cytokines were measured during the early and late timepoints of each model and from control animals to gauge the level of inflammation during disease progression (Table 4.1). While we aimed to measure five markers in each group (IL-10, IL-17A, IL-6, IL-1 β , and TNF- α) some analytes were below the limit of detection of the Multiplex assay and are denoted as not determined (ND) in Table 4.2.

In MIA animals, levels of the pro-inflammatory mediators IL-6 and TNF- α were elevated at day 3 (IL-6: 33.8 ± 6.3 pg/mL, TNF- α : 360.8 ± 106 pg/mL) and decreased by day 14 (IL-6: 12.6 ± 3.1 pg/mL, TNF- α : 114.4 ± 29.3 pg/mL) ($p < 0.05$, $n = 6-7$, one-way ANOVA). In naïve animals, IL-6 levels were below the limit of detection while TNF- α concentration was lower than measured at either MIA timepoint (61.44 ± 24.0 pg/mL) ($p < 0.05$, $n = 6-7$). IL-10 was also significantly elevated at the earlier timepoint ($p < 0.05$, $n = 7$) compared to day 14, while lower levels were detected in naïve animals. IL-17A concentration was non-significantly different as the model developed ($p > 0.05$, $n = 7$). Additionally, serum concentration of IL- β was below the limit of detection in many of the samples from MIA and control animals.

In MMT animals, a similar early inflammatory trend was observed with each detected analyte significantly elevated at day 7 when compared to day 7 sham-surgery

animals ($p < 0.05$, $n = 5$). IL-1 β , and IL-17A levels were also significantly higher 7 days following PTOA induction compared to day 28 suggesting an enhanced inflammatory state at the earlier timepoint. TNF- α concentration was below the limit of detection in many of the samples from MMT and sham-surgery animals.

4.4 Single-Unit Recordings of Joint Afferent Fibres in MIA and MMT Models of OA and the Effect of PAR4 Blockade on Evoked Firing

4.4.1 Methods

MIA (day 3 and 14) and MMT (day 7 and 28) animals were deeply anaesthetised with urethane (25% solution, 2 g/kg i.p.) and underwent surgical preparation for electrophysiological recordings as outlined in section 2.3. Upon identification of a joint afferent fibre, baseline rotation of the knee joint were carried out and pepducin P4pal10 (300 μ g/kg i.p.) or saline (5 ml/kg i.p.) was administered. Joint nociceptor mechanosenitivity was assessed for an additional 60 minutes by applying a rotational stimulus to the knee joint every ten minutes. The percentage change in afferent firing rate following drug treatment was calculated offline using Spike2 software.

The dose of pepducin P4pal10 was chosen based on previous behavioural and electrophysiology experiments carried out in mice and rats [155, 260, 272].

4.4.2 Results

4.4.2.1 Characterisation of Joint Afferent Electrophysiological Activity in the Early and Late Phases of Experimental OA

Mechanosensitive A δ - and C- joint afferent fibres from naïve, MIA, and MMT animals were recorded and electrophysiological characteristics are summarised in Table 4.2. Sensitisation was observed in nociceptors from MIA and MMT animals compared to naïve animals; however, no electrophysiological differences were discerned across timepoints of either model. Mechanical thresholds were reduced in day 3 MIA animals (10 ± 1 mNm) compared with naïve (23 ± 3 mNm) but a non-significant difference was observed with day 14 (16 ± 3 mNm). Hyper-rotation of the knee also evoked significantly more firing from both early and late phase MIA animals compared to naïve controls ($p < 0.05$, $n = 10-11$ fibres per group, one-way ANOVA). Spontaneous firing was present in 73% of fibres recorded in day 3 MIA animals and 50% of day 14 animals, but only evoked firing was observed in naïve joint afferents.

In the MMT model, a similar proportion of joint afferents exhibited spontaneous firing, with 56 and 57% in day 7 and 28 animals, respectively. Fibres from early and late phase PTOA animals had similar mechanical thresholds but both groups were significantly lower than thresholds in naïve animals ($p > 0.05$, $n = 11-16$ fibres per group, one-way ANOVA). Evoked firing rates were also similar between day 7 and day 28 animals (day 7: 35 ± 5 action potentials/movement; day 28: 38 ± 5 action potentials/movement) but significantly elevated compared to naïve (12 ± 2 action potentials/movement) ($p < 0.05$, $n = 11-16$). There were no significant differences in either the electrical thresholds or the conduction velocities between either group.

4.4.2.2 PAR4 Blockade Attenuates Joint Afferent Firing in Early Experimental OA

Examples of single unit electrophysiological recordings before and after administration of saline and pepducin P4pal10 in day 3 MIA and day 7 MMT animals are presented in Figure 4.3A-B.

Blockade of PAR4 with pepducin P4pal10 significantly reduced joint afferent firing in day 3 MIA animals compared with saline vehicle ($p < 0.05$, $n = 8$, 2-way rm ANOVA). A maximal reduction of $35 \pm 6\%$, compared to baseline firing, was reached by 60 minutes post-drug administration. In day 7 MMT animals, pepducin P4pal10 also significantly reduced nociceptor activity ($p < 0.05$, $n = 8-10$). A maximal effect was observed at 50 minutes where firing was decreased by $40 \pm 10\%$.

4.4.2.3 PAR4 Blockade Fails to Affect Joint Afferent Firing in Late Experimental OA

Representative traces of single unit recordings before and after saline and pepducin P4pal10 treatment in day 14 MIA and day 28 MMT animals are depicted in Figure 4.3E-F.

Systemic pepducin P4pal10 failed to attenuate joint afferent firing in day 14 MIA animals over the 60-minute timecourse ($p > 0.05$, $n = 7-9$, 2-way rm ANOVA, Figure 4.3G). Blockade of PAR4 in day 28 MMT animals, similarly, had no effect on nociceptor firing compared to baseline ($p > 0.05$, $n = 10-11$, Figure 4.3H).

4.5 Effect of PAR4 Blockade on Pain Behaviour in the Early and Late Phases of Experimental OA

4.5.1 Methods

Male Wistar rats underwent behavioural pain testing on days 3 and 14 following MIA administration and days 7 and 28 post MMT surgery. von Frey hair algiesiometry and dynamic weight bearing measurements were taken in series at baseline to measure secondary allodynia and weight bearing deficits, respectively. Animals were then separated into two cohorts that received either pepducin P4pal10 (300 µg/kg i.p.) or saline (5 mL/kg i.p.). Behavioural pain measurements were taken at 30, 60, 120, and 180 minutes following drug treatment.

4.5.2 Results

4.5.2.1 PAR4 Blockade Improves Referred Pain in Early Phases of Experimental OA

Day 3 MIA animals exhibited secondary mechanical allodynia compared to day zero (day 3: 6.1 ± 0.5 g, day 0: 14.9 ± 0.0 g) which was significantly improved with pepducin P4pal10 treatment ($p < 0.05$, $n = 7$, two-way rm ANOVA, Figure 4.4A). *Post hoc*-analysis revealed PAR4 blockade was analgesic from 30 minutes following treatment until 120 minutes compared to saline vehicle. Severe hindlimb weight bearing defects were also present in these animals (Day 3: 32.3 ± 2 % ipsilateral weight bearing) compared with day zero baseline measurements (Pre-MIA: 49.9 ± 0.6 %) ($p < 0.05$, $n = 7$, student's t-test). Treatment with pepducin P4pal10 was unable to attenuate these weight bearing deficits over the timecourse recorded ($p > 0.05$, $n = 7$, two-way RM ANOVA, Figure 4.4B).

Seven days following MMT surgery, animals withdrawal thresholds reduced to 10.3 ± 0.6 g from 14.9 ± 0.07 g at pre-surgery measurement. Pepducin P4pal10 significantly increased withdrawal thresholds over the same 30 to 120-minute time period ($p < 0.05$, $n = 7-8$, Figure 4.4C) as observed in MIA animals. A maximal recovery of 13.8 ± 0.7 g was achieved 60 minutes following drug administration. A mild reduction in hindlimb weight bearing was detected at day 7 where animals placed 46.6 ± 1.4 % of their hindlimb weight on their ipsilateral limb compared with 51.3 ± 1.4 % on day zero. Blockade of PAR4 attenuated this mild deficit when compared with saline over the 3-hour timecourse ($p < 0.05$, $n = 7-8$, Figure 4.4D).

4.5.2.2 PAR4 Blockade Fails to Improve Pain Behaviour During the Late phase of Experimental OA

Referred pain persisted on day 14 of the MIA model as detected by reduced withdrawal thresholds (Day 14: 6.4 ± 0.6 g vs Day 0: 14.9 ± 0.0 g). PAR4 blockade was ineffective in mitigating the mechanical allodynia observed in these animals ($p > 0.05$, $n = 7-8$, Figure 4.4E). At this end-stage phase of the disease, weight bearing deficits were less severe; animals bore 42.2 ± 1.5 % weight on the ipsilateral hindpaw compared to 32.3 ± 2 % on day 3 ($p < 0.05$, $n = 14-15$). Pepducin P4pal10 treatment also failed to elicit any significant effect on hindlimb incapacitance compared to vehicle control ($p > 0.05$, $n = 7-8$, Figure 4.4F).

Twenty-eight days following MMT surgery, the referred pain and weight bearing deficits observed on day 7 persisted and were not significantly different from the earlier

timepoint ($p > 0.05$, $n = 12-16$). Pepducin P4pal10 had no effect on von Frey hair mechanosensitivity ($p > 0.05$, $n = 8$, Figure 4.4G) but did significantly improve hindlimb incapacitance compared to saline control ($p < 0.05$, $n = 8$, Figure 4.4H).

4.6 Measuring Joint Inflammation in Experimental OA and the Effects of Systemic PAR4 Blockade

4.6.1 Methods

Male Wistar rats underwent joint inflammation assessment using IVM and LASCA at days 3 and 14 of the MIA model and days 7 and 28 of the MMT model.

Briefly, animals were deeply anaesthetised using urethane (25% solution, 2 g/kg i.p.) and underwent surgical preparation for IVM and LASCA experiments as outlined in section 2.8. The skin and fascia overlying the knee were removed in order to visualise the knee microvascular. Circulating leukocytes were fluorescently labelled using Rhodamine 6G (100 μ l of 0.05% solution in saline, i.v.).

4.6.1.1 IVM

Unbranched post-capillary venules were identified in the knee capsule. Three one-minute videos were taken at baseline. Following baseline measurements, animals were administered either pepducin P4pal10 (300 μ g/kg i.p.) or saline (5 mL/kg i.p.). Three additional videos were taken at each of the following time points post-drug administration: 15, 30, 60, 90, and 120 minutes. Rolling and adherent leukocyte values were quantified and averaged for each timepoint and compared to baseline values.

4.6.1.2 LASCA

LASCA measurements were completed immediately proceeding IVM recordings at baseline and for each timepoint after pepducin P4pal10 or saline treatment. Immediately following euthanasia, a dead scan was recorded and the value of which was subsequently subtracted from all experimental LASCA measurements. To account for differences in MAP between the animals and during the course of the experiment, the mean perfusion values obtained from LASCA were divided by MAP to calculate vascular conductance as detailed in section 2.82. Vascular conductance at each timepoint was compared to baseline values.

4.6.2 Results

4.6.2.1 Comparison of Joint Inflammation in Early and Late OA

When compared to historical lab data of IVM and LASCA conducted on naïve animals, MIA induces increases in rolling and adherent leukocytes as well as vascular conductance at both day 3 and day 14 (naïve rolling: 5.6 ± 1.8 leukocytes/minute, adherent: 0.8 ± 0.2 leukocytes/minute, vascular conductance: 2.1 ± 0.3). Three days following MIA administration, some measures of joint inflammation were enhanced compared to day 14. Rolling leukocytes were significantly increased in the early timepoint compared to the endstage timepoint ($p < 0.05$, $n = 6-12$, Table 4.3), while a non-significant difference was observed in adherent leukocytes. Vascular conductance also was not significantly different between early and late stage MIA ($p > 0.05$, $n = 6-12$).

In the MMT model, 7 days following surgery all joint inflammatory parameters were significantly increased compared to 28 days after PTOA induction. Enhanced leukocyte trafficking was observed at the early timepoint (rolling: 62.4 ± 3 /minute and adherent: 2.2 ± 0.5 /minute) while lower values were observed at the later timepoint (rolling: 36.8 ± 3 /minute and adherent: 0.6 ± 0.2 /minute) ($p < 0.05$, $n = 8-18$). Joint perfusion was also significantly increased in day 7 animals compared to day 28 ($p < 0.05$, $n = 8-18$).

4.6.2.2 Effect of PAR4 Blockade on Joint Inflammation in Early Timepoints

When treated with pepducin P4pal10 on day 3 of the MIA model, rolling leukocytes were significantly reduced compared with saline vehicle ($p < 0.05$, $n = 6$, Figure 4.5A). Conducting *post-hoc* analysis revealed significance at 15, 30, 90 and 120-minute timepoints demonstrating a rapid and prolonged response to treatment with pepducin P4pal10. The antagonist failed to elicit an effect, however, on either adherent leukocyte trafficking or synovial hyperaemia ($p > 0.05$, $n = 6$, Figure 4.5B-C) over the two-hour timecourse.

In day 7 MMT animals, PAR4 blockade had mild effects on joint inflammation. Pepducin P4pal10 significantly reduced the number of rolling leukocytes compared to saline vehicle, with post-hoc analysis revealing significance at only the 60-minute timepoint ($p < 0.05$, $n = 9-12$, Figure 4.5D). There was a non-statistical difference in both adherent leukocytes trafficking and vascular conductance between treatment groups ($p > 0.05$, $n = 9-12$, Figure 4.5E-F).

4.7 Evaluation of PAR4 expression in DRG Joint Neurons

4.7.1 Methods

Fluoro-gold dye was used to identify joint neurones within the DRG of MIA and MMT animals. The retrograde tracer was injected into the ipsilateral knee (10 μ l of 2% FG in saline, i.artic. MIA: day -2 or 9, MMT: day 2 or 23) as outlined in section 2.4.1. Five days later, animals were perfused with saline and paraformaldehyde and ipsilateral L3 DRGs harvested and prepared for histology.

Following sectioning, tissues from L3 DRGs were stained with rabbit-anti-PAR4 (1:250, Abcam, Cambridge, UK) primary antibody overnight at 4 °C followed by Alexa fluor 488 goat-anti-rabbit (1:500, Invitrogen, Carlsbad, CA, USA) secondary antibody for one hour at room temperature. Slides were viewed under a Zeiss Axio Imager 2 (Zeiss, Oberkochen, Germany) at 10x magnification and analysed offline using Image J software. The total number of Fluoro-Gold-positive neurones were counted and the percentage that expressed PAR4 was calculated.

4.7.2 Results

4.7.2.1 PAR4 Expression is Higher in Joint DRG Neurons at Early OA Timepoints

Immunohistochemical analysis of Fluoro-gold DRG neurones revealed higher expression of PAR4 in earlier timepoints of both the MIA and MMT models compared to later timepoints. In day 3 MIA animals, $78 \pm 2\%$ of joint neurones express PAR-4 compared with $65 \pm 3\%$ two-weeks post induction ($p < 0.01$, $n = 4$ animals, students t-test). Seven days following MMT surgery, a similar level was observed with $79 \pm 2\%$ of

Fluoro-gold positive neurones co-expressing PAR-4 compared to $58 \pm 2\%$ on day 28 of the model ($p < 0.0001$, $n = 4$ animals).

4.8 Chapter Summary

4.8.1 The MIA and MMT models of OA Exhibit Enhanced Inflammation at Early Timepoints and Nerve Damage at Later Timepoints

Analysis of the MIA and MMT models reveals distinct early and late phases of disease progression. The early phase is characterised by pronounced inflammation and the later stage by the presence of peripheral neuropathy. Measurement of serum cytokines revealed increased levels of proinflammatory mediators at early model timepoints. IL-6 and TNF- α were elevated in day 3 MIA animals and IL-1 β and IL-17A in day 7 MMT. The heightened cytokine levels decreased at later timepoints. Additionally, assessment of the joint microvasculature in these animals verified the presence of local joint inflammation. Enhanced leukocyte trafficking was present in the knee joints of day 3 MIA animals while the number of adherent leukocytes and the magnitude of joint perfusion was not enhanced in this phase. In contrast, both rolling and adherent leukocytes and joint hyperaemia were increased during the early phase of the MMT model which resolved in the end-stage of the model.

Analysis of the saphenous nerve revealed demyelination and irregular axonal morphology in the late phase of MIA which was absent during the early timepoint. In the MMT model, g-ratio analysis did not indicate a change in myelin thickness at either timepoint; however, in day 28 animals a significant increase in non-uniform axons was observed.

The distinct phases modelled here with high inflammation and the absence of neuropathy early in the models followed by low grade inflammation and peripheral nerve damage during later phases in the MIA and MMT models allowed for the examination of a PAR4 antagonist under different joint conditions.

4.8.2 Pepducin P4pal10 Treatment was Analgesic and Mildly Anti-Inflammatory During Early Timepoints in the MIA and MMT Models

Treatment with the PAR4 antagonist pepducin P4pal10 was anti-nociceptive in animals during the early phase of both the MIA and MMT models but failed to produce consistent analgesia at end-stage timepoints. In single-unit electrophysiology experiments, PAR4 blockade attenuated joint afferent firing in day 3 MIA and day 7 MMT animals but not did not alter firing in day 14 and 28 animals. When tested using behavioural pain assays, improvements in withdrawal thresholds were observed in the early phase of both models following pepducin P4pal10 treatment. Mild improvements in weight bearing deficits were also detected in day 7 MMT animals but not MIA animals. Treatment failed to elicit robust anti-nociceptive behaviour during the later timepoint in animals of either model.

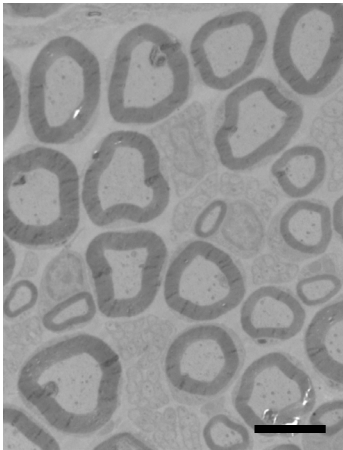
Mild anti-inflammatory effects were observed following PAR4 blockade in IVM and LASCA experiments. While leukocyte trafficking was reduced for a short-time frame in day 3 MIA animals, joint perfusion was not affected. In contrast, treatment reduced vascular conductance in day 7 MMT animals but failed to modulate leukocyte trafficking.

4.8.3 PAR4 Expression in DRG Joint Neurones is Greater During Early Timepoints in the MIA and MMT Models

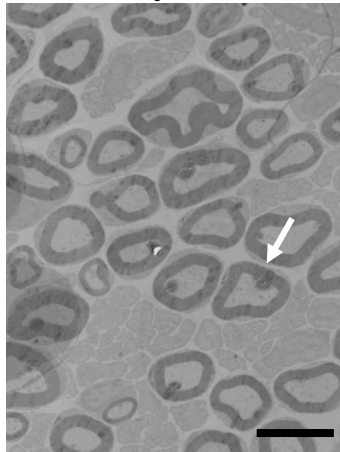
The expression of PAR4 in Fluoro-gold traced positive neurones in the L3 DRG was assessed during early and late phases of the MIA and MMT models to determine if changes in receptor expression may be contributing to the differential effect of PAR4 blockade. Higher expression of PAR4 was detected in day 3 MIA and day 7 MMT joint neurones compared to day 14 MIA and day 28 MMT.

A

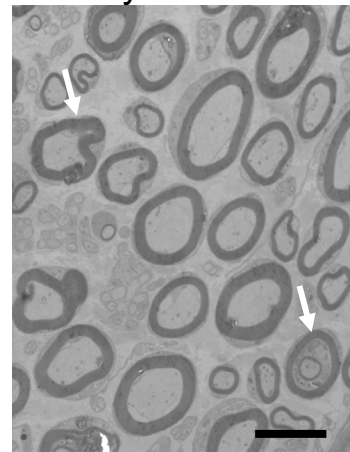
Naive



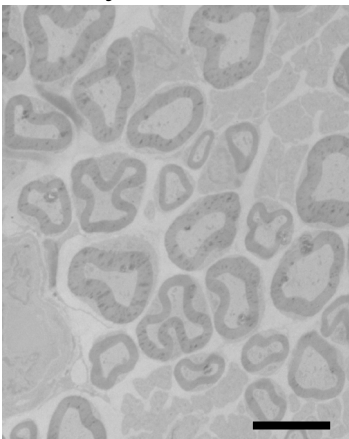
Day 3 MIA



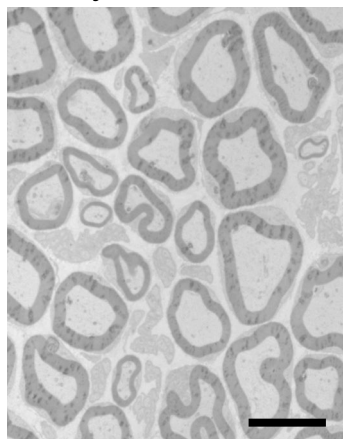
Day 14 MIA



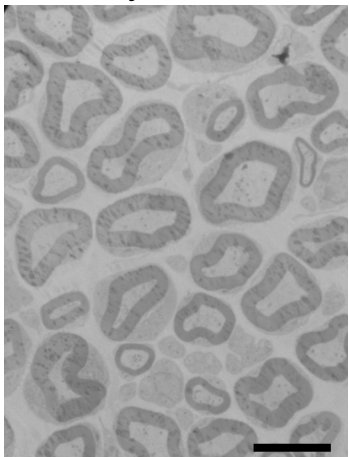
Day 7 Sham



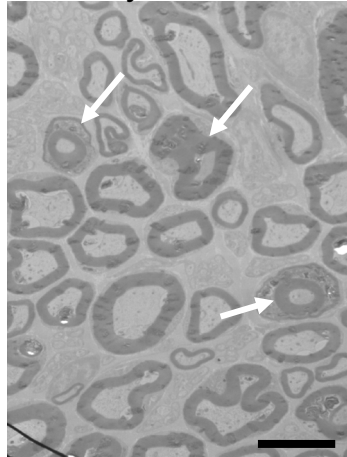
Day 28 Sham



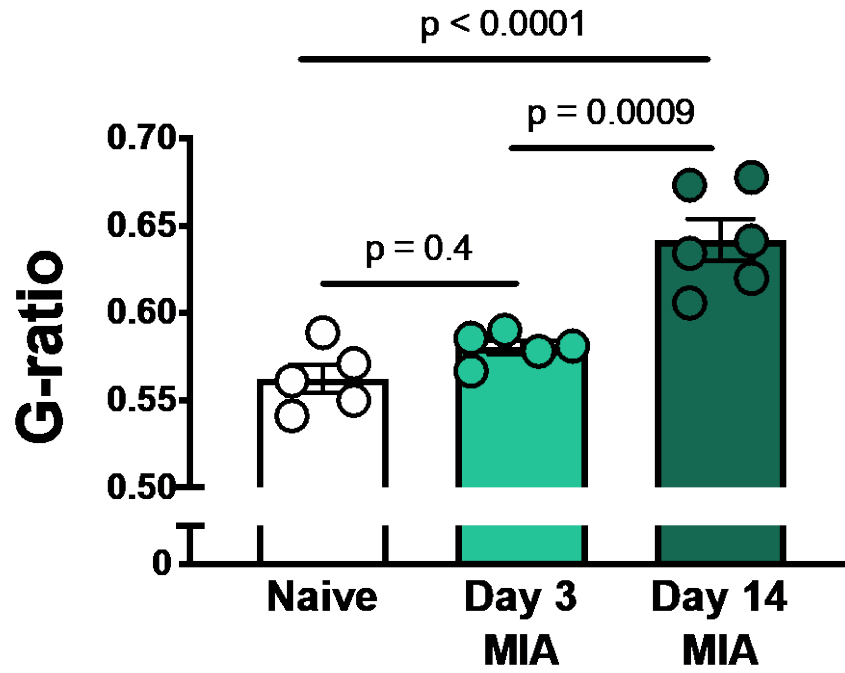
Day 7 MMT



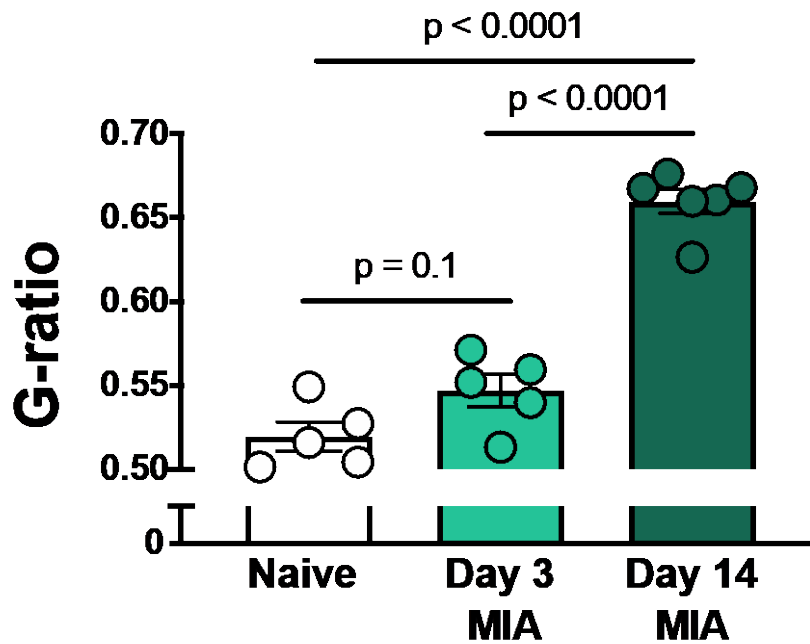
Day 28 MMT

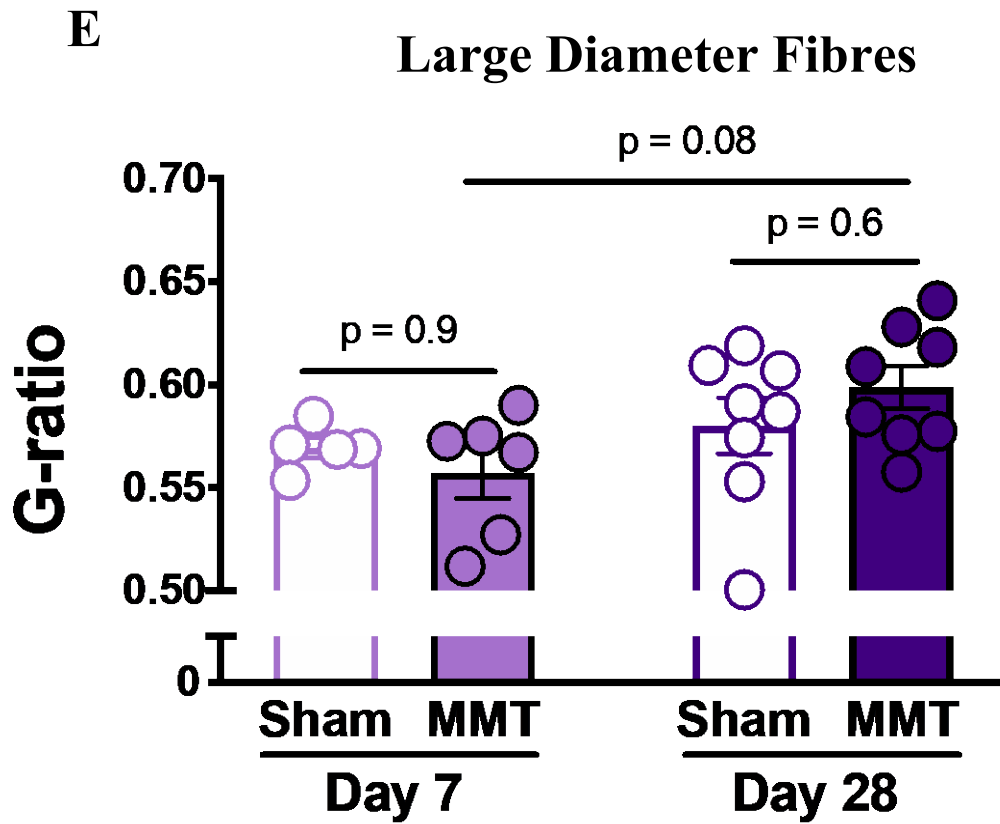
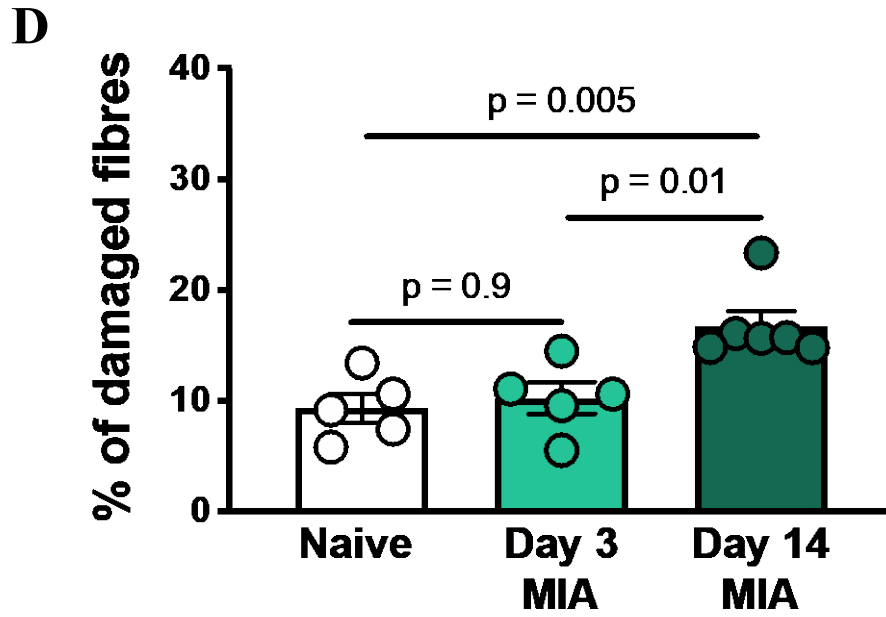


B Large Diameter Fibres



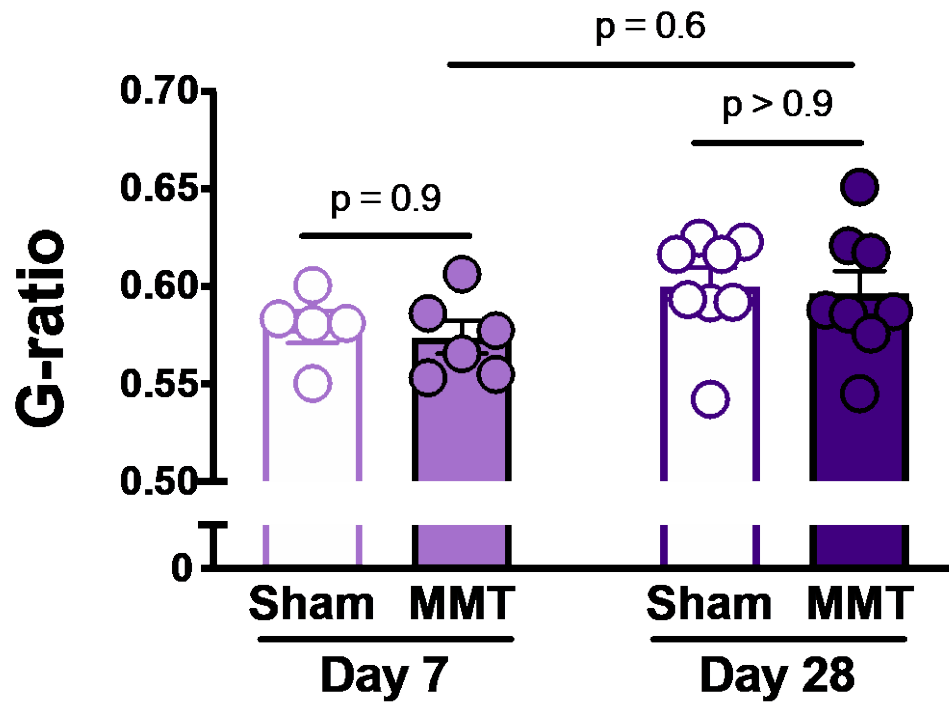
C Small Diameter Fibres





F

Small Diameter Fibres



G

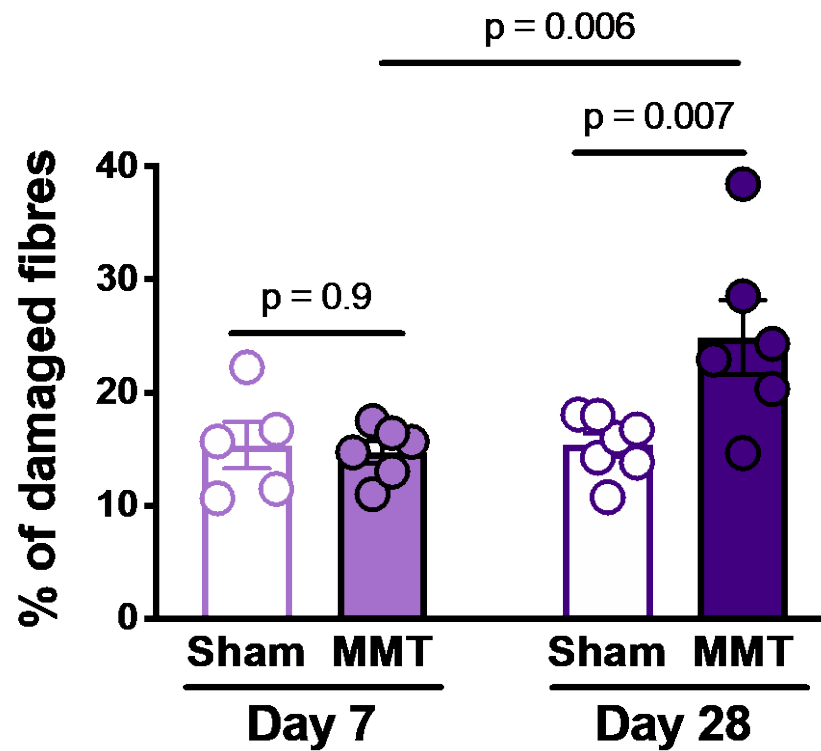


Figure 4. 2 MIA and MMT-induced Nerve Damage.

Representative electron photomicrographs of saphenous nerve axons from naïve, day 3 MIA, day 14 MIA, day 7 MMT, day 28 MMT and sham-surgery animals. **(A)**. G-ratio values were calculated for both large and small diameter fibres from each model. The MIA model resulted in higher g-ratio values in both large **(B)** and small **(C)** fibres at day 14 compared to day 3. The percentage of axons with irregular morphology was also assessed for each model **(D, G)** and demonstrated significantly more axons with abnormal myelin at day 14 following MIA administration (n = 534-595 axons from 5-6 animals per group) **(D)**. G-ratios from day 7 and day 28 MMT animals did not differ in either small **(E)** or large-diameter fibres **(F)**. The percentage of axons with irregular morphology was significantly higher in day 28 MMT animals compared to sham or day 7 MMT animals (n = 514-757 axons from 5-8 animals per group) **(G)**. Data are presented as means \pm SEM, one-way ANOVA. Arrows indicate axons with irregular morphology, scale bar = 6 μ m.

| | IL-10 | IL-1 β | IL-17A | IL-6 | TNF- α | n |
|----------------------|---------------------|--------------------------|------------------------|------------------|-------------------|---|
| MIA + Control | | | | | | |
| Day 3 | 1377 \pm 301.7*## | ND | 257.3 \pm 32.1 | 33.8 \pm 6.3* | 360.8 \pm 106*# | 7 |
| Day 14 | 625.2 \pm 88.9# | ND | 162.4 \pm 31.5 | 12.6 \pm 3.1 | 114.4 \pm 29.3 | 7 |
| Naïve | 319.5 \pm 122.9 | ND | ND | ND | 61.44 \pm 24.0 | 6 |
| MMT + Control | | | | | | |
| Day 7 | 329.2 \pm 48.3# | 703.5 \pm 110.5## * | 37.29 \pm 4.1## * | 78.65 \pm 7.6# | ND | 5 |
| Day 7 Sham | 97.64 \pm 16.3 | 164.7 \pm 60.1 | 8.63 \pm 2.3 | 17.86 \pm 5.4 | ND | 5 |
| Day 28 | 188.1 \pm 48.0 | 252.9 \pm 77.3 | 15.3 \pm 5.7 | 53.69 \pm 14.6 | ND | 5 |
| Day 28 Sham | 249.6 \pm 92.6 | 186.2 \pm 153.3 | 15.1 \pm 11.1 | 23.14 \pm 11.7 | ND | 5 |

Table 4. 1: Measurement of Serum Cytokines in MIA and MMT Animals.

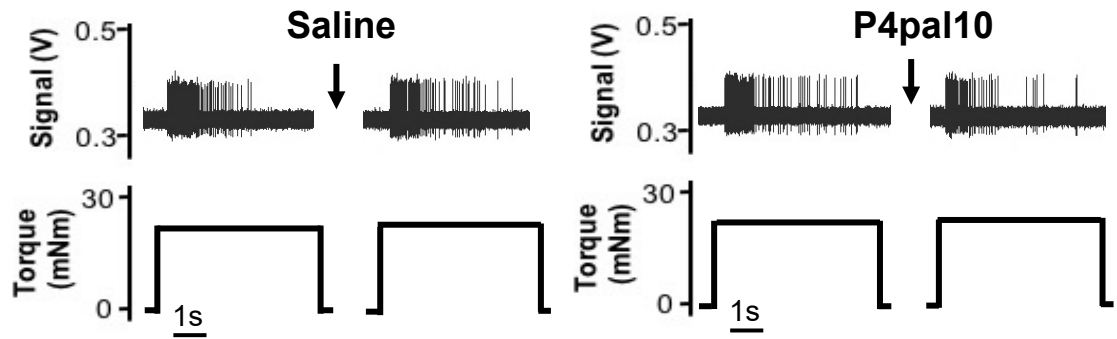
Serum cytokines IL-10, IL-1 β , IL-17A, IL-6, and TNF- α were measured at early and late time points in MIA, MMT, as well as control animals. #P<0.05 and ##P<0.01 denotes model vs control statistical significance using Tukey's multiple comparisons test. *P<0.05 denotes statistical significance using Tukey's multiple comparisons test comparing day 3 MIA vs day 14 MIA or day 7 MMT vs day 28 MMT. Data are means \pm SEM, one-way ANOVA.

| Fibre type | Mechanical Threshold (mNm) | Evoked Baseline Firing (action potentials/rotation) | Spontaneous Fibres (%) | Electrical Threshold (V) | Conduction Velocity (m/s) | n |
|---------------|----------------------------|---|------------------------|--------------------------|---------------------------|----|
| <i>Naive</i> | 23 ± 3 (10-40) | 12 ± 2 (4-27) | 0 | 4.1 ± 0.3 (3.25-5) | 2.4 ± 0.9 (1.0-3.5) | 11 |
| MIA | | | | | | |
| Day 3 | 10 ± 1 (4-19)## | 65 ± 8 (25-112)# | 73### | 3 ± 0.1 (2.5-3.0) | 1.6 ± 0.9 (0.61-2.18) | 11 |
| Day 14 | 16 ± 3 (2-30) | 41 ± 8 (11-100)# | 50## | 3 ± 0.4 (2.0-4.0) | 3.1 ± 1.2 (1.85-4.66) | 10 |
| MMT | | | | | | |
| Day 7 | 11 ± 2 (4-25)### | 35 ± 5 (13-75)## | 56## | 3 ± 0.4 (2.5-3.75) | 2.3 ± 0.8 (1.60-3.63) | 16 |
| Day 28 | 10 ± 2 (3-25)### | 38 ± 5 (13-83)## | 57## | 3.5 ± 0.4 (3.0-4.0) | 2.6 ± 1.4 (0.66-4.24) | 14 |

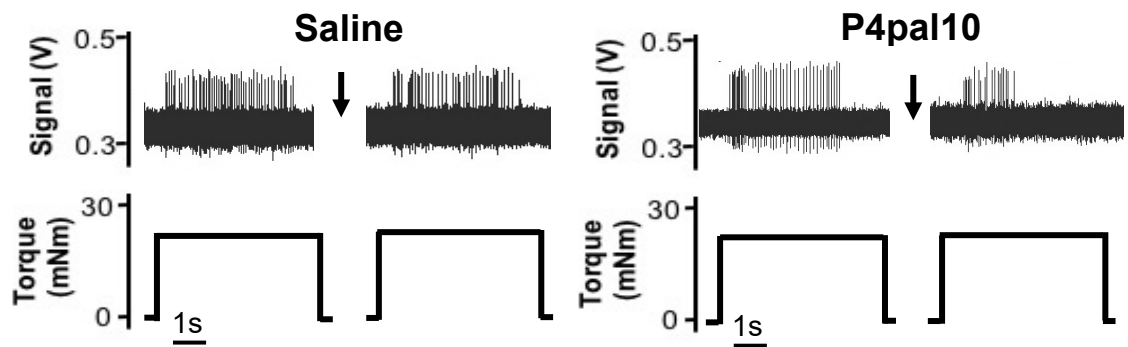
Table 4.2: Electrophysiological Properties of MIA and MMT Joint Afferents.

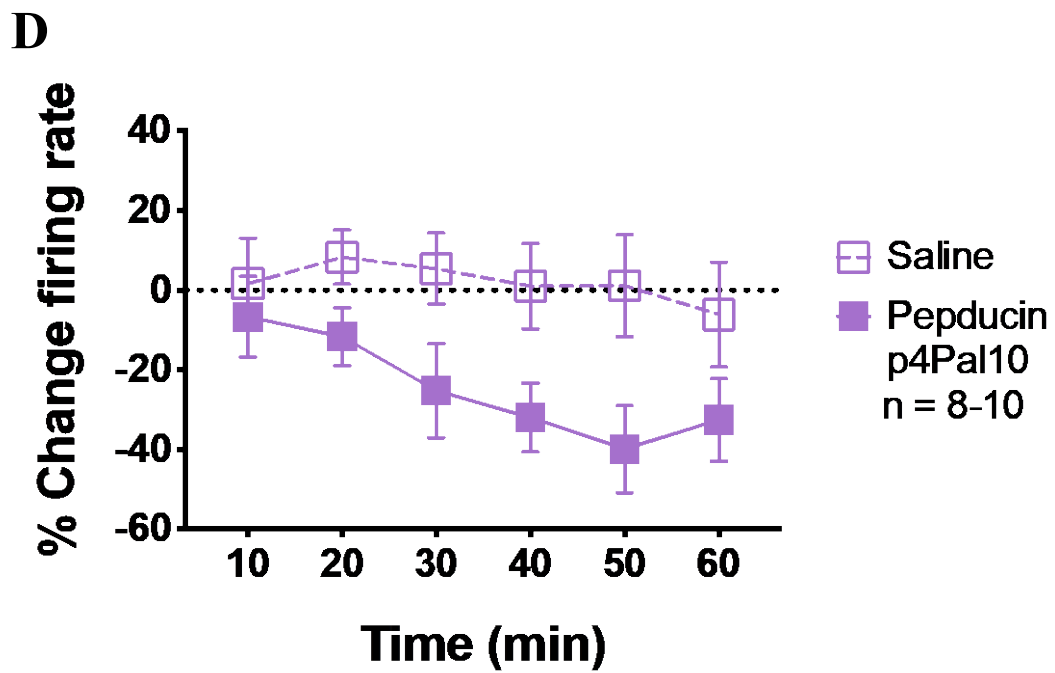
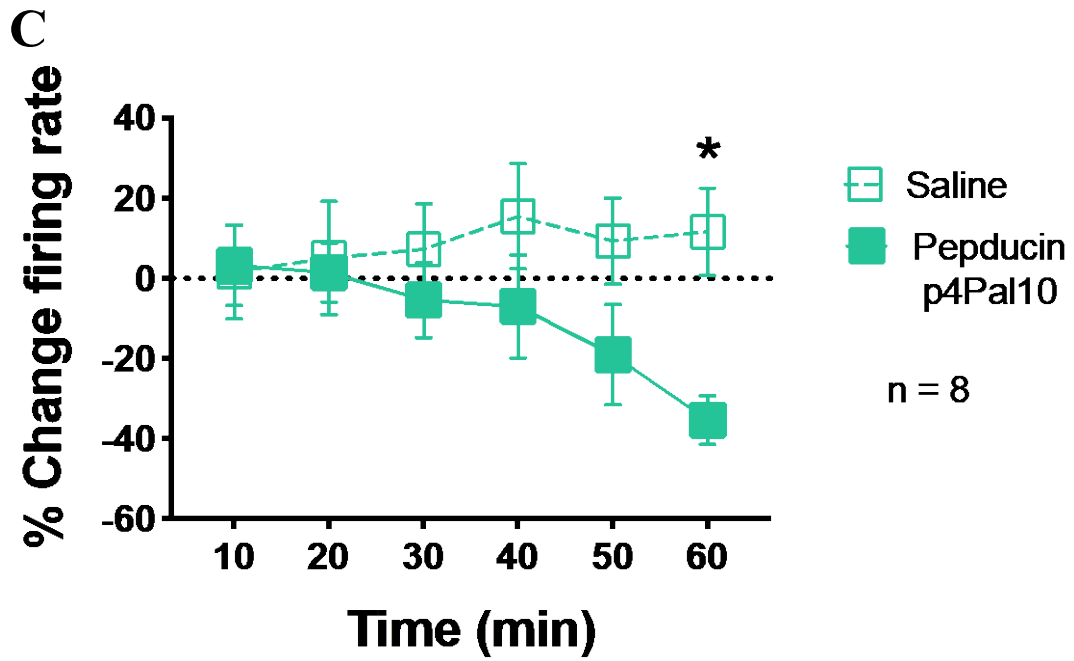
Fibres recorded from naïve, day 3 and 14 MIA, and day 7 and 28 MMT animals are characterised based on mechanical thresholds, evoked firing rates, the percentage of spontaneous fibres present, electrical thresholds, and conduction velocity. #P<0.05, ##P<0.01, ###P<0.001 denotes statistical significance between model fibres and naïve using Tukey's multiple comparisons test. Data are means ± SEM, one-way ANOVA.

A

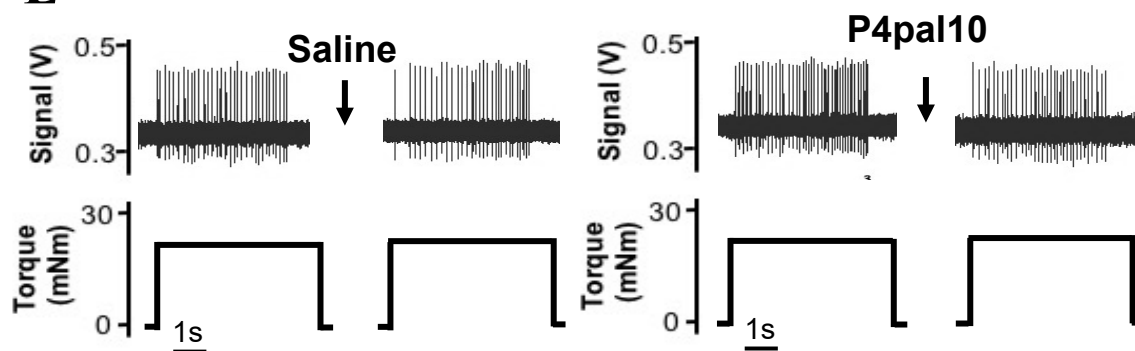


B

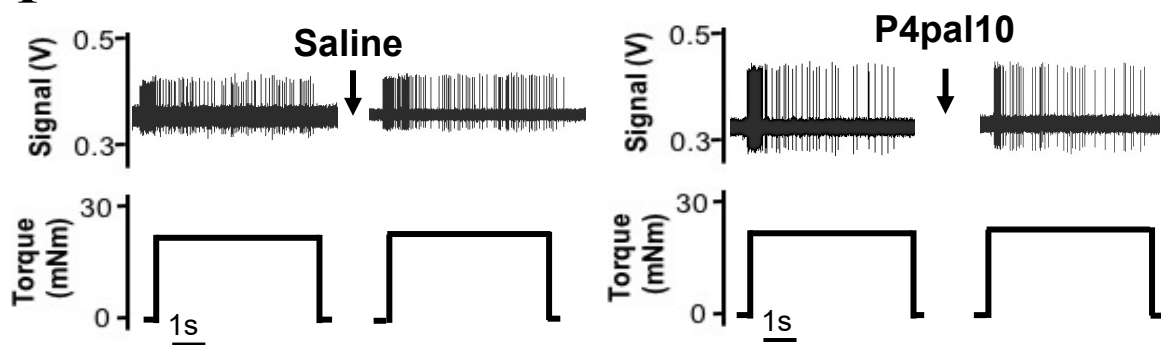




E



F



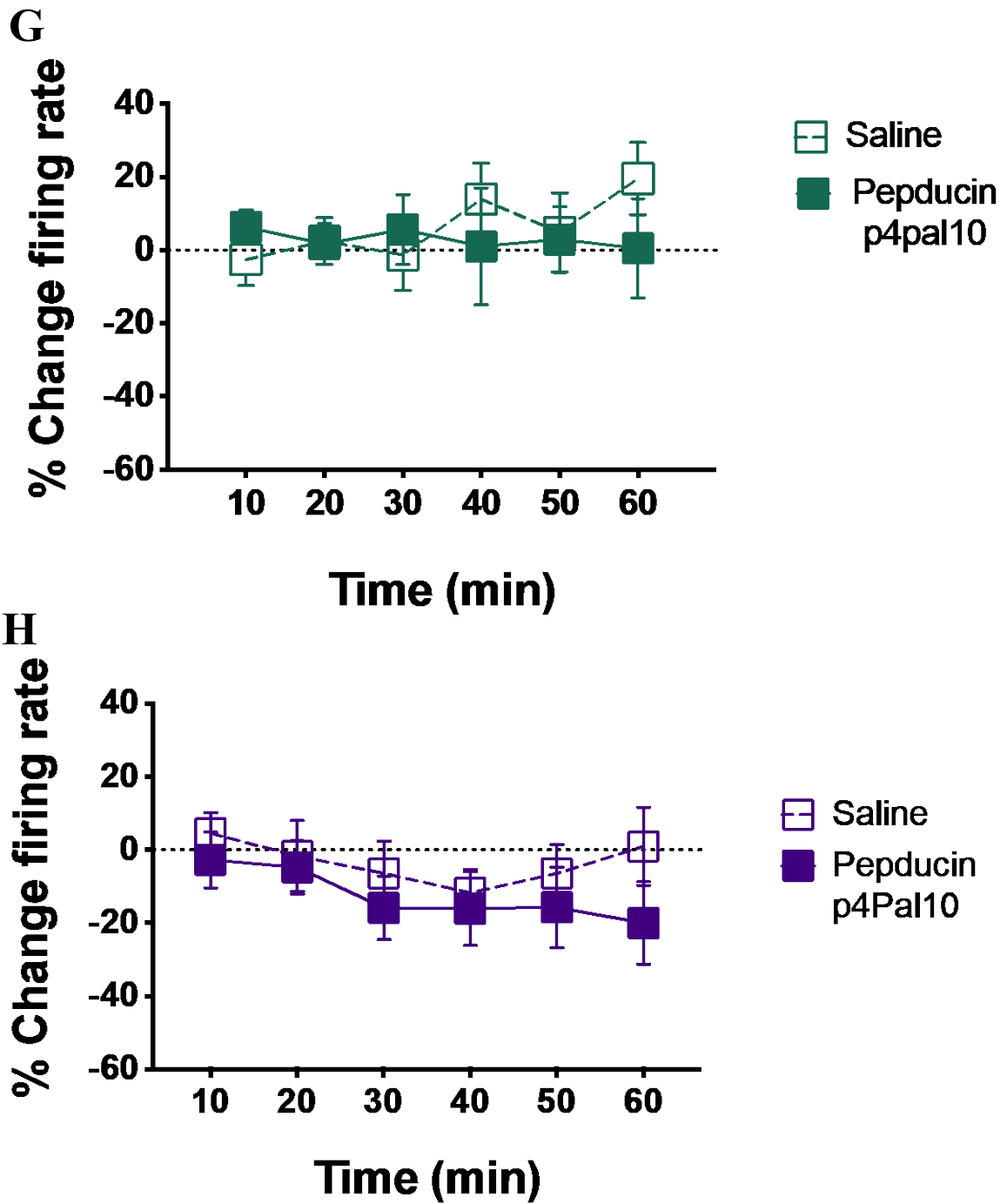
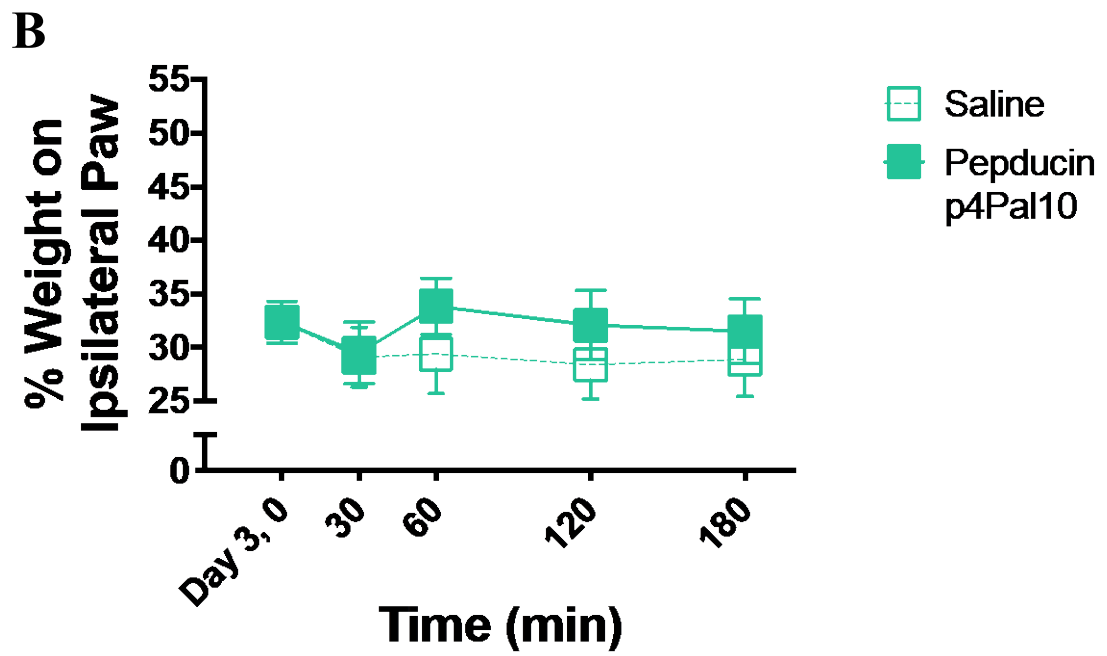
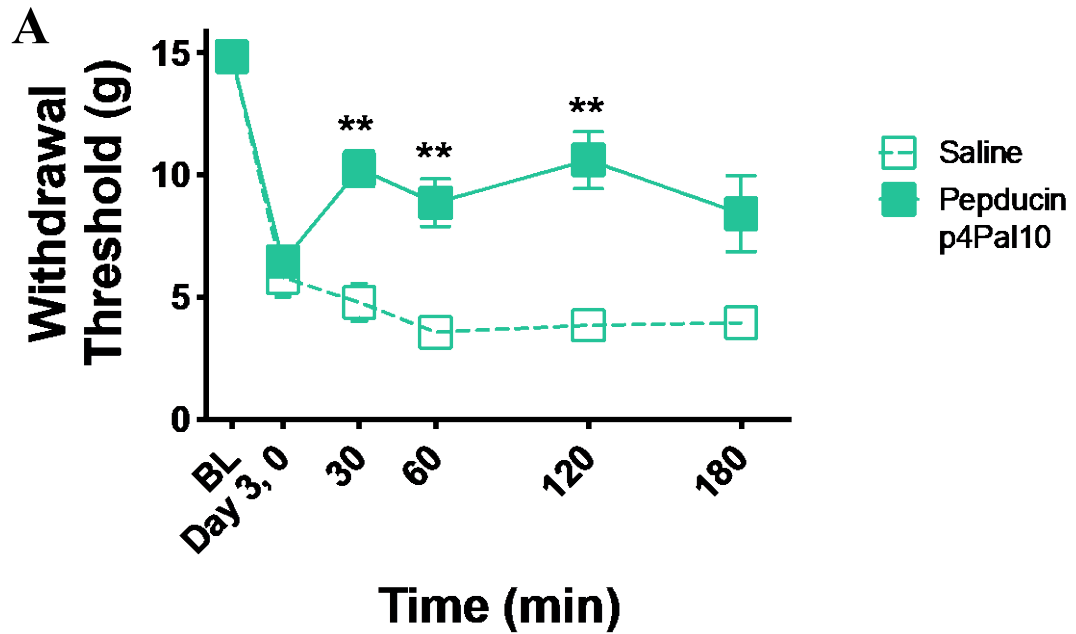


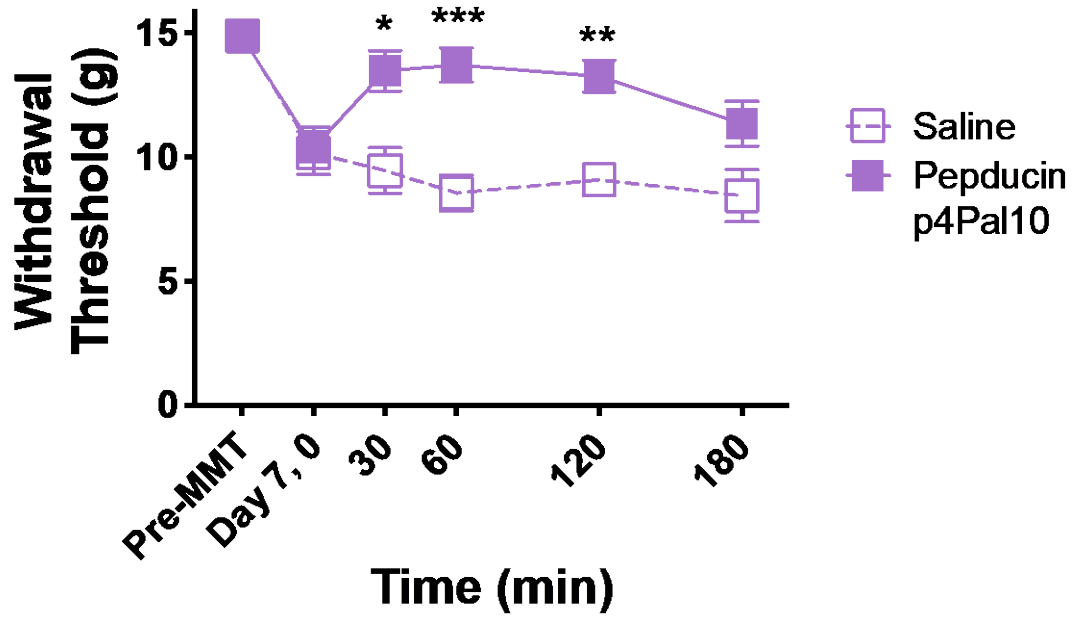
Figure 4. 3 Effect of PAR4 Blockade on Joint Afferent Firing in Early and Late Stages of the MIA and MMT Models.

Representative traces from day 3 MIA (A) and day 7 MMT (B) animals demonstrate afferent firing before and after administration of saline and pepducin P4pal10. Systemic pepducin P4pal10 reduced joint afferent firing relative to baseline over the 60-minute timecourse when compared to saline vehicle in both day 3 MIA (C) and day 7 MMT

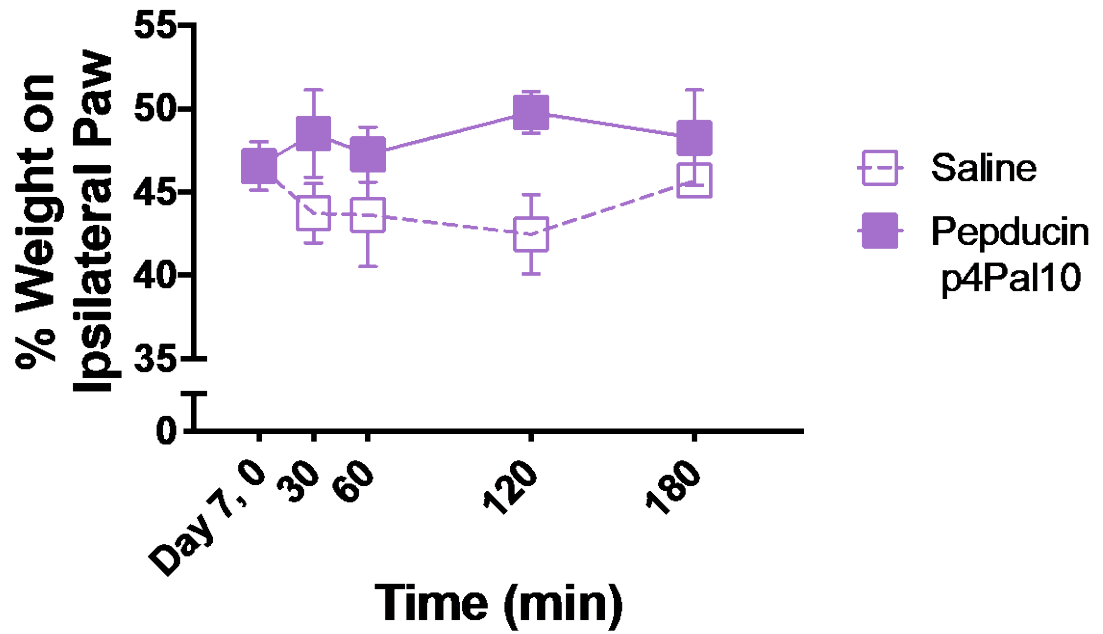
animals **(D)** (n = 8-10 fibres per group, 2-way rm ANOVA). Representative traces of joint afferent recording from day 14 MIA **(E)** and day 28 MMT **(F)** animals illustrate the effect of treatment at the later timepoint. Pepducin P4pal10 failed to attenuate nociceptive evoked firing when compared to saline in either MIA **(G)** or MMT **(H)** animals (n = 7-11 fibres per group, 2-way rm ANOVA). *P<0.05 denotes post hoc significance between pepducin P4pal10 and saline treated animals using Sidak's multiple comparisons test. Data are means \pm SEM.

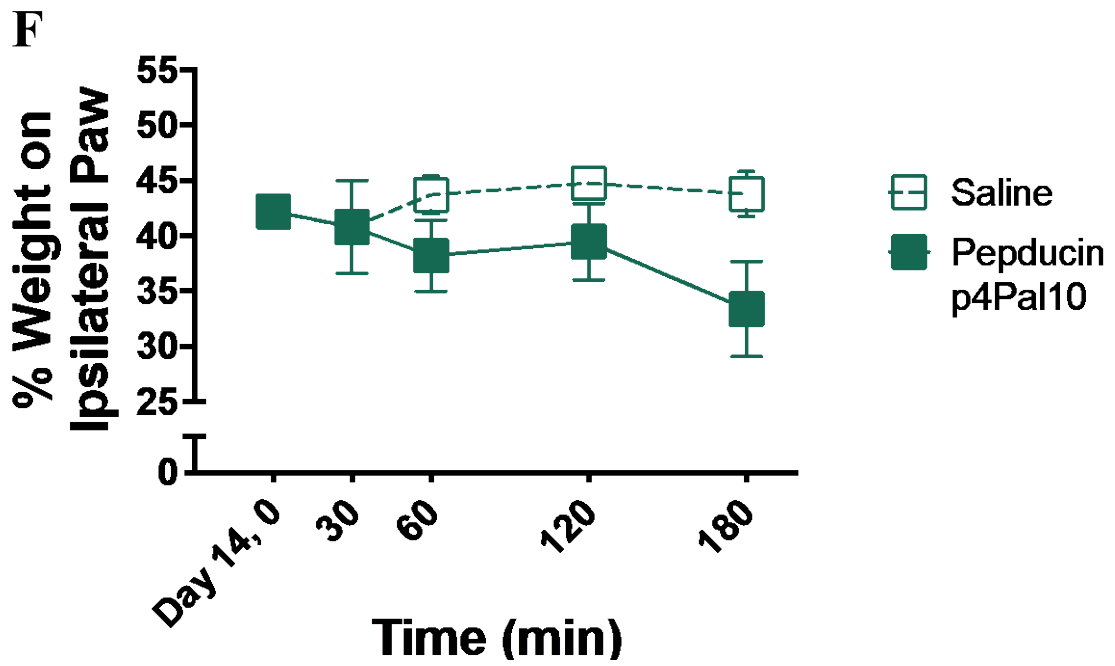
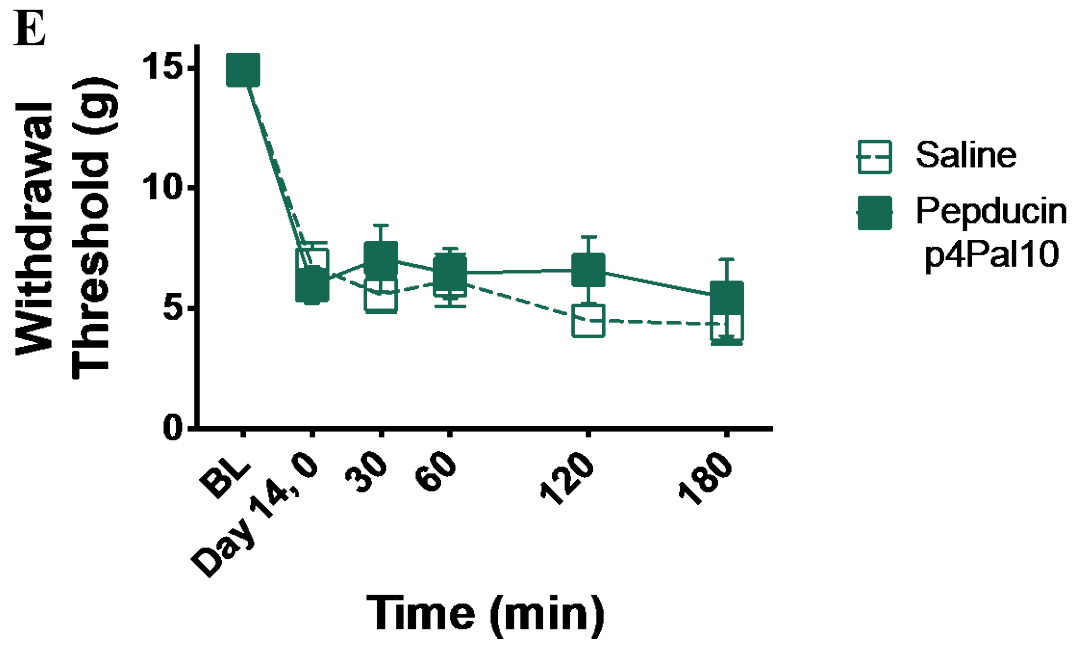


C



D





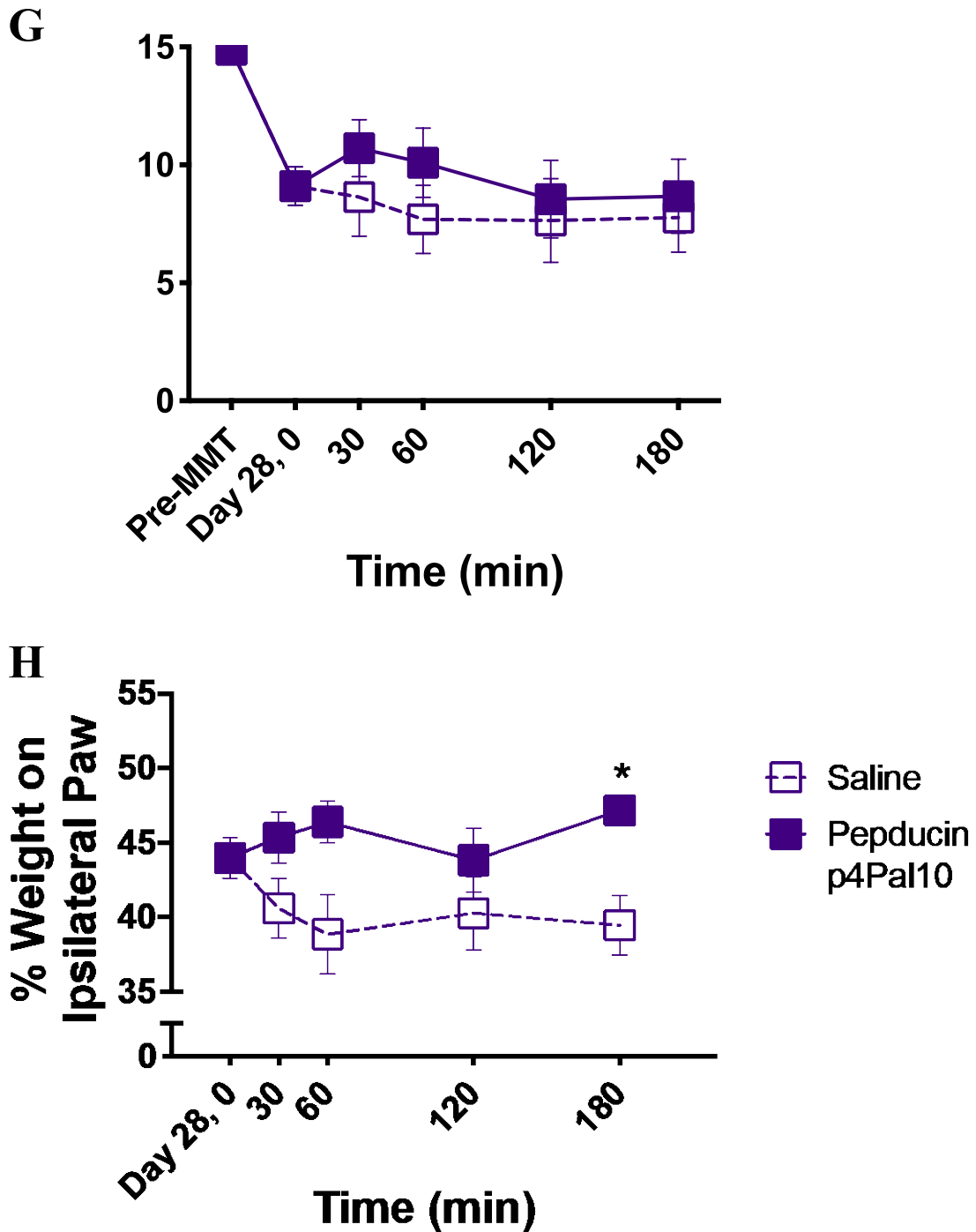


Figure 4. 4 Effect of PAR4 Blockade on Pain Behaviour in Early and Late Stages of the MIA and MMT Models.

Administration of pepducin P4pal10 improved withdrawal thresholds compared to saline vehicle in day 3 MIA animals (A), weight bearing deficits were not improved following drug administration in the same animals (B). Systemic treatment with pepducin P4pal10 in day 7 MMT animals resulted in reversal of secondary allodynia (C) and weight bearing

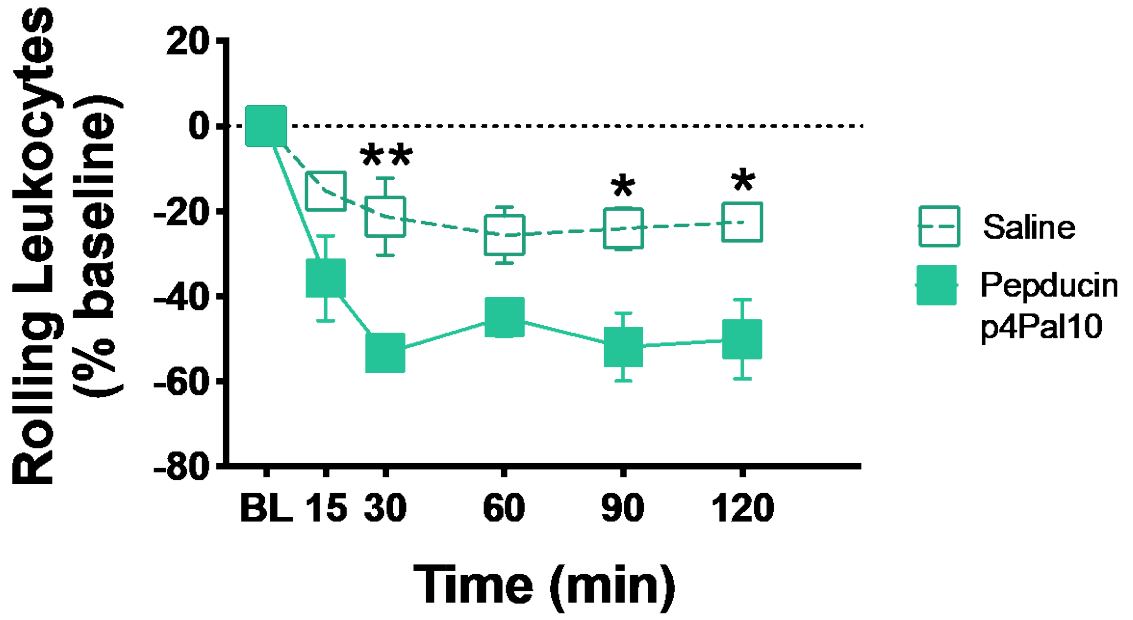
deficits (**D**). No significant effects were observed in day 14 MIA animals in either secondary allodynia (**E**) or weight bearing deficits (**F**) following PAR4 blockade. When day 28 MMT animals were treated with pepducin P4pal10, it did not improve withdrawal threshold (**G**) but did reduce hindlimb weight bearing deficits at 180 minutes (**H**). Data presented as means \pm SEM, n = 7 animals per group, 2-way rm ANOVA. *P<0.05 denotes post hoc statistical significance between pepducin P4pal10 and saline treated animals as determined by Tukey's multiple comparisons test.

| | Rolling Leukocytes | Adherent Leukocytes | Vascular Conductance | n |
|---------------|----------------------------------|----------------------|-----------------------|----|
| MIA | | | | |
| Day 3 | 71.6 ± 4 (51.7-87.7)*** | 2.9 ± 0.7 (0.0-7.6) | 4.2 ± 0.3 (2.2-5.7) | 12 |
| Day 14 | 41.4 ± 4 (29.0-54.3) | 1.6 ± 0.5 (0.3-4.0) | 3.6 ± 0.2 (3.3-4.4) | 6 |
| MMT | | | | |
| Day 7 | 62.4 ± 3 (34.7-86.3)*** ##### | 2.2 ± 0.5 (0.5-5.7)* | 4.8 ± 0.7 (1.9-13.0)* | 18 |
| Day 28 | 36.8 ± 3 (24.0-53.5) | 0.6 ± 0.2 (0.0-2.0) | 2.2 ± 0.1 (1.7-2.6) | 8 |

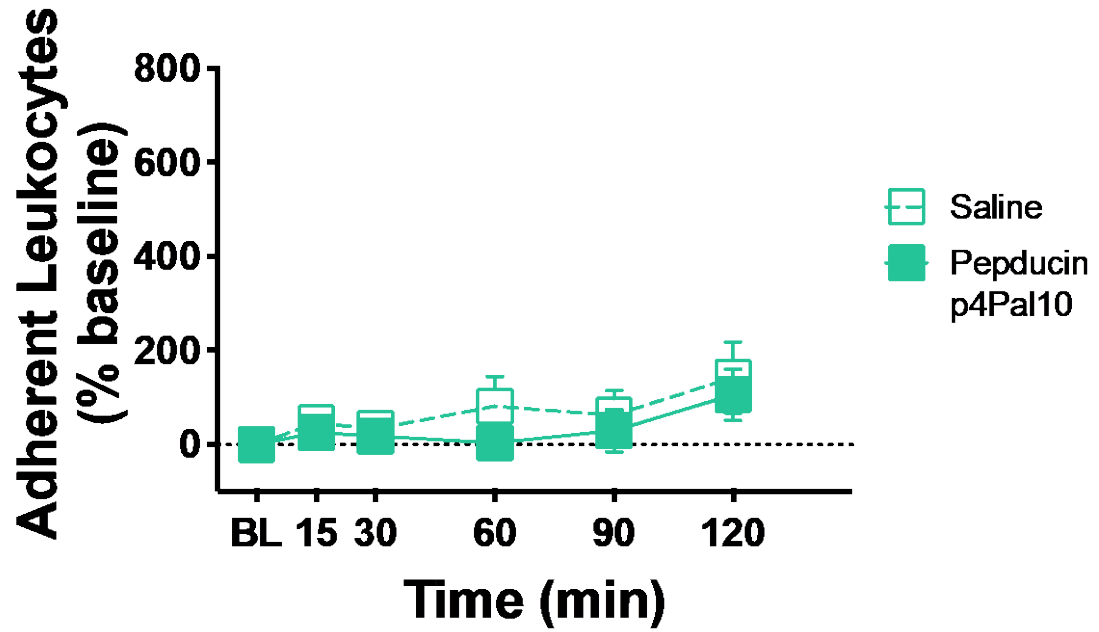
Table 4. 3: Measurement of Leukocyte Trafficking and Joint Perfusion in MIA and MMT Animals.

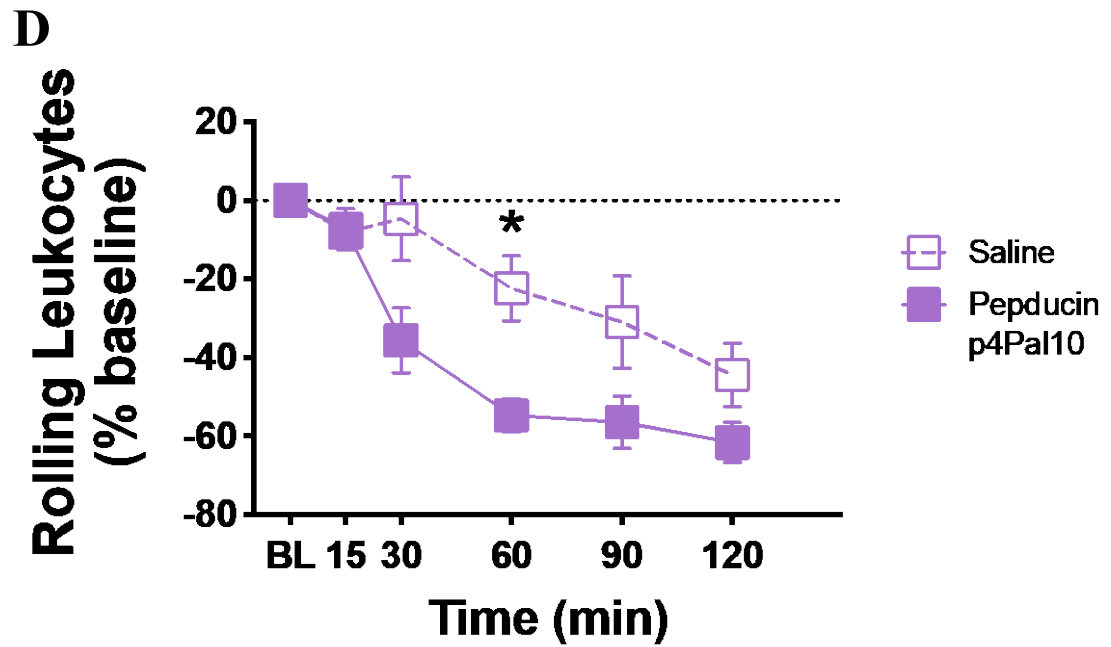
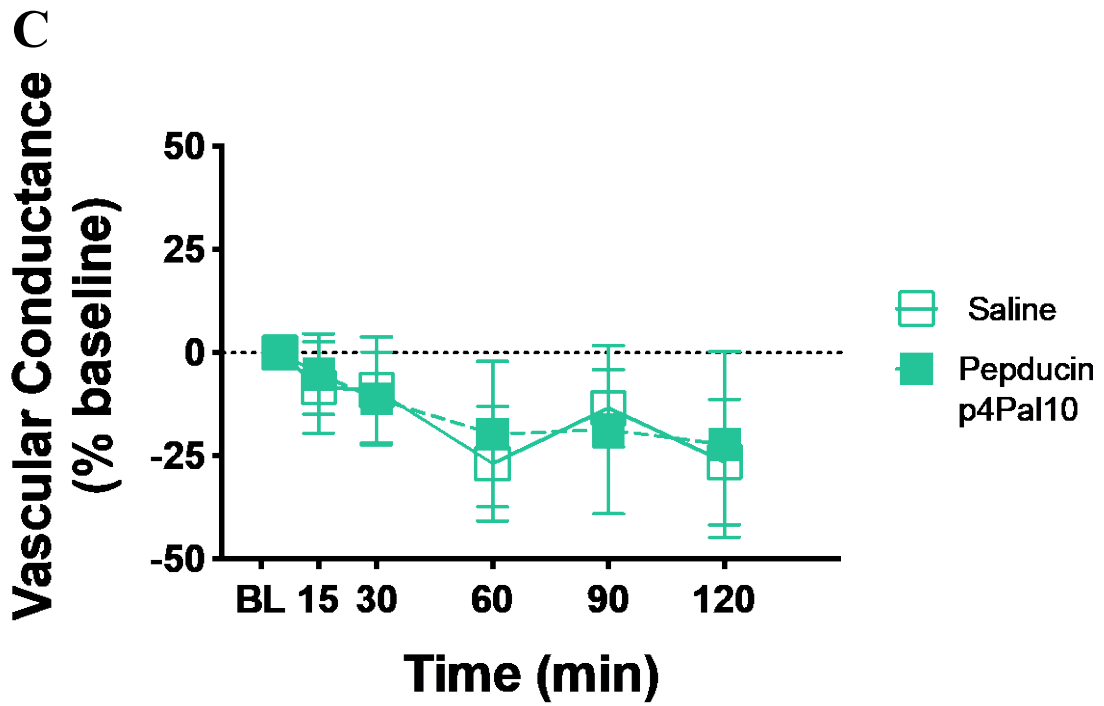
The number of rolling leukocytes were significantly higher 3 days following MIA administration compared to 14 days. Adherent leukocyte and vascular conductance values were not different during baseline recordings in day 3 and 14 MIA animals. All measurements were significantly higher in day 7 MMT animals compared to day 28. *P<0.05, ***P<0.001 denotes statistical significance between day 3 vs day 14 MIA or day 7 vs da 28 MMT using a student's t-test. Data are means ± SEM.

A



B





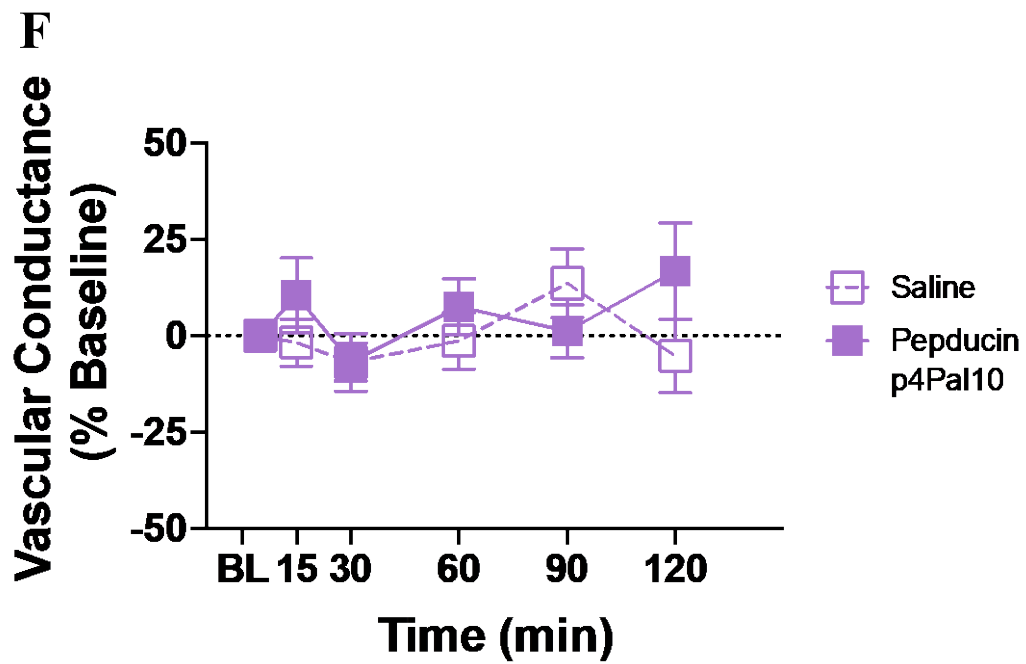
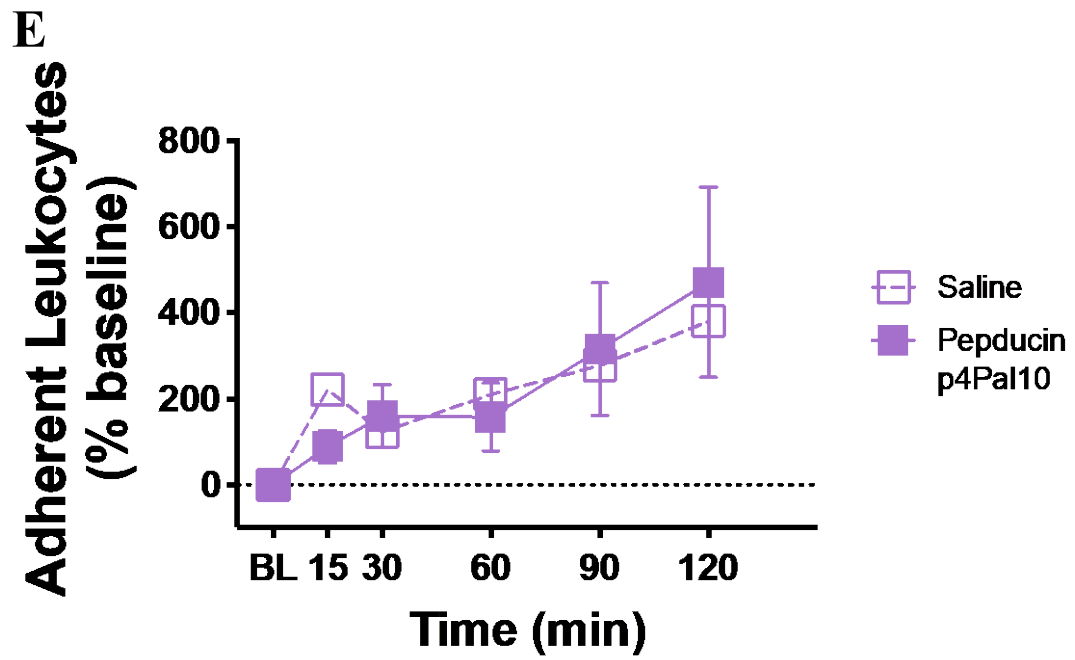
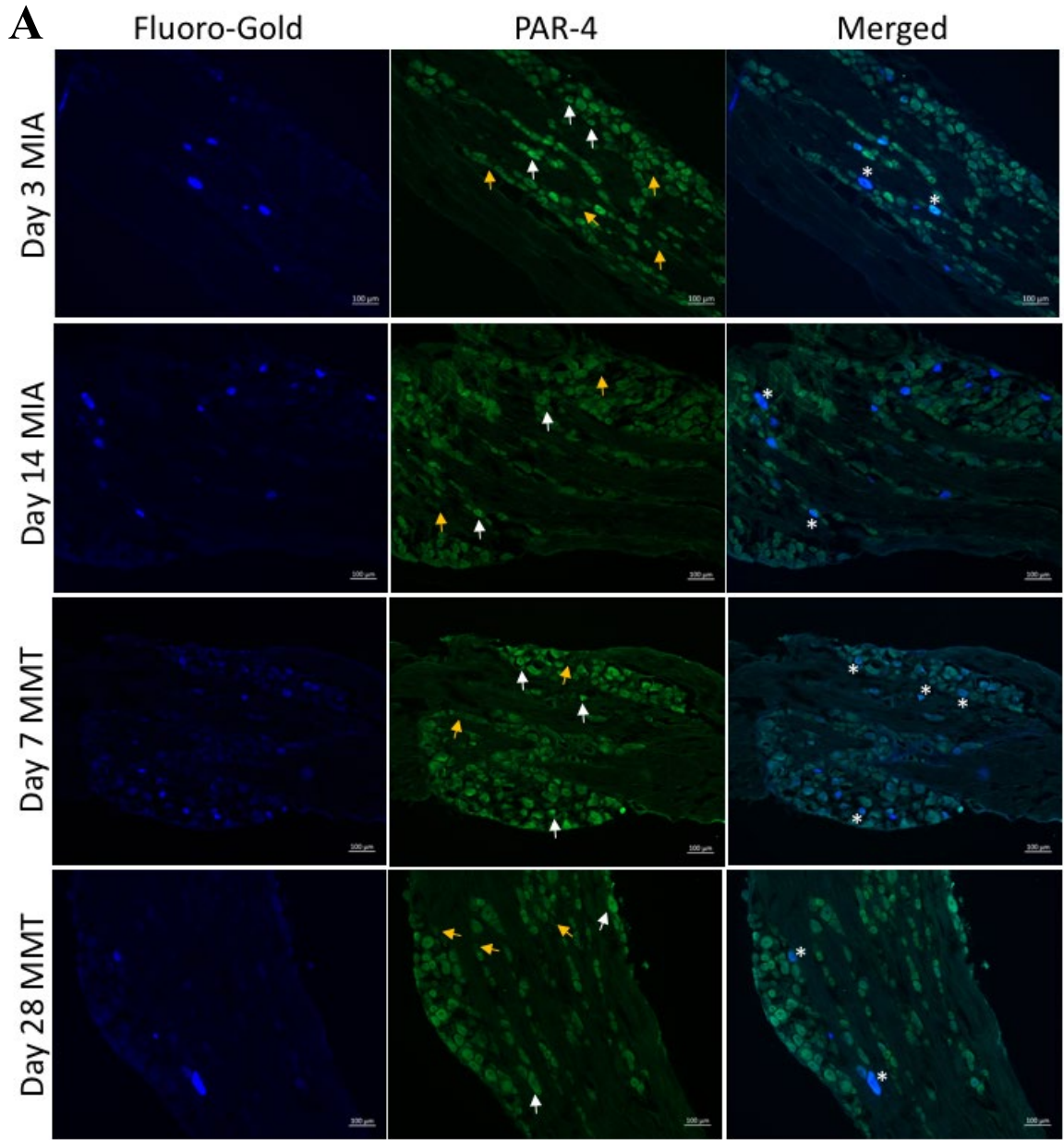


Figure 4. 5 Effect of PAR4 Blockade on Joint Inflammation in MIA and MMT Models.

Administration of pepducin P4pal10 significantly reduced rolling leukocytes in day 3 MIA animals (**A**) but failed to improve adherent leukocyte trafficking (**B**) or vascular conductance (**C**) (n=6 animals per group, 2-way rm ANOVA). Similarly, treatment in day 7 MMT animals elicited significant reductions rolling leukocytes (**D**) but failed to attenuate adherent leukocyte movement (**E**). Vascular conductance in MMT animals was not affected by PAR4 blockade (**F**) (n = 9-12 animals per group, 2-way rm ANOVA). *P<0.05 denotes post hoc significance between pepducin P4pal10 and saline treated animals as determined by Tukey's multiple comparisons test. Data are means \pm SEM.



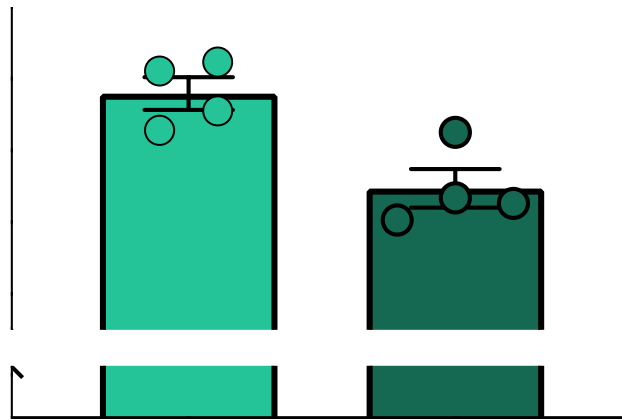
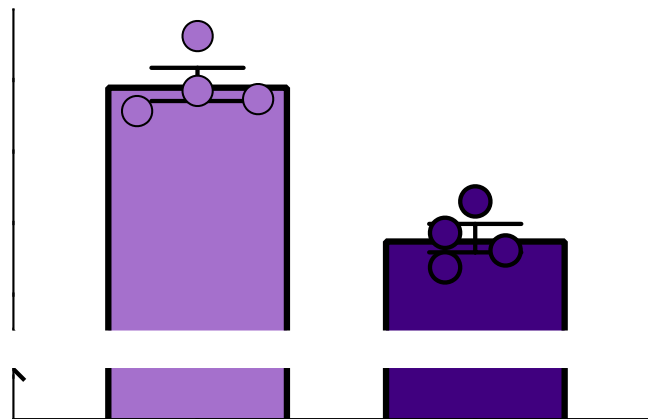
B**C**

Figure 4. 6 PAR4 Expression in DRG Joint Neurons in MIA and MMT Models.

Representative photomicrographs of PAR4 expression in Fluoro-gold (FG) traced L3-DRG neurones from MIA and MMT animals (A). PAR4 immunoreactivity was calculated for FG neurones from each treatment group. The percentage of FG-neurones that expressed PAR4 was significantly higher in day 3 MIA animals compared with day 14 (B). Higher expression of PAR4 was also observed in the earlier timepoint of the MMT model (C). Data are means \pm SEM, n = 4 animals per group, student's t-test. White arrows indicate positive expression of PAR4 and yellow arrows indicate a lack of expression, asterisks represent coexpression.

Chapter 5: Human Arthritic Synovial Fluid Contributes to Joint Afferent Sensitisation, in Part by Activation of PAR4

Disclosures: There are no disclosures to report for this chapter.

5.1 Background and Hypotheses:

A growing body of evidence suggests that the constituents within the synovial fluid contribute to pain associated with OA [273, 274]. Several studies have examined the potential role of pro-inflammatory cytokines, neuropeptides, adipokines, and to a lesser extent proteases, as mediators of arthritic pain because of their presence in synovial fluid. Conflicting data linking cytokine levels to OA pain exist. While some studies find that molecules such as TNF- α , IL-1 β , and IL-6 are associated with clinically defined pain scores [273, 274], others find no correlation between these cytokines and OA pain [275]. Similarly, neuropeptides such as CGRP, substance P, and neuropeptide Y have been probed because of their algogenic properties but failed to consistently correlate with pain in arthritic patients [275-277]. The adipokines adiponectin and leptin have been found to be predictive of patient-reported pain [278] but levels vary depending on the site of arthritis. While proteases are elevated in arthritic joints, few studies have directly investigated whether synovial fluid proteases contribute to arthritic pain. Fan et al., measured the catabolic metalloproteases, MMP-3 and MMP-13, and ADAMTS5 in OA patients and observed a small correlation between reported pain and MMP-13 but not the other proteases [275].

Despite the lack of clinical studies evaluating the potential role of synovial fluid proteases and arthritic pain, both clinical and pre-clinical data exist to support the hypothesis that serine proteases present in arthritic joints modulate pain. A plethora of

clinical work has demonstrated that serine proteases are elevated in arthritic joints [4, 64, 213, 214]. Proteases such as thrombin and trypsin are elevated in the synovial fluid of both OA and RA joints, while proteases such as cathepsin G is found in RA joints and tissue-plasminogen activator is only abundant in OA synovial fluid [4]. Each of these proteases are known to cleave PAR4 and thus have the potential to activate joint nociceptors and cause pain.

Hypotheses Evaluated in this Study:

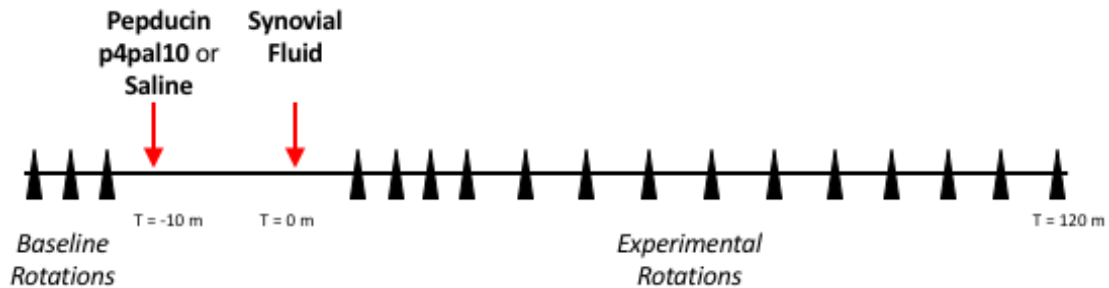
- I: Human arthritic synovial fluid contributes to nociception and will sensitise rat joint nociceptors.**
- II: PAR4 cleaving proteases are present in arthritic synovial fluid and contribute to joint afferent sensitization.**

5.2 Effect of Human Synovial Fluid on Rodent Joint Nociceptors and the Contribution of PAR4

5.2.1. Methods

Naïve male Wistar rats (307-517 g) were deeply anaesthetised with urethane (25% solution, 2 g/kg i.p.) and underwent surgical preparation for electrophysiology experiments as outlined in section 2.3. Upon identification of a joint afferent fibre, three sets of 10-second long joint hyper-rotations were carried out over 15-minutes to assess baseline activity of the nociceptor. Immediately following baseline rotations, pepducin P4pal10 (100 µg in 100 µl saline) or saline (100 µl) was administered via the saphenous artery. Ten minutes later, human synovial fluid (OA or RA; 100 µl) was administered via the saphenous artery and joint rotation resumed 5-minutes later. Joint mechanosensation was assessed every 5 minutes for the first 20 minutes and then every 10 minutes until 120

minutes. The percentage change in firing rate from baseline was calculated and reported as mean \pm SEM. The number of spontaneously active fibres in each treatment group was also counted.



5.2.2. Results

5.2.2.1 Neuronal Characteristics of Afferent Fibres

One mechanosensitive joint afferent fibre was recorded in each naïve animal and neuronal characteristics were quantified (Table 5.1). 54% of fibres had conduction velocities in the C-fibre range (<2.0 m/s) and 16% in the $A\delta$ -fibre range (>2.0 m/s). In 30% of experiments, conduction velocities could not be determined. The two cohorts of fibres that were treated with OA synovial fluid (saline and pepducin P4pal10 pre-treated) appear to be very similar in both mechanosensitivity and applied torque. The fibres in the RA treated groups were somewhat divergent in that overall the saline-treated group had more high-threshold fibres and the pepducin P4pal10 pretreated group had more low-threshold fibres. Although, the mean mechanical thresholds of the groups were not

statistically different (saline: 21 ± 4.5 mNm, pepducin P4pal10: 14.5 ± 3.5 , 2-way ANOVA, $p > 0.05$).

5.2.2.2 Human Arthritic Synovial Fluid Sensitised Rodent Nociceptors

Human OA synovial fluid sensitised naïve rodent joint nociceptors (Figure 5.1). OA synovial fluid resulted in a maximum increase in firing of 111 ± 31 % at 120 minutes following administration relative to baseline. Pretreatment with pepducin P4pal10 significantly augmented this sensitization. Fibres reached a maximum increase of 40 ± 17 % earlier in the time-course at 60 minutes when treated with the PAR4 blocker ($p < 0.05$, two-way rm ANOVA, $n = 7-9$). The cumulative effect over the 120-minute time-course was a 69 ± 8 % increase in firing in saline-pretreated joint afferents and a 23 ± 5 % increase in firing in joint nociceptors that were pre-treated with pepducin P4pal10 ($p < 0.05$, one-way ANOVA, $n = 7-9$).

Administration of human osteoarthritic synovial fluid also increased the number and activity of spontaneously active fibres (Figure 5.1 E-F). The total number of spontaneously firing fibres was counted in each recording to determine whether synovial fluid could activate previously silent nociceptors. Compared with saline, pre-treatment with pepducin P4pal10 did not affect the number of spontaneously active fibres following administration of synovial fluid ($p > 0.05$, one-way ANOVA, $n = 7-9$).

Local administration of RA synovial fluid to naïve rodent joint nociceptors also resulted in afferent sensitisation (Figure 5.2). In saline pre-treated animals, a maximal response was observed at 110 minutes following RA synovial fluid administration with a 131 ± 56 % increase in firing. In contrast, animals that received pre-treatment with

pepducin P4pal10 demonstrated an increase of only $8 \pm 15 \%$ at 120 minutes following synovial fluid administration ($p < 0.05$, $n = 5-6$). The cumulative effect of the RA synovial fluid over the time-course was similar to that of OA, with a $74 \pm 9 \%$ increase in firing detected in saline-treated fibres. PAR4 blockade was more effective against RA sensitisation, as a $6 \pm 3 \%$ decrease in firing in pepducin P4pal10-treated fibres was observed ($p < 0.05$, $n = 5-6$).

5.3 Proteomic Analysis of Arthritic Synovial Fluid

5.3.1. Methods

OA and RA synovial fluid samples were prepared for mass spectrometry and underwent LC/MS-MS as outlined in section 2.10.

5.3.2. Results

5.3.2.1 Proteomic Analysis Reveals High Levels of Proteases and Protease Inhibitors in Synovial Fluid

Untargeted proteomic analysis of human arthritic synovial fluid identified 115 proteins in the OA exudate and 118 proteins in the RA sample (Appendix D). When the proteins were compared, 10 were unique to the OA fluid and 13 were only found in the RA fluid. Since a large number of proteins were identified in each sample that mediate diverse biological processes, pathway analysis was conducted on the protein datasets using Metascape to determine if OA and RA samples shared significantly enriched pathways. A heatmap of the twenty most enriched pathways were associated with ECM regulation, zymogen activation, and complement activation within both samples (Figure 5.6A). The most enriched pathway in both samples was the Gene Ontology ‘protein

activation cascade' which included 47 proteins from the RA sample and 43 from the OA sample. Among these were plasminogen, fibrinogen, kininogen, and a large number of complement proteins. Overall, the analysis revealed that the samples had proteins with very similar signalling pathways. Minor variations in lipoprotein functions were highlighted (elevated in RA) as previously outlined in the literature [279, 280].

String-networks were also generated to allow for easier visualisation of the datasets and identify potential functional or structural interactions between synovial fluid proteins (Figure 5.6B-C). This analysis revealed that the RA sample had a larger number of serine proteases present compared to the OA sample (RA: 13 versus OA:10). Additionally, there were more proteases with trypsin-like domains present in the RA sample which is of interest because these types of proteases are known to cleave PAR4 [219]. Six serine protease inhibitors were common to both samples. The relative abundance of proteases and protease inhibitors quantified in arthritic synovial fluid are depicted in Figure 5.7. Proteases that have PAR4 modulating effects, i.e. plasminogen and C4a, are underlined.

5.4 Chapter Summary

5.4.1 PAR4 cleaving proteins are present in OA and RA synovial fluid

Proteomic examination revealed that the OA and RA synovial fluid samples used for these studies had a similar proteomic composition as previously published reports [281-283]. The RA sample had a larger number of trypsin-like serine proteases compared to the OA synovial fluid, which was of interest because of the proclivity of these

proteases to cleave PAR4 [219]. Both samples contained the PAR4 activators plasminogen and the complement component C4a with concentrations being higher in the OA synovial fluid. The presence of serine protease inhibitors such as anti-chymotrypsin and the absence of their protease substrates, suggests that targeted mass spectrometry may reveal additional low abundance serine proteases that were not identified using our untargeted LC-MS/MS approach.

5.4.2 Human Arthritic Synovial Fluid Sensitises Rodent Nociceptors in part via PAR4 Activation

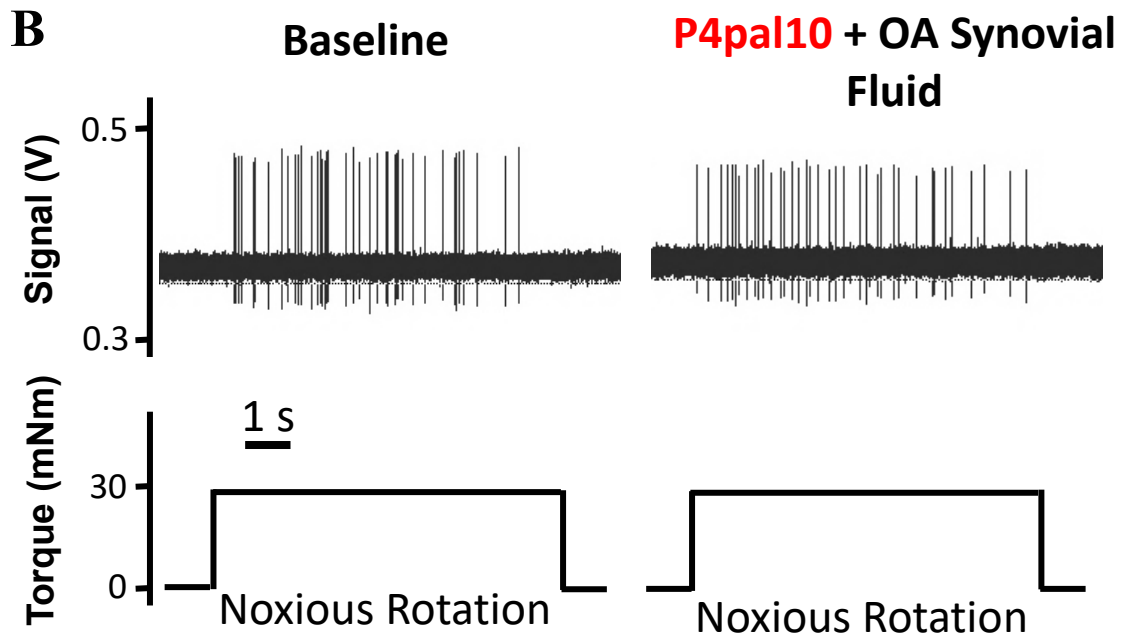
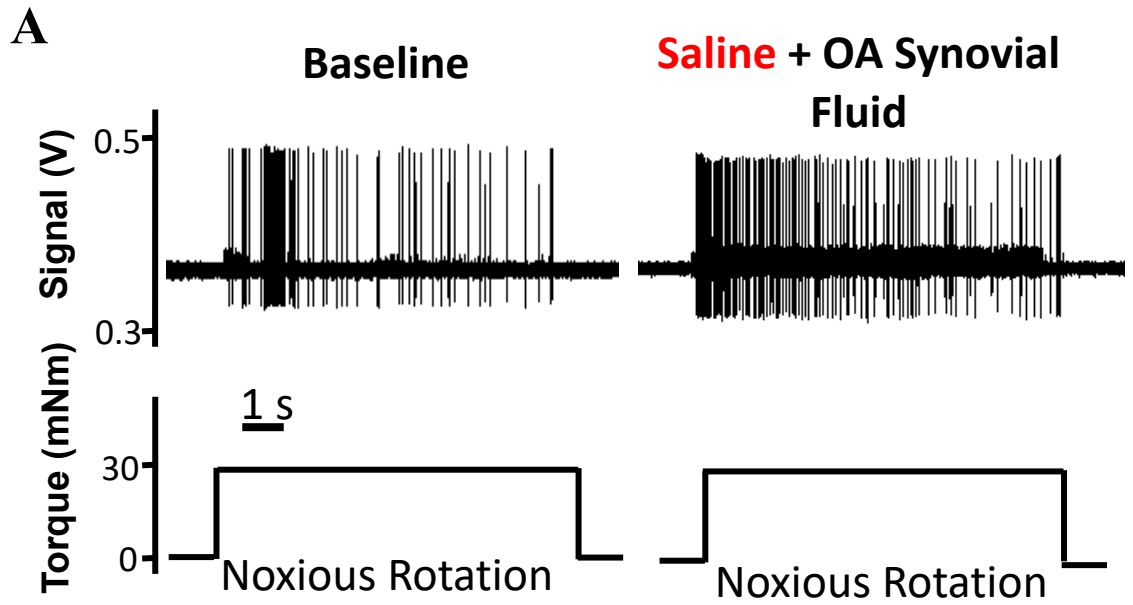
Human synovial fluid from an OA and a RA joint caused sensitisation of rodent mechanosensitive nociceptors. Increases in evoked firing were similar in response to OA and RA synovial fluid and both types of synovial fluid also caused spontaneous firing of silent joint afferents. Pre-treatment with the PAR4 blocker pepducin P4pal10 produced disparate responses when OA or RA synovial fluid was administered. In the OA treated animals, pepducin P4pal10 pre-treatment augmented the effect of the synovial fluid-induced mechanosensitisation while having no effect on spontaneous activity. PAR4 blockade in the RA treated animals prevented the movement-evoked increase in firing and reduced the number of spontaneously active fibres.

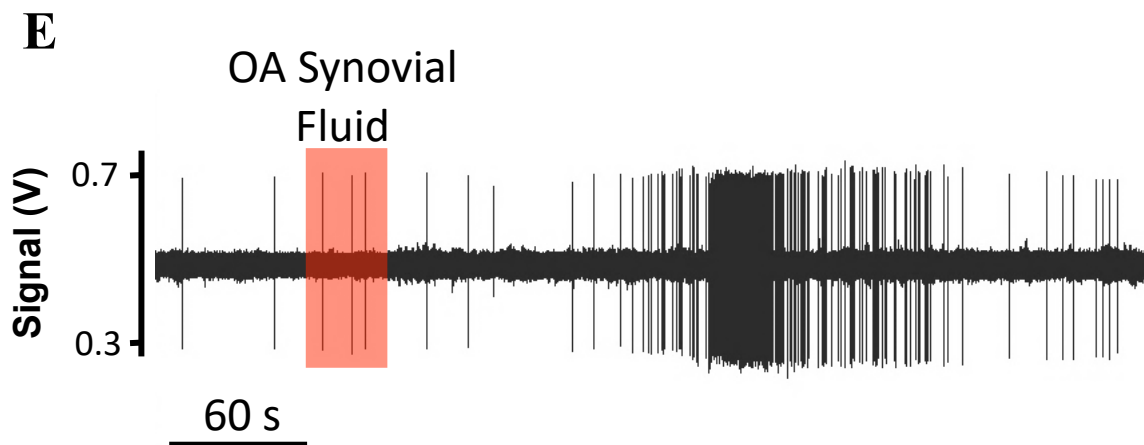
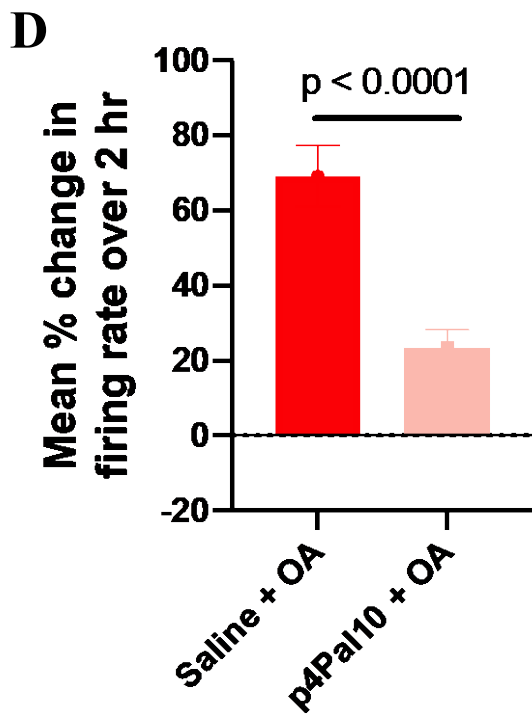
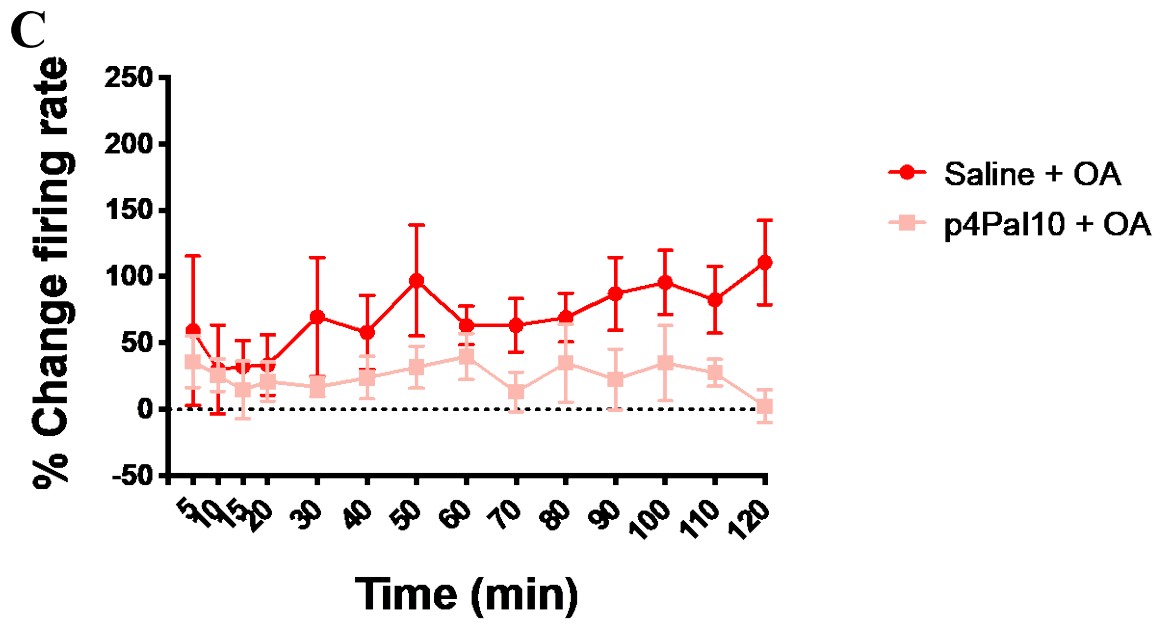
| Fibre type | Mechanical Threshold (mNm) | Noxious Rotation Torque (mNm) | Electrical Threshold (V) | Conduction Velocity (m/s) | n |
|--|-----------------------------------|--------------------------------------|---------------------------------|----------------------------------|----------|
| Naïve Animals Treated with Saline and OA Synovial Fluid | | | | | |
| All Fibres | 17.5 ± 3.3 (10-28) | 27.3 ± 2.7 (20-33) | 3.2 ± 0.5 (1.2-4) | 1.9 ± 0.7 (0.7-2.2) | 6 |
| III | 12 | 22 | 4 | 2.2 | 1 |
| IV | 18.0 ± 5.3 (10-28) | 27.7 ± 3.9 (20-33) | 2.9 ± 0.6 (2-4) | 1.2 ± 0.3 (0.7-1.2) | 3 |
| ND | 19.5 ± 7.5 (12-27) | 29.5 ± 3.5 (26-33) | | | 2 |
| Naïve Animals Treated with Pepducin P4pal10 and OA Synovial Fluid | | | | | |
| All Fibres | 21.0 ± 3.1 (10-28) | 28.2 ± 1.8 (22-33) | 2.65 ± 0.2 (2-3) | 1.2 ± 0.2 (0.7-1.7) | 5 |
| IV | 21.0 ± 3.1 (10-28) | 28.2 ± 1.8 (22-33) | 2.65 ± 0.2 (2-3) | 1.2 ± 0.2 (0.7-1.7) | 5 |
| Naïve Animals Treated with Saline and RA Synovial Fluid | | | | | |
| All Fibres | 21 ± 4.5 (12-30) | 28.4 ± 1.9 (20-38) | 3.1 ± 0.5 (2.75-4) | 1.9 ± 0.5 (0.8-3.5) | 10 |
| III | 19.5 ± 0.5 (19-20) | 29.0 ± 6.0 (23-35) | 3.5 ± 0.5 (3-4) | 2.9 ± 0.6 (2.3-3.5) | 2 |
| IV | 22.8 ± 2.4 (20-30) | 29.0 ± 2.6 (22-33) | 3.2 ± 0.3 (2.75-4) | 1.2 ± 0.2 (0.8-1.5) | 4 |
| ND | 20.0 ± 2.7 (12-24) | 27.5 ± 3.8 (20-38) | | | 4 |
| Naïve Animals Treated with Pepducin P4pal10 and RA Synovial Fluid | | | | | |
| All Fibres | 14.5 ± 3.5 (7-30) | 24.1 ± 2.8 (18-35) | 2.7 ± 0.3 (2-3.5) | 1.7 ± 0.5 (1.0-3.3) | 5 |

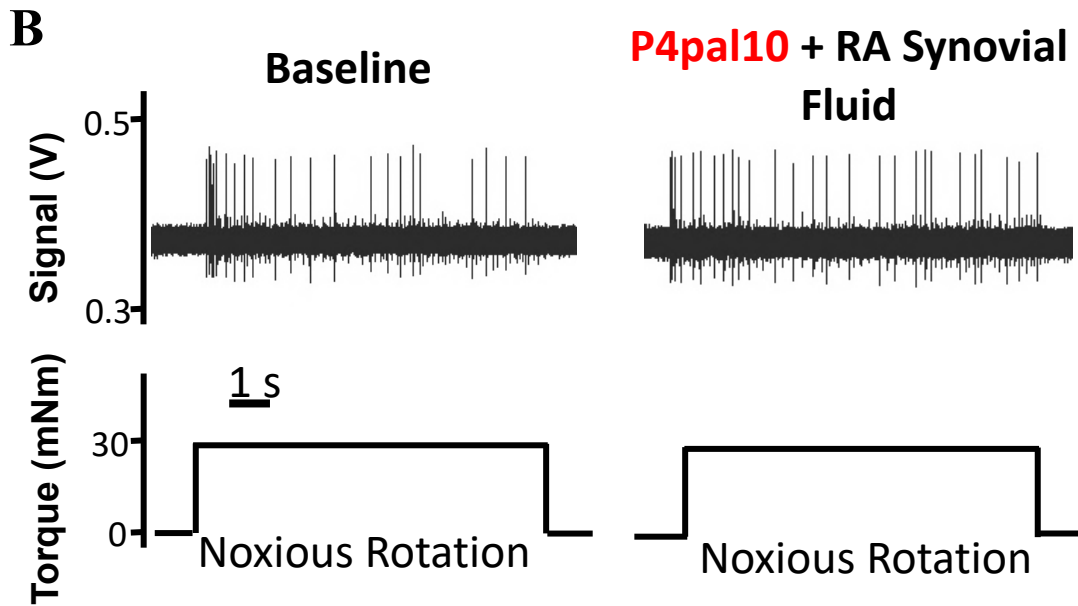
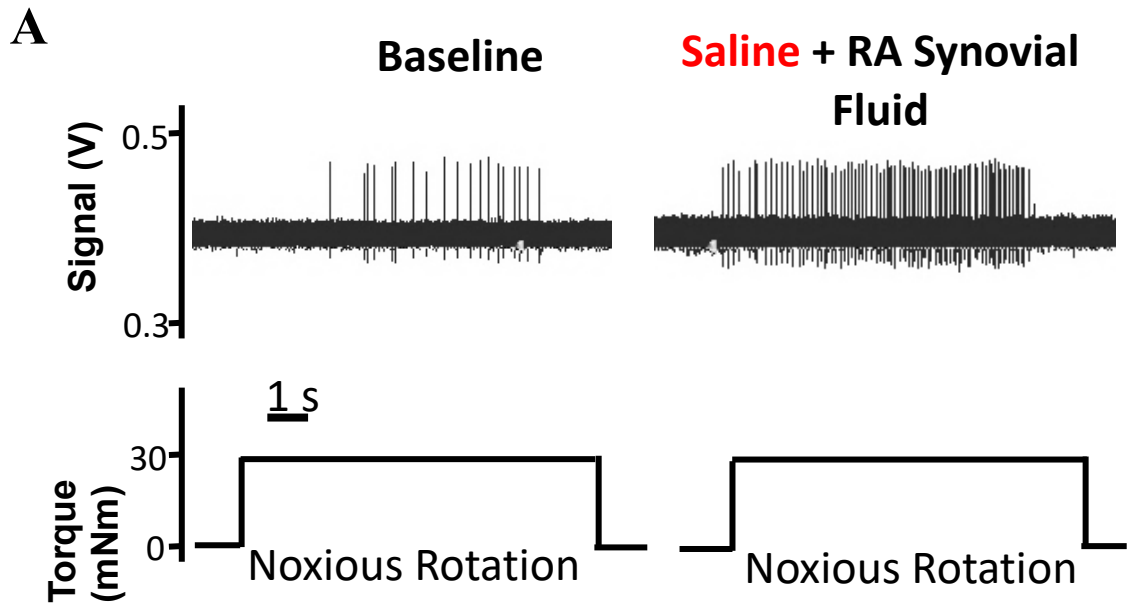
| | | | | | |
|-----|-------------------|--------------------|-----------------|---------------------|---|
| III | 18 | 22 | 3.5 | 3.3 | 1 |
| IV | 15.3 ± 7.3 (7-30) | 23.7 ± 5.7 (18-35) | 2.5 ± 0.3 (2-3) | 1.3 ± 0.2 (1.0-1.6) | 3 |
| ND | 13.3 ± 3.2 (6-13) | 23.8 ± 2.4 (22-30) | | | 3 |

Table 5. 1: Electrophysiological Properties of Naïve Joint Afferent Fibres Treated with Human Arthritic Synovial Fluid.

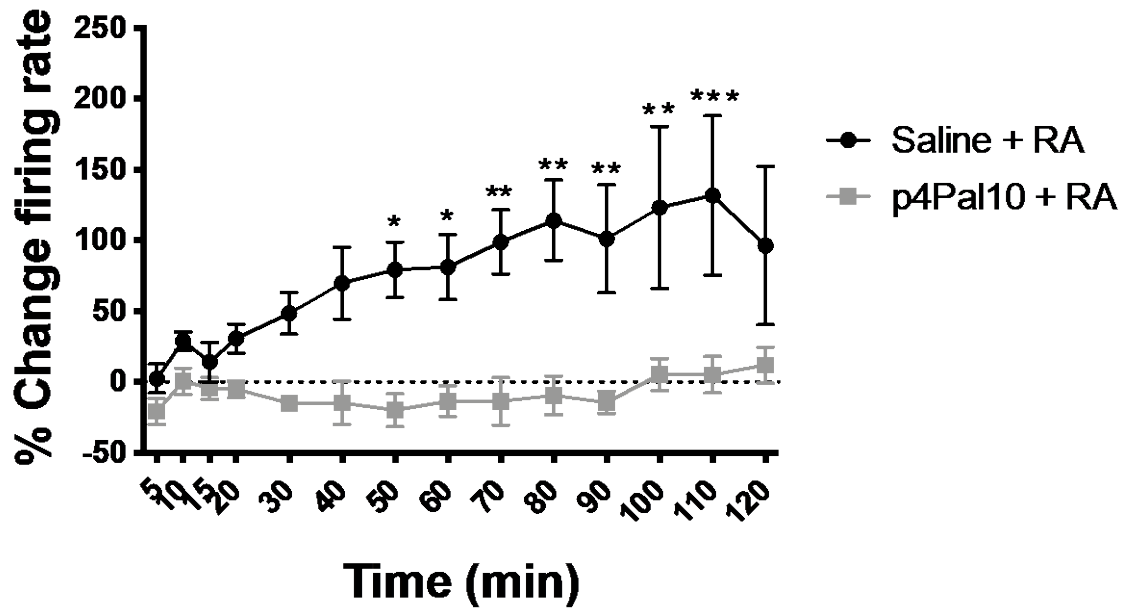
Fibres were categorised as type III (A δ) or IV (C) based on calculated conduction velocities. In experiments where conduction velocities could not be calculated, the fibres are denoted as ‘not determined’ (ND). Data are means ± SEM (range).



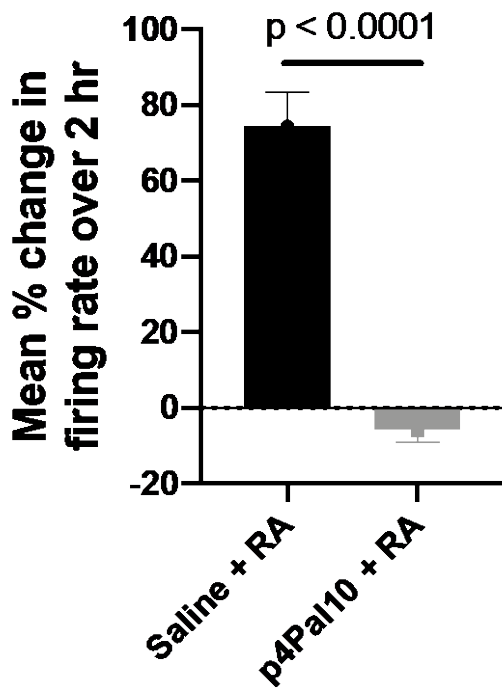




C



D



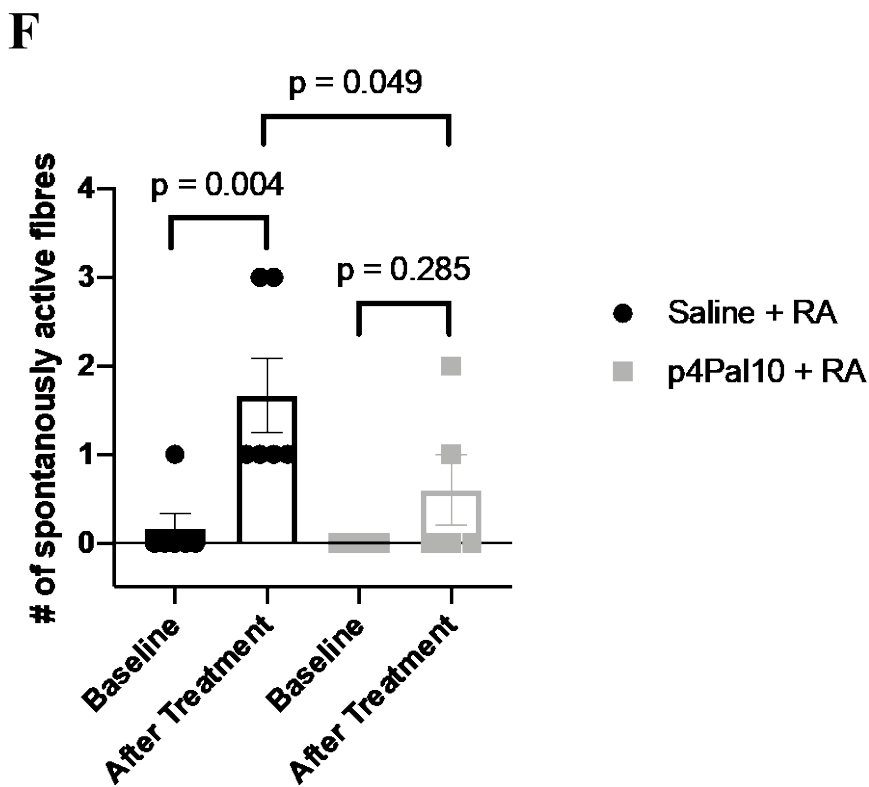
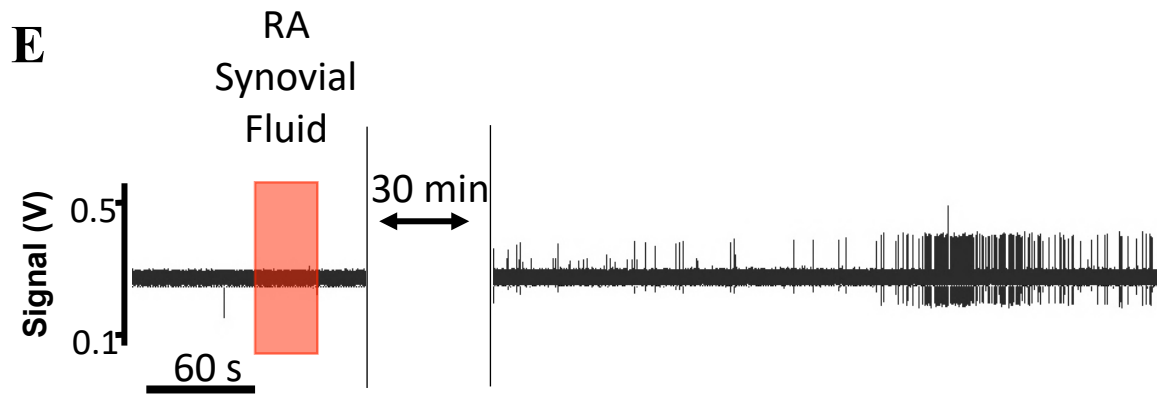
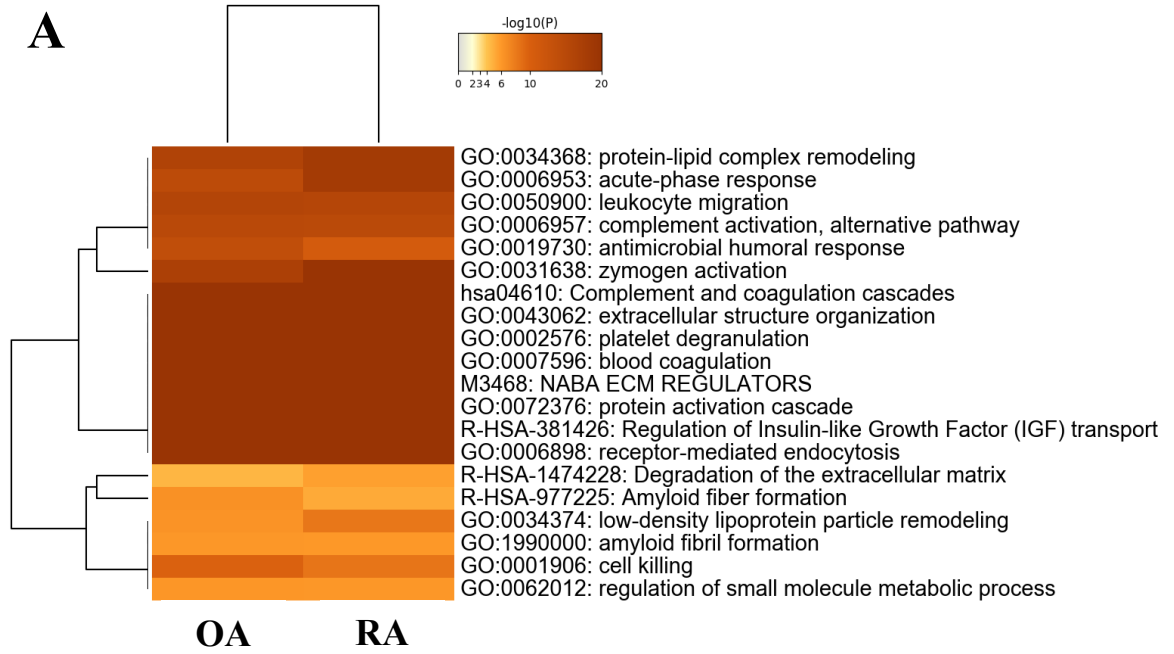


Figure 5. 2 The Effect of PAR4 Blockade on RA Synovial Fluid-Induced Joint Afferent Sensitisation.

A representative trace demonstrates the effect of saline (**A**) or pepducin P4pal10 (**B**) pre-treatment on RA synovial fluid-induced sensitisation (nociceptive C-fibres shown). RA synovial fluid increased joint afferent firing over the course of 120-minutes compared to baseline in saline-pretreated animals. Pre-treatment with pepducin P4pal10 prevented this sensitisation (**C**). The cumulative change in firing over the 120-minute time-course

demonstrates the mean effect of RA synovial fluid in saline-versus pepducin-P4pal10-treated animals **(D)**. Spontaneous firing was also observed following RA synovial fluid administration. The representative trace depicts a delayed response to RA synovial fluid **(E)**. The number of spontaneously active fibres increased following treatment with synovial fluid in saline pretreated animals **(F)**. In contrast, in animals that were pretreated with pepducin P4pal10 there was a small reduction in the number of spontaneously active fibres following RA fluid administration. Data are presented as means \pm SEM. Two-way rm ANOVA or two-way ANOVA followed by Sidak's multiple comparisons test *post-hoc* analysis was used for multivariate analysis. A student's t-test was used to analyse mean percent change in firing. * $p < 0.05$, ** $p < 0.01$, *** $p < 0.001$.



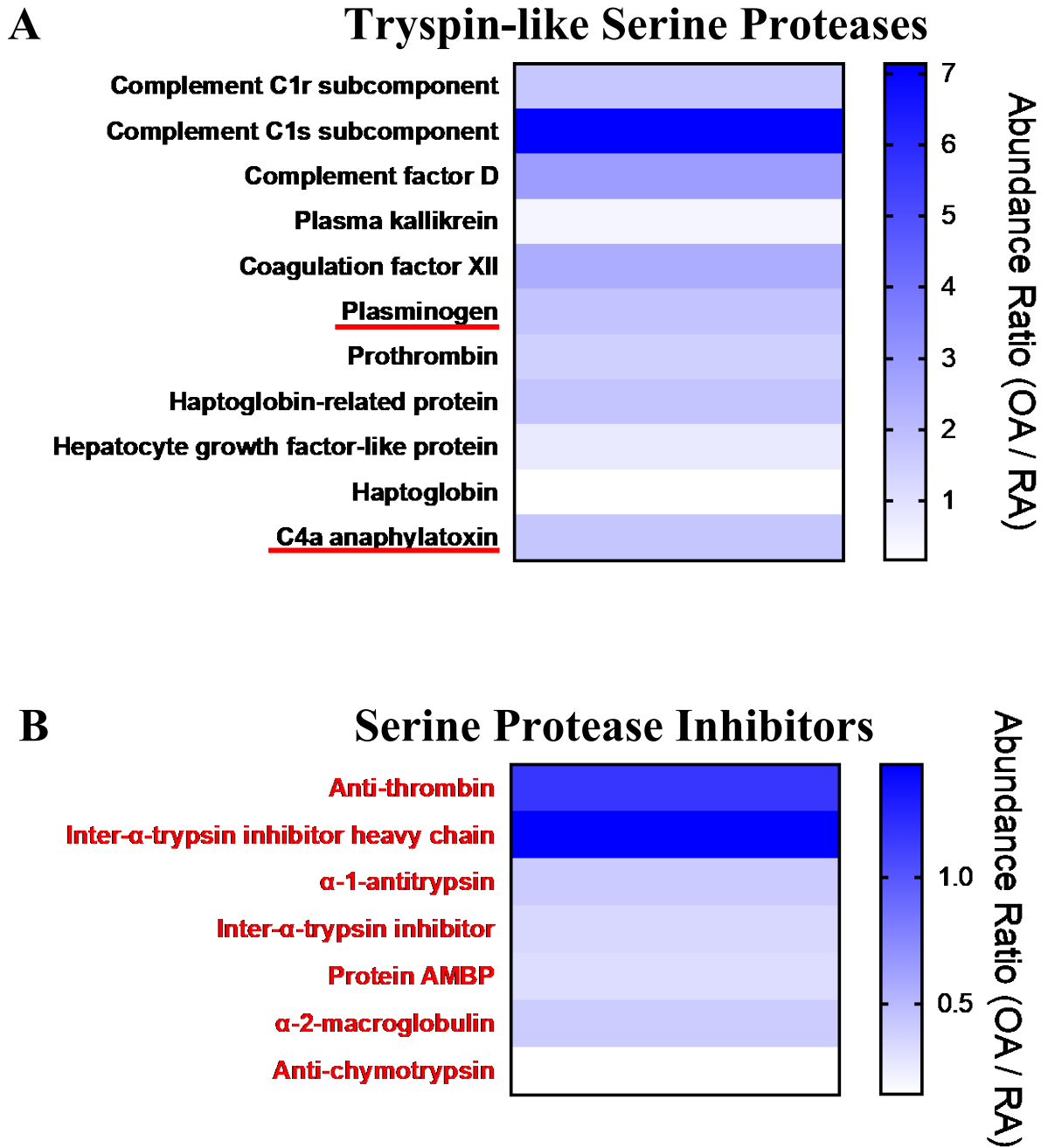


Figure 5. 4 Abundance of Serine Proteases and SERPINS of Interest.

A heat map of trypsin-like serine proteases and C4a anaphylatoxin abundance in arthritic synovial fluid (**A**). Known PAR4 activators (plasminogen and C4a anaphylatoxin) are underlined in red and were detected in higher levels in OA synovial fluid. Seven serine protease inhibitors were detected in arthritic synovial fluid (**B**), many of which were greater in the RA joint.

Chapter 6: Discussion

Pain is the defining clinical symptom of OA; however, over 60% of people living with the disease often cite poorly controlled pain [102]. In addition to a lack of efficacy of currently used therapeutics, a dangerous side-effect profile, especially with long-term use, is putting patients in harm's way [102]. One hypothesis is that analgesics would be more effective if they were disease-oriented, targeting the specific pain mechanisms underlying a given condition. The drugs currently used to treat OA have not been designed in such a manner; however, there have been many drug targets identified in preclinical animal studies and most of these agents subsequently failed in clinical trials. This suggests a disconnect between preclinical testing and clinical utility.

An enigma in OA research has been the disconnect between structural joint damage and patient reported pain. Many studies have tried to identify joint structures that either correlate with pain and or predict escalation of pain over time. One structure that has been identified as a driver of joint pain is the meniscus which is prone to damage [268, 284]. While over 20% of older adults have mild radiographic signs of meniscal damage, 80% of OA patients have meniscal damage with maceration, root tears, and extrusion of the meniscus [285, 286]. Studies have also demonstrated that a traumatic meniscal injury accelerates the development of OA, and that women are more likely to develop the disease after such an injury [36]. Undergoing arthroscopic surgery to repair the meniscus after traumatic injury increases the risk of developing OA even further in women compared with men [36]. In patients with fully developed OA, evidence of meniscal extrusion has been associated with an increased propensity to develop neuropathic pain-revealing a mechanistic pathway that has yet to be fully explored preclinically [268].

Another major clinical issue is that OA is more prevalent in women who also experience more pain than men with the same disease severity [287]. While there are some anatomical factors that predispose women to develop OA, the reasons for the differences in pain intensity remain largely elusive. Despite these clear sex-differences, male animals are predominantly used in pre-clinical studies. These include studies aimed at elucidating disease pathophysiology, pain mechanisms, and pre-clinical screening for candidate analgesics. The exclusion of female animals may be a contributing factor to the poor translatability of drugs from lab animal to human. Additionally, striking sex-differences in pain neurobiology have been identified in animal pain models but have not been widely explored in models of OA [288, 289].

Thus, our first aim was to understand the pain phenotype better in both sexes in a commonly used preclinical model of post-traumatic OA induced by damaging the meniscus. The occurrence of peripheral neuropathy was also explored.

6.1 Medial Meniscus Transection Causes Sexually Disparate Nociceptive Responses in Rats

Transection of the medial meniscus has previously been shown in male animals to recapitulate PTOA-like joint damage and pain behaviour, but its effects in female animals have not been explored [94, 290]. The data presented here demonstrate that following transection of the medial meniscus, both male and female animals develop joint damage consistent with post-traumatic OA. On day 28 following surgery, animals of both sexes developed cartilage loss on the medial tibial plateau with sclerotic subchondral bone, large osteophytes, and mild synovitis. Interestingly, female mammals across multiple species including humans and rats have thinner cartilage compared to their male

counterparts which predisposes them to developing OA [291, 292]. When cartilage lesions in MMT rats were normalised to total cartilage thickness, no difference in lesion severity was observed across the sexes. A recent study by Pucha *et al.*, characterized MMT-induced joint damage in both sexes 21-days following surgery and observed similar levels of damage in males and females [293]. However, they also utilised μ -CT to analyze the structure and composition of bone and discovered that female animals had more cartilage loss in the medial tibial condyle following MMT when normalised for weight. The study only assessed joint damage and concluded that both male and female animals should be included in MMT studies because joint trauma occurred in both sexes. This conclusion is in stark contrast to the findings from our studies that also assessed the pain pathway in these animals.

In Chapter 3, the nociceptive behaviour that follows MMT surgery is described where divergent pain responses were observed in male and female animals. In males, persistent mechanical allodynia and mild weight bearing deficits were observed while in females a recovery in withdrawal thresholds was detected after two-weeks and weight bearing deficits were absent. Single unit recordings from joint afferent fibres corroborated these findings when nociceptors from male MMT animals exhibited lower mechanical thresholds and enhanced evoked firing rates, whereas in female MMT animals peripheral sensitisation was not observed. Given that both sexes developed PTOA but only the males maintained a heightened nociceptive state, we wanted to discern what types of pain were present in the model and why the females appeared to be spared. Since three types of pain (inflammatory, nociceptive, and neuropathic) contribute to the pain phenotype in OA patients, we wondered if these pain states were also present in the MMT model.

Inflammation appeared to play a minor role in pain at day 28 of the MMT model. Synovial lining hyperplasia and cellular infiltration were not statistically elevated in day 28 MMT animals compared to sham-operated animals. There were also no significant signs of joint edema in PTOA animals in end-stage disease.

The presence of appreciable joint damage suggests that nociceptive pain may be contributing to the pain phenotype observed in MMT animals. Nociceptive pain occurs in response to abnormal loading of the damaged joint, where mechanogated ion channels are activated [294]. The presence of weight-bearing deficits in male animals is suggestive of nociceptive pain. The absence of significant weight-bearing deficits in females was at first puzzling for two reasons: (1) they had significant joint damage, and (2) since the centre of mass in female rats lies more anterior than males, they should be able to shift their weight off the affected hindlimb with more ease than males. Experiments that followed began to unravel this mystery.

Peripheral nerve damage was also examined to assess whether neurodegeneration was contributing to the pain phenotype following meniscal transection. Measurement of myelin thickness and nerve morphology of the saphenous nerve revealed that male MMT animals had significantly greater axonal damage compared to sham-operated animals. In contrast, the axons in female MMT animals were indistinguishable from sham-operated animals. No evidence of demyelination was observed in either sex. Previous studies investigating other models of OA revealed peripheral nerve damage and demyelination [149, 164]. In the MIA model, for example, demyelination occurs at day 14 which is considered end-stage disease but is absent at earlier timepoints [149, 295]. Thus, by only looking at one timepoint in the MMT model, we may be missing demyelination that

could occur at later stages. Following meniscal transection, we terminated the model at day 28 but others have extended it further to day 42, although they found that joint damage did not differ between the two time points [296]. Since nerve damage can be induced by sustained abnormal loading, we cannot exclude the possibility that demyelination may occur at a later timepoint. The irregular structural morphology of the nerves observed here has been reported in other models of neuropathy, however, including chronic constriction injury and paclitaxel-induced peripheral neuropathy [297].

In the DRGs, immunohistochemistry was utilised to identify neuronal apoptosis (cleaved caspase-3) and activated SGCs (GFAP) in FG-traced joint neurones. We did not observe any difference in cleaved caspase-3 expression between any of the surgical groups at day 28 of the model. However, there was a significant increase in the percentage of joint neurones that were surrounded by activated GFAP-positive SGCs in MMT animals of both sexes. Glial cell activation has been demonstrated to play a key role in the development and maintenance of neuropathic pain as well as OA pain [288, 289, 298]. Accumulating evidence suggests that through the release of mainly pro-inflammatory mediators, such as TNF- α , IL-6, and BDNF, glial cells alter neuronal excitability thereby contributing to peripheral and central sensitisation [299-302]. Using the destabilisation of the medial meniscus (DMM) PTOA model in mice, Tran *et al.*, observed microglial activation in the spinal cord that they deemed was mediated by peripheral input from fractalkine-signalling DRG neurones [303]. Other studies have demonstrated that by blocking the activity of glial cells with drugs such as fluorocitrate or minocycline, neuropathic-like pain behaviour can be abolished in animal models of OA [298, 304]. In the present study, the female MMT animals also surprisingly exhibited

enhanced GFAP immunoreactivity when pain behaviour and joint afferent sensitisation were absent. There are several potential explanations for this perceived discrepancy between SGC activation and the lack of pain in female PTOA animals. Persistent microglia activation in the dorsal horn of the spinal cord have similarly been observed in female rats while pain behaviours had resolved in a nerve transection model [305]. At the level of the DRG, SGCs may be acting in the same fashion and may still be active despite pain resolution. Despite the majority of the literature describing a pro-nociceptive activity of glial cells, these cells can also exhibit some anti-nociceptive properties. Activated glial cells can release anti-nociceptive mediators such as interleukin-10 and -4, or modulate the endogenous analgesic system by upregulating cannabinoid receptors and opioids to dampen the nociceptive system [306-310]. Thus, in female animals, the SGCs may be preferentially releasing anti-nociceptive mediators but more investigation is required to test this.

Many studies have demonstrated sex-specific pain processing in rodents [270, 271, 289, 311] and our data revealed a striking sex-difference in pain despite similar levels of joint damage. Males exhibited nerve damage, which we would expect to enhance afferent sensitisation and mechanical allodynia. Female animals on the other hand did not exhibit peripheral sensitisation and recovered from tactile sensitivity suggesting a resolution in pain despite joint damage still being present. It has previously been shown that the adrenergic systemic is more active in females, leading to a desensitisation of hyperalgesic β -adrenoceptors and anti-nociception [271]. A recent study by Brederson and colleagues have also reported increased tyrosine hydroxylase staining in the L3 DRG of MMT animals suggesting sympathetic sprouting; however, these experiments were only carried

out in male animals [312]. When we measured noradrenaline in serum it was elevated in the female MMT animals compared to sham-operated but there was no difference between male and female PTOA animals. In both male and female MMT animals, the concentration of noradrenaline was quite variable compared to sham-operated animals. Factors including the degree of animal handling and anesthesia can affect serum levels of noradrenaline and may have influenced the results observed here [313, 314]. Increased handling of animals is associated with higher levels of stress-induced plasma catecholamines. Additionally, the use of urethane has been shown to increase plasma noradrenaline [315].

There is also evidence to suggest that sex differences in the endogenous opioid system contribute to antinociception in female animals [316]. Using the partial meniscectomy model in mice, Knights *et al.* noted similar results to ours where male animals exhibit persistent pain behaviour while female animals recover after an initial nociceptive response [270]. In their study, it was found that administration of naloxone as well as the selective μ -opioid receptor antagonist naloxonazine both enhanced pain sensitivity in female mice, suggesting that endogenous opioids and specifically β -endorphin are, in part, responsible for the pain recovery observed in female animals. When we measured serum β -endorphin, it was significantly elevated in female MMT animals compared to males but not compared to sham-operated animals. In females, serum β -endorphin concentration was also inversely correlated with joint afferent firing, yet no relationship was detectable in male animals. In day 28 female MMT animals, administration of naloxone resulted in secondary mechanical allodynia which was comparable to male MMT animals; however it did not have a significant effect on animal

weight bearing. Overall, the weight bearing deficits observed in this model were quite mild, with male MMT animals placing 43% of their hindlimb weight on the ipsilateral limb at day 28. These data suggest that in the MMT model, female animals are afforded analgesic relief by endogenous opioids.

In the male MMT animals, there were indications that neuropathy may be contributing to the pain phenotype, so we decided to test this pharmacologically with the neuropathic analgesic agent amitriptyline. Amitriptyline is a tricyclic antidepressant that non-selectively inhibits the reuptake of noradrenaline and serotonin. The main mechanism of action of amitriptyline in pain treatment is thought to be facilitation of the descending inhibitory pathway. The systemic dose of amitriptyline was chosen because of its ability to extinguish central sensitisation-mediated behaviour in the formalin test [317]. Systemic amitriptyline attenuated both tactile mechanical sensitivity and weight bearing deficits in male animals but had no effect on female animals. A study by Bove *et al.*, have similarly reported a potential neuropathic component in the MMT model, with male animals favourably responding to another neuropathic drug, gabapentin [94]. When administered locally to the knee, amitriptyline dramatically reduced movement-evoked afferent firing in both male and female animals. Peripheral targets of amitriptyline include voltage-gated sodium channels, where it has been shown to act like a local anesthetic [318]. Thus, the mechanism of action appears to be similar in both sexes and not necessarily related to neuropathy. Modification of sodium channel expression on peripheral axons following nerve damage have been reported. For example, after sciatic nerve ligation in rats, Nav1.8 expression increases strikingly along the sciatic nerve [319, 320]. The rapid response to amitriptyline in male animals compared to females may

suggest higher expression of sodium channels in male animals. Further investigation with a Nav1.8 channel antagonist may provide further insight. Interestingly, we have previously found that in a model of joint neuropathy, where females animals develop more pronounced nerve damage and pain, the Nav1.8 antagonist A-803467 was more effective at blocking afferent firing in female animals compared to males [164].

The data presented here characterise for the first time the peripheral nociceptive pathway of male and female animals in the MMT model of PTOA. We have shown that the model is likely a mix of nociceptive and neuropathic phenotypes in male animals with very little inflammatory contribution. In female MMT animals, the endogenous opioid system is engaged which greatly complicates the use of female animals for testing potential analgesic agents in this model. It highlights that male and female animals do not always respond similarly to the same injury and the importance of studying both females and males when investigating nociceptive processes. We have not assessed spinal or supra-spinal centres which are also important relay centres in the pain pathway which have also shown sex differences [321]. To have a complete appreciation of pain processing in this model, the neurobiology of the dorsal horn and higher centres need to be explored.

6.2 Effects of PAR4 Antagonism in Early and Late Phases of MMT and MIA

Considering both PAR1 and PAR2 have shown potential as therapeutic targets for neuropathic pain, we wanted to explore whether PAR4 may also have analgesic potential in preclinical OA models [156, 157, 238]. We decided to use only male MMT animals in these experiments because of the confounding influence of the endogenous opioid system

in female animals and the lack of a pain phenotype. Since analgesics show variable efficacy in different models of OA, MMT and MIA rats were tested [322, 323]. We compared the electrophysiological properties of joint afferents and saphenous nerve morphology of female and male MIA animals and observed no differences between the sexes. Therefore, we continued the experiments with just male MIA animals to make a direct comparison with male MMT animals.

One of our central hypotheses was that PAR4 blockade would be analgesic against neuropathic-like OA pain. Neuropathy had already been confirmed in the MMT model at day 28 from data presented in Chapter 3 and was identified at day 14 of the MIA model by a reduction in myelin thickness as well as irregular axonal morphology. This finding was in-line with work from others that have identified ATF-3 expression in the DRG of MIA animals and responsiveness to neuropathic analgesics at this later timepoint [100, 324]. Administration of pepducin P4pal10 during the end-stage neuropathic timepoints, however, failed to produce consistent analgesia in behaviour pain testing or reduce joint afferent firing in either model. These results demonstrate that PAR4 may not be a viable target for endstage OA pain where neuropathy is present. In contrast, blocking PAR2 at day 14 of the MIA model has previously been shown to be analgesic [157], suggesting divergent roles of the protease receptors in OA pain. Previous studies demonstrate that activation of articular PAR4 mediates inflammatory pain with the PAR4 activating peptide AYPGKF-NH₂ acting in conjunction with the bradykinin B₂ receptor to sensitise joint afferents [155, 325]. To determine if blockade of PAR4 would be analgesic at an earlier, more inflammatory, timepoint further classification of these models was required.

To characterise the early timepoints in each model, serum inflammatory markers were measured, and saphenous nerves were assessed to determine if signs of nerve damage were present. Inflammatory markers including TNF- α and IL-6 were elevated on day 3 in the MIA model compared to day 14. Whereas proinflammatory cytokines IL-1 β and IL-17A were increased in the serum in MMT animals at day 7 compared to day 28. Demyelination was not present in either model and axons exhibited myelin with a compact appearance. These findings corroborate other studies that have demonstrated an early inflammatory component in the MIA model with synovitis, elevated joint cytokines, and the pain being attenuated with diclofenac but not gabapentin [100, 101, 324]. There are few studies that have assessed inflammatory changes throughout the MMT model. Willett *et al.*, used a multiplex cytokine panel to measure inflammatory mediators in synovial fluid in MMT animals at day 3 and 21 and found the only elevated factor was monocyte chemoattractant protein-1 (MCP-1) at day 3 [326]. In contrast, Mapp *et al.* assessed the histopathology of the model over days 7 to 28 and noted increased synovial vascular density on day 14 and mild synovial hypertrophy over the entire period [93]. These authors cauterized the joint tissue to expose the MCL and removed the surrounding connective tissue which may have introduced a greater inflammatory response and altered the healing process compared to the milder induction employed in the present study. Thus, while MIA has a clear biphasic response with an early inflammatory phase and a later neuropathic phase, conflicting literature suggests that the MMT model may have some mild inflammation throughout.

Pepducin P4pal10 was anti-nociceptive in behavioural experiments and reduced joint afferent firing in both the MIA and MMT model at early timepoints. These data are in

line with other findings where PAR4 inactivation was analgesic in inflammatory joint conditions. In mice that received intraarticular carrageenan, pepducin P4pal10 reduced thermal hyperalgesia and mechanical allodynia [260]. The nociceptive and inflammatory actions of PAR4 activation within the joint have been deemed to be partly dependent on the kallikrein-kinin system and on mast cell activation [155, 272]. A study by Russell *et al.* demonstrated that PAR4 is expressed on mast cells within the rat knee joint in addition to neurones, and pretreatment with the mast cell stabiliser cromolyn, attenuated the pronociceptive actions of PAR4 activation [272]. Additionally, using single unit electrophysiology, the sensitising effect of AYPGKF-NH₂ can be attenuated with the bradykinin B₂ antagonist HOE-140, suggesting a kinin-dependent effect. These experiments suggest that PAR4 can be activated on neurones but also non-neuronal tissue to induce its sensitising effects.

In contrast to the data presented here, preclinical studies of inflammatory pain in other organs suggest mostly nociceptive responses to PAR4 antagonism. PAR4 is widely expressed in the gut and has been implicated in inflammatory bowel conditions [229]. Patch clamp recordings of colon projecting DRG neurones established that PAR4 activation suppresses their excitability [327]. When administered into the colon, sub-inflammatory doses of AYPGKF-NH₂ inhibit nociceptive responses to colon distension in mice [229]. Additionally, PAR4 deficient mice exhibit exaggerated allodynia and hyperalgesia following intracolonic mustard oil administration compared with wild-type animals. Thus, it appears that PAR4 activation produces different nociceptive responses depending on where in the body it is expressed. In our electrophysiology experiments, while pepducin P4pal10 was administered systemically, the central projecting branch of

the saphenous nerve was cut so we were only measuring the effects of PAR4 antagonism locally in the joint. Further experiments would be needed to determine the effect of PAR4 blockade at higher centres of the nervous system with joint input. If necessary, we would have to test the effects of a local administration of a PAR4 targeting drug and determine if systemic levels can be kept adequately low to negate the potential pronociceptive effects of the antagonist in non-articular structures.

It has been previously shown in joint tissue that inflammatory mediators regulate protease receptor expression [255]. In the present study, we found that at early timepoints pro-inflammatory serum cytokines were elevated when compared to later timepoints in both models. The relationship between inflammatory mediators and PAR2 expression has been studied in chondrocytes whereby application of IL-6 or TNF- α increase PAR mRNA and protein expression, and further increase the release of proinflammatory cytokines, suggesting a positive feedback cycle [255]. When the expression of PAR4 in joint DRG-neurones was assessed in early and late timepoints of the MIA and MMT models, enhanced receptor expression was found in the early inflammatory phase of both models, compared to the later timepoints. Thus, higher PAR4 expression correlated with timepoints of greater systemic inflammation in our models. During the early inflammatory phase, 78% and 79% of joint neurones expressed PAR4 in MIA and MMT neurones respectively, which decreased to 65% and 58% by the end-stage of the diseases. By comparison, Russell *et al.* measured a similar level in naïve animals where 60% of joint neurones expressed the receptor [155]. The changes in PAR expression observed here may contribute to the difference in efficacy of pepducin P4pal10 at early versus late stage disease. A full dose-response study would further test any such relationship.

In addition to the coagulation cascade, the discovery that the activity of thrombin acts on PARs opened a new realm of therapeutic intrigue. Current interest in PAR4 focuses largely on its viability as a potential antithrombotic agent largely because of its expression on platelets and endothelial cells. Vergnolle and colleagues demonstrated that thrombin also exhibits numerous pro-inflammatory properties including increased vascular permeability and neutrophil chemotaxis which have been shown to be mediated through PAR4 activation [328]. Thrombin and AYPGKF-NH₂ induced leukocyte rolling and adhesion in mesenteric vessels in rats which was independent of platelet interactions. PAR4 activation also provokes full recruitment of leukocytes as evidenced by leukocyte extravasation into the peritoneal cavity following administration of a synthetic activating peptide [328]. The expression of PAR4 on endothelial cells, leukocytes, as well as vascular smooth muscle were deemed to facilitate these pro-inflammatory processes. Owing to the fact that synovitis is an important contributor to pain and disease progression in early OA, we wanted to determine if pepducin P4pal10 exhibited anti-inflammatory properties in our models. When the microvasculature of early OA animals was examined, there was enhanced leukocyte trafficking. In MIA animals, the number of rolling leukocytes was increased at day 3 compared with day 14, while adherent leukocytes were not significantly different between the timepoints. In MMT animals in contrast, the number of both rolling and adherent leukocytes was greater at the early timepoint. Joint perfusion was also significantly increased seven days after MMT surgery compared with day 28 but wasn't different between early and late timepoints in the MIA model. Treatment with pepducin P4pal10 produced mild anti-inflammatory responses in MMT and MIA animals during these early timepoints. It significantly reduced the

number of rolling leukocytes in both models but had no effect on any of the other parameters. The anti-inflammatory potential of PAR blockade was previously tested in a model of joint inflammation (carrageenan) where it had robust effects. In mice, pepducin P4pal10 decreased joint blood flow and edema and prevented synovial hyperplasia and cellular infiltration [260]. While the effect observed here was mild compared to that seen in the carrageenan model, it may be due to differing joint pathology where carrageenan produces a more severe inflammatory response. Similarities between the thrombotic and inflammatory effects of PAR4 activation may also explain the results observed in the current study. In platelets, PAR4 activation by thrombin or synthetic activating peptides induce surface expression of adhesion molecules which are the primary facilitators of the rolling phase of leukocyte trafficking [329, 330]. In P-selectin knockout mice, intra-articular treatment with AYPGKF-NH₂ or pepducin P4pal10 had no effect on leukocyte kinetics [202]. Thus, it appears that PAR4 induced inflammation is mediated in part through P-selectin and antagonism of the receptor is more sensitive to the rolling phase of leukocyte trafficking. Antagonism of the PAR4 receptor was not tested at the later timepoints in the current study because of the absence of any overt inflammation.

The findings presented here support further investigation of the utility of PAR4 modulation for the treatment of early OA pain. In advanced stages of OA, a multitude of factors contribute to nerve damage including chronic low-grade inflammation, serine proteinases, myelin-destroying lysophosphatidic acid, and physical joint trauma [163, 268]. Following classification of neuropathic-like pain, patients report poorly managed symptoms, and are often treated with serotonin-norepinephrine reuptake inhibitors such as duloxetine [331]. A recent study by Muley *et al.* demonstrated that in the MIA

animals, PAR2 cleaving serine proteases are elevated during the early phase of the model [156]. MIA-induced neuropathy was prevented in these animals by either inhibiting the activity of the proteases or using a PAR2 knockout demonstrating the role of PAR activation in mediating nerve damage. Since we observed anti-inflammatory effects with PAR4 blockade in both models and other studies have reported that early attenuation of joint inflammation prevents the development of joint neuropathy in the MIA model, the neuroprotective potential of early PAR4 antagonism is worth exploring.

6.3 Arthritic Synovial Fluid is Pro-Nociceptive and Contains Serine Proteases

With evidence that PAR cleaving serine proteases are present in arthritic synovial fluid we decided to explore the potential sensitizing effect of human synovial fluid on naïve rat nociceptors. Additionally, having identified PAR4 as a viable target for OA pain, a subset of animals was pretreated with pepducin P4pal10 to determine if PAR4 cleaving proteases present in the synovial fluid could be responsible for altering afferent firing. An OA and a RA synovial fluid sample were tested on the premise that differences in protease profiles are known to occur between diseases [4].

Human OA and RA synovial fluid both caused progressive sensitization of rat joint nociceptors over two hours. An enhancement of both spontaneous and noxious movement-evoked firing was observed. Unfortunately, synovial fluid from a non-arthritic joint was not available to act as a control. Chakrabarti *et al.*, recently carried out a similar electrophysiology study *in vitro* in dissociated mouse DRG neurones that were treated with OA synovial fluid [332]. The authors found that acute treatment with the synovial fluid increased intracellular calcium levels. The effects were blocked by nifedipine and

tetrodotoxin pre-treatment suggesting voltage-gated ion channel activation. G_q protein coupled receptors were also implicated in synovial fluid induced sensitisation as the inhibitor YM-245890 attenuated calcium fluorescence. Surprisingly, other ion channels that have been implicated in arthritis pain were unable to block this synovial fluid-induced flux (e.g. TRPV1, ASIC). A longer synovial fluid incubation period overnight lead to increased neurone sensitisation where decreased resting membrane potentials and enhanced responsiveness of TRPV1 and TRMP8 channels were recorded. In the present study, pre-treatment with pepducin P4pal10 prevented movement-evoked sensitization induced by OA and RA synovial fluid samples. Pepducin P4pal10 also moderately reduced the number of spontaneously active fibres following RA synovial fluid treatment but had no effect on fibres treated with OA synovial fluid. These data suggest that one source of arthritis pain may be the direct activation of articular nerves by serine proteases in synovial fluid. Since joint structures such as the synovium, infrapatellar fat pad, and meniscus are richly innervated by nociceptors and are in direct contact with synovial fluid, the identification of these PAR cleaving proteases may reveal new pain targets.

Untargeted LC-MS/MS was used to identify the proteins present in each synovial fluid sample. In the OA sample, 115 proteins were identified, 10 of which were unique. The RA synovial fluid had 118 proteins identified of which 13 were unique. Among the uniquely identified proteins were markers that have been acknowledged as being dominant in either RA or OA joints [281, 283, 333]. Examples from the RA fluid include the catabolic enzyme, MMP-1, and calgranulin B (S100-A9), an alarmin that mediates pro-inflammatory responses in autoimmune conditions [281, 282, 333, 334]. OA-specific

proteins included the protease inhibitor, SERPIN A2, and the aggrecan core protein, a major constituent of ECM and indicator of active cartilage destruction.

The proteins in each sample were compared using Metascape which identified enriched protein biochemical pathways. The most highly enriched pathways included protein activation, zymogen activation, and ECM regulators, acknowledging the strong presence of proteases and complement proteins in our samples. The Gene Ontology 'protein activation cascade' was the most enriched pathway in both samples, with the RA fluid comprising 47 such proteins and the OA sample containing 43. Included in this pathway are enzymes and substrates of proteolytic cleavage and covalent modification as part of the blood coagulation and kinin pathways. These included molecules such as plasminogen, fibrinogen, kininogen, and a large number of complement proteins.

Further analysis using the String Consortium revealed that there were more serine proteases present in the RA sample (RA:13 versus OA:10). When the structure of those proteases was examined, a greater number of proteases with trypsin-like domains were found in the RA fluid. These are of interest because trypsin-like proteases are capable of cleaving PAR4. Despite there being more proteases in the RA sample, the relative abundance of known PAR4-modulating proteases (e.g. plasminogen and complement factor C4a) were higher in OA fluids. Since the method of mass spectrometry used cannot distinguish between active and inactive proteases, the presence of plasminogen for example, is likely a mixture of the inactive zymogen and its active protease, plasmin. Plasmin cleaves PAR4 at its canonical site and in platelets causes intracellular calcium mobilisation and platelet aggregation [335]. Comparing the activity of plasmin at human and murine PAR4, larger responses to plasmin were observed at the mouse receptor

which was attributed to species differences in the tethered ligand sequences [309]. Differences in the N-terminus of rat and human PAR4 also exist. Thus, the sensitising effect of synovial fluid observed in the present study may also be attributed to a heightened effect of plasmin on the rat specific PAR4 sequence. The relative contribution of synovial fluid plasmin to joint afferent sensitisation in these experiments is unknown. While we have identified that PAR4 contributes to the sensitising effect of synovial fluid, the use of specific serine protease inhibitors would provide further mechanistic insights. In arthritis models, plasmin activity is correlated with cartilage and bone matrix degradation and the elevation of proinflammatory cytokines, IL-1 β , IL-6, and MMPs [197, 336]. It can also mediate the activation of complement proteins known to contribute to arthritis [337, 338]. Thus, plasmin can act on nociceptors directly by cleaving PAR4 or indirectly via these secondary mediators that can also sensitise nociceptors within the joint.

The other PAR4 ligand identified in this study was complement C4a which was 1.8-fold higher in OA synovial fluid. Recently, Wang *et al.*, discovered that this anaphylatoxin was a potent but atypical agonist at PAR4 [339]. Using a cell-based reporter assay, the authors screened C4a against known and orphan GPCRs and identified that C4a acts as a full agonist at PAR4 and a partial agonist at PAR1. C4a activation of PAR4 could not be inhibited with antagonists that block the activity of thrombin and synthetic activating peptides suggesting a non-competitive activation with the complement factor. Whether C4a is cleaving the N-terminus of PAR4 or acting as a ligand itself will need further investigation. Other studies have implicated complement factors C3 and C5 in numerous models of pain; however, C4a has not been widely

studied, in part because a putative receptor was unknown [338, 340, 341]. The recent identification of C4a as a PAR4 activator and its presence in the synovial fluid warrants further investigation into the effect of C4a on nociception and arthritis.

Seven serine protease inhibitors were identified in both synovial fluid samples, and apart from anti-chymotrypsin, the relative abundance of inhibitors favoured the RA fluid. This suggests that despite there being a more diverse population of proteases in the RA fluid, the overall abundance of serine proteases may be higher in the OA sample. Mass spectrometry analysis does not measure proteolytic activity and identification of proteases here are likely a mix of the inactive zymogen and the active form. The use of an activity-based probe would circumvent this limitation and provide a quantification of serine protease bioactivity [342]. The identification of SERPINs in the absence of their cognate substrates (e.g. anti-chymotrypsin was present but cathepsin-G was not) suggests that a targeted mass spectrometry approach is warranted to locate low abundant peptides. In our untargeted approach, we did not deplete the samples of immunoglobulins and other high abundance proteins prior to analysis, as was done elsewhere [281, 283]. Therefore, proteins in low abundance were likely not detected in this analysis and other PAR4 cleaving proteases may be present in our samples.

Given the complexity of synovial fluid samples analysed herein and the many inflammatory mediators elevated in the MIA and MMT models, a polypharmacy approach to treating OA may be desirable. By combining drugs that act synergistically to treat OA pain, the doses of each drug can be lowered, thereby decreasing off-target tissue effects. Identifying what synovial fluid proteins are algogenic and if the antagonism of

their receptors act in a complementary manner may provide a mechanism by which off-site actions of therapeutics can be minimised.

6.3.1 Summary

The results presented and discussed here suggest that despite the importance of studying OA in the female sex, the MMT model does not recapitulate OA pain in female animals. Our findings also demonstrated that PAR4 may be a useful target for early inflammatory pain associated with OA but not endstage disease. Furthermore, the data suggest that human arthritic synovial fluid directly sensitises joint nociceptors to contribute to OA and RA pain, in part, via PAR4 cleaving proteases.

6.4 Limitations of Experimentation

6.4.1 The Use of Animals to Study Arthritis and Pain

The use of animals in experimental research is a privilege that I believe must be undertaken with great respect and foresight. Every opportunity was taken to minimise the number of animals in accordance with the Canadian Council on Animal Care guidelines. Several decisions were made on the basis of minimising the use of animals and are explained throughout the limitations section.

There is no animal model of OA that fully recapitulates the human condition. Large animals such as pigs, horse, or sheep are preferred because their joints are similar to humans and they develop OA spontaneously. In the confines of an academic laboratory environment, however, the use of rats and mice are more common because of size, cost, and genetic homogeneity of animals. In this thesis, I used Wistar rats in the MMT and MIA models of OA. At the onset of studies, animals were sexually-mature but they were considered young adults (< 16 weeks old), which is dissimilar to the average onset of OA

in humans. In the MMT model, induction in 3-, 6-, and 9-month-old Lewis rats produced cartilage lesions that correlated with age; however, no pain measurements were undertaken [343]. Assessing the effect of age in the MMT model is an ongoing project in our laboratory. In the MIA model, induction of the model in aged animals (Fisher 344 rats) resulted in severe weight bearing deficits when compared with younger controls [344]. We have not assessed the MIA model in older females but did confirm joint afferent sensitisation in younger female animals. One of the benefits afforded by the MIA model is the rapid onset of joint pain; however, compared to other OA models it is more severe [324]. These features (excessive cartilage loss and bone destruction), while advantageous in an experimental setting, are often criticized because of the lack of translation to the human disease. In comparison, the MMT model develops at a slower pace with the joint damage being more consistent with human OA [92, 324].

While sham animals were used as a control for MMT animals in most experiments, naïve animals were used for MIA animals. Previous publications demonstrate no difference between i.artic. saline animals and naïve [345]. Since we chose to use two timepoints in MIA, day 3 and day 14, two timepoints would also be required for saline-injected animals. Thus, on the basis of reducing animal use, we decided to use naïve animals as a control.

OA patients often have comorbidities including diabetes or depression, either of which can affect nociceptive processing. Diabetes and OA in humans can be modelled, in part, by combining metabolic disorder and osteoarthritic models. The psychological impact of living with a chronic disease, however, is a complex and subjective experience which cannot be fully appreciated in a model.

6.4.2 Electrophysiology

Electrophysiology is a powerful tool to measure the activity of neurones *in vivo* but several experimental factors need to be considered when interpreting the results of these experiments. To carry out *in vivo* electrophysiology, animals need to be deeply anaesthetised and as such neuronal activity is diminished. Animals in this thesis were anaesthetised with urethane because of the long duration of effect and minimal effects on the autonomic and cardiovascular systems [346]. At anaesthetic concentrations, NMDA, and AMPA receptors are inhibited while glycine and GABA_A receptors are potentiated by urethane leading to overall inhibition of neuronal excitability [346]. Several changes to the local joint environment may have affected the recordings as well. Gallamine triethiodide, a non-depolarising muscle relaxant, was administered to animals to silence muscle afferents and aid in the identification of joint nociceptors. The saphenous nerve was cut distally from the joint to prevent spinal reflexes and thus the nociceptive circuit was not intact. Since different animal groups were anaesthetised in the same manner and administered the same dose of gallamine, the comparison of neuronal activity between cohorts is sound. Nevertheless, the neuronal response to the stimuli applied in an alert animal is likely much higher than in our anaesthetised models. As an alternative, to circumvent the need to cut the saphenous nerve, the activity of joint neurones could be measured at the level of the DRG although this would be technically demanding.

In several experiments, it was not possible to determine the conduction velocity of some fibres. This occurred either because the receptive field was difficult to reach with the stimulating electrode, or the receptive field was too close to the recording electrode

such that system noise prevented identification of the signal on the oscilloscope. In these cases, the fibre had already been identified as having a receptive field in the joint and not the surrounding muscle. It was also categorised according to its characteristic sound upon firing to differentiate muscle and joint afferents.

6.4.3 Pain Behaviour

Since rodents are prey animals much controversy exists as to whether nociceptive behaviour can be effectively measured using these animals and what assays best interrogate pain. There exists both non-evoked and evoked pain measurements. We opted to use dynamic incapacitance, a non-evoked measurement of nociception, and von Frey hair algometry, an evoked measurement of nociception which were carried out on the same day. A criticism of dynamic incapacitance is that the animals may hide their lameness from predator (experimenters) and placing the animals in a darkened, rather than clear, chamber might mitigate this behaviour.

With von Frey hair algometry, animals were also placed in a clear Perspex chamber but as they cannot anticipate the application of the von Frey hair (applied by the experimenter), they are less likely to conceal their response. Special care needs to be taken when applying the hair; holding the von Frey hair for too long may lead to false positive responses, and not holding it long enough can lead to a false negative. In unrestrained animals, the von Frey hair is applied to the plantar surface of the hindpaw rather than directly to the affected knee because of ease of accessibility. As such, secondary rather than primary mechanical allodynia is measured. There may be an added stimulus at the hindpaw, however, as the animals are standing on a mesh floor and

supporting varying levels of weight. Tactile mechanosensitivity at the knee joint could also be measured; however, this would require restraining the animals.

Owing to the emotional aspects of pain and the important psychological impact of OA, there are increasing efforts to measure cognitive/affective aspects of pain. Tests such as conditioned place preference and burrowing behaviour are thought to assess these affective pain states [347]. In place preference testing, animals in pain must choose between a preferred environment (conditioned analgesia) versus an aversive environment (control). Burrowing behaviour is a natural rodent activity and an animal in pain is less likely to burrow [348]. Due to regular monitoring and handling of the animals, especially after MMT surgery, we opted to limit the behavioural testing to once per week. The reason for this was overhandling of the animals has been shown to contribute to stress-induced analgesia or freezing [167]. Since the dynamic incapacitance as well as von Frey hair algometry assays were carried out on the same day, this meant we did not have enough time to also complete additional tests that would have assessed the affective component of pain.

6.4.4 Measures of Inflammation

6.4.4.1 Preparatory Surgery-Induced Inflammation

IVM and LASCA were used to assess joint inflammation. Surgical removal of the skin overlying the joint as well as the fascia was necessary to expose the joint capsule for vascular measurements. This surgery could have induced a minor local vascular reaction which could influence the inflammation measurements. The effect of pepducin P4pal10 on leukocyte trafficking and joint perfusion was compared to baseline measurements in each model, however, so any influence of surgery is consistent in all groups.

6.4.4.2 Rhodamine 6-G Staining of Leukocytes

A limitation of using rhodamine 6-G in our IVM experiments is that it is a non-specific stain of nucleated cells. Therefore, we are unable to differentiate between different types of leukocytes that may be in the joint microvasculature.

6.4.4.3 LASCA

Several factors need to be considered when undertaking joint perfusion experiments. The depth of tissue penetration of the 785 nm LASCA laser is approximately 300 μm in skin [349], and synovial blood vessels are largely found 6-20 μm beneath the surface of the joint capsule [350]. Therefore, by removing the skin and fascia of the joint, we believe we are acquiring synovial blood flow measurements. Since joints do not pressure autoregulate, differences in systemic blood pressure could influence joint perfusion measurements [17]. To control for differences in systemic blood pressure, vascular conductance was calculated and reported rather than raw perfusion values. Vascular conductance has arbitrary units and can thus only describe relative changes.

6.4.4.4 Measurement of Serum Cytokines

We used serum cytokine levels as a surrogate measure of inflammation in the early and late stages of the PTOA models. A more refined approach would have been to measure synovial fluid levels of these mediators. The amount of synovial fluid in a rat knee joint, however, is very low (15-20 μl) and often needs to be either pooled with other animals or diluted in saline. There is evidence that the concentrations of cytokines in

serum and the joint are similar in rodent models of arthritis [351], so to minimise the use of animals and limit dilution of our analyte we used serum instead.

6.4.5 Pharmacological Tools

6.4.5.1 PAR4 Antagonism

We chose to use pepducin P4pal10 to antagonize PAR4 because it has previously been shown to block the actions of PAR4 agonists in joints. Although pepducin P4pal10 has good selectivity for PAR4 over other PARs, activity at structurally similar receptors has been reported [352, 353]. Pepducins mimic the sequence of the third-intracellular loop of a receptor and are conjugated to a N-terminal palmitate (pal) that anchors the sequence to the lipid membrane of a cell. By mimicking the third-intracellular loop, these drugs are proposed to inhibit signalling by binding to G-proteins thereby preventing their interaction with the receptor. A confounding factor of using pepducin P4pal10 is that it can also act as an inhibitor at several other G_q protein-coupled receptors. There is evidence of receptor inhibition by pepducin P4pal10 at bradykinin B₂, muscarinic M₃, histamine H₁, and purinergic P2Y_{1/2} [354]. These receptors share an amino acid sequence (SGRRYG) with pepducin P4pal10 within their intracellular or transmembrane domains, such that binding of the pepducin may alter their ability to signal. Other G_q protein-coupled receptors, such as β-adrenoceptor and chemokine CXCR4, also possess the SGRRYG sequence but in the extracellular domain. These receptors were not affected by pepducin P4pal10 treatment, demonstrating that this reagent does not inhibit all G_q protein-coupled receptors although further screening is greatly needed [354]. With regard to the receptors identified, B₂, H₁, and P2Y_{1/2} are all implicated in nociception. B₂ and H₁ receptors both sensitise joint nociceptors while P2Y receptors are expressed on microglia

[355-357]. While the effect of pepducin P4pal10 has not been compared in the same cell type, the calculated IC_{50} values suggest its most potent at PAR4 and B₂ [353, 354]. An alternate PAR4 antagonist should be used to compare with pepducin P4pal10 to probe the role of PAR4 in OA pain.

6.4.5.2 Male vs Female Animals

We decided to solely use male animals to test the effect of pepducin P4pal10 in the MMT and MIA model. While the rationale for doing so was because the level of nociception appeared similar between male and female MIA animals, that does not mean that both sexes would respond similarly to treatment. Therefore, the effect of PAR4 blockade should be tested in female animals as well to determine if targeting the receptor is appropriate for both sexes.

6.4.5.3 Testing a Single Dose of Pepducin P4pal10

In these experiments we used only one dose of pepducin P4pal10 which was based on an effective analgesic dose in other models of joint pain. While it was effective at reducing pain at early timepoints it failed to produce analgesia in endstage disease. Without testing other doses of pepducin P4pal10 it is impossible to make a firm conclusion regarding PAR4 as a target overall. Instead, the conclusions made are based on the efficacy of the one dose tested, where a higher or lower dose may have been antinociceptive in endstage OA animals.

6.4.5.4 The Use of Post-Surgical Buprenorphine

A sustained-release formulation (48-72 hr) of buprenorphine was administered to all MMT and sham-surgery animals perioperatively. Although buprenorphine acts at all opioid receptors, it provides a safer alternative to classic opioid analgesics because of slow receptor kinetics and minimal respiratory depression [358]. It has the highest affinity at μ -receptors where it acts as an agonist, but it is also a partial agonist at nociceptin/orphanin-FQ receptors, and an antagonist at both κ - and δ -opioid receptors [359]. Sex-differences have been noted in humans, rhesus monkeys, and rats, where the analgesic effects of buprenorphine are more pronounced in males compared to females [360-362]. The implications in this observation is that if male animals were afforded more analgesia in the early timepoints of the MMT model, they may have borne more weight on the affected hindlimb causing further damage. There is also evidence in rats of opioid medications inducing transcriptional changes on genes that encode opioid receptors and endogenous opioids. When the acute transcriptional effects of morphine, methadone, and buprenorphine treatment were compared in the dorsal striatum, thalamus, and nucleus acumbens, the effect of buprenorphine was minimal compared to the other opioids [363].

6.4.6 Untargeted Mass Spectrometry

In these studies we used a ‘shot gun, untargeted’ approach to the initial synovial fluid proteomics experiments to determine if we could identify any proteins in our samples. While it was necessary to complete this first run to determine what type of proteins were present, several refinements can be made. In these initial experiments, we did not deplete the samples of high abundance proteins (e.g. albumin, IgGs), which hindered our ability to detect low abundance proteins. First depleting these contaminants, or running a

targeted analysis, may identify low abundance peptides that were initially missed.

Additionally, the use of an activity-based probe would identify bioactive serine proteases instead of just the constitutive, inert enzyme.

6.4.7 Immunohistochemistry

To assess potential signs of neuronal damage and the expression of PAR4 in the DRG, we used immunohistochemistry. Rather than assessing the entire neuronal population of the hindlimb, a retrograde tracer was used to fluorescently label only joint neurones. One of the limitations of these experiments is that we only evaluated expression at the cell body. Evidence suggests that following injury to nociceptors, receptor expression can change differentially along axons compared to DRG soma [320, 364]. Since in the PAR4 electrophysiology experiments, the outcome of pepducin P4pal10 treatment was dependent on joint expression of PAR4 rather than afferent cell body expression, further experiments are warranted to determine expression of the receptor on the peripheral nerve terminals.

Our histology experiments would have also been strengthened by accompanying Western blot experiments to determine protein levels of epitopes of interest.

6.5 Future Directions

6.5.1 Determine What Other Receptors are Inhibited by Pepducin P4pal10

Ideally, we would like to know what other receptors are inhibited, or modulated by pepducin P4pal10. As mentioned above, Pepducin P4pal10 is known to interact with B2, H1, and P2Y₁₂ receptors in addition to PAR4. Measuring the effect of pepducin P4pal10

on GPCR signalling in a high-throughput assay such as, PRESTO-TANGO, would provide some clarity to interpreting the specificity of the drug in joint tissues.

6.5.2 Assess PAR4 Antagonism using another Agent

To confirm that PAR4 antagonism is a major contributor to the analgesic responses observed in this thesis, another antagonist could be tested at the early OA timepoints. Trans-cinnamoyl-YPGKF-NH₂ (tcY-NH₂) is a peptide that binds to PAR4 but doesn't activate it and prevents its activation via other proteases [365]. It has been shown to have activity at rat and mouse PAR4 but not at the human receptor and thus is used purely for experimental purposes [258].

6.5.3 Use Serine Protease Probes in Mass Spectrometry and Activity-Based Probes to Ascertain Protease Bioactivity in Synovial Fluid

To measure active serine proteases in LC-MS/MS, a tagged substrate probe can be added to the samples. When an active serine protease cleaves the probe, it becomes irreversibly tagged which will allow for the identification of active-site peptides during analysis [342]. This will differentiate between bioactive proteases and inactive forms (zymogens, inhibitor-bound proteases) in the synovial fluid. Another refinement would be to deplete the samples of high abundance proteins and leaving low abundance proteins to be more easily identified.

6.5.4 Assess the Effect of Complement Factor C4a on Afferent Firing and Pain

Having identified C4a as being elevated in OA synovial fluid and the recent finding that it acts as an agonist at PAR4, we would like to further study the role of this factor in

joint nociception. Specifically, can C4a modulate joint afferent firing and does it affect rodent pain behaviour in naïve animals? Evidence of elevated C4a levels have been noted in multiple sclerosis and lupus but studies examining its relationship to pain have not been undertaken [366, 367].

6.5.5 Future Electrophysiology Experiments

To understand better the relationship between primary afferents and spinal neurones and how they both respond to joint injury and analgesia, I would like to record from both the DRG and spinal cord simultaneously. First a DRG neurone with joint input would need to be identified, following which I would need to identify a spinal cord neurone that is functionally connected to the DRG neurone. Once this complete circuit had been assembled, analgesic agents could be applied locally to the joint, DRG, or spinal cord while primary afferent and spinal neurone activity is measured. Additionally, the effect of chronic treatments with analgesics can be tested to determine if they can prevent peripheral and central sensitisation. For example, both joint afferents and spinal cord neurones in the MIA model have been shown to be sensitised. Whether or not chronic PAR4 inhibition can prevent both peripheral and central sensitisation is currently unknown. This approach could answer these questions and provide many mechanistic insights in OA pain.

6.6 Conclusion

The results presented in this study demonstrate that the MMT model is a useful tool to study nociceptive and neuropathic PTOA pain in male animals. Interestingly,

destabilisation of the joint does not lead to significant peripheral sensitisation in female animals thus limiting the utility of the MMT model to study nociception in females. These results suggest that other models such as MIA and LPA, where female animals develop nociceptive sensitisation similar to clinical scenarios may be more appropriate to study female nociception even though the pathophysiology is less similar to clinical disease.

These data have confirmed that serine proteases are present in human arthritic synovial fluid where they activate PAR4 to contribute to joint pain. The results also demonstrated that PAR4 may be a useful target for pain treatment in early-onset OA where patients have inflammatory flares. Further study is warranted to determine the effects of chronic PAR4 treatment and if it has any disease modifying effects.

References

1. Organization, W.H. *Chronic Rheumatic Conditions* [cited 2020 July 15].
2. McAlindon, T.E., et al., *OARSI guidelines for the non-surgical management of knee osteoarthritis*. *Osteoarthritis Cartilage*, 2014. **22**(3): p. 363-88.
3. Tonelli, S.M., et al., *Women with knee osteoarthritis have more pain and poorer function than men, but similar physical activity prior to total knee replacement*. *Biol Sex Differ*, 2011. **2**: p. 12.
4. Russell, F.A. and J.J. McDougall, *Proteinase-Activated Receptors and Arthritis*, in *Proteases and Their Receptors in Inflammation*, N. Vergnolle and M. Chignard, Editors. 2011, Springer Basel: Basel. p. 217-242.
5. Drake, R., A.W. Vogl, and A.W.M. Mitchell, *Gray's Anatomy for Students*. 2014, Saint Louis, United States: Elsevier.
6. Englund, M., et al., *Meniscus pathology, osteoarthritis and the treatment controversy*, in *Nature Reviews Rheumatology*. 2012, Nature Publishing Group. p. 412-419.
7. Norton, W.L. and M. Ziff, *Electron microscopic observations on the rheumatoid synovial membrane*. *Arthritis & Rheumatism*, 1966. **9**(4): p. 589-610.
8. Jayson, M.I.V. *Pressures Within the Human Knee: The Changes During Quadriceps Contraction in Normal and Diseased Joints*. 1974. Berlin, Heidelberg: Springer Berlin Heidelberg.
9. Caughey, D.E. and E.G. Bywaters, *Joint fluid pressure in chronic knee effusions*. *Annals of the rheumatic diseases*, 1963. **22**(2): p. 106-109.
10. Rutherford, D.J., *Intra-articular pressures and joint mechanics: Should we pay attention to effusion in knee osteoarthritis?* *Medical Hypotheses*, 2014. **83**(3): p. 292-295.
11. Kennedy, J.C., I.J. Alexander, and K.C. Hayes, *Nerve supply of the human knee and its functional importance*. *The American Journal of Sports Medicine*, 1982. **10**(6): p. 329-335.
12. Hines, A.E., et al., *Fiber type composition of articular branches of the tibial nerve at the knee joint in man*. *The Anatomical Record*, 1996. **246**(4): p. 573-578.
13. Langford, L.A. and R.F. Schmidt, *Afferent and efferent axons in the medial and posterior articular nerves of the cat*. *The Anatomical Record*, 1983. **206**(1): p. 71-78.
14. Schaible, H.G. and R.F. Schmidt, *Responses of fine medial articular nerve afferents to passive movements of knee joints*. *Journal of Neurophysiology*, 1983. **49**(5): p. 1118-1126.
15. Schaible, H.G. and R.F. Schmidt, *Activation of groups III and IV sensory units in medial articular nerve by local mechanical stimulation of knee joint*. *Journal of Neurophysiology*, 1983. **49**(1): p. 35-44.
16. Catre, M.G. and P.T. Salo, *Quantitative analysis of the sympathetic innervation of the rat knee joint*. *Journal of Anatomy*, 1999. **194**(2): p. 233-239.
17. McDougall, J.J., W.R. Ferrell, and R.C. Bray, *Spatial variation in sympathetic influences on the vasculature of the synovium and medial collateral ligament of*

- the rabbit knee joint*. The Journal of physiology, 1997. **503 (Pt 2)**(Pt 2): p. 435-443.
18. Jessop, D.S., L.J. Richards, and M.S. Harbuz, *Opioid peptides endomorphin-1 and endomorphin-2 in the immune system in humans and in a rodent model of inflammation*. Ann N Y Acad Sci, 2002. **966**: p. 456-63.
 19. Ferrell, W.R. and N.J. Russell, *Extravasation in the knee induced by antidromic stimulation of articular C fibre afferents of the anaesthetized cat*. J Physiol, 1986. **379**: p. 407-16.
 20. Karimian, M. and W.R. Ferrell, *Plasma protein extravasation into the rat knee joint induced by calcitonin gene-related peptide*. Neurosci Lett, 1994. **166**(1): p. 39-42.
 21. Lam, F.Y. and W.R. Ferrell, *Mediators of substance P-induced inflammation in the rat knee joint*. Agents Actions, 1990. **31**(3-4): p. 298-307.
 22. Scott, D.T., F.Y. Lam, and W.R. Ferrell, *Time course of substance P-induced protein extravasation in the rat knee joint measured by micro-turbidimetry*. Neurosci Lett, 1991. **129**(1): p. 74-6.
 23. Krustev, E., D. Rioux, and J.J. McDougall, *Mechanisms and Mediators That Drive Arthritis Pain*, in *Current Osteoporosis Reports*. 2015. p. 216-224.
 24. Badley, E.M., et al., *The Status of Arthritis in Canada: National Report*. 2019: The Arthritis Society.
 25. Kraus, V.B., et al., *Call for standardized definitions of osteoarthritis and risk stratification for clinical trials and clinical use*, in *Osteoarthritis and Cartilage*. 2015. p. 1233-1241.
 26. Neogi, T., *The epidemiology and impact of pain in osteoarthritis*, in *Osteoarthritis and cartilage*. 2013, NIH Public Access. p. 1145-53.
 27. Altman, R., et al., *Development of criteria for the classification and reporting of osteoarthritis: Classification of osteoarthritis of the knee*. Arthritis & Rheumatism, 1986. **29**(8): p. 1039-1049.
 28. Zhang, W., et al., *EULAR evidence-based recommendations for the diagnosis of knee osteoarthritis*. Annals of the Rheumatic Diseases, 2010. **69**(3): p. 483-489.
 29. Johnson, V.L. and D.J. Hunter, *The epidemiology of osteoarthritis*. Best Pract Res Clin Rheumatol, 2014. **28**(1): p. 5-15.
 30. Loeser, R.F., *Age-related changes in the musculoskeletal system and the development of osteoarthritis*, in *Clinics in Geriatric Medicine*. 2010, Elsevier Ltd. p. 371-386.
 31. Loeser, R.F., *Aging and osteoarthritis: the role of chondrocyte senescence and aging changes in the cartilage matrix*, in *Osteoarthritis and Cartilage*. 2009, Elsevier Ltd. p. 971-979.
 32. Loeser, R.F., J.A. Collins, and B.O. Diekman, *Ageing and the pathogenesis of osteoarthritis*, in *Nature Publishing Group*. 2016.
 33. Brown, T.D., et al., *Posttraumatic Osteoarthritis: A First Estimate of Incidence, Prevalence, and Burden of Disease*, in *Journal of Orthopaedic Trauma*. 2006. p. 739-744.
 34. Thomas, A.C., et al., *Epidemiology of Posttraumatic Osteoarthritis*. J Athl Train, 2017. **52**(6): p. 491-496.

35. Aït Si Selmi, T., D. Fithian, and P. Neyret, *The evolution of osteoarthritis in 103 patients with ACL reconstruction at 17 years follow-up*. *The Knee*, 2006. **13**(5): p. 353-358.
36. Abram, S.G.F., et al., *Long-term rates of knee arthroplasty in a cohort of 834 393 patients with a history of arthroscopic partial meniscectomy*. *Bone Joint J*, 2019. **101-B**(9): p. 1071-1080.
37. Grotle, M., et al., *Obesity and osteoarthritis in knee, hip and/or hand: an epidemiological study in the general population with 10 years follow-up*. *BMC musculoskeletal disorders*, 2008. **9**: p. 132-132.
38. Thijssen, E., A. van Caam, and P.M. van der Kraan, *Obesity and osteoarthritis, more than just wear and tear: pivotal roles for inflamed adipose tissue and dyslipidaemia in obesity-induced osteoarthritis*. *Rheumatology*, 2014. **54**(4): p. 588-600.
39. Zhai, G., et al., *The genetic contribution to muscle strength, knee pain, cartilage volume, bone size, and radiographic osteoarthritis: A sibpair study*. *Arthritis & Rheumatism*, 2004. **50**(3): p. 805-810.
40. Valdes, A.M., et al., *Sex and ethnic differences in the association of ASPN, CALM1, COL2A1, COMP, and FRZB with genetic susceptibility to osteoarthritis of the knee*. *Arthritis & Rheumatism*, 2007. **56**(1): p. 137-146.
41. Loughlin, J., et al., *Association of the interleukin-1 gene cluster on chromosome 2q13 with knee osteoarthritis*. *Arthritis & Rheumatism*, 2002. **46**(6): p. 1519-1527.
42. Southam, L., et al., *Association analysis of the interleukin 17 genes IL17A and IL17F as potential osteoarthritis susceptibility loci*. *Annals of the rheumatic diseases*, 2006. **65**(4): p. 556-557.
43. Holden, P., et al., *Identification of Novel pro- α 2(I)X Collagen Gene Mutations in Two Families with Distinctive Oligo-Epiphyseal Forms of Multiple Epiphyseal Dysplasia*. *The American Journal of Human Genetics*, 1999. **65**(1): p. 31-38.
44. Hannan, M.T., et al., *Estrogen use and radiographic osteoarthritis of the knee in women*. *Arthritis & Rheumatism*, 1990. **33**(4): p. 525-532.
45. Nevitt, M.C. and D.T. Felson, *Sex hormones and the risk of osteoarthritis in women: epidemiological evidence*. *Annals of the rheumatic diseases*, 1996. **55**(9): p. 673-676.
46. Wluka, A.E., et al., *Tibial cartilage volume change in healthy postmenopausal women: a longitudinal study*. *Annals of the rheumatic diseases*, 2004. **63**(4): p. 444-449.
47. Hame, S.L. and R.A. Alexander, *Knee osteoarthritis in women*. *Current reviews in musculoskeletal medicine*, 2013. **6**(2): p. 182-187.
48. Burr, D.B. and M.A. Gallant, *Bone remodelling in osteoarthritis*. *Nature Reviews Rheumatology*, 2012. **8**(11): p. 665-673.
49. Bettica, P., et al., *Evidence for increased bone resorption in patients with progressive knee osteoarthritis: Longitudinal results from the Chingford study*. *Arthritis & Rheumatism*, 2002. **46**(12): p. 3178-3184.
50. Bolbos, R.I., et al., *Relationship between trabecular bone structure and articular cartilage morphology and relaxation times in early OA of the knee joint using parallel MRI at 3 T*. *Osteoarthritis and cartilage*, 2008. **16**(10): p. 1150-1159.

51. Neogi, T., et al., *Cartilage loss occurs in the same subregions as subchondral bone attrition: A within-knee subregion-matched approach from the multicenter osteoarthritis study*. Arthritis Care & Research, 2009. **61**(11): p. 1539-1544.
52. Setton, L.A., D.M. Elliott, and V.C. Mow, *Altered mechanics of cartilage with osteoarthritis: human osteoarthritis and an experimental model of joint degeneration*. Osteoarthritis and Cartilage, 1999. **7**(1): p. 2-14.
53. Lorenzo, P., M.T. Bayliss, and D. Heinegård, *Altered patterns and synthesis of extracellular matrix macromolecules in early osteoarthritis*. Matrix Biology, 2004. **23**(6): p. 381-391.
54. Freemont, A.J., et al., *Gene expression of matrix metalloproteinases 1, 3, and 9 by chondrocytes in osteoarthritic human knee articular cartilage is zone and grade specific*. Annals of the rheumatic diseases, 1997. **56**(9): p. 542-549.
55. Saito, I., et al., *Increased cellular infiltrate in inflammatory synovia of osteoarthritic knees*. Osteoarthritis and Cartilage, 2002. **10**(2): p. 156-162.
56. Fernandez-Madrid, F., et al., *Synovial thickening detected by MR imaging in osteoarthritis of the knee confirmed by biopsy as synovitis*. Magnetic Resonance Imaging, 1995. **13**(2): p. 177-183.
57. Loeuille, D., et al., *Macroscopic and microscopic features of synovial membrane inflammation in the osteoarthritic knee: Correlating magnetic resonance imaging findings with disease severity*. Arthritis & Rheumatism, 2005. **52**(11): p. 3492-3501.
58. Roemer, F.W., et al., *Presence of MRI-detected joint effusion and synovitis increases the risk of cartilage loss in knees without osteoarthritis at 30-month follow-up: the MOST study*. Annals of the rheumatic diseases, 2011. **70**(10): p. 1804-1809.
59. Felson, D.T., et al., *Synovitis and the risk of knee osteoarthritis: the MOST Study*. Osteoarthritis and cartilage, 2016. **24**(3): p. 458-464.
60. Neogi, T., et al., *Association of Joint Inflammation With Pain Sensitization in Knee Osteoarthritis: The Multicenter Osteoarthritis Study*. Arthritis & rheumatology (Hoboken, N.J.), 2016. **68**(3): p. 654-661.
61. Benito, M.J., et al., *Synovial tissue inflammation in early and late osteoarthritis*. Annals of the rheumatic diseases, 2005. **64**(9): p. 1263-1267.
62. Fukushima, K., et al., *Relationship between synovial inflammatory cytokines and progression of osteoarthritis after hip arthroscopy: Experimental assessment*. Journal of Orthopaedic Surgery, 2018. **26**(2): p. 2309499018770922.
63. Smith, M.D., et al., *Synovial membrane inflammation and cytokine production in patients with early osteoarthritis*. Journal of Rheumatology, 1997. **24**(2): p. 365-71.
64. Martel-Pelletier, J. and J.P. Pelletier, *Neutral proteases in human osteoarthritic synovium: quantification and characterization*. J Rheumatol, 1987. **14 Spec No**: p. 38-40.
65. Pelletier, J.P., et al., *Proteoglycan-degrading acid metalloprotease activity in human osteoarthritic cartilage, and the effect of intraarticular steroid injections*. Arthritis & Rheumatism, 1987. **30**(5): p. 541-548.

66. Boettger, M.K., et al., *Antinociceptive effects of tumor necrosis factor alpha neutralization in a rat model of antigen-induced arthritis: evidence of a neuronal target*. *Arthritis Rheum*, 2008. **58**(8): p. 2368-78.
67. Brenn, D., F. Richter, and H.G. Schaible, *Sensitization of unmyelinated sensory fibers of the joint nerve to mechanical stimuli by interleukin-6 in the rat: an inflammatory mechanism of joint pain*. *Arthritis Rheum*, 2007. **56**(1): p. 351-9.
68. Richter, F., et al., *Tumor necrosis factor causes persistent sensitization of joint nociceptors to mechanical stimuli in rats*. *Arthritis Rheum*, 2010. **62**(12): p. 3806-14.
69. Fukuoka, H., et al., *Cutaneous hyperalgesia induced by peripheral injection of interleukin-1 beta in the rat*. *Brain Res*, 1994. **657**(1-2): p. 133-40.
70. Mohtai, M., et al., *Expression of interleukin-6 in osteoarthritic chondrocytes and effects of fluid-induced shear on this expression in normal human chondrocytes in vitro*. *Journal of Orthopaedic Research*, 1996. **14**(1): p. 67-73.
71. Ashraf, S., et al., *Increased vascular penetration and nerve growth in the meniscus: a potential source of pain in osteoarthritis*, in *Annals of the Rheumatic Diseases*. 2011. p. 523-529.
72. McDougall, J., R. Bray, and K. Sharkley, *Morphological and immunohistochemical examination of nerves in normal and injured collateral ligaments of rat, rabbit, and human knee joints*, in *The Anatomical Record*. 1997. p. 29-39.
73. French, H.P., K.M. Smart, and F. Doyle, *Prevalence of neuropathic pain in knee or hip osteoarthritis: A systematic review and meta-analysis*. *Seminars in Arthritis and Rheumatism*, 2017. **47**(1): p. 1-8.
74. McCarberg, B. and P. Tenzer, *Complexities in the pharmacologic management of osteoarthritis pain*, in *Current Medical Research and Opinion*. 2013. p. 539-548.
75. Anand, P. and K. Bley, *Topical capsaicin for pain management: therapeutic potential and mechanisms of action of the new high-concentration capsaicin 8% patch*. *British journal of anaesthesia*, 2011. **107**(4): p. 490-502.
76. Bannuru, R.R., et al., *Comparative Effectiveness of Pharmacologic Interventions for Knee Osteoarthritis*, in *Annals of Internal Medicine*. 2015. p. 46.
77. Zeng, C., et al., *Intra-articular corticosteroids and the risk of knee osteoarthritis progression: results from the Osteoarthritis Initiative*. *Osteoarthritis and Cartilage*, 2019. **27**(6): p. 855-862.
78. Liu, S.-H., et al., *Longterm Effectiveness of Intraarticular Injections on Patient-reported Symptoms in Knee Osteoarthritis*. *The Journal of Rheumatology*, 2018. **45**(9): p. 1316-1324.
79. Brown, M.T., et al., *Tanezumab Reduces Osteoarthritic Knee Pain: Results of a Randomized, Double-Blind, Placebo-Controlled Phase III Trial*. *The Journal of Pain*, 2012. **13**(8): p. 790-798.
80. Brown, M.T., et al., *Tanezumab Reduces Osteoarthritic Hip Pain: Results of a Randomized, Double-Blind, Placebo-Controlled Phase III Trial*. *Arthritis & Rheumatism*, 2013. **65**(7): p. 1795-1803.
81. Schnitzer, T.J., et al., *Effect of Tanezumab on Joint Pain, Physical Function, and Patient Global Assessment of Osteoarthritis Among Patients With Osteoarthritis of the Hip or Knee: A Randomized Clinical Trial*. *JAMA*, 2019. **322**(1): p. 37-48.

82. Dakin, P., et al., *The Efficacy, Tolerability, and Joint Safety of Fasinumab in Osteoarthritis Pain: A Phase IIb/III Double-Blind, Placebo-Controlled, Randomized Clinical Trial*. *Arthritis & Rheumatology*, 2019. **71**(11): p. 1824-1834.
83. Hochberg, M.C., et al., *When Is Osteonecrosis Not Osteonecrosis?: Adjudication of Reported Serious Adverse Joint Events in the Tanezumab Clinical Development Program*. *Arthritis & Rheumatology*, 2016. **68**(2): p. 382-391.
84. McInnes, I.B. and G. Schett, *The pathogenesis of rheumatoid arthritis*. *N Engl J Med*, 2011. **365**(23): p. 2205-19.
85. Aletaha, D., et al., *2010 Rheumatoid arthritis classification criteria: an American College of Rheumatology/European League Against Rheumatism collaborative initiative*. *Arthritis Rheum*, 2010. **62**(9): p. 2569-81.
86. Singh, J.A., et al., *2015 American College of Rheumatology Guideline for the Treatment of Rheumatoid Arthritis*. *Arthritis & Rheumatology*, 2016. **68**(1): p. 1-26.
87. Okada, Y., et al., *Genetics of rheumatoid arthritis contributes to biology and drug discovery*. *Nature*, 2014. **506**(7488): p. 376-381.
88. Stastny, P., et al., *HLA-DR4 and other genetic markers in rheumatoid arthritis*. *Br J Rheumatol*, 1988. **27 Suppl 2**: p. 132-8.
89. Symmons, D.P.M., et al., *Blood transfusion, smoking, and obesity as risk factors for the development of rheumatoid arthritis. Results from a primary care-based incident case-control study in Norfolk, England*. *Arthritis & Rheumatism*, 1997. **40**(11): p. 1955-1961.
90. van Vollenhoven, R.F., *Sex differences in rheumatoid arthritis: more than meets the eye*. *BMC medicine*, 2009. **7**: p. 12-12.
91. Malfait, A.M., C.B. Little, and J.J. McDougall, *A commentary on modelling osteoarthritis pain in small animals*. *Osteoarthritis Cartilage*, 2013. **21**(9): p. 1316-26.
92. Janusz, M.J., et al., *Induction of osteoarthritis in the rat by surgical tear of the meniscus: Inhibition of joint damage by a matrix metalloproteinase inhibitor*. *Osteoarthritis and Cartilage*, 2002. **10**(10): p. 785-791.
93. Mapp, P.I., et al., *Angiogenesis in two animal models of osteoarthritis*. *Osteoarthritis and Cartilage*, 2008. **16**(1): p. 61-69.
94. Bove, S.E., et al., *Surgically induced osteoarthritis in the rat results in the development of both osteoarthritis-like joint pain and secondary hyperalgesia*, in *Osteoarthritis and Cartilage*. 2006. p. 1041-1048.
95. King, W., et al., *Human blood-based anti-inflammatory solution inhibits osteoarthritis progression in a meniscal-tear rat study*. *Journal of Orthopaedic Research*, 2017. **35**(10): p. 2260-2268.
96. LaBranche, T.P., et al., *Nerve growth factor inhibition with tanezumab influences weight-bearing and subsequent cartilage damage in the rat medial meniscal tear model*. *Annals of the Rheumatic Diseases*, 2017. **76**(1): p. 295-302.
97. de Sousa Valente, J., *The Pharmacology of Pain Associated With the Monoiodoacetate Model of Osteoarthritis*. *Frontiers in pharmacology*, 2019. **10**: p. 974-974.

98. Foxall, D.L., et al., *The inhibition of erythrocyte glyceraldehyde-3-phosphate dehydrogenase in situ PMR studies*. Biochimica et Biophysica Acta (BBA) - Molecular Cell Research, 1984. **804**(2): p. 209-215.
99. Jiang, L., et al., *Monosodium iodoacetate induces apoptosis via the mitochondrial pathway involving ROS production and caspase activation in rat chondrocytes in vitro*. Journal of Orthopaedic Research, 2013. **31**(3): p. 364-369.
100. Orita, S., et al., *Pain-related sensory innervation in monoiodoacetate-induced osteoarthritis in rat knees that gradually develops neuronal injury in addition to inflammatory pain*, in *BMC Musculoskeletal Disorders*. 2011. p. 134.
101. Ivanavicius, S.P., et al., *Structural pathology in a rodent model of osteoarthritis is associated with neuropathic pain: Increased expression of ATF-3 and pharmacological characterisation*. PAIN, 2007. **128**(3): p. 272-282.
102. Crichton, B. and M. Green, *GP and patient perspectives on treatment with non-steroidal anti-inflammatory drugs for the treatment of pain in osteoarthritis.*, in *Current medical research and opinion*. 2002. p. 92-6.
103. Raja, S.N., et al., *The revised International Association for the Study of Pain definition of pain: concepts, challenges, and compromises*. Pain, 2020.
104. Meyer, A., et al., *Peripheral mechanisms of cutaneous nociception*, in *Textbook of Pain*, S.B. McMahon and M. Koltzenburg, Editors. 2006.
105. Bonet, I.J.M., et al., *Involvement of TACAN, a Mechanotransducing Ion Channel, in Inflammatory But Not Neuropathic Hyperalgesia in the Rat*. The Journal of Pain.
106. Kim, S.E., et al., *The role of Drosophila Piezo in mechanical nociception*. Nature, 2012. **483**(7388): p. 209-212.
107. Szczot, M., et al., *PIEZO2 mediates injury-induced tactile pain in mice and humans*. Science Translational Medicine, 2018. **10**(462): p. eaat9892.
108. Beaulieu-Laroche, L., et al., *TACAN Is an Ion Channel Involved in Sensing Mechanical Pain*. Cell, 2020. **180**(5): p. 956-967.e17.
109. Julius, D. and E. McCleskey, *Cellular and molecular properties of primary afferent neurons*, in *Textbook of Pain*, S. McMahon and M. Koltzenburg, Editors. 2006.
110. Todd, A. and R. Koerber, *Neuroanatomical substrates of spinal nociception*, in *Textbook of Pain*, S. McMahon and M. Koltzenburg, Editors. 2006.
111. Heinricher, M.M., et al., *Descending control of nociception: Specificity, recruitment and plasticity*. Brain research reviews, 2009. **60**(1): p. 214-225.
112. Costigan, M. and C.J. Woolf, *Pain: molecular mechanisms*. J Pain, 2000. **1**(3 Suppl): p. 35-44.
113. Schuelert, N. and J.J. McDougall, *Grading of monosodium iodoacetate-induced osteoarthritis reveals a concentration-dependent sensitization of nociceptors in the knee joint of the rat*, in *Neuroscience Letters*. 2009. p. 184-188.
114. Woolf, C.J. and M. Salter, *Plasticity and pain: role of the dorsal horn*, in *Textbook of Pain*, S. McMahon and M. Koltzenburg, Editors. 2006.
115. Felson, D.T., *Developments in the clinical understanding of osteoarthritis*. Arthritis Res Ther, 2009. **11**(1): p. 203.

116. Hannan, M., D. Felson, and T. Pincus, *Analysis of the discordance between radiographic changes and knee pain in osteoarthritis of the knee.*, in *J Rheumatol*. 2000. p. 1513-1517.
117. Lawrence, R.C., et al., *Estimates of the prevalence of arthritis and selected musculoskeletal disorders in the United States*, in *Arthritis & Rheumatism*. 1998. p. 778-799.
118. Hochberg, M.C., et al., *Epidemiologic associations of pain in osteoarthritis of the knee: data from the National Health and Nutrition Examination Survey and the National Health and Nutrition Examination-I Epidemiologic Follow-up Survey*. *Semin Arthritis Rheum*, 1989. **18**(4 Suppl 2): p. 4-9.
119. Neogi, T., et al., *Association between radiographic features of knee osteoarthritis and pain: results from two cohort studies*. *BMJ*, 2009. **339**: p. b2844.
120. Dye, S.F., G.L. Vaupel, and C.C. Dye, *Conscious neurosensory mapping of the internal structures of the human knee without intraarticular anesthesia*. *Am J Sports Med*, 1998. **26**(6): p. 773-7.
121. Kellgren, J.H. and E.P. Samuel, *The sensitivity and innervation of the articular capsule* *The Journal of Bone and Joint Surgery.* , 1950. **32-B**(1): p. 84-92.
122. Lewis, T., *Pain*. 1942, New York: MacMillan. xiii, 2 , 192 p., 2 leaves of plates.
123. Carlesso, L.C., et al., *Association of intermittent and constant knee pain patterns with knee pain severity, radiographic knee osteoarthritis duration and severity*. *Arthritis Care Res (Hoboken)*, 2020.
124. McDougall, J.J., et al., *Unravelling the relationship between age, nociception and joint destruction in naturally occurring osteoarthritis of Dunkin Hartley guinea pigs*, in *Pain*. 2009. p. 222-232.
125. Zhang, Y., et al., *Fluctuation of knee pain and changes in bone marrow lesions, effusions, and synovitis on magnetic resonance imaging*. *Arthritis Rheum*, 2011. **63**(3): p. 691-9.
126. Eitner, A., et al., *Pain sensation in human osteoarthritic knee joints is strongly enhanced by diabetes mellitus*. *PAIN*, 2017. **158**(9): p. 1743-1753.
127. Brenn, D., F. Richter, and H.-G. Schaible, *Sensitization of unmyelinated sensory fibers of the joint nerve to mechanical stimuli by interleukin-6 in the rat: An inflammatory mechanism of joint pain*. *Arthritis & Rheumatism*, 2007. **56**(1): p. 351-359.
128. Richter, F., et al., *Tumor necrosis factor causes persistent sensitization of joint nociceptors to mechanical stimuli in rats*. *Arthritis & Rheumatism*, 2010. **62**(12): p. 3806-3814.
129. Kanaka, R., H.G. Schaible, and R.F. Schmidt, *Activation of fine articular afferent units by bradykinin*. *Brain Research*, 1985. **327**(1): p. 81-90.
130. Schaible, H.G. and R.F. Schmidt, *Excitation and sensitization of fine articular afferents from cat's knee joint by prostaglandin E2*. *The Journal of Physiology*, 1988. **403**(1): p. 91-104.
131. Gold, M.S., J.D. Levine, and A.M. Correa, *Modulation of TTX-R INa by PKC and PKA and their role in PGE2-induced sensitization of rat sensory neurons in vitro*. *J Neurosci*, 1998. **18**(24): p. 10345-55.

132. Cesare, P. and P. McNaughton, *A novel heat-activated current in nociceptive neurons and its sensitization by bradykinin*. Proc Natl Acad Sci U S A, 1996. **93**(26): p. 15435-9.
133. Neugebauer, V. and H.G. Schaible, *Peripheral and spinal components of the sensitization of spinal neurons during an acute experimental arthritis*. Agents and Actions, 1988. **25**(3): p. 234-236.
134. König, C., et al., *Involvement of Peripheral and Spinal Tumor Necrosis Factor α in Spinal Cord Hyperexcitability During Knee Joint Inflammation in Rats*. Arthritis & Rheumatology, 2014. **66**(3): p. 599-609.
135. Grubb, B.D., R.U. Stiller, and H.G. Schaible, *Dynamic changes in the receptive field properties of spinal cord neurons with ankle input in rats with chronic unilateral inflammation in the ankle region*. Exp Brain Res, 1993. **92**: p. 441-452.
136. Arendt-Nielsen, L., *Pain sensitisation in osteoarthritis*. Clin Exp Rheumatol, 2017. **35 Suppl 107**(5): p. 68-74.
137. Arendt-Nielsen, L., et al., *Sensitization in patients with painful knee osteoarthritis*. Pain, 2010. **149**(3): p. 573-81.
138. Lee, Y.C., et al., *Pain sensitivity and pain reactivity in osteoarthritis*. Arthritis Care Res (Hoboken), 2011. **63**(3): p. 320-7.
139. Finan, P.H., et al., *Discordance between pain and radiographic severity in knee osteoarthritis: findings from quantitative sensory testing of central sensitization*. Arthritis Rheum, 2013. **65**(2): p. 363-72.
140. Neogi, T., et al., *Sensitivity and sensitisation in relation to pain severity in knee osteoarthritis: trait or state?* Ann Rheum Dis, 2015. **74**(4): p. 682-8.
141. Puttfarcken, P.S., et al., *A-995662 [(R)-8-(4-methyl-5-(4-(trifluoromethyl)phenyl)oxazol-2-ylamino)-1,2,3,4-tetrahydronaphthalen-2-ol], a novel, selective TRPV1 receptor antagonist, reduces spinal release of glutamate and CGRP in a rat knee joint pain model*. PAIN, 2010. **150**(2): p. 319-326.
142. Ferland, C.E., et al., *Gait analysis and pain response of two rodent models of osteoarthritis*. Pharmacol Biochem Behav, 2011. **97**(3): p. 603-10.
143. Neugebauer, V., T. Lucke, and H.G. Schaible, *N-methyl-D-aspartate (NMDA) and non-NMDA receptor antagonists block the hyperexcitability of dorsal horn neurons during development of acute arthritis in rat's knee joint*. Journal of Neurophysiology, 1993. **70**(4): p. 1365-1377.
144. Neugebauer, V., P. Rümenapp, and H.-G. Schaible, *The Role of Spinal Neurokinin-2 Receptors in the Processing of Nociceptive Information from the Joint and in the Generation and Maintenance of Inflammation-evoked Hyperexcitability of Dorsal Horn Neurons in the Rat*. European Journal of Neuroscience, 1996. **8**(2): p. 249-260.
145. Neugebauer, V., et al., *The involvement of substance P and neurokinin-1 receptors in the responses of rat dorsal horn neurons to noxious but not to innocuous mechanical stimuli applied to the knee joint*. Brain Research, 1994. **666**(2): p. 207-215.
146. Neugebauer, V. and H.G. Schaible, *Evidence for a central component in the sensitization of spinal neurons with joint input during development of acute arthritis in cat's knee*. Journal of Neurophysiology, 1990. **64**(1): p. 299-311.

147. Eitner, A., et al., *The innervation of synovium of human osteoarthritic joints in comparison with normal rat and sheep synovium*. *Osteoarthritis Cartilage*, 2013. **21**(9): p. 1383-91.
148. Suri, S., et al., *Neurovascular invasion at the osteochondral junction and in osteophytes in osteoarthritis*. *Ann Rheum Dis*, 2007. **66**(11): p. 1423-8.
149. Philpott, H.T., M. O'Brien, and J.J. McDougall, *Attenuation of early phase inflammation by cannabidiol prevents pain and nerve damage in rat osteoarthritis*, in *PAIN*. 2017. p. 2442-2451.
150. Aso, K., et al., *Contribution of nerves within osteochondral channels to osteoarthritis knee pain in humans and rats*. *Osteoarthritis Cartilage*, 2020. **28**(9): p. 1245-1254.
151. Rodriguez-Raecke, R., et al., *Brain Gray Matter Decrease in Chronic Pain Is the Consequence and Not the Cause of Pain*. *The Journal of Neuroscience*, 2009. **29**(44): p. 13746-13750.
152. Gwilym, S.E., et al., *Thalamic atrophy associated with painful osteoarthritis of the hip is reversible after arthroplasty: A longitudinal voxel-based morphometric study*. *Arthritis & Rheumatism*, 2010. **62**(10): p. 2930-2940.
153. Apkarian, A.V., et al., *Chronic Back Pain Is Associated with Decreased Prefrontal and Thalamic Gray Matter Density*. *The Journal of Neuroscience*, 2004. **24**(46): p. 10410-10415.
154. Russell, F.A., et al., *Activation of PAR2 receptors sensitizes primary afferents and causes leukocyte rolling and adherence in the rat knee joint*, in *British Journal of Pharmacology*. 2012. p. 1665-1678.
155. Russell, F.A., et al., *Proteinase-activated receptor-4 (PAR4) activation leads to sensitization of rat joint primary afferents via a bradykinin B2 receptor-dependent mechanism.*, in *Journal of neurophysiology*. 2010. p. 155-63.
156. Muley, M.M., et al., *Prophylactic inhibition of neutrophil elastase prevents the development of chronic neuropathic pain in osteoarthritic mice*. *Journal of neuroinflammation*, 2017. **14**(1): p. 168-168.
157. Muley, M.M., et al., *Neutrophil elastase induces inflammation and pain in mouse knee joints via activation of proteinase-activated receptor-2*, in *British Journal of Pharmacology*. 2016. p. 766-777.
158. Lucena, F. and J.J. McDougall, *Pain responses to protease-activated receptor-2 stimulation in the spinal cord of naive and arthritic rats*. *Neurosci Lett*, 2020. **739**: p. 135391.
159. Richardson, D., et al., *Characterisation of the cannabinoid receptor system in synovial tissue and fluid in patients with osteoarthritis and rheumatoid arthritis*, in *Arthritis Research & Therapy*. 2008. p. R43.
160. Schuelert, N., et al., *Paradoxical effects of the cannabinoid CB2 receptor agonist GW405833 on rat osteoarthritic knee joint pain*. *Osteoarthritis Cartilage*, 2010. **18**(11): p. 1536-43.
161. Azim, S., et al., *Endocannabinoids and acute pain after total knee arthroplasty*. *Pain*, 2015. **156**(2): p. 341-347.
162. Burston, J.J., et al., *Cannabinoid CB2 receptors regulate central sensitization and pain responses associated with osteoarthritis of the knee joint*. *PLoS One*, 2013. **8**(11): p. e80440.

163. McDougall, J.J., et al., *Lysophosphatidic acid provides a missing link between osteoarthritis and joint neuropathic pain.*, in *Osteoarthritis and cartilage*. 2017. p. 926-934.
164. O'Brien MS, P.H., McDougall JJ, *Targeting the Nav1.8 ion channel engenders sex-specific responses in lysophosphatidic acid-induced joint neuropathy*, in *Pain*. 2019. p. 269-278.
165. O'Brien, M., H.T. Philpott, and J.J. McDougall, *Understanding osteoarthritis pain through animal models*. Clin Exp Rheumatol, 2017. **35 Suppl 107(5)**: p. 47-52.
166. Bodnar, R.J., *18 - Measurement of Stress-Induced Analgesia*, in *Methods in Neurosciences*, P.M. Conn, Editor. 1993, Academic Press. p. 281-293.
167. Butler, R.K. and D.P. Finn, *Stress-induced analgesia*. Progress in Neurobiology, 2009. **88(3)**: p. 184-202.
168. Hurwitz, D.E., et al., *Knee pain and joint loading in subjects with osteoarthritis of the knee*. Journal of Orthopaedic Research, 2000. **18(4)**: p. 572-579.
169. Thorp, L.E., et al., *Relationship between pain and medial knee joint loading in mild radiographic knee osteoarthritis*. Arthritis Care & Research, 2007. **57(7)**: p. 1254-1260.
170. Allen, K.D., et al., *Kinematic and dynamic gait compensations resulting from knee instability in a rat model of osteoarthritis*. Arthritis research & therapy, 2012. **14(2)**: p. R78-R78.
171. Mogil, J.S., *Qualitative sex differences in pain processing: emerging evidence of a biased literature*. Nat Rev Neurosci, 2020. **21(7)**: p. 353-365.
172. Gardner, E., *Spike potentials in sensory fibers from the knee joint of the cat*. Anat Rec, 1947. **97(3)**: p. 336.
173. Hutchison, W.D., M.A. Luhn, and R.F. Schmidt, *Responses of lateral thalamic neurons to algescic chemical stimulation of the cat knee joint*. Exp Brain Res, 1994. **101(3)**: p. 452-64.
174. Coggeshall, R.E., et al., *Discharge characteristics of fine medial articular afferents at rest and during passive movements of inflamed knee joints*. Brain Research, 1983. **272(1)**: p. 185-188.
175. Neugebauer, V., H.G. Schaible, and R.F. Schmidt, *Sensitization of articular afferents to mechanical stimuli by bradykinin*. Pflügers Archiv, 1989. **415(3)**: p. 330-335.
176. Schaible, H.G. and R.F. Schmidt, *Time course of mechanosensitivity changes in articular afferents during a developing experimental arthritis*. Journal of Neurophysiology, 1988. **60(6)**: p. 2180-2195.
177. Heppelmann, B., et al., *Effects of acetylsalicylic acid and indomethacin on single groups III and IV sensory units from acutely inflamed joints*. Pain, 1986. **26(3)**: p. 337-351.
178. Vestweber, D., *How leukocytes cross the vascular endothelium*. Nat Rev Immunol, 2015. **15(11)**: p. 692-704.
179. Hickey, M.J. and P. Kubes, *Use of Intra Vital Microscopy to Analyze Leukocyte Rolling and Adhesion In Vivo*. Microscopy and Microanalysis, 1997. **3(S2)**: p. 323-324.
180. McEver, R.P., *Selectins: initiators of leucocyte adhesion and signalling at the vascular wall*. Cardiovasc Res, 2015. **107(3)**: p. 331-9.

181. Huang, M.T., et al., *ICAM-2 mediates neutrophil transmigration in vivo: evidence for stimulus specificity and a role in PECAM-1-independent transmigration*. Blood, 2006. **107**(12): p. 4721-7.
182. Nourshargh, S., F. Krombach, and E. Dejana, *The role of JAM-A and PECAM-1 in modulating leukocyte infiltration in inflamed and ischemic tissues*. J Leukoc Biol, 2006. **80**(4): p. 714-8.
183. Muller, W.A., *The role of PECAM-1 (CD31) in leukocyte emigration: studies in vitro and in vivo*. J Leukoc Biol, 1995. **57**(4): p. 523-8.
184. Krustev, E., A. Reid, and J.J. McDougall, *Tapping into the endocannabinoid system to ameliorate acute inflammatory flares and associated pain in mouse knee joints*. Arthritis Res Ther, 2014. **16**(5): p. 437.
185. de Vries, B.A., et al., *Quantitative DCE-MRI demonstrates increased blood perfusion in Hoffa's fat pad signal abnormalities in knee osteoarthritis, but not in patellofemoral pain*. Eur Radiol, 2020. **30**(6): p. 3401-3408.
186. Toth, J., et al., *Serine Proteases*, in *Handbook of Neurochemistry and Molecular Neurobiology*, A. Lajtha and N. Banik, Editors. 2007.
187. Page, M.J. and E. Di Cera, *Serine peptidases: classification, structure and function*. Cell Mol Life Sci, 2008. **65**(7-8): p. 1220-36.
188. Heutinck, K.M., et al., *Serine proteases of the human immune system in health and disease*. Mol Immunol, 2010. **47**(11-12): p. 1943-55.
189. Sharony, R., et al., *Protein targets of inflammatory serine proteases and cardiovascular disease*. J Inflamm (Lond), 2010. **7**: p. 45.
190. Clements, J.A., et al., *The tissue kallikrein family of serine proteases: functional roles in human disease and potential as clinical biomarkers*. Crit Rev Clin Lab Sci, 2004. **41**(3): p. 265-312.
191. Hedstrom, L., *Serine protease mechanism and specificity*. Chem Rev, 2002. **102**(12): p. 4501-24.
192. Southan, C., *A genomic perspective on human proteases*. FEBS Letters, 2001. **498**(2): p. 214-218.
193. Ossovskaya, V.S. and N.W. Bunnett, *Protease-activated receptors: contribution to physiology and disease*. Physiol Rev, 2004. **84**(2): p. 579-621.
194. Blow, D.M., J.J. Birktoft, and B.S. Hartley, *Role of a buried acid group in the mechanism of action of chymotrypsin*. Nature, 1969. **221**(5178): p. 337-40.
195. Blow, D.M., *6 The Structure of Chymotrypsin*, in *The Enzymes*, P.D. Boyer, Editor. 1971, Academic Press. p. 185-212.
196. Morris, R., et al., *Thrombin receptor expression in rheumatoid and osteoarthritic synovial tissue*. Annals of the Rheumatic Diseases, 1996. **55**(11): p. 841-843.
197. Busso, N. and J.A. Hamilton, *Extravascular coagulation and the plasminogen activator/plasmin system in rheumatoid arthritis*. Arthritis & Rheumatism, 2002. **46**(9): p. 2268-2279.
198. Busso, N., et al., *Plasminogen activation in synovial tissues: differences between normal, osteoarthritis, and rheumatoid arthritis joints*. Annals of the Rheumatic Diseases, 1997. **56**(9): p. 550-557.
199. Ferrell, W.R., et al., *Protease-activated receptor 2: a novel pathogenic pathway in a murine model of osteoarthritis*. Annals of the Rheumatic Diseases, 2010. **69**(11): p. 2051-2054.

200. Ferrell, W.R., et al., *Essential role for proteinase-activated receptor-2 in arthritis*. The Journal of clinical investigation, 2003. **111**(1): p. 35-41.
201. Huesa, C., et al., *Proteinase-activated receptor 2 modulates OA-related pain, cartilage and bone pathology*. Annals of the Rheumatic Diseases, 2016. **75**(11): p. 1989-1997.
202. McDougall, J.J., *Proteinase Activated Receptor-4 Stimulation Promotes Leukocyte Adhesion in the Rat knee Joint*. Arthritis & Rheumatism, 2012. **64**(S10): p. S876-S877.
203. Yang, Y.H., et al., *Reduction of arthritis severity in protease-activated receptor-deficient mice*. Arthritis & Rheumatism, 2005. **52**(4): p. 1325-1332.
204. Varisco, P.A., et al., *Effect of thrombin inhibition on synovial inflammation in antigen induced arthritis*. Annals of the Rheumatic Diseases, 2000. **59**(10): p. 781-787.
205. Sanchez-Pernaute, O., et al., *Fibrin generated in the synovial fluid activates intimal cells from their apical surface: a sequential morphological study in antigen-induced arthritis*. Rheumatology (Oxford), 2003. **42**(1): p. 19-25.
206. Fan, S.T. and T.S. Edgington, *Integrin regulation of leukocyte inflammatory functions. CD11b/CD18 enhancement of the tumor necrosis factor-alpha responses of monocytes*. The Journal of Immunology, 1993. **150**(7): p. 2972-2980.
207. Perez, R.L. and J. Roman, *Fibrin enhances the expression of IL-1 beta by human peripheral blood mononuclear cells. Implications in pulmonary inflammation*. The Journal of Immunology, 1995. **154**(4): p. 1879-1887.
208. Qi, J. and D.L. Kreutzer, *Fibrin activation of vascular endothelial cells. Induction of IL-8 expression*. The Journal of Immunology, 1995. **155**(2): p. 867-876.
209. Harley, S.L., J. Sturge, and J.T. Powell, *Regulation by Fibrinogen and Its Products of Intercellular Adhesion Molecule-1 Expression in Human Saphenous Vein Endothelial Cells*. Arteriosclerosis, Thrombosis, and Vascular Biology, 2000. **20**(3): p. 652-658.
210. Liu, X. and T.H. Piela-Smith, *Fibrin(ogen)-Induced Expression of ICAM-1 and Chemokines in Human Synovial Fibroblasts*. The Journal of Immunology, 2000. **165**(9): p. 5255-5261.
211. Flick, M.J., et al., *Fibrin(ogen) exacerbates inflammatory joint disease through a mechanism linked to the integrin α M β 2 binding motif*. The Journal of Clinical Investigation, 2007. **117**(11): p. 3224-3235.
212. Marty, I., et al., *Amelioration of collagen-induced arthritis by thrombin inhibition*. The Journal of Clinical Investigation, 2001. **107**(5): p. 631-640.
213. Ronday, H.K., et al., *Difference in expression of the plasminogen activation system in synovial tissue of patients with rheumatoid arthritis and osteoarthritis*. Rheumatology, 1996. **35**(5): p. 416-423.
214. Cerinic, M.M., et al., *Synoviocytes from osteoarthritis and rheumatoid arthritis produce plasminogen activators and plasminogen activator inhibitor-1 and display u-PA receptors on their surface*. Life Sciences, 1998. **63**(6): p. 441-453.
215. Martel-Pelletier, J., et al., *In vitro effects of interleukin 1 on the synthesis of metalloproteases, TIMP, plasminogen activators and inhibitors in human articular cartilage*. J Rheumatol Suppl, 1991. **27**: p. 80-4.

216. Mochan, E. and T. Keler, *Plasmin degradation of cartilage proteoglycan*. Biochim Biophys Acta, 1984. **800**(3): p. 312-5.
217. Cook, A.D., et al., *Differing roles for urokinase and tissue-type plasminogen activator in collagen-induced arthritis*. Am J Pathol, 2002. **160**(3): p. 917-26.
218. Vu, T.-K.H., et al., *Molecular cloning of a functional thrombin receptor reveals a novel proteolytic mechanism of receptor activation*. Cell, 1991. **64**(6): p. 1057-1068.
219. Xu, W.-f., et al., *Cloning and characterization of human protease-activated receptor 4*. Proceedings of the National Academy of Sciences, 1998. **95**(12): p. 6642-6646.
220. Kahn, M.L., et al., *A dual thrombin receptor system for platelet activation*. Nature, 1998. **394**(6694): p. 690-694.
221. Ossovskaya, V.S. and N.W. Bunnnett, *Protease-Activated Receptors: Contribution to Physiology and Disease*. Physiological Reviews, 2004. **84**(2): p. 579-621.
222. Macfarlane, S.R., et al., *Proteinase-Activated Receptors*. Pharmacological Reviews, 2001. **53**(2): p. 245-282.
223. Steinhoff, M., et al., *Proteinase-Activated Receptors: Transducers of Proteinase-Mediated Signaling in Inflammation and Immune Response*. Endocrine Reviews, 2005. **26**(1): p. 1-43.
224. Soh, U.J., et al., *Signal transduction by protease-activated receptors*. British Journal of Pharmacology, 2010. **160**(2): p. 191-203.
225. Faruqi, T.R., et al., *Structure-Function Analysis of Protease-activated Receptor 4 Tethered Ligand Peptides: Determinants of Specificity and Utility in Assays of Receptor Function* Journal of Biological Chemistry, 2000. **275**(26): p. 19728-19734.
226. Hirano, K., et al., *Distinct Ca²⁺ Requirement for NO Production between Proteinase-Activated Receptor 1 and 4 (PAR1 and PAR4) in Vascular Endothelial Cells*. Journal of Pharmacology and Experimental Therapeutics, 2007. **322**(2): p. 668-677.
227. Momota, F., et al., *Involvement of Gi/o in the PAR-4-induced NO production in endothelial cells*. Biochemical and Biophysical Research Communications, 2006. **342**(2): p. 365-371.
228. Russo, A., et al., *Caveolae are required for protease-selective signaling by protease-activated receptor-1*. Proc Natl Acad Sci U S A, 2009. **106**(15): p. 6393-7.
229. Augé, C., et al., *Protease-activated receptor-4 (PAR4): a role as inhibitor of visceral pain and hypersensitivity*. Neurogastroenterology & Motility, 2009. **21**(11): p. 1189-e107.
230. DeFea, K.A., et al., *beta-arrestin-dependent endocytosis of proteinase-activated receptor 2 is required for intracellular targeting of activated ERK1/2*. The Journal of cell biology, 2000. **148**(6): p. 1267-1281.
231. Paing, M.M., et al., *β-Arrestins Regulate Protease-activated Receptor-1 Desensitization but Not Internalization or Down-regulation*. Journal of Biological Chemistry, 2002. **277**(2): p. 1292-1300.

232. Shapiro, M.J., et al., *Protease-activated Receptors 1 and 4 Are Shut Off with Distinct Kinetics after Activation by Thrombin*. Journal of Biological Chemistry, 2000. **275**(33): p. 25216-25221.
233. Smith, T.H., et al., *Protease-activated Receptor-4 Signaling and Trafficking Is Regulated by the Clathrin Adaptor Protein Complex-2 Independent of beta-Arrestins*. J Biol Chem, 2016. **291**(35): p. 18453-64.
234. Adams, M.N., et al., *Structure, function and pathophysiology of protease activated receptors*. Pharmacology & Therapeutics, 2011. **130**(3): p. 248-282.
235. Suidan, H.S., S.P. Niclou, and D. Monard. *The thrombin receptor in the nervous system*. in *Seminars in thrombosis and hemostasis*. 1996. Copyright© 1996 by Thieme Medical Publishers, Inc.
236. Garavilla, L.d., et al., *Agonists of proteinase-activated receptor 1 induce plasma extravasation by a neurogenic mechanism*. British Journal of Pharmacology, 2001. **133**(7): p. 975-987.
237. Narita, M., et al., *Protease-activated receptor-1 and platelet-derived growth factor in spinal cord neurons are implicated in neuropathic pain after nerve injury*. The Journal of neuroscience : the official journal of the Society for Neuroscience, 2005. **25**(43): p. 10000-10009.
238. Shavit-Stein, E., et al., *The role of thrombin in the pathogenesis of diabetic neuropathy*. PLOS ONE, 2019. **14**(7): p. e0219453.
239. Suidan, H.S., et al., *Thrombin causes neurite retraction in neuronal cells through activation of cell surface receptors*. Neuron, 1992. **8**(2): p. 363-75.
240. Vaughan, P.J., et al., *Thrombin receptor activation protects neurons and astrocytes from cell death produced by environmental insults*. J Neurosci, 1995. **15**(7 Pt 2): p. 5389-401.
241. Asfaha, S., et al., *Protease-activated receptor-4: a novel mechanism of inflammatory pain modulation*. British journal of pharmacology, 2007. **150**(2): p. 176-185.
242. Martin, L., et al., *Thrombin receptor: An endogenous inhibitor of inflammatory pain, activating opioid pathways*. PAIN, 2009. **146**(1): p. 121-129.
243. Yoon, H., et al., *Blocking the Thrombin Receptor Promotes Repair of Demyelinated Lesions in the Adult Brain*. The Journal of neuroscience : the official journal of the Society for Neuroscience, 2020. **40**(7): p. 1483-1500.
244. Amadesi, S., et al., *Protease-Activated Receptor 2 Sensitizes the Capsaicin Receptor Transient Receptor Potential Vanilloid Receptor 1 to Induce Hyperalgesia*. The Journal of Neuroscience, 2004. **24**(18): p. 4300-4312.
245. Amadesi, S., et al., *Protease-activated receptor 2 sensitizes TRPV1 by protein kinase C ϵ - and A-dependent mechanisms in rats and mice*. The Journal of Physiology, 2006. **575**(2): p. 555-571.
246. Bao, Y., et al., *PAR2-Mediated Upregulation of BDNF Contributes to Central Sensitization in Bone Cancer Pain*. Molecular Pain, 2014. **10**: p. 1744-8069-10-28.
247. Chen, K., et al., *Blocking PAR2 attenuates oxaliplatin-induced neuropathic pain via TRPV1 and releases of substance P and CGRP in superficial dorsal horn of spinal cord*. Journal of the Neurological Sciences, 2015. **352**(1): p. 62-67.

248. Huang, Z.-J., et al., *Chronic compression or acute dissociation of dorsal root ganglion induces cAMP-dependent neuronal hyperexcitability through activation of PAR2*. PAIN, 2012. **153**(7): p. 1426-1437.
249. Zhu, W.-J., et al., *Expression of mRNA for four subtypes of the proteinase-activated receptor in rat dorsal root ganglia*. Brain Research, 2005. **1041**(2): p. 205-211.
250. Hirano, F., et al., *Thrombin-induced expression of RANTES mRNA through protease activated receptor-1 in human synovial fibroblasts*. Annals of the Rheumatic Diseases, 2002. **61**(9): p. 834-837.
251. Chiu, Y.-C., et al., *Thrombin-induced IL-6 production in human synovial fibroblasts is mediated by PAR1, phospholipase C, protein kinase Ca, c-Src, NF-kappaB and p300 pathway*. Molecular Immunology, 2008. **45**(6): p. 1587-1599.
252. Salvi, R., et al., *Enhanced expression of genes involved in coagulation and fibrinolysis in murine arthritis*. Arthritis Research & Therapy, 2000. **2**(6): p. 504.
253. Nakano, S., et al., *Distinct expression of mast cell tryptase and protease activated receptor-2 in synovia of rheumatoid arthritis and osteoarthritis*. Clin Rheumatol, 2007. **26**(8): p. 1284-92.
254. Boileau, C., et al., *Activation of proteinase-activated receptor 2 in human osteoarthritic cartilage upregulates catabolic and proinflammatory pathways capable of inducing cartilage degradation: a basic science study*. Arthritis research & therapy, 2007. **9**(6): p. R121-R121.
255. Xiang, Y., et al., *Expression of proteinase-activated receptors (PAR)-2 in articular chondrocytes is modulated by IL-1 β , TNF- α and TGF- β* . Osteoarthritis and Cartilage, 2006. **14**(11): p. 1163-1173.
256. Abraham, L.A., et al., *Expression of protease-activated receptor-2 by osteoblasts*. Bone, 2000. **26**(1): p. 7-14.
257. Palmer, H.S., et al., *Protease-activated receptor 2 mediates the proinflammatory effects of synovial mast cells*. Arthritis & Rheumatism, 2007. **56**(11): p. 3532-3540.
258. Hollenberg, M.D., et al., *Proteinase-activated receptor-4: evaluation of tethered ligand-derived peptides as probes for receptor function and as inflammatory agonists in vivo*. British journal of pharmacology, 2004. **143**(4): p. 443-454.
259. Houle, S., et al., *Neutrophils and the kallikrein-kinin system in proteinase-activated receptor 4-mediated inflammation in rodents*. British journal of pharmacology, 2005. **146**(5): p. 670-678.
260. McDougall, J.J., et al., *Triggering of proteinase-activated receptor 4 leads to joint pain and inflammation in mice*. Arthritis Rheum, 2009. **60**(3): p. 728-37.
261. Williams, G. and P. Faulkner, *Detection of viral and cellular structures by post-embedding immunocytochemistry*, in *Immuno-gold electron microscopy in virus diagnosis and research*, A.D. Hyatt and B.T. Eaton, Editors. 1993. p. 177-230.
262. Basbaum AI, G.M., Jazat F, Mayes M, Guilbaud G, *The spectrum of fiber loss in a model of neuropathic pain in the rat: an electron microscopic study*, in *Pain*. 1991. p. 359-67.
263. Chaplan, S.R., et al., *Quantitative assessment of tactile allodynia in the rat paw.*, in *Journal of neuroscience methods*. 1994. p. 55-63.

264. Andruski, B., et al., *Leukocyte trafficking and pain behavioral responses to a hydrogen sulfide donor in acute monoarthritis*. *Am J Physiol Regul Integr Comp Physiol*, 2008. **295**(3): p. R814-20.
265. Baatz, H., et al., *Kinetics of white blood cell staining by intravascular administration of rhodamine 6G*. *Int J Microcirc Clin Exp*, 1995. **15**(2): p. 85-91.
266. Zhou, Y., et al., *Metascape provides a biologist-oriented resource for the analysis of systems-level datasets*. *Nat Commun*, 2019. **10**(1): p. 1523.
267. Frey-Law, L.A., et al., *Pain sensitivity profiles in patients with advanced knee osteoarthritis*. *Pain*, 2016. **157**(9): p. 1988-1999.
268. Roubille, C., et al., *The presence of meniscal lesions is a strong predictor of neuropathic pain in symptomatic knee osteoarthritis: a cross-sectional pilot study.*, in *Arthritis research & therapy*. 2014, BioMed Central. p. 507.
269. Krenn, V., et al., *Synovitis score: discrimination between chronic low-grade and high-grade synovitis*. *Histopathology*, 2006. **49**(4): p. 358-64.
270. Knights, C., C. Gentry, and S. Bevan, *Partial medial meniscectomy produces osteoarthritis pain-related behaviour in female C57BL/6 mice*, in *Pain*. 2012. p. 281-292.
271. Khasar, S., et al., *Estrogen regulates adrenal medullary function producing sexual dimorphism in nociceptive threshold and beta-adrenergic receptor-mediated hyperalgesia in the rat.*, in *European Journal of Neuroscience*. 2005. p. 3379-3386.
272. Russell, F.A., et al., *The pronociceptive effect of proteinase-activated receptor-4 stimulation in rat knee joints is dependent on mast cell activation*, in *Pain*. 2011, International Association for the Study of Pain. p. 354-360.
273. Orita, S., et al., *Associations between proinflammatory cytokines in the synovial fluid and radiographic grading and pain-related scores in 47 consecutive patients with osteoarthritis of the knee*. *BMC musculoskeletal disorders*, 2011. **12**: p. 144-144.
274. Leung, Y.Y., et al., *Synovial fluid pro-inflammatory profile differs according to the characteristics of knee pain*. *Osteoarthritis and Cartilage*, 2017. **25**(9): p. 1420-1427.
275. Li, L., et al., *Profiling of inflammatory mediators in the synovial fluid related to pain in knee osteoarthritis*. *BMC Musculoskeletal Disorders*, 2020. **21**(1): p. 99.
276. Dong, T., et al., *Calcitonin gene-related peptide can be selected as a predictive biomarker on progression and prognosis of knee osteoarthritis*. *International Orthopaedics*, 2015. **39**(6): p. 1237-1243.
277. Wang, L., et al., *Levels of neuropeptide Y in synovial fluid relate to pain in patients with knee osteoarthritis*. *BMC Musculoskeletal Disorders*, 2014. **15**(1): p. 319.
278. Calvet, J., et al., *Differential involvement of synovial adipokines in pain and physical function in female patients with knee osteoarthritis. A cross-sectional study*. *Osteoarthritis and Cartilage*, 2018. **26**(2): p. 276-284.
279. Ananth, L., P.E. Prete, and M.L. Kashyap, *Apolipoproteins A-I and B and cholesterol in synovial fluid of patients with rheumatoid arthritis*. *Metabolism - Clinical and Experimental*, 1993. **42**(7): p. 803-806.

280. Bresnihan, B., et al., *Apolipoprotein A-I infiltration in rheumatoid arthritis synovial tissue: a control mechanism of cytokine production?* *Arthritis Res Ther*, 2004. **6**(6): p. R563.
281. Mateos, J., et al., *Differential protein profiling of synovial fluid from rheumatoid arthritis and osteoarthritis patients using LC-MALDI TOF/TOF.* *J Proteomics*, 2012. **75**(10): p. 2869-78.
282. Balakrishnan, L., et al., *Differential proteomic analysis of synovial fluid from rheumatoid arthritis and osteoarthritis patients.* *Clinical Proteomics*, 2014. **11**(1): p. 1.
283. Bhattacharjee, M., et al., *Synovial fluid proteome in rheumatoid arthritis.* *Clin Proteomics*, 2016. **13**: p. 12.
284. Berthiaume, M.-J., et al., *Meniscal tear and extrusion are strongly associated with progression of symptomatic knee osteoarthritis as assessed by quantitative magnetic resonance imaging,* in *Annals of the Rheumatic Diseases*. 2005. p. 556-563.
285. Antony, B., et al., *The relationship between meniscal pathology and osteoarthritis depends on the type of meniscal damage visible on magnetic resonance images: data from the Osteoarthritis Initiative.* *Osteoarthritis and Cartilage*, 2017. **25**(1): p. 76-84.
286. Wenger, A., et al., *Relationship of 3D meniscal morphology and position with knee pain in subjects with knee osteoarthritis: a pilot study.* *Eur Radiol*, 2012. **22**(1): p. 211-20.
287. Glass, N., et al., *Examining sex differences in knee pain: the multicenter osteoarthritis study.* *Osteoarthritis and cartilage*, 2014. **22**(8): p. 1100-1106.
288. Mapplebeck, J.C.S., S. Beggs, and M.W. Salter, *Molecules in pain and sex: a developing story.*, in *Molecular brain*. 2017, BioMed Central. p. 9.
289. Sorge, R.E., et al., *Different immune cells mediate mechanical pain hypersensitivity in male and female mice.*, in *Nature neuroscience*. 2015, NIH Public Access. p. 1081-3.
290. Flannery, C.R., et al., *Prevention of cartilage degeneration in a rat model of osteoarthritis by intraarticular treatment with recombinant lubricin,* in *Arthritis and Rheumatism*. 2009. p. 840-847.
291. Ding, C., et al., *Sex differences in knee cartilage volume in adults: role of body and bone size, age and physical activity.* *Rheumatology (Oxford)*, 2003. **42**(11): p. 1317-23.
292. Mosavian Naeini, R., M. Sahebalzamani, and M.N. Nazem, *Histomorphometrical Changes on the Knee Joints of Male and Female Rats After Moderate Exercise Program.* *Anatomical Sciences Journal*, 2018. **15**(2): p. 41-46.
293. Pucha, K.A., et al., *Characterization of OA development between sexes in the rat medial meniscal transection model.* *Osteoarthritis and Cartilage Open*, 2020. **2**(3): p. 100066.
294. Fu, K., S.R. Robbins, and J.J. McDougall, *Osteoarthritis: the genesis of pain,* in *Rheumatology*. 2018, Oxford University Press. p. iv43-iv50.
295. McDougall, J.J., et al., *Early blockade of joint inflammation with a fatty acid amide hydrolase inhibitor decreases end-stage osteoarthritis pain and peripheral neuropathy in mice,* in *Arthritis Research & Therapy*. 2017. p. 106.

296. Kloefkorn, H.E., et al., *Spatiotemporal gait compensations following medial collateral ligament and medial meniscus injury in the rat: correlating gait patterns to joint damage*. *Arthritis Res Ther*, 2015. **17**: p. 287.
297. Zhang, Y.-L., et al., *Microencapsulated Schwann cell transplantation inhibits P2X3 receptor expression in dorsal root ganglia and neuropathic pain.*, in *Neural regeneration research*. 2018, Medknow Publications and Media Pvt. Ltd. p. 1961-1967.
298. Sagar, D.R., et al., *The contribution of spinal glial cells to chronic pain behaviour in the monosodium iodoacetate model of osteoarthritic pain*. *Molecular pain*, 2011. **7**: p. 88-88.
299. Mousseau, M., et al., *Microglial pannexin-1 channel activation is a spinal determinant of joint pain*. *Science Advances*, 2018. **4**(8): p. eaas9846.
300. Ding, H., et al., *BDNF promotes activation of astrocytes and microglia contributing to neuroinflammation and mechanical allodynia in cyclophosphamide-induced cystitis*. *Journal of Neuroinflammation*, 2020. **17**(1): p. 19.
301. Ledebøer, A., et al., *Minocycline attenuates mechanical allodynia and proinflammatory cytokine expression in rat models of pain facilitation*. *Pain*, 2005. **115**(1): p. 71-83.
302. Zhou, L.-J., et al., *Microglia Are Indispensable for Synaptic Plasticity in the Spinal Dorsal Horn and Chronic Pain*. *Cell Reports*, 2019. **27**(13): p. 3844-3859.e6.
303. Tran, P., et al., *Spinal microglial activation in a murine surgical model of knee osteoarthritis*, in *Osteoarthritis and Cartilage*. 2017. p. 718-726.
304. Adães, S., et al., *Glial activation in the collagenase model of nociception associated with osteoarthritis*. *Molecular pain*, 2017. **13**: p. 1744806916688219-1744806916688219.
305. Leinders, M., et al., *Up-regulation of spinal microglial Iba-1 expression persists after resolution of neuropathic pain hypersensitivity*, in *Neuroscience Letters*. 2013. p. 146-150.
306. Svíženská, I.H., et al., *Bilateral Changes of Cannabinoid Receptor Type 2 Protein and mRNA in the Dorsal Root Ganglia of a Rat Neuropathic Pain Model*. *Journal of Histochemistry & Cytochemistry*, 2013. **61**(7): p. 529-547.
307. Zhang, J., et al., *Induction of CB2 receptor expression in the rat spinal cord of neuropathic but not inflammatory chronic pain models*. *European Journal of Neuroscience*, 2003. **17**(12): p. 2750-2754.
308. Ru-Rong, J., B. Temugin, and M. Nedergaard, *Glia and pain: Is chronic pain a gliopathy?*, in *Pain*. 2013. p. S10-S28.
309. Huang, Q., et al., *Cynandione A attenuates neuropathic pain through p38 β MAPK-mediated spinal microglial expression of β -endorphin*. *Brain, Behavior, and Immunity*, 2017. **62**: p. 64-77.
310. Wu, H.-Y., et al., *Autocrine interleukin-10 mediates glucagon-like peptide-1 receptor-induced spinal microglial β -endorphin expression*. *Journal of Neuroscience*, 2017. **37**(48): p. 11701-11714.
311. Ma, H., et al., *Osteoarthritis severity is sex dependent in a surgical mouse model.*, in *Osteoarthritis and Cartilage*. 2007. p. 695-700.

312. Brederson, J.D., et al., *Characterization and comparison of rat monosodium iodoacetate and medial meniscal tear models of osteoarthritic pain*. J Orthop Res, 2018.
313. Maignan, E., et al., *Sympathetic activity in the rat: effects of anaesthesia on noradrenaline kinetics*. Journal of the Autonomic Nervous System, 2000. **80**(1): p. 46-51.
314. Bühler, H.U., et al., *Plasma adrenaline, noradrenaline and dopamine in man and different animal species*. The Journal of physiology, 1978. **276**: p. 311-320.
315. Carruba, M.O., et al., *Effects of diethyl ether, halothane, ketamine and urethane on sympathetic activity in the rat*. Eur J Pharmacol, 1987. **134**(1): p. 15-24.
316. Gaumond, I., M. Spooner, and S. Marchand, *Sex differences in opioid-mediated pain inhibitory mechanisms during the interphase in the formalin test.*, in *Neuroscience*. 2007. p. 366-374.
317. Sawynok, J. and A. Reid, *Antinociception by tricyclic antidepressants in the rat formalin test: differential effects on different behaviours following systemic and spinal administration*. Pain, 2001. **93**(1): p. 51-59.
318. Sudoh, Y., et al., *Tricyclic antidepressants as long-acting local anesthetics*, in *Pain*. 2003. p. 49-55.
319. England, J.D., et al., *Sodium channels accumulate at the tips of injured axons*. Muscle & Nerve, 1994. **17**(6): p. 593-598.
320. Gold, M.S., et al., *Redistribution of Nav1.8 in Uninjured Axons Enables Neuropathic Pain*. The Journal of Neuroscience, 2003. **23**(1): p. 158-166.
321. Ge, H.Y., P. Madeleine, and L. Arendt-Nielsen, *Sex differences in temporal characteristics of descending inhibitory control: an evaluation using repeated bilateral experimental induction of muscle pain*. Pain, 2004. **110**(1-2): p. 72-8.
322. Boyce-Rustay, J.M., et al., *Characterization of Fasudil in Preclinical Models of Pain*. The Journal of Pain, 2010. **11**(10): p. 941-949.
323. TenBroek, E.M., et al., *Randomized controlled studies on the efficacy of antiarthritic agents in inhibiting cartilage degeneration and pain associated with progression of osteoarthritis in the rat*. Arthritis Research & Therapy, 2016. **18**(1): p. 24.
324. Fernihough, J., et al., *Pain related behaviour in two models of osteoarthritis in the rat knee*, in *Pain*. 2004. p. 83-93.
325. Russell, F.A., et al., *Proteinase-Activated Receptor-4 (PAR 4) Activation Leads to Sensitization of Rat Joint Primary Afferents Via a Bradykinin B 2 Receptor-Dependent Mechanism Proteinase-Activated Receptor-4 (PAR 4) Activation Leads to Sensitization of Rat Joint Primary A*. 2011. p. 155-163.
326. Willett, N.J., et al., *Intra-articular injection of micronized dehydrated human amnion/chorion membrane attenuates osteoarthritis development*. Arthritis Research & Therapy, 2014. **16**(1): p. R47.
327. Karanjia, R., et al., *Activation of protease-activated receptor-4 inhibits the intrinsic excitability of colonic dorsal root ganglia neurons*. Neurogastroenterology & Motility, 2009. **21**(11): p. 1218-1221.
328. Vergnolle, N., et al., *Characterization of Thrombin-Induced Leukocyte Rolling and Adherence: A Potential Proinflammatory Role for Proteinase-Activated Receptor-4*. The Journal of Immunology, 2002. **169**(3): p. 1467-1473.

329. Rigg, R.A., et al., *Protease-activated receptor 4 activity promotes platelet granule release and platelet-leukocyte interactions*. *Platelets*, 2019. **30**(1): p. 126-135.
330. Ivanov, I.I., et al., *Platelet P-selectin triggers rapid surface exposure of tissue factor in monocytes*. *Scientific Reports*, 2019. **9**(1): p. 13397.
331. Smith, H.S., E.J. Smith, and B.R. Smith, *Duloxetine in the management of chronic musculoskeletal pain.*, in *Therapeutics and clinical risk management*. 2012, Dove Press. p. 267-77.
332. Chakrabarti, S., et al., *Human osteoarthritic synovial fluid increases excitability of mouse dorsal root ganglion sensory neurons: an in-vitro translational model to study arthritic pain*. *Rheumatology*, 2019. **59**(3): p. 662-667.
333. Cunnane, G., et al., *Early joint erosions and serum levels of matrix metalloproteinase 1, matrix metalloproteinase 3, and tissue inhibitor of metalloproteinases 1 in rheumatoid arthritis*. *Arthritis & Rheumatism*, 2001. **44**(10): p. 2263-2274.
334. Baillet, A., et al., *Synovial fluid proteomic fingerprint: S100A8, S100A9 and S100A12 proteins discriminate rheumatoid arthritis from other inflammatory joint diseases*. *Rheumatology*, 2010. **49**(4): p. 671-682.
335. Mao, Y., et al., *Regulation of plasmin-induced protease-activated receptor 4 activation in platelets*. *Platelets*, 2009. **20**(3): p. 191-198.
336. Syrovets, T., et al., *Plasmin-induced expression of cytokines and tissue factor in human monocytes involves AP-1 and IKK β -mediated NF- κ B activation*. *Blood*, 2001. **97**(12): p. 3941-3950.
337. Foley, J.H., et al., *Complement Activation in Arterial and Venous Thrombosis is Mediated by Plasmin*. *EBioMedicine*, 2016. **5**: p. 175-182.
338. Woodruff, T.M., et al., *Antiarthritic activity of an orally active C5a receptor antagonist against antigen-induced monarticular arthritis in the rat*. *Arthritis & Rheumatism*, 2002. **46**(9): p. 2476-2485.
339. Wang, H., D. Ricklin, and J.D. Lambris, *Complement-activation fragment C4a mediates effector functions by binding as untethered agonist to protease-activated receptors 1 and 4*. *Proceedings of the National Academy of Sciences of the United States of America*, 2017. **114**(41): p. 10948-10953.
340. Jang, J.H., et al., *Nociceptive sensitization by complement C5a and C3a in mouse*. *PAIN*, 2010. **148**(2): p. 343-352.
341. Liang, D.-Y., et al., *The complement component C5a receptor mediates pain and inflammation in a postsurgical pain model*. *PAIN*, 2012. **153**(2): p. 366-372.
342. Patricelli, M.P., et al., *Direct visualization of serine hydrolase activities in complex proteomes using fluorescent active site-directed probes*. *PROTEOMICS*, 2001. **1**(9): p. 1067-1071.
343. Allen, K.D., et al., *The effects of age on the severity of joint damage and intra-articular inflammation following a simulated medial meniscus injury in 3, 6, and 9 month old male rats*. *Connective Tissue Research*, 2020. **61**(1): p. 82-94.
344. Ro, J.Y., et al., *Age and Sex Differences in Acute and Osteoarthritis-Like Pain Responses in Rats*. *The journals of gerontology. Series A, Biological sciences and medical sciences*, 2020. **75**(8): p. 1465-1472.

345. Bove, S.E., et al., *Weight bearing as a measure of disease progression and efficacy of anti-inflammatory compounds in a model of monosodium iodoacetate-induced osteoarthritis*. *Osteoarthritis Cartilage*, 2003. **11**(11): p. 821-30.
346. Hara, K. and R.A. Harris, *The anesthetic mechanism of urethane: the effects on neurotransmitter-gated ion channels*. *Anesth Analg*, 2002. **94**(2): p. 313-8, table of contents.
347. Pedersen, L.H. and G. Blackburn-Munro, *Pharmacological characterisation of place escape/avoidance behaviour in the rat chronic constriction injury model of neuropathic pain*. *Psychopharmacology (Berl)*, 2006. **185**(2): p. 208-17.
348. Jirkof, P., J. Rudeck, and L. Lewejohann, *Assessing Affective State in Laboratory Rodents to Promote Animal Welfare-What Is the Progress in Applied Refinement Research?* *Animals (Basel)*, 2019. **9**(12).
349. O'Doherty, J., et al., *Comparison of instruments for investigation of microcirculatory blood flow and red blood cell concentration*. *J Biomed Opt*, 2009. **14**(3): p. 034025.
350. Knight, A.D. and J.R. Levick, *The density and distribution of capillaries around a synovial cavity*. *Q J Exp Physiol*, 1983. **68**(4): p. 629-44.
351. Finn, A., et al., *Influence of model and matrix on cytokine profile in rat and human*. *Rheumatology (Oxford)*, 2014. **53**(12): p. 2297-305.
352. Covic, L., et al., *Activation and inhibition of G protein-coupled receptors by cell-penetrating membrane-tethered peptides*. *Proceedings of the National Academy of Sciences*, 2002. **99**(2): p. 643-648.
353. Covic, L., et al., *Pepducin-based intervention of thrombin-receptor signaling and systemic platelet activation*. *Nature Medicine*, 2002. **8**(10): p. 1161-1165.
354. Carr, R., 3rd, et al., *Interdicting Gq Activation in Airway Disease by Receptor-Dependent and Receptor-Independent Mechanisms*. *Mol Pharmacol*, 2016. **89**(1): p. 94-104.
355. Herbert, M.K., H. Just, and R.F. Schmidt, *Histamine excites groups III and IV afferents from the cat knee joint depending on their resting activity*. *Neurosci Lett*, 2001. **305**(2): p. 95-8.
356. Gomis, A., et al., *Blockade of nociceptive sensory afferent activity of the rat knee joint by the bradykinin B2 receptor antagonist fasinabant, in Osteoarthritis and Cartilage*. 2013, Elsevier. p. 1346-1354.
357. Trang, T., S. Beggs, and M.W. Salter, *Purinoreceptors in microglia and neuropathic pain*. *Pflugers Arch*, 2006. **452**(5): p. 645-52.
358. Pergolizzi, J., et al., *Current knowledge of buprenorphine and its unique pharmacological profile*. *Pain Pract*, 2010. **10**(5): p. 428-50.
359. Ding, Z. and R.B. Raffa, *Identification of an additional supraspinal component to the analgesic mechanism of action of buprenorphine*. *Br J Pharmacol*, 2009. **157**(5): p. 831-43.
360. Cook, C.D., et al., *Sex-related differences in the antinociceptive effects of opioids: importance of rat genotype, nociceptive stimulus intensity, and efficacy at the μ opioid receptor*. *Psychopharmacology*, 2000. **150**(4): p. 430-442.
361. Turner, J.M., et al., *Pharmacogenetic analysis of sex differences in opioid antinociception in rats*. *Pain*, 2003. **106**(3): p. 381-391.

362. Negus, S.S. and N.K. Mello, *Opioid antinociception in ovariectomized monkeys: comparison with antinociception in males and effects of estradiol replacement*. J Pharmacol Exp Ther, 1999. **290**(3): p. 1132-40.
363. Belkai, E., et al., *Comparison of the transcriptional responses induced by acute morphine, methadone and buprenorphine*. Eur J Pharmacol, 2013. **711**(1-3): p. 10-8.
364. Lai, J., et al., *Inhibition of neuropathic pain by decreased expression of the tetrodotoxin-resistant sodium channel, Nav1.8.*, in *Pain*. 2002. p. 143-52.
365. Hollenberg, M.D. and M. Saifeddine, *Proteinase-activated receptor 4 (PAR4): activation and inhibition of rat platelet aggregation by PAR4-derived peptides*. Canadian Journal of Physiology and Pharmacology, 2001. **79**(5): p. 439-442.
366. Ingram, G., et al., *Elevated plasma C4a levels in multiple sclerosis correlate with disease activity*. Journal of Neuroimmunology, 2010. **223**(1): p. 124-127.
367. Wild, G., et al., *C4a anaphylatoxin levels as an indicator of disease activity in systemic lupus erythematosus*. Clinical & Experimental Immunology, 1990. **80**(2): p. 167-170.

Appendix A: OARSI Scoring of Knee Joints

A modified OARSI scoring of MMT- and sham-surgery joints was utilised to assess histopathological changes in male and female animals.

The following parameters were measured and/or scored in rat MMT joints:

Tibial and Femoral Cartilage Degeneration Score

Joints were partitioned into outside (z1), middle (z2), and inner (z3) zones to measure cartilage degeneration. General cartilage degeneration includes chondrocyte death/loss, proteoglycan (PG) loss, and collagen loss or fibrillation. Zones were scored individually and a sum of all three zones was calculated.

| Parameter | Score | Description |
|------------------------|-------|---|
| Cartilage degeneration | 0 | No degeneration |
| | 0.5 | Very minimal degeneration; >5% of the total projected cartilage area affected by matrix or chondrocyte loss |
| | 1 | Minimal degeneration; 5–10% affected |
| | 2 | Mild degeneration; 11–25% affected |
| | 3 | Moderate degeneration; 26–50% affected |
| | 4 | Marked degeneration; 51–75% affected |
| | 5 | Severe degeneration; greater than 75% affected |

Normalised Medial Tibial Cartilage Damage

The depth to tidemark at the midpoint in each of the 3 zones of the tibial plateau are measured using an ocular micrometer. The total depth to tidemark can serve as an

average measure of cartilage thickness. The depth of any lesion is measured. A depth ratio of

any matrix change is calculated by dividing the lesion depth by the total depth.

Osteophyte Score and Measurement

Osteophyte thickness (tidemark to furthest point extending toward synovium) is measured with

an ocular micrometer. Scores are assigned to the largest osteophyte according to the following criteria:

| Parameter | Score | Description |
|------------------|--------------|--|
| Osteophytes | 0 | Marginal zone proliferative changes <200 μm |
| | 1 | Small 200–299 μm |
| | 2 | Moderate 300–399 μm |
| | 3 | Large 400–499 μm |
| | 4 | Very large 500-599 μm |
| | 5 | Very Large $\geq 600 \mu\text{m}$ |

Medial Tibial Bone Damage Score

A single score is assigned for all 3 sections of the joint. Damage to the calcified cartilage layer and subchondral bone (worst case scenario for all sections) is scored using the following criteria:

| Parameter | Score | Description |
|---|--------------|---|
| Calcified cartilage and subchondral bone damage | 0 | No changes |
| | 1 | Increased basophilia at tidemark, - no fragmentation of tidemark, - no marrow changes or, if present, minimal and focal (affects <10% linear width of tidemark) |
| | 2 | Increased basophilia at tidemark, - minimal to mild focal fragmentation of calcified cartilage of tidemark (1-10% width of tidemark), - mesenchymal change in marrow (fibroblastic cells) involving about 1/4 of subchondral region under lesion, |
| | 3 | Increased basophilia at tidemark, - mild to marked fragmentation (multiple larger areas) of calcified cartilage (11-25% width of tidemark), subchondral bone loss - mesenchymal change in marrow in up to 3/4 of total area, - areas of marrow chondrogenesis may be evident but no major collapse of articular cartilage into epiphyseal bone (definite depression in surface). |
| | 4 | Increased basophilia at tidemark, - marked to severe fragmentation of calcified cartilage (26-50% of width of tidemark), |

| Parameter | Score | Description |
|-----------|-------|--|
| | | <ul style="list-style-type: none"> - marrow mesenchymal change involves up to 3/4 of area, - articular cartilage has collapsed into the epiphysis to a depth of 250 µm or less from tidemark (see definite depression in surface cartilage). |
| | 5 | <p>Increased basophilia at tidemark,</p> <ul style="list-style-type: none"> - marked to severe fragmentation of calcified cartilage (>50% of the width of the tidemark), - marrow mesenchymal change involves up to 3/4 of area, - articular cartilage has collapsed into the epiphysis to a depth of greater than 250 µm from tidemark. |

Total Joint Scores

The tibial and femoral cartilage degeneration scores, and the osteophyte score were combined to determine a total joint score.

Synovitis Score

Synovial inflammation (concentrated on the medial side) was scored as follows:

| Parameter | Grade | Description |
|--------------------------------|-------|---|
| Synovial membrane inflammation | 0 | No changes (1–2 layers of synovial lining cells) |
| | 0.5 | Minimal changes- generally focal or scattered minimal diffuse |

| Parameter | Grade | Description |
|------------------|--------------|--|
| | 1 | Increased number of lining cell layers (≥ 3 –4 layers) or <ul style="list-style-type: none"> - slight proliferation of subsynovial tissue. - generally focal or scattered minimal diffuse |
| | 2 | Increased number of lining cell layers (≥ 3 –4 layers) and/or <ul style="list-style-type: none"> - proliferation of subsynovial tissue. - mild mononuclear cell infiltration |
| | 3 | Increased number of lining cell layers (> 4 layers) and/or <ul style="list-style-type: none"> - proliferation of subsynovial tissue and - moderate mononuclear cell infiltration |
| | 4 | Increased number of lining cell layers (> 4 layers) and/or <ul style="list-style-type: none"> - proliferation of subsynovial tissue, - marked mononuclear cell infiltration |
| | 5 | Increased number of lining cell layers (> 4 layers) and/or <ul style="list-style-type: none"> - proliferation of subsynovial tissue, - severe mononuclear cell infiltration |

Appendix B: Drugs, Reagents, and Devices

| Drug | Source | Description |
|---------------------------|--|--|
| Amitriptyline | Sigma Aldrich (St. Louis, MO, USA) | <ul style="list-style-type: none"> • Tricyclic antidepressant • Used to treat neuropathic pain |
| Buprenorphine | Chiron Compounding (Hamilton, ON, CAN) | <ul style="list-style-type: none"> • Opioid • Used to manage post-operative pain |
| Heparin | CDMV (Dartmouth, NS, CAN) | <ul style="list-style-type: none"> • Anticoagulant |
| Isoflurane | CDMV (Dartmouth, NS, CAN) | <ul style="list-style-type: none"> • Gaseous general anesthetic agent • 1-chloro-2,2,2-trifluoroethyl difluoromethyl ether |
| Naloxone | Sigma Aldrich (St. Louis, MO, USA) | <ul style="list-style-type: none"> • Non-selective opioid receptor antagonist |
| Pepducin P4pal10 | Genscript (Piscataway, NY, USA) | <ul style="list-style-type: none"> • PAR4 antagonist • Pepducin p4Palomide10 |
| Saline (0.9% NaCl) | Procured in house | <ul style="list-style-type: none"> • Used as a vehicle control for amitriptyline and pepducin P4pal10 |
| Urethane | Sigma Aldrich (St. Louis, MO, USA) | <ul style="list-style-type: none"> • Anesthetic agent • Ethyl carbamate |

| Reagent | Source | Description |
|--|------------------------------------|--|
| Anti-cleaved Caspase-3 (rabbit) | Cell Signalling (Danvers, MA, USA) | <ul style="list-style-type: none"> • Primary antibody against cleaved caspase-3 |

| Reagent | Source | Description |
|---|--|---|
| Anti-Glial Fibrillary Acidic Protein (mouse) | Cell Signalling (Danvers, MA, USA) | <ul style="list-style-type: none"> • Primary antibody against GFAP |
| Anti-PAR4 (rabbit) | Abcam (Cambridge, MA, USA) | <ul style="list-style-type: none"> • Primary antibody against PAR4 |
| Fluoro-Gold | Fluorochrome (Denver, CO, USA) | <ul style="list-style-type: none"> • Fluorochrome used for retrograde labelling of joint neurons |
| Glu-C | Promega (Madison, WI, USA) | <ul style="list-style-type: none"> • Endoprotease used for sample digestion in mass spectrometry experiments |
| Glutaraldehyde | Electron Microscopy Sciences (Hatfield, PA, USA) | <ul style="list-style-type: none"> • Fixative for electron microscopy |
| Magnesium Sulfate (MgSO₄) | Sigma Aldrich (St. Louis, MO, USA) | <ul style="list-style-type: none"> • Component of physiological buffer solution |
| Normal Goat Serum (NGS) | Abcam (Cambridge, MA, USA) | <ul style="list-style-type: none"> • Blocking Agent |
| Paraformaldehyde | Sigma Aldrich (St. Louis, MO, USA) | <ul style="list-style-type: none"> • Fixative for Immunohistochemistry |
| Phosphate Buffered Saline | Sigma Aldrich (St. Louis, MO, USA) | <ul style="list-style-type: none"> • Solvent used for Immunohistochemistry and Fluoro-Gold |
| Potassium Chloride (KCl) | Sigma Aldrich (St. Louis, MO, USA) | <ul style="list-style-type: none"> • Component of physiological buffer solution |
| Rhodamine 6-G | Sigma Aldrich (St. Louis, MO, USA) | <ul style="list-style-type: none"> • Fluorescent dye that accumulates in mitochondria of cells • Used in IVM to identify leukocytes |

| Reagent | Source | Description |
|---|--|--|
| Saline (0.9% NaCl) | Procured in house | <ul style="list-style-type: none"> • Vehicle for amitriptyline and pepducin P4pal10 |
| Sodium Bicarbonate (NaHCO₃) | Sigma Aldrich (St. Louis, MO, USA) | <ul style="list-style-type: none"> • Component of physiological buffer solution |
| Sodium cacodylate buffer (1.0M) | Electron Microscopy Sciences (Hatfield, PA, USA) | <ul style="list-style-type: none"> • Buffer for electron microscopy |
| Sodium Chloride (NaCl) | Sigma Aldrich (St. Louis, MO, USA) | <ul style="list-style-type: none"> • Component of physiological buffer solution |
| Sodium Monoiodoacetate | Sigma Aldrich (St. Louis, MO, USA) | <ul style="list-style-type: none"> • GAPDH inhibitor • Used to induce MIA model of experimental OA |

| Device | Model | Manufacturer |
|--|---|---|
| AC Differential Amplifier | DAM80 | World Precision Instruments (Sarasota, FL, USA) |
| Amplifier & Low Pass Filter | 202A | Warner Instrument Corporation (Hamden, CT, USA) |
| Blood Perfusion Imager | PeriCam PSI Normal Resolution with PimSoft Software | Perimed Incorporated (Ardmore, PA, USA) |
| Blood Pressure Monitor & Transducer | BP-1 | World Precision Instruments (Sarasota, FL, USA) |
| CED Board | Power 1401 | Cambridge Electronic Design (Cambridge, UK) |
| Cryostat | HM 525NX | Thermo Fisher Scientific (Waltham, MA, USA) |
| Dynamic Weight | BIO-DWB-AUTO-R for | DWB system and software |

| Device | Model | Manufacturer |
|---|---|--|
| Bearing System | rats with DFK22AUC03 camera with Bioseb software version 1.4.2.92 | from Bioseb (Boulogne, France) Camera from ImagingSource (Charlotte, NC, USA) |
| Fluorescent Microscope (for IHC) | Zeiss Axio Imager 2 and AxioCam HRm camera | Zeiss (Oberkochen, Germany) |
| Fluorescent Microscope (for IVM) | Leica DM2500 microscope and Leica DFC 3000 camera | Leica Microsystems Inc. (Concord, Ontario, Canada) |
| Luminex Bead Analysis System | Bio-Plex 200 system and Bio-Plex Manager 6.0 software | (Bio-Rad, Hercules, CA, USA) |
| Mass Spectrometer | Q-Exactive Orbitrap mass spectrometer | Thermo Fisher Scientific (Waltham, MA, USA) |
| Oscilloscope (analogue) | VC-6023 | Hitachi (Tokyo, Japan) |
| Oscilloscope (digital) | TDS 3032B | Tektronix (Beaverton, OR, USA) |
| Plate Reader | FLUOstar Omega | BMG Labtech (Ortenberg, Germany) |
| Recording Electrode | Self-made | N/A |
| Small Animal Ventilator | Model 683 | Harvard Apparatus (Holliston, MA, USA) |
| Stimulating Electrode | Self-made | N/A |
| Stimulator | S48 | Grass Instruments (West Warwick, RI, USA) |
| Temperature Controller & Heating Pad | TC1000 | CWE Inc (Ardmore, PA, USA) |
| Torque Meter | Data Track 244-1-R | Intertechnology (Toronto, ON, CAN) |
| Transmission Electron Microscope (TEM) | JEOL JEM 1230 and Hamamatsu ORCA-HR digital camera | TEM from JEOL Corp. Ltd. (Tokyo, Japan) Hamamatsu Photonics (Hamamatsu City, Japan) |
| Von Frey Chamber | Custom made | Concept Plastics Inc. (Dartmouth, NS, Canada) |
| Von Frey Hairs | Semme Weinstein Microfilaments | North Coast Medical (Gilroy, CA, USA) |

| Device | Model | Manufacturer |
|-----------------------------|--------------|---|
| Window Discriminator | 121 | World Precision Instruments (Sarasota, FL, USA) |

Appendix C: Comparison of Day 14 MIA in Male and Female Animals

Single unit electrophysiology was carried out in male and female animals (374-498 and 318-346g) on day 14 of the MIA model to measure joint afferent activity (Figure A.1). Both male and female MIA animals exhibited peripheral sensitization with enhanced evoked afferent firing ($p < 0.05$, $n = 8-11$, 2-way ANOVA) and an increased number of spontaneously active fibres ($p < 0.05$, $n = 8-11$, chi-square test) when compared with naïve control animals. There was no statistical difference observed between the sexes in any measurement.

The presence of neuropathy was assessed in female MIA animals by calculating saphenous nerve G-ratios and comparing to male MIA and naïve animals (Figure A.2). 14 days following MIA administration, myelin thickness was significantly reduced in large and small diameter fibres in female saphenous nerves compared with naïve animals ($p < 0.01$, $n = 4-6$, 2-way ANOVA). G-ratio values were also significantly different between small diameter fibres from male and female MIA animals ($p < 0.01$, $n = 5-6$).

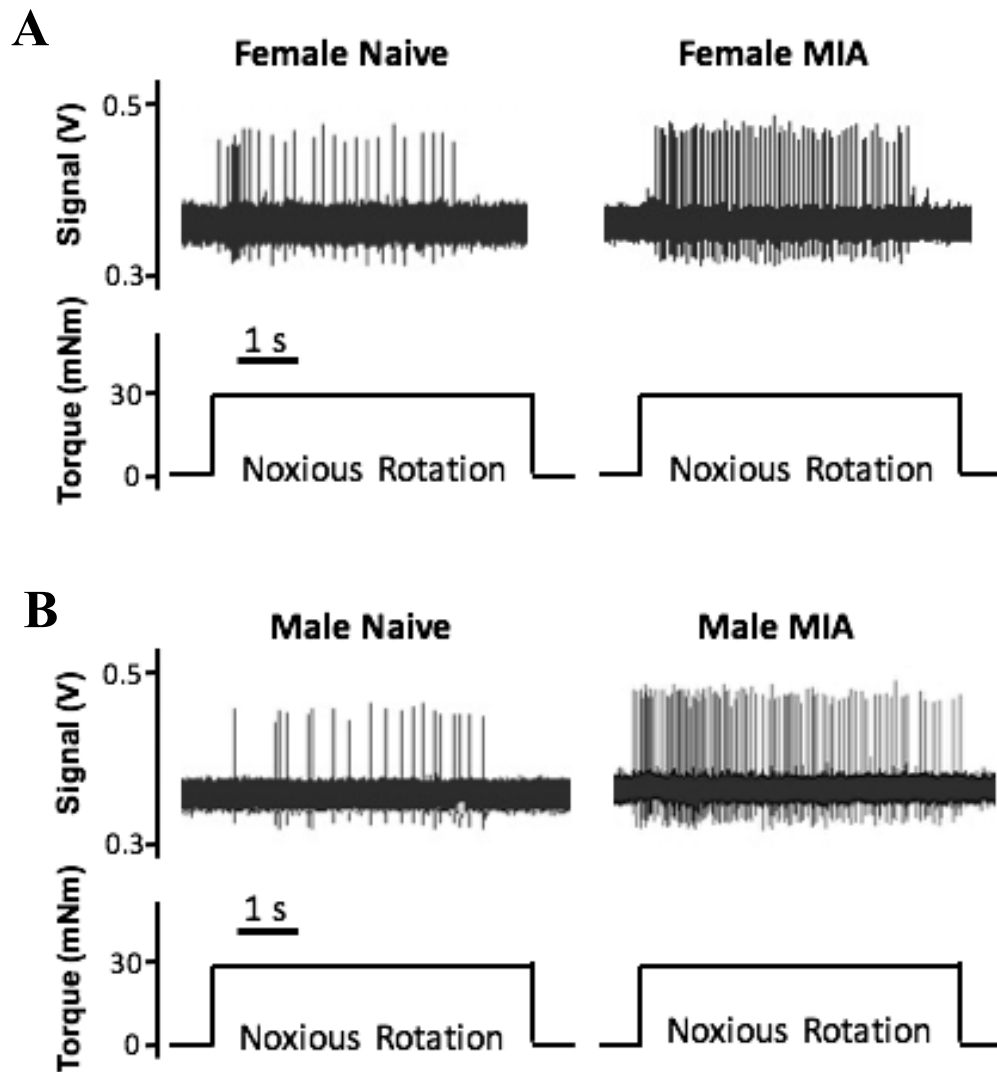


Figure A.1: MIA-induced Sensitisation of Joint Afferents in Female and Male Animals

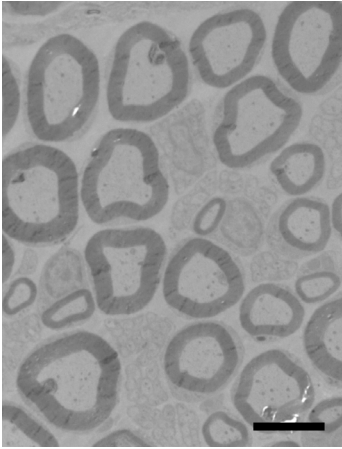
Representative traces of joint afferents recorded from female naïve and MIA animals (A) and male naïve and MIA animals (B).

| Fibre type | Mechanical Threshold (mNm) | Evoked Firing (action potentials/rotation) | Spontaneous Fibres (%) | Electrical Threshold (V) | Conduction Velocity (m/s) | n |
|---------------|----------------------------|--|------------------------|--------------------------|---------------------------|----|
| Naïve | | | | | | |
| Male | 23 ± 3 (10-40) | 12 ± 2 (4-27) | 0 | 4 ± 0.3 (3.5-5.0) | 2.4 ± 0.9 (1.0-3.5) | 11 |
| Female | 23 ± 3 (8-40) | 14 ± 3 (4-26) | 0 | 4 ± 0.4 (3.0-5.0) | 2.4 ± 0.4 (1.8-4.4) | 9 |
| MIA | | | | | | |
| Male Day 14 | 16 ± 3 (2-30) | 41 ± 8 (11-100)** | 50* | 3 ± 0.4 (2.0-4.0) | 3.1 ± 1.2 (1.9-4.7) | 10 |
| Female Day 14 | 14 ± 2 (2-23) | 38 ± 7 (18-69)* | 50* | 3 ± 0.4 (2.5-4.0) | 3.5 ± 1.0 (1.7-6.1) | 8 |

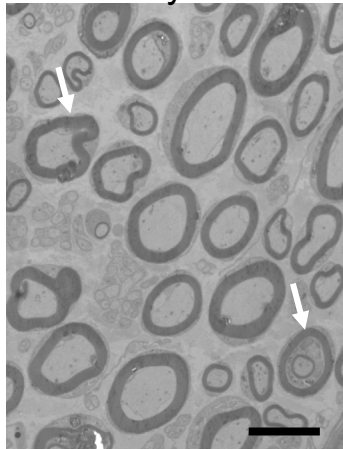
Table A.1: Electrophysiological Characteristics of Joint Afferents from Naïve and MIA Animals. Fibres were recorded from male and female naïve and 14 days MIA animals. Mechanical thresholds, evoked action potentials, electrical thresholds, and conduction velocities were calculated for each group. The percentage of fibres that exhibited spontaneous firing was also calculated. Data are presented as mean ± SEM (range). *p<0.05, **p<0.01, denotes statistical significance between MIA and Naïve fibres of the same sex.

A

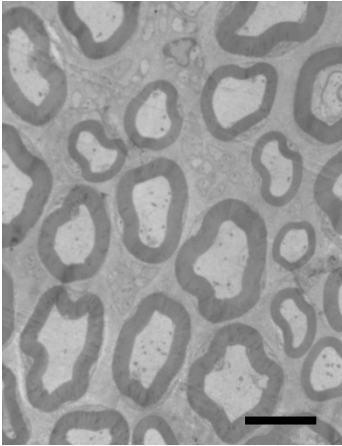
Male Naive



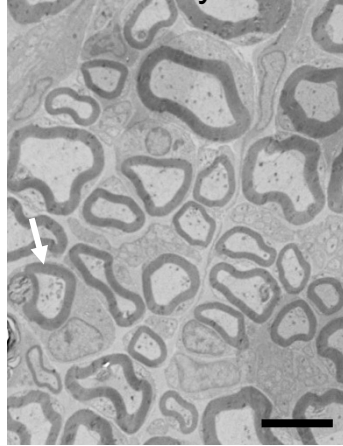
Male Day 14 MIA



Female Naive



Female Day 14 MIA



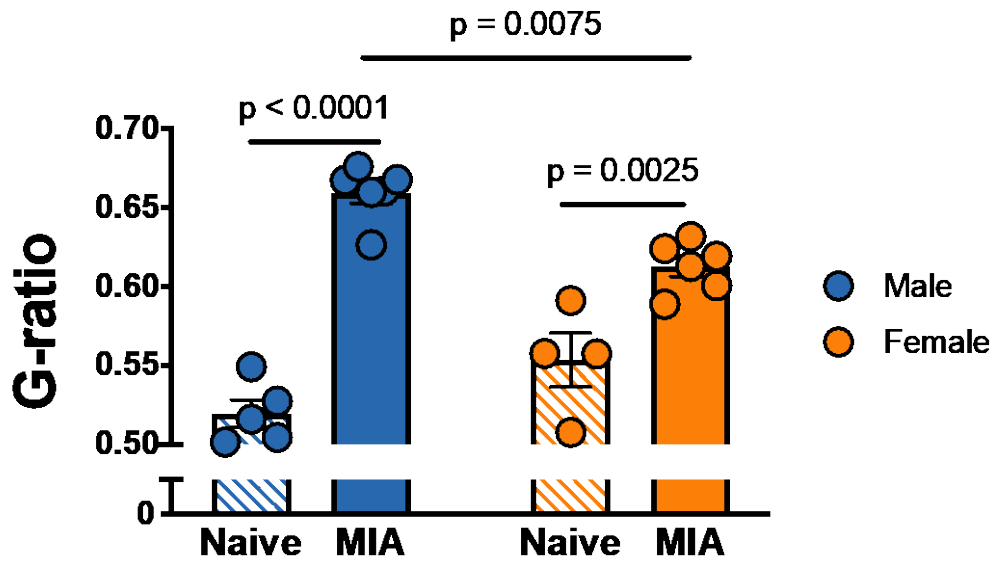
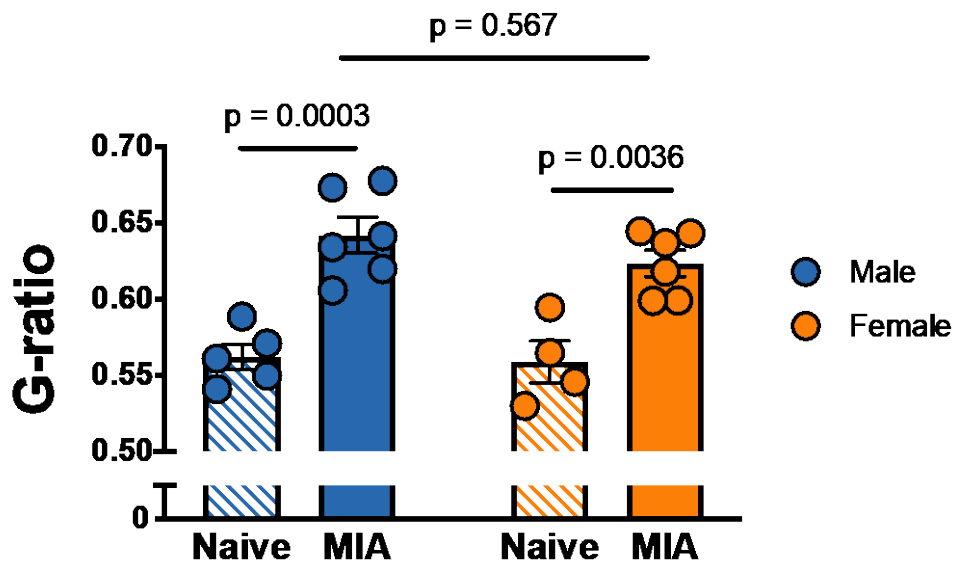
B**Small Diameter Fibres****C****Large Diameter Fibres**

Figure A.2: G-ratio analysis in Male and Female MIA Animals. Representative electron photomicrographs of saphenous nerves from naïve and day 14 MIA male and

female animals **(A)**. G-ratio analysis revealed significantly reduced myelin thickness in both small diameter **(B)** and large diameter **(C)** fibres in MIA animals of both sexes. Arrows indicate axons with non-compact myelin. Scale bar = 6 μm .

Appendix D: Synovial Fluid Proteomics Result

| Protein name | RA | OA | Abundance Ratio (OA/RA) |
|-----------------------------------|----|----|-------------------------|
| 2-phospho-D-glycerate hydro-lyase | ✓ | ✓ | 0.172 |
| Actin, cytoplasmic 1 | ✓ | ✓ | 0.064 |
| Adipsin | ✓ | ✓ | 2.831 |
| Afamin | ✓ | ✓ | 1.847 |
| Aggrecan core protein | | ✓ | nd |
| Alpha-1-acid glycoprotein 1 | ✓ | ✓ | 0.417 |
| Alpha-1-acid glycoprotein 2 | ✓ | ✓ | 0.891 |
| Alpha-1-antichymotrypsin | ✓ | ✓ | 0.143 |
| Alpha-1-antitrypsin | ✓ | ✓ | 0.405 |
| Alpha-1B-glycoprotein | ✓ | ✓ | 0.948 |
| Alpha-2-HS-glycoprotein | ✓ | ✓ | 2.851 |
| Alpha-2-macroglobulin | ✓ | ✓ | 0.401 |
| Angiotensinogen | ✓ | ✓ | 1.207 |
| Antithrombin-III | ✓ | ✓ | 1.168 |
| Apolipoprotein A-I | ✓ | ✓ | 1.384 |
| Apolipoprotein A-II | ✓ | ✓ | 0.971 |
| Apolipoprotein A-IV | ✓ | ✓ | 2.137 |
| Apolipoprotein B-100 | ✓ | ✓ | 0.365 |
| Apolipoprotein C-I | ✓ | ✓ | 0.452 |
| Apolipoprotein C-II | ✓ | ✓ | 0.987 |
| Apolipoprotein C-III | ✓ | ✓ | 2.332 |
| Apolipoprotein D (Fragment) | ✓ | ✓ | 1.019 |
| Apolipoprotein E | ✓ | ✓ | 0.612 |
| Apolipoprotein L1 | ✓ | ✓ | 0.639 |
| Apolipoprotein M | ✓ | ✓ | 1.619 |
| Apolipoprotein(a) | | ✓ | nd |
| Attractin | ✓ | | nd |
| Beta-2-glycoprotein 1 | ✓ | ✓ | 3.12 |
| Beta-2-microglobulin | ✓ | ✓ | 1.122 |
| C-reactive protein | ✓ | | nd |
| C3/C5 convertase | ✓ | ✓ | 0.757 |

| Protein name | RA | OA | Abundance Ratio (OA/RA) |
|--|-----------|-----------|--------------------------------|
| C4a anaphylatoxin | ✓ | ✓ | 1.718 |
| C4b-binding protein alpha chain | ✓ | ✓ | 1.057 |
| Cartilage acidic protein 1 | ✓ | ✓ | 2.106 |
| Cartilage oligomeric matrix protein | ✓ | ✓ | 15.419 |
| CD5 antigen-like | ✓ | ✓ | 0.448 |
| Ceruloplasmin | ✓ | ✓ | 0.547 |
| Clusterin | ✓ | ✓ | 1.091 |
| Coactosin-like protein | ✓ | ✓ | nd |
| Coagulation factor IX | ✓ | ✓ | nd |
| Coagulation factor XII | ✓ | ✓ | 2.392 |
| Coagulation factor XIII B chain | ✓ | ✓ | 0.505 |
| Collagen alpha-2(I) chain | | ✓ | nd |
| Complement C1r subcomponent-like protein | ✓ | | nd |
| Complement C1s subcomponent | ✓ | ✓ | 7.141 |
| Complement C3 | ✓ | ✓ | 0.928 |
| Complement C5 | ✓ | ✓ | 0.668 |
| Complement component C6 | ✓ | ✓ | 0.633 |
| Complement component C7 | ✓ | ✓ | 0.77 |
| Complement component C8 alpha chain | ✓ | ✓ | 0.998 |
| Complement component C9 | ✓ | ✓ | 0.357 |
| Complement factor H | ✓ | ✓ | 0.984 |
| Complement factor H-related protein 1 | ✓ | ✓ | 1.026 |
| Complement subcomponent C1r | ✓ | | 1.683 |
| Extracellular matrix protein 1 | | ✓ | nd |
| Fibrinogen alpha chain | ✓ | ✓ | 0.437 |
| Fibrinogen beta chain | ✓ | ✓ | 0.529 |
| Fibrinogen gamma chain | ✓ | ✓ | 0.472 |
| Fibroblast growth factor-binding protein 2 | | ✓ | nd |
| Fibronectin | ✓ | ✓ | 3.982 |
| Gc-globulin | ✓ | ✓ | 1.516 |
| Gelsolin | ✓ | ✓ | 3.857 |

| Protein name | RA | OA | Abundance Ratio (OA/RA) |
|--|-----------|-----------|--------------------------------|
| Haptoglobin | ✓ | ✓ | 0.169 |
| Haptoglobin-related protein | ✓ | ✓ | 1.775 |
| Hemopexin | ✓ | ✓ | 0.836 |
| Heparin cofactor 2 | ✓ | ✓ | 1.677 |
| Hepatocyte growth factor-like protein | ✓ | ✓ | 0.73 |
| Histidine-rich glycoprotein | ✓ | ✓ | 0.947 |
| Immunoglobulin heavy constant alpha 1 | ✓ | ✓ | 0.35 |
| Immunoglobulin heavy constant alpha 2 (Fragment) | ✓ | ✓ | 2.923 |
| Immunoglobulin heavy constant gamma 1 | ✓ | ✓ | 0.757 |
| Immunoglobulin heavy constant gamma 2 | ✓ | ✓ | 1.841 |
| Immunoglobulin heavy constant gamma 3 (Fragment) | ✓ | ✓ | 0.735 |
| Immunoglobulin heavy constant gamma 4 | ✓ | ✓ | 0.699 |
| Immunoglobulin heavy constant mu | ✓ | ✓ | 0.626 |
| Immunoglobulin heavy variable 5-51 | ✓ | | nd |
| Immunoglobulin J chain | ✓ | ✓ | 1.608 |
| Immunoglobulin kappa constant (Fragment) | ✓ | ✓ | 0.549 |
| Immunoglobulin kappa joining 1 | ✓ | ✓ | 2.233 |
| Immunoglobulin kappa variable 1D-17 | ✓ | ✓ | 0.416 |
| Immunoglobulin kappa variable 3-20 | ✓ | ✓ | 0.884 |
| Immunoglobulin kappa variable 4-1 | | ✓ | nd |
| Immunoglobulin lambda constant 2 | ✓ | ✓ | 0.55 |
| Immunoglobulin lambda constant 3 | ✓ | ✓ | 0.547 |
| Immunoglobulin lambda constant 7 (Fragment) | ✓ | ✓ | 0.994 |
| Immunoglobulin lambda variable 2-14 | ✓ | | nd |
| Immunoglobulin lambda variable 3-21 | | ✓ | 1.257 |
| Immunoglobulin lambda-like polypeptide 5 | ✓ | ✓ | 0.931 |
| Insulin-like growth factor II | | ✓ | nd |
| Insulin-like growth factor-binding protein 3 | ✓ | ✓ | 0.554 |
| Insulin-like growth factor-binding protein 4 | ✓ | ✓ | 1.218 |
| Insulin, isoform 2 | ✓ | ✓ | 1.608 |
| Integral membrane protein 2B | | ✓ | nd |



| Protein name | RA | OA | Abundance Ratio (OA/RA) |
|--|-----------|-----------|--------------------------------|
| Inter-alpha-trypsin inhibitor heavy chain H1 | ✓ | ✓ | 6.326 |
| Inter-alpha-trypsin inhibitor heavy chain H2 | ✓ | ✓ | 1.446 |
| Inter-alpha-trypsin inhibitor heavy chain H4 | ✓ | ✓ | 0.34 |
| Interstitial collagenase (MMP-1) | ✓ | | nd |
| Kininogen-1 | ✓ | ✓ | 1.125 |
| L-selectin | ✓ | | nd |
| Leucine-rich alpha-2-glycoprotein | ✓ | ✓ | 0.167 |
| Lumican | ✓ | ✓ | 1.278 |
| Microfibrillar-associated protein 5 | | ✓ | nd |
| N-acetylmuramoyl-L-alanine amidase | | ✓ | nd |
| Neutrophil defensin 1 | ✓ | | nd |
| Phospholipid transfer protein | ✓ | ✓ | 0.091 |
| Pigment epithelium-derived factor | ✓ | ✓ | 1.608 |
| Plasma kallikrein (Fragment) | ✓ | ✓ | 0.438 |
| Plasminogen | ✓ | ✓ | 1.807 |
| Pregnancy zone protein | ✓ | | nd |
| Properdin | ✓ | ✓ | 1.189 |
| Prostaglandin-H2 D-isomerase | ✓ | ✓ | 1.157 |
| Protein AMBP | ✓ | ✓ | 0.312 |
| Protein S100-A9 | ✓ | | nd |
| Proteoglycan 4 | ✓ | ✓ | 6.035 |
| Prothrombin | ✓ | ✓ | 1.443 |
| Putative alpha-1-antitrypsin-related protein (SERPIN A2) | | ✓ | nd |
| Retinol-binding protein 4 | ✓ | ✓ | 2.426 |
| Scavenger receptor cysteine-rich type 1 protein M130 | ✓ | | nd |
| Selenoprotein P | ✓ | ✓ | 2.568 |
| Serum amyloid A protein | ✓ | ✓ | 1.435 |
| Stromelysin-1 (MMP-3) | ✓ | ✓ | 0.558 |
| Tetranectin | ✓ | ✓ | 0.487 |
| Thymosin beta-4 | ✓ | | nd |
| Transthyretin | ✓ | ✓ | 4.805 |


| Protein name | RA | OA | Abundance Ratio (OA/RA) |
|--|-----------|-----------|--------------------------------|
| Vitamin K-dependent protein S (Fragment) | ✓ | ✓ | 0.091 |
| Vitronectin | ✓ | ✓ | 2.218 |
| Zinc-alpha-2-glycoprotein | ✓ | ✓ | 1.827 |

Abundance Ratio = abundance of protein in OA sample/abundance of protein in RA sample.

A ratio was not calculated if the protein was only identified in one sample, denoted as 'nd', not determined.

Appendix E: Copyright Permission

HomeHelpEmail SupportSign inCreate Account



Neurophysiological assessment of joint nociceptors in the rat medial meniscus transection model of post-traumatic osteoarthritis
Author: M.S. O'Brien, J.J. McDougall
Publication: Osteoarthritis and Cartilage
Publisher: Elsevier
Date: September 2020
© 2020 Osteoarthritis Research Society International. Published by Elsevier Ltd. All rights reserved.

Please note that, as the author of this Elsevier article, you retain the right to include it in a thesis or dissertation, provided it is not published commercially. Permission is not required, but please ensure that you reference the journal as the original source. For more information on this and on your other retained rights, please visit: <https://www.elsevier.com/about/our-business/policies/copyright#Author-rights>

[BACK](#) [CLOSE WINDOW](#)

© 2021 Copyright - All Rights Reserved | Copyright Clearance Center, Inc. | [Privacy statement](#) | [Terms and Conditions](#)
Comments? We would like to hear from you. E-mail us at customer@copyright.com